University of Stavanger

FACULTY OF SCIENCE AND TECHNOLOGY

MASTER'S THESIS

Study programme/specialisation: Petroleum Geoscience Engineering	Spring/ Autumn semester, 2018 Open / ~~Confidential~~
Author: Jacob Dieset	…… (signature of author)
Programme coordinator: Supervisor(s): Udo Zimmermann	
Title of master's thesis: Age and Provenance study of Paleoarchean rocks from the Singhbhum Craton (India)	
Credits:	
Keywords: Singhbhum Craton Paleoarchean, India U-Pb age Hf-isotope Zircon Apatite Singhbhum Granite, OMGT	Number of pages: ……51…… + supplemental material/other: …82…… Stavanger, August 13th/2018 date/year

Abstract

This study has performed *in situ* U-Pb and Lu-Hf isotope analysis on zircons and *in situ* U-Pb isotope analysis on apatites, by LA-ICP-MS and MC-ICP-MS, from three Tonalite-Trondhjemite-Granodiorite (TTG) samples from the Paleoarchean rocks of the Singhbhum Craton, eastern India. One sample, RM1, from the Older Metamorphic Tonalite Gneiss (OMTG) and two samples, RT11 and CH2, from the Singhbhum Granites. Presenting $^{207}Pb/^{206}Pb$ zircon crystallization ages for the three samples: RT11 - 3384.4 ± 3.9 Ma, CH2 - 3308.4 ± 7.6 Ma and RM1 - 3396 ± 14 Ma. These U-Pb zircon ages are supported by very similar U-Pb apatite ages. Hf-isotopes in zircons indicates a dominantly juvenile provenance, but single zircons aged ∼3.6 Ga from RT11 and RM1 indicates reworking of at least one older Archean component. RM1 yielded eight concordant $^{207}Pb/^{206}Pb$ ages of ∼4.0 Ga, which rendered both radiogenic and unradoigenic $^{176}Hf/^{176}Hf$ values. Four zircons exhibited $\varepsilon_{Hf,t}$ values of -10.6 to -13.6, indicating an enriched source with a separation age of 4.5 Ga, and may indicate an initially enriched reservoir at the formation of the Earth.

Acknowledgement

I would like to thank Dr. Rajat Mazumder, for providing the sample information and material for this thesis work. Without the contribution of the samples, this thesis would have been conducted on a totally different subject.

Thanks to Dr. Thomas J. Lapen and Dr. Minako Righter for welcoming me in Houston, and providing me with access and support to their isotopic laboratories at the University in Houston.

Thanks to Caroline Ruud and Mina Minde for laboratory expertise and help in preparing samples and operating the Scanning Electron Microscope at the University in Stavanger.

Special thanks to my supervisor Dr. Udo Zimmermann. Without his experience and connections the project would simply not be possible. Coupled with an enormous patience and trust, he has guided me through this project, and made it possible for me to finish my education!

I would also like to thank friends, co-students and family for all their needed support.

Table of Contents

List of Figures

List of Tables

1. Introduction

The objective of this thesis is to perform *in situ* U-Pb and Hf-isotope analysis, by LA-ICP-MS and MC-ICP-MS, on zircons from three different samples from the oldest suite of rocks in the Singhbhum Craton, eastern India. By coupling U-Pb ages with Hf-isotope compositions, the rocks will be analyzed for magmatic provenance, where the objective is to resolve the crustal formation activity in the Singhbhum Craton.

Further the project will perform *in situ* U-Pb analysis on apatites, to test if this phase of U-bearing mineral can provide additional information on these rocks.

1.1. Crustal geology

Earth is unique among the rocky planets of the Solar System in possessing a chemically evolved continental crust. It is the presence of such a crust that has ultimately permitted the appearance of human life (Brown and Rushmer 2006). So it has for a long time been an interest of geology to understand the origin and evolution of the planet that we origin from. It is not the purpose of this thesis to figure out why life appeared on the Earth, but to contribute to the knowledge of the geological formation and evolution of the crust as it is known

today.

When looking at the Earth, and the geological evidences it provides, it is clear that the Earth is on longer what it used to be (Rollinson 2007). Be it sedimentological evidences of marine sediments on top of mountains or magnetic evidence that lead to the theory of plate tectonics. To understand the evolution of the Earth, it is important to know the components which from it is derived. Regrettably, there is very little unaltered geologic evidence left from the early history of the Hadean (4.0-4.6 Ga). In this text millions of years ago are abbreviated to Mega-years ago (Ma - 10^6 years ago), billions of years ago is abbreviated to Giga-years ago (Ga - 10^9 years ago) and durations, like 3 million or 3 billion years, will be abbreviated to 3 My and 3 Gy respectively.

The prevailing method for geochemical scientists to look at the major components and interactions of the Earth today is through a box-model. The model shown in Figure 1.1 is most comprehensive box model for the whole modern Earth, and its purpose is to provide a geochemical reference model for the Earth (Rollinson 2007). This approach recognizes that the big components (crust, mantle, core and atmosphere) can not be divided into separate, closed off compartments, but is rather open systems that interact with each other (Rollinson 2007). The Earth System approach also consider the interaction between the solid crust and the atmosphere, including the evolution of life and biological interference. These systems interact on timescales of milliseconds to billions of years and spatially from microns to thousands of kilometer.

During the first 100 My, or even as short as 30 My, the Earth differentiated into some of its principal reservoirs - the core, mantle, ocean and atmosphere. At this time, an initial basaltic crust was formed, followed by a felsic crust a little time later (Rollinson 2007). Hastie et al. (2016) argues that the first continental crust is a result of partial melting of an $\sim$35-40 km thick Eoarchean oceanic crust due to subduction. Johnson et al. (2017), however, argues that the formation of continental crust did not require subduction, but partial melting

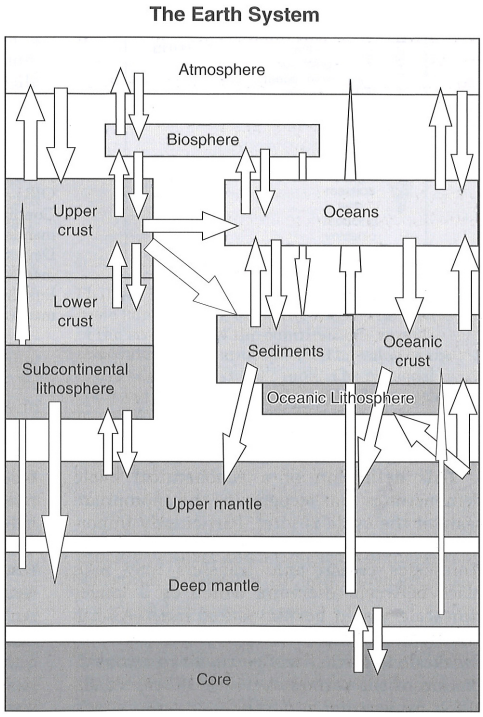

Figure 1.1.: A box model for the Earth System, showing some of the major reservoirs and the interaction (white arrows) between them (from Rollinson (2007)).

of basaltic sources, due to a higher geothermal gradient in the earlier stage of the Earth's history. The mechanics of the early Earth is clearly disputed.

Information about the Early earth processes and composition is scarce. Because of the various dynamic recycling processes operating, very little of the oldest rock record is left (Rollinson 2007; Brown and Rushmer 2006). Most of the compositional information that is known is derived from cosmological studies on meteorites. The oldest fragments that is known, are the various meteorites that plunge to the Earth from time to time, and the radiometric dating of these has lead us to infer the age of the formation of the Earth to be 4.56 Ga. Of the various meteorites, there is one kind that is believed to be representative of the material forming the first planetesimals, it it is the rocky, undifferentiated group of chondrites.

The prevailing model for the formation of the Earth, is thus that the initial composition was chondritic, before collisional and radioactive heat lead to the differentiation, and the fractionation of the Earth in the different components that is known today, namely: The core, lower and upper mantle and the oceanic and continental crust.

This far, little is known of the timing of the separation of these geochemical reservoirs. Isotope geochemistry has been a valuable tool in investigating this evolution, as different compositions of radioactive and radiogenic elements will have different evolutions, and is thus traceable, providing that there is instruments capable of measuring the correct amounts.

1.2. Geology of India

The Indian continental plate is what is known as a Precambrian shield, and is a mosaic of cratons and fold belts that has remained stable since the Precambrian. The Indian shield is, as most Precambrian shields, distinguished by granite-greenstone terrains or low-grade terrains surrounded by curvilinear, high-grade, gneiss-granulite belts which is separated from the cratons by crustal scale ductile share zones (Ramakrishnan and Vaidyanadhan 2008). India is subdivided into several geological provinces, and based on different geological criteria the continent is subdivided in different ways. Figure 1.2 depicts one such subdivision based on tectonic division.

The Indian shield consists of five major Archean cratons: Dharwar, Bastar, Singhbhum, Bundelkhand and Aravalli. There are three prominent Proterozoic mobile belts, Eastern Ghats mobile belt bordering Dharwar, Bastar and Singhbhum cratons, Pandyan mobile belt bordering Dharwar craton, and Satpura mobile belt bordering Bastar, Singhbhum, Bundelkand and Aravalli cratons

Figure 1.2.: Tectonic subdivision of the Indian shield. From Ramakrishnan and Vaidyanadhan (2008).

and extending into the Shillong Plateau. This thesis will focus on the Singhbhum Craton, which is bordered to the north by the Satpura mobile belt, the Mahanadi rift and Bastar craton to the west and the Eastern Ghats to the south (Ramakrishnan and Vaidyanadhan 2008).

The Paleoarchean Singhbhum Craton consists of an Archean nucleus of large volumes of Tonalite-Trondhjemite-Granodiorite (TTG) gneisses and intrusive granitoids of ∼3.5 to 3.2 Ga age. Flanking the nucleus are three Paleoarchean greenstone successions, which are collectively known as the Iron Ore Group (IOG) (D. Mukhopadhyay 2001; J. Mukhopadhyay et al. 2008). The Archean nucleus is unconformably overlain by Paleoproterozoic supracrustals, which will not be covered here.

The Older Metamorphic Group (OMG) comprises interlayered metabasalt (amphibolite) and metasedimentary rocks (biotite-muscovite schist, quartz-sericite schist, quartzites and calc-silicates). The OMG is constrained by a $^{207}Pb/^{206}Pb$ ion microprobe age of ∼3.5 Ga, obtained from a detrital zircon from quartzites from the Champua area (type location for the OMG) (Mishra et al. 1999). Older, inherited, cores of ∼3.55 to 3.6 Ga suggests an older crust (Mishra et al. 1999).

The Older Metamorphic Tonalitic Gneiss (OMTG) consists of thinly layered, medium-grained tonalitic to granodioritic gneisses. The OMTG represents a metamorphic suite of TTGs that formed over an extended period between 3.53-3.45 Ga, while the OMG represents a supracrustal group that formed as a greenstone succession (Chaudhuri et al. 2018). Most $^{207}Pb/^{206}Pb$ zircon ages of the OMTG from previous studies centers around 3.4 Ga, but Chaudhuri et al. (2018) reports two xenocrysts from the OMGT with $^{207}Pb/^{206}Pb$ ages of 4.0 and 4.2 Ga, giving a strong indication that felsic crustal formation was going on in the Singhbhum Craton before the emplacement of the OMTG.

A voluminous TTG-granitoid suite (most commonly referred to as the Singhb-

hum Granites) was emplaced in at least two phases (Mishra et al. 1999; Tait et al. 2011). The oldest emplacement at 3.45 to 3.44 Ga coincides highly with the emplacement of the OMGT, and the youngest phase is constrained from 3.35 to 3.32 Ga (Upadhyay et al. 2014). Surrounding the Singhbhum Granite is three distinct Archean greenstone successions of the IOG. J. Mukhopadhyay et al. (2008) confirms the Paleoarchean age of these rocks with a SHRIMP U-Pb zircon age of 3507 ± 2 Ma of dacitic lava from the southern IOG.

This thesis will perform further studies on one of the OMGT samples from Chaudhuri et al. (2018), and two samples from the Singhbhum Granites.

1.2.1. Samples

Three samples, RT11, CH2 (from the Singhbhum Granites) and RM1 (from OMTG), were sent to the University of Stavanger with courtesy of Dr. Rajat Mazumder at the Department of Applied Geology, Faculty of Engineering and Science, Curtin University Malaysia.

RT11 and CH2 are, according to the geological map from (Chaudhuri et al. 2018) (Figure 1.3), from the Singhbhum Granite TTGs, first emplacement phase, and are course-grained igneous rocks. No outcrop information was provided with the samples, so no further description will be provided for these two samples. Sample location for RT11 are N 22°37′11″ and E 86°13′30″, and location for CH2 are N 22°15′ and E 85°47′.

Sample RM1 are from the Rimuli Formation of the OMTG and is collected at N 21°58′2.8″ and E 85°35′53.6″, ∼1.5 km northwest of Rimuli village, to the south of Champua.

The following description of the Rimuli Formation is found in Chaudhuri et al.

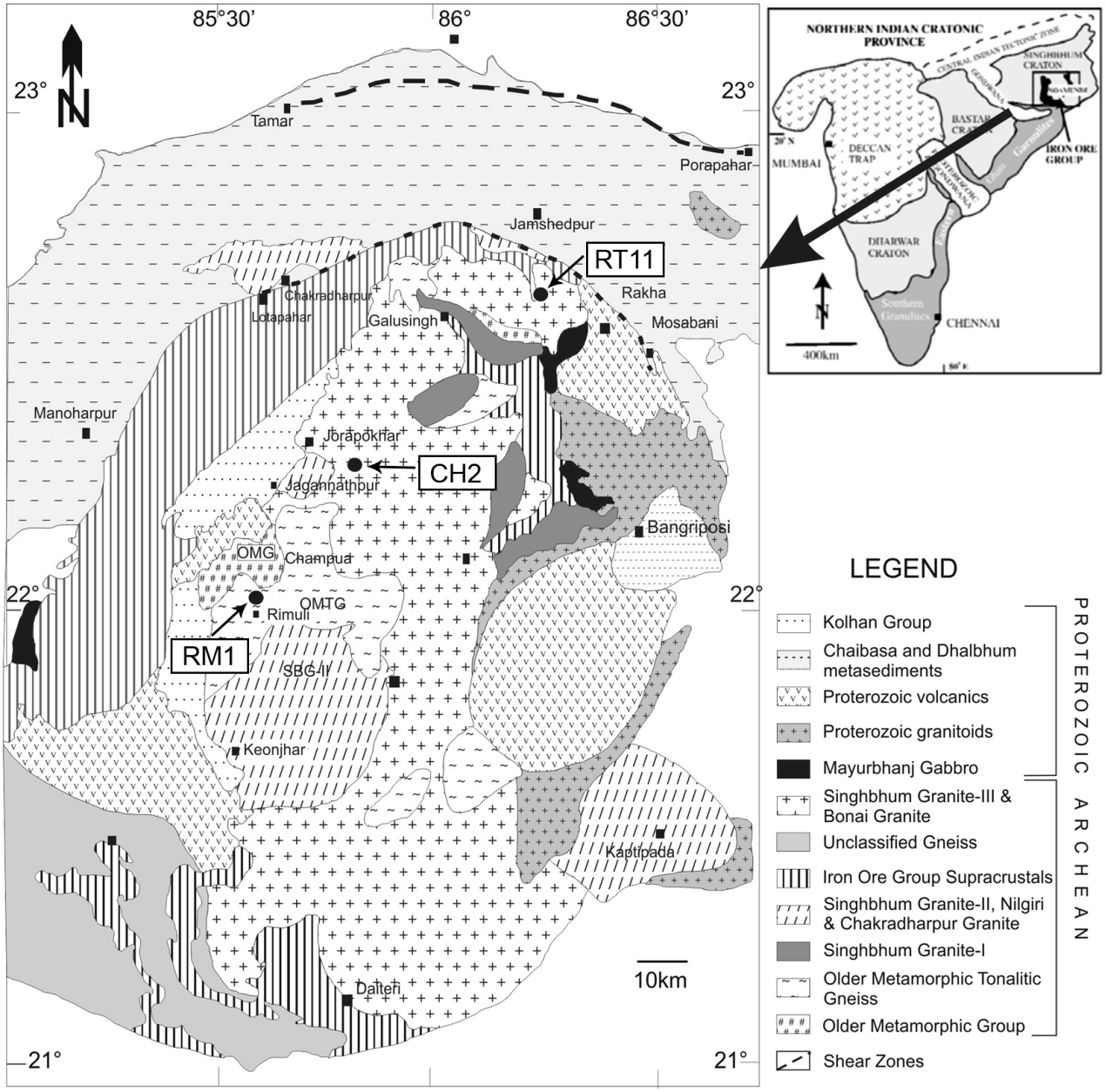

Figure 1.3.: Geological map of the Singhbhum Craton with locations of the three samples investigated in this thesis. (Modified after Chaudhuri et al. (2018))

(2018): These rocks occur as small, patchy exposures of granite gneiss (OMTG) within a terrain dominated by the OMTG, which contains abundant enclaves

of the OMG amphibolite. These are medium-grained, mesocratic, partially weathered TTG gneisses displaying thin (5–10 mm) compositional banding. The mesocratic bands comprise medium-grained (1–5 mm) quartz, potassic feldspar, plagioclase and muscovite, whereas the darker bands are mostly comprised of biotite and minor amphibole.

1.3. Isotope geochemistry

Geochronology made its entry in the geological toolbox after Becquerel's discovery of radioactivity in the late 1800s. It was soon clear that radioactive isotopes not only gave the Earth an internal energy source and the Sun the ability to burn over a much longer timespan than previously thought possible, but that long-lived radioactive decay systems could be used to date geological events with potentially high precision. The first radioactive element U, and then the discovery of Ra by the Courier couple, lead to the realization of the first two decay series called "radium" and "actinium" (Davis et al. 2003). From this basis, the field of geochronology has developed a range of different tools for the study of the evolution of the Earth. In this thesis the focus will be on the decay of U to Pb and a Lu decaying into Hf.

Half-life ($t_{1/2}$) is the time it takes (in year or even Gy) from the original amount of an amount of one particular isotope to be reduced to 50 %. The decay constant (λ) is in the unit $year^{-1}$, and is a negative number that reflects the decrease of the original amount of isotope atoms per year. The relation can be equated to:

$$t_{1/2} = \frac{\ln 2}{\lambda} \tag{1.1}$$

Two important assumptions is made when working with geochronological systems: 1. The initial composition of the starting material was in isotopic

equilibrium, meaning the system had an initial uniform distribution of isotopes. 2. Radioactive decay has been operating in a closed system, so no transfer of parent or daughter isotopes has taken place since the initiation of the system. With these two assumptions, the equation of radioactive decay in a closed system can be written as,

$$N_t = N_i e^{-\lambda t}$$

where N_t is amount of radioactive isotopes at time t, N_i is amount of radioactive isotopes initially, λ is the decay constant, e is Eulers number and t is time passed, one can calculate the amount of isotopes present at any time after the system closes. Substituting the amount of initially present isotopes with the present number of radioactive parent isotope, N_P, plus the stable daughter isotope; N_D, $N_i = N_P + N_D$, the amount of parent isotope after a given t, $N_t = N_P$, and the decay constant for the appropriate parent isotope, λ_P, we get:

$$N_P = (N_P + N_D)e^{-\lambda_P t}$$

Rearranging the equation:

$$\begin{aligned} \frac{N_P}{N_P + N_D} &= e^{-\lambda_P t} \\ 1 + \frac{N_D}{N_P} &= e^{\lambda_P t} \\ \frac{N_D}{N_P} &= e^{\lambda_P t} - 1 \end{aligned} \tag{1.2}$$

Equation 1.2 is true, and is the basis for all geochronological systems, relating the measured daughter-parent ratios of any given radiogenic system to the time passed and the decay constant of this system.

The two most important methods of decay are α-decay and β-decay. α-decay

happens when a $^4He^{2+}$ nucleus (two protons and two neutrons), called an alpha-particle, is spontaneously emitted from an unstable parent isotope nucleus, resulting in a (stable or unstable) daughter isotope, 1^4He and energy. An α-decay always results in a reduction in atomic number by two and atomic mass by four. β-decay happens in an unstable isotope nucleus where there is an unbalance in the proton to neutron ratio. There is two possible decays, where a neutron emits a β^--particle (an electron) and converts into a proton, or a proton emits a β^+-particle (destroying an electron) and converts into a neutron. Either way, the spontaneous decay changes the atomic number by one, but the atomic mass does not change.

1.3.1. U-Pb dating

The element U has three naturally occurring isotopes, all of which is radioactive. The main isotope ^{238}U constitutes more than 99 % of naturally occurring U, ^{235}U constitutes approximately 0.7 %. The isotope ^{234}U is a intermediate daughter isotope in the ^{238}U decay series, with $t_{1/2} = 245500$ years, and is utilized in fission-track dating, but will not be covered in this thesis.

^{238}U decays through eight α-particles and six β^--particles into ^{206}Pb and ^{235}U decays through seven α-particles and four β^--particles into ^{207}Pb, the full decay series is illustrated in Figure 1.4 (also illustrating the decay of ^{232}Th to ^{208}Pb, but this series will not be discussed further in this thesis.) (Schoene 2014). Because the intermediate daughter isotopes has $t_{1/2} \ll t_{1/2}$-U, these are neglected in the further calculations.

$t_{1/2}$ of ^{238}U and ^{235}U was first measured with high accuracy with α-counting by Jaffey et al. (1971). Knowing the relation between a radioactive half-life and its decay constant from equation 1.1, the decay constant of the two isotopes can be calculated, and utilized to construct ages for measured quantities of

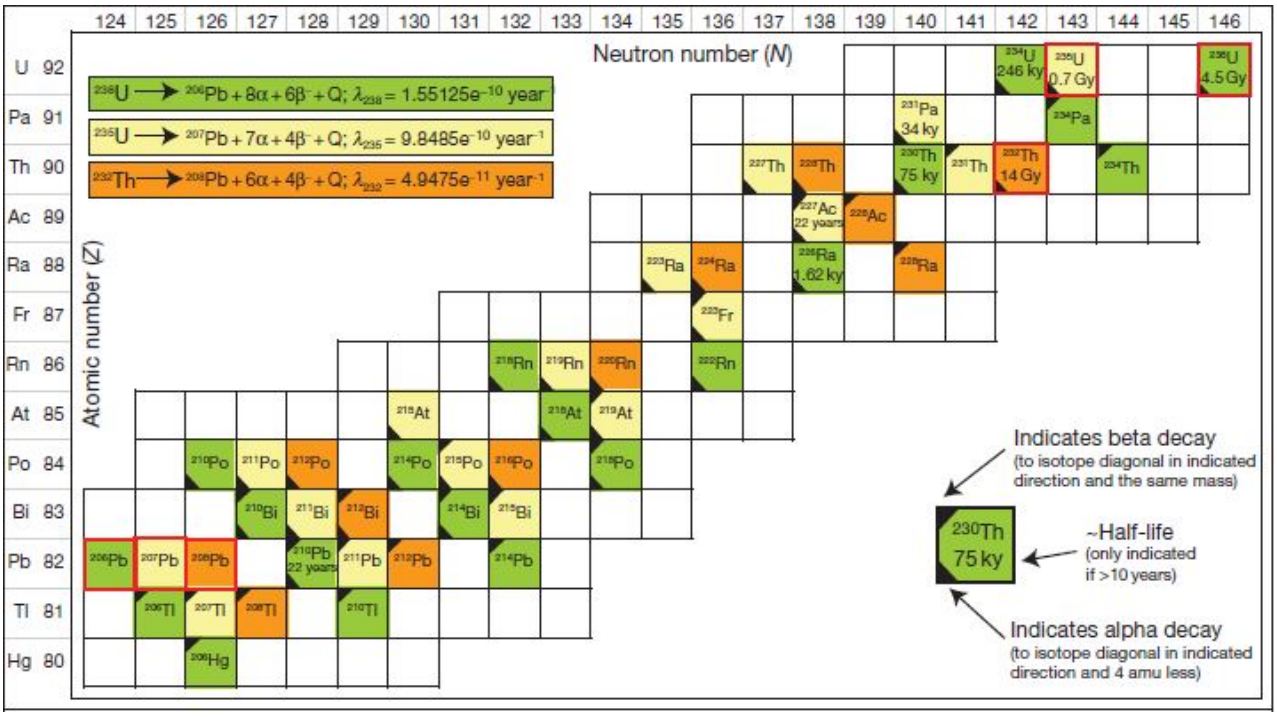

Figure 1.4.: An illustration of the U-Th-Pb decay chains. Each isotope occurring in a given decay chain is color-coded to its parent isotope, which are outlined in red, as are the stable daughter isotopes of Pb. See inset for description of symbols in each box. α is an alpha-particle, β is a beta-particle, and Q is energy released during decay. (Schoene 2014)

daughter/parent fractions. The decay constants has later been refined by Schoene et al. (2006) and Mattinson (2010), by comparing real datasets to the concordia curve. The values has been recalculated within uncertainty of the original values of Jaffey et al. (1971), but 0.09 % different from the mean value and decreases the uncertainty by one power of magnitude. This thesis utilizes the calculated decay constants from Schoene et al. (2006), $\lambda_{238} = 1.54993 \pm 0.00026 \times 10^{-10}\ year^{-1}$ and $\lambda_{235} = 9.8569 \pm 0.0017 \times 10^{-10}\ year^{-1}$.

Substituting for the two U-Pb systems into equation 1.2, we get:

$$\frac{^{206}\mathrm{Pb}^{*}}{^{238}\mathrm{U}} = e^{\lambda_{238} t} - 1 \tag{1.3}$$

and

$$\frac{^{207}\mathrm{Pb}^{*}}{^{235}\mathrm{U}} = e^{\lambda_{235}t} - 1 \tag{1.4}$$

where Pb^{*} is radiogenic Pb, and t, time since the system closed, is only dependent on the measured daughter/parent isotope ratio and the respective decay constant. Dividing equation 1.4 with equation 1.3 gives the relation

$$\left(\frac{^{207}\mathrm{Pb}^{*}}{^{206}\mathrm{Pb}^{*}}\right) = \left(\frac{^{235}\mathrm{U}}{^{238}\mathrm{U}}\right)\frac{(e^{\lambda_{235}t} - 1)}{(e^{\lambda_{238}t} - 1)} \tag{1.5}$$

where t is only dependent in the measured, radiogenic, daughter isotope ratio and the $^{238}\mathrm{U}/^{235}\mathrm{U}$ ratio and decay constants are, well, constants. The value for $^{238}\mathrm{U}/^{235}\mathrm{U} = 137.88$ used in this thesis, is the value adopted by Steiger and Jäger (1977) after compiling measurements performed in uranium ore deposits. Recent, deviations up to $\sim$1 ‰has been observed in low-temperature environments and crustal rocks, but since the $^{238}\mathrm{U}/^{235}\mathrm{U}$ ratio influences the calculations for the decay constants (Schoene 2014; Schoene et al. 2006; Mattinson 2010), this thesis will stick to the value of Steiger and Jäger (1977).

The U-decay system has a huge advantage in geochronology. Because of the two long-lived systems with different $t_{1/2}$ that exists simultaneously, they can be cross checked to confirm that both systems give the same age. If the two systems give the same age, the data point is said to be concordant, and discordant if not. Concordance is often interpreted as the system having remained closed since the date calculated, thus yielding an accurate crystallization age for the sample (Vervoort and Kemp 2016). Wetherill (1956) introduced a graphical way of inspecting data for concordance, in what is now known as the concordia diagram. The diagram plots $^{206}\mathrm{Pb}^{*}/^{238}\mathrm{U}$ versus $^{207}\mathrm{Pb}^{*}/^{235}\mathrm{U}$ of the same analysis, and then draws over the *concordia curve*. The concordia cure is drawn as the set of solutions to equation 1.3 and equation 1.4 for equal values of t. Samples

who plots on the concordia curve has remained closed systems since the time of crystallization, while samples which has experienced open-system behavior plots off the line.

Pb loss, Pb gain, U loss, U gain and mixing of different-aged sources can all generate discordant results, where Pb-loss and and mixing of different-aged sources is the most commonly analyzed features (Schoene 2014). In the concordia diagram, a suite of zircons which has experienced Pb-loss, will plot beneath the concordia curve in a linear fashion (provided they were of the same age before Pb-loss) towards the age of the event providing the Pb-loss. On a population of same original age, a linear regression can be performed on the discordant data points, and a lower and upper intercept with the concordia curve can be calculated. This lower intercept will represent the Pb-loss event and the upper intercept will represent the true crystallization age. Caveats to this method, is when several events of Pb-loss has occurred, for which the lower and upper intercept will represent the *average* time of Pb-loss and crystallization.

1.3.2. Hf-Isotopes

Lu lies at the end of the lanthanide series as the heaviest of the Rare Earth Elements (REE). Lu has two naturally occurring isotopes, ^{175}Lu which is stable and ^{176}Lu which is unstable, whose respective abundances are 97.4 % and 2.6 %. ^{176}Lu displays a branched isobaric decay, by β^- emission to ^{176}Hf and by electron capture to ^{176}Yb. However, the latter makes up a tiny amount of the total activity and can be more or less ignored. ^{176}Hf is left in an excited state after the β decay, and decays to the ground state by γ emission. It is one of six Hf-isotopes and makes up 5.2 % of total Hf, an element which is not a REE, but resembles Zr very closely in its crystal chemical behavior (Dickin 2005), see section 1.4.

The Lu-Hf system is analogous to the Sm-Nd system, however it is a more sensitive tracer (Kinny and Maas 2003) applied on single zircon grains, as Sm-Nd is commonly applied on whole rock samples.

Lu and Hf are refractory elements, which means they condensed early in the cooling of the solar system, and it is considered that the distribution was in equilibrium (Brown and Rushmer 2006). Both elements are immobile and to a certain extent quite compatible. However Hf is less compatible than Lu, and has been fractionated between the mantle and continental crust through the evolution of an enriched continental crust and depleted mantle during partial melting (Dickin 2005). The resulting reservoirs of Hf-isotopes can be tracked, utilizing the slow decay of ^{176}Lu. By convention it is usual to compare fractions, based on the stable isotope of ^{177}Hf, so different quantities of measured material can readily be compared.

At the time of earth formation, the isotopic composition of the Earth was chondritic, and the fractionation of the different reservoirs is measured in parts per ten thousand deviations from a Chondritic Uniform Reservoir (CHUR):

$$\varepsilon_{Hf,t} = \left[\left(\frac{(\frac{^{176}\mathrm{Hf}}{^{177}\mathrm{Hf}})_{sample,t}}{(\frac{^{176}\mathrm{Hf}}{^{177}\mathrm{Hf}})_{CHUR,t}} \right) - 1 \right] \times 10^4$$

Positive $\varepsilon_{Hf,t}$ (often referred to as suprachondritic) indicates that the sample has higher ^{176}Hf/^{177}Hf values than CHUR at the time t, and is interpreted to derive from a depleted source. Negative $\varepsilon_{Hf,t}$ (subchondritic) on the other hand, indicate a derivation from an enriched source.

Calculating the $\varepsilon_{Hf,t}$ to the crystallization age of a measured zircon crystal gives the opportunity to compare the amount of radiogenic Hf with regards to a model of the depleted mantle, and evaluate if the magma source was separated

recently before crystallization or had experienced longer residence time. This can be done visually in a time vs $\varepsilon_{Hf,t}$ diagram, and compared to various evolution models (Figure 1.5). This thesis will compare measured results to the CHUR, with values after Bouvier et al. (2008), and Depleted Mantle Model, with values after Griffin et al. (2000).

When combining zircon crystallization ages and Hf-isotopic it is important to evaluate the U-Pb ages with care (Vervoort and Kemp 2016). The problem arise when discordance or internal complexities in the zircon grain is not resolved, which will shift the Hf-isotopic results and result in meaningless interpretations (Figure 1.5). The answer to this problem is to utilize CL imagery and careful spot placements, both when measuring U-Pb isotopes and Hf-isotopes, coupled with a concordance filter (Vervoort and Kemp 2016).

1.3.3. Model ages

Model ages differ from crystallization ages in rocks and minerals in that it utilizes an isotopic system to infer the time of separation from a modeled reservoir, instead of determining the last crystallization. In isotope geochemistry, the model age represents the time of magma separation from the mantle, or for mixed sources, the *average* time of separation (Arndt and Goldstein 1987).

To provide a time estimate for the separation of magma from the mantle source has the potential to provide insight regarding regional provenance and early Earth evolution (Bodet and Schärer 2000; Gehrels and Pecha 2014; Hawkesworth and Kemp 2006; Hawkesworth, Cawood, et al. 2017; Knudsen et al. 2001; Andersen et al. 2011; Bahlburg et al. 2009). The point of separation is often evaluated for the DMM

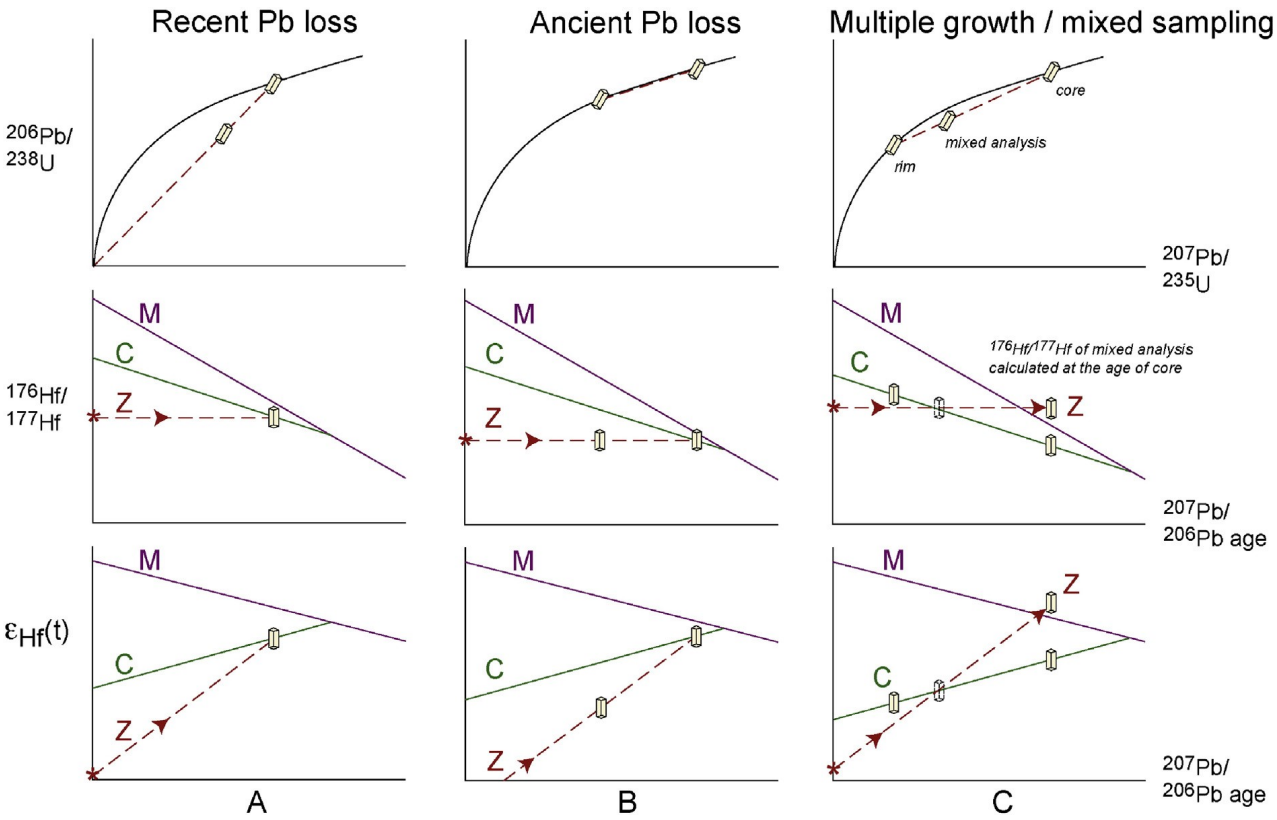

Figure 1.5.: Schematic representation of the effects of zircon age complexity on the calculation of initial $^{176}Hf/^{177}Hf$ and $\varepsilon_{Hf,t}$, showing generalized evolutionary trajectories for the mantle (M), crust (C) and zircon (Z). For the latter, the asterisk at the intersection with the y axis denotes the measured (i.e., present day) zircon Hf isotope composition, and the arrows hows the back calculation of this to the chosen U–Pb age. Three scenarios are shown, depicting (A) recent Pb loss, (B) ancient Pb loss, and (C) a simplified case of mixed sampling of a zircon core and rim of different age and Hf isotope composition, where the initial $^{176}Hf/^{177}Hf$ and $\varepsilon_{Hf,t}$ values are then erroneously calculated at the age of the core. From Vervoort and Kemp (2016).

$$T_{DMM} = \frac{1}{\lambda} \times \ln\left(\frac{(\frac{^{176}\mathrm{Hf}}{^{177}\mathrm{Hf}})_{sample} - (\frac{^{176}\mathrm{Hf}}{^{177}\mathrm{Hf}})_{DM}}{(\frac{^{176}\mathrm{Lu}}{^{177}\mathrm{Hf}})_{sample} - (\frac{^{176}\mathrm{Lu}}{^{177}\mathrm{Hf}})_{DM}} + 1\right) \tag{1.6}$$

, but can also be evaluated as T_{CHUR}, by substitution $^{176}\mathrm{Lu}/^{177}\mathrm{Hf}$ and $^{176}\mathrm{Hf}/^{177}\mathrm{Hf}$ values for CHUR instead of DM in equation 1.6.

1.4. Zircon

Zircon is a silicate mineral with the general chemical equation $ZrSiO_4$. The mineral forms tetragonal crystals that varies in length and breath according to physical and chemical conditions during growth (Mange and Maurer 1992). Zircon is a remarkably widespread in rocks of crustal origin, and is particularly ubiquitous in silicic and intermediate igneous rocks (Mange and Maurer 1992).

Zircon is one of the most stable minerals, resistant to both chemical and mechanical weathering and has a relatively high closing temperature with respect to diffusion of elements (Mange and Maurer 1992). Zircon also has a low solubility in silicic melts (Watson and Harrison 1983), which makes it possible to survive as refractory relics in granitic suits. The applicability of zircon in geochronology comes down to its crystal structure and elemental composition. Zrs very similar atomic radius to both U and Hf, coupled with a similar valency of +4, makes zircon highly agreeable for incorporation of these trace elements in the crystal lattice (Kinny and Maas 2003). Zi also has similar properties to Th and the light REEs, and incorporates these element as well. Pb has a significant larger atomic radius, and is therefore expelled in the formation of the zircon crystal. This means that when the migration-system of a zircon crystal closes, at approximately 900 °C, the crystal can be treated as a closed system with near to no daughter isotopes present. Zircon also discriminates against both Lu, which means that the Hf-isotope ratio of the magma source is preserved at crystallization, as shown by a study in detrital zircons by Knudsen et al. (2001). Of course this is not always the reality, but correction for initial Pb and high $^{176}Lu/^{177}Hf$ can be performed, as explained in the Methods chapter.

When preparing zircons for a isotope study, it is important to consider the complex internal growth structure of a zircon crystal . This can very often entail growth zones, core and rim structures or reveal metamictization and internal

fracturing. This is revealed by cathodoluminescense (CL) imagery of the grains, often performed in a Scanning Electron Microscope (SEM), prior to isotope measurements. CL imagery is performed by bombarding the sample with an high-energy electron beam, and recording the emission of photons (Egerton 2016). The patterns revealed reflects a complex function of composition, lattice structure and superimposed strain or damage on the material.

1.5. Apatite

Apatite is one of three naturally occurring phosphorous minerals. It has the general chemical formula $CaPO_5$[F,Cl,OH], where the anions F, Cl and OH represents three different apatite series. Regardless of the anion present, the structure and morphology is always the same.

Apatite is a common accessory mineral in many rock types, which incorporates a range of trace minerals and REEs. It is a low U-mineral, but with the use of instruments like LA-ICP-MS, there it is possible to measure U content with precision (Thomson et al. 2012; Chew et al. 2011; Chamberlain and Bowring 2000). Unlike the mineral zircon, which discriminates against incorporation of Pb in the crystal, apatite incorporates Pb well. That means that a robust common Pb-correction is needed for U-Pb age determination. But with increasing popularity in U-Pb apatite dating, several standards has been evolved so that the common Pb-correction can be performed with precision.

Low U-content and a high abundance of common Pb is still a challenge in U-Pb dating of apatites, but (Thomson et al. 2012) showed that by utilizing larger spot sizes for laser ablation, and performing a robust common Pb-correction, these challenges can be overcome.

Chamberlain and Bowring (2000) assessed the closure temperature for Pb-diffusion in apatites to the range 450-500 °C, which means that U-Pb ages from apatites from the same igneous rocks as U-Pb zircon ages should be similar or slightly older, or they may reveal low-temperature metamorphism that is not resolved in the zircon data.

2. Methods

2.1. Sample preparation

A small piece of each of the samples CH 2, RT 11 and RM 1 were cut off to keep as a reference, before the rest of the samples were weighted and sent to Geotrack International in Australia for heavy mineral separation and zircon extraction.

The following procedure for heavy mineral separation is provided by Geotrack International:

Samples are initially reduced in size using a jaw crusher, followed by a disc pulverizer, designed to disaggregate the rock, rather than crush the constituent mineral grains. Fine material is removed by hand washing (larger samples are processed over a separating table) and the resulting fine-sand sized material is dried in a low temperature oven (60°C).

Frantz Isodynamic Magnetic separators and heavy liquid mineral separations are then used to separate mineral grains by gravity and magnetic susceptibility. First the dry sample is run through a vertical Frantz Magnetic Separator, removing the ferromagnetic fraction of the sample. The non ferromagnetic fraction is then put in Tetrabromoethane (TBE - Specific Gravity = 2.95),

separating the material into two fractions: Light fraction $<$ 2.95 SG, consisting of mainly quartz and feldspar, and heavy fraction $>$ 2.95 SG. The heavy fraction is then run through horizontal Frantz magnetic separator configuration (25° slope, 10° angle and full scale separation). The magnetic fraction in this step is bagged and labeled as the Magnetic fraction, consisting of monazite, garnet, sphene etc. The non-magnetic fraction is the treated in another heavy liquid, Methyl Iodide (SG = 3.3). The light fraction of this separation (2.95 $<$ SG $<$ 3.3) is consistent of apatite, fluorite, carbonates, andalusite etc, and is bagged and labeled the Apatite fraction. The remaining heavy fraction (2.95 $<$ SG $<$3.3) fraction is put through a final Frantz magnetic separator, where the purest non-magnetic material at the configurations of 25° slope, 2° slope and full scale separation, is bagged and labeled Zircon Concentrate, consistent almost purely of zircons. The rest of the non-magnetic, heavy fraction, is labeled as the Zircon Fraction and consists of barite, rutile and darker (metamict) more magnetic zircons.

Zircons and apatites were both randomly selected and manually hand picked from the zircon concentrate and apatite fraction respectively, to ensure that all grain variations, with respect to grain size and morphology, were represented. The grains were cast in epoxy mounts, 2.5 cm in diameter, and polished to expose the interior of the grains. Cathodoluminescence (CL) images were taken of the zircons to map the grains and control spot placements for fractures, inclusions, growth structures and inherited cores. Secondary electron images were taken of the apatite fraction to identify the apatite grains within the fraction, and provide a grain map for the isotope analysis.

2.2. LA-ICP-MS

The Laser Ablation Inductively coupled Plasma Mass Spectrometer (LA-ICP-MS) is one of many instruments utilized in measuring isotopic compositions in geochronology. It is by far the most utilized method by number of publications (cite), and is shown to produce accurate and reproducible measurements of isotope composition in *in situ* grain analyses (Shaulis et al. 2010). It has the advantage over Thermal Ionization Mass Spectrometry (TIMS) that it can preform *in situ* measurements on single grains, thus conserving the grain for further analysis, compared to the need for dissolving the grain in acid which is a requirement for TIMS analysis. Similar in precision (Horn et al. 2000) the Sensitive High-Resolution Ion Microprobe (SHRIMP) offers higher spatial resolution (spot sizes from 5 to >30 µm) on *in situ* analysis, but consumes a lot more time per analysis. A comparison of the three different measurement methods can be seen in Table 2.1.

Shortly explained the LA-ICP-MS is divided in to parts: The laser ablation system which vaporizes the sample material and feeds it to the plasma. The plasma further disintegrate molecules into elements and ionizes them, before acceleration into the mass spectrometer which converts the ions to a quantifiable voltage. A more detailed explanation on the instruments utilized in this study follows:

The sample material is mounted in the air-tight sample chamber on a automated moving stage, beneath a high resolution camera and laser beam. The sample chamber is then purged with N_2-gas to get rid of all oxygen. This is an important step to prevent making UO and ThO molecules when the mineral is vaporized by the laser. Each grain should be examined for surface inclusions and internal structure (CL image) before deciding ablation spot. He-gas is utilized to flush the vaporized sample out of the sample chamber and carry it to the detector, with a constant flow of 500 ml/ min.

Table 2.1.: Charted strengths and weaknesses of the three methods of U-Pb dating. (Modified after Schaltegger et al. (2015))

	ID-TIMS	SIMS	LA-ICP-MS
Absolute age resolution (2σ)	U-Pb high to very high: $\leq 0.1\%$ precision and accuracy	U–Th and U–Pb ca. 1–2 %; very high ($\sim 10^3$ - 10^4 years) for U–Th dating <300 ka	U-Pb ca. 2% Th-Pb ca. 3%
Spatial resolution	Poor (mixing of age domains in single crystals hardly avoidable)	Excellent (sub-µm in depth profiling); quasi non-destructive	Good (20-30 µm laterally, single µm vertically, depending on analytical system)
Time requirement for sample preparation and analysis	Slow (digestion and chemical separation)	Fast (CL imagery, volumetric excavation rate ~ 0.1 µm^3/s/nA primary beam)	Very fast (CL imagery, volumetric excavation rate ~ 0.125 µm^3/pulse at 2.4 J cm^{-2} fluence)
Preferred geologic applicability	Volcanic and plutonic systems of any age	Young volcanic systems with volcanic and plutonic enclaves; metamorphic systems; microcrystal and in situ analysis	Detrital provenance studies, young volcanic and plutonic systems, metamorphic systems, *in situ* analysis

The laser used on this project is a Photon Machines Analyte.193 Excimer laser ablation system, operating with 193 nm wavelength, power setting of 3 J cm^{-2} and ablation time of 30 s (300 shots at 10 Hz). Spot sizes used were 24,6 µm circle for U-Pb measurements of zircons and 49,3 µm for U-Pb measurements on apatites and Lu-Hf isotopes in zircons.

After the sample is vaporized and carried from the sample chamber, it is introduced to the ICP-MS. For this thesis the Varian 810 ICP-MS is used for all U-Pb ratio measurements. The induction coupled plasma consists of three cylindrical quartz tubes, which separates the cooling gas flow, the Ar discharge gas and the flow of carrier gas . The electrode coil which creates a time varying magnetic field, provides the plasma generation and creates the plasma torch from the rarefied gas. Temperature and flux is calibrated for optimal ionization of the target elements.

The ionized sample beam is then focused through a series of skimmers and cones and passed into a vacuum. Further the beam passes through a ion-deflector, getting rid of all neutral and negatively charged ions, before going through a collision cell (filled with He gas), where interfering ions are neutralized.

Finally the sample passes through the four cylindrical metal rods, called the quadrupole mass analyzer. The rods are positioned parallel to each other, with each opposing pair having the same charge. This allows the sample beam to be separated based on the mass-to-charge ratio, before the target isotopes ends up in a detector and converted into a quantifiable signal, where voltage intensity equals amount of ions. The signal is recorded as a intensity vs time plot and stored for each sample-spot.

60 s of reading time is recorded for each shot, where the first ∼15 s are blank, providing a stable and consistent baseline for the extraction and quantification, followed by the 30 s sample ablation time and the last ∼15 s are left for the gas wash out and stabilizing of the detector. Because the carrier gas, Ar, contains trace amounts of Hg, and the isobaric interference between ^{204}Hg and ^{204}Pb, ^{202}Hg is also measured, so that the correct amount of ^{204}Pb can be used for common-Pb correction in the calculation. The measured isotopes are ^{238}U, ^{232}Th, ^{206}Pb, ^{207}Pb, ^{208}Pb, ^{204}Pb (mixed with ^{204}Hg) and ^{202}Hg.

For zircon U-Pb, the standards Plešovise and FC5z were measured before, during (between every 10 unknown) and after each analytical session. For apatite U-Pb, three apatite standards were utilized, called Madagascar, Yates and Bear (laboratory standards of known isotopic composition and age at the University of Houston).

2.3. MC-ICP-MS

Because of the isobaric interference between ^{176}Hf, ^{176}Lu and ^{176}Yb, a Multi Collector ICP-MS (MC-ICP-MS) is utilized to measure and quantify the Hf-isotope ratios. The MC-ICP-MS were used together with the Photon Machines Analyte.193 Excimer laser ablation system, for *in situ* measurements of the

Hf-isotope system on zircons with concordant U-Pb-ages. Concordance was defined to ±5% difference between $^{206}Pb/^{207}Pb$-age and $^{206}Pb/^{238}U$-age. The laser setup for Hf-isotope measurements were identical to U-Pb analysis, with a spot size of 49,3 µm. The measurements were performed on a NuPlasma II mass spectrometer equipped with 16 Faraday collectors and 5 Ion counters.

After laser ablation, the sample material is carried to the same kind of plasma torch, as for LA-ICP-MS, by Ar carrier gas. Ionization of elements takes place before the ion-beam is focused and accelerated into a magnetic separator, and collected by the Faraday collectors.

Hf-isotopic analyses were performed on ∼50 concordant zircons grains from each sample, on top of or as close to the U-Pb analytical spot as possible, according to internal structure and impurities visible on CL image or in reflected and transmitted light in the sample chamber view. 60 s reading time for each analysis, where 30 s was left blank to produce a stable baseline for data extraction and 30 second reading time during the sample ablation to record the sample signal. During analysis, the following Hf-isotopes were measured: ^{174}Hf, ^{176}Hf, ^{177}Hf, ^{178}Hf, ^{179}Hf and ^{180}Hf. In addition the isotopes: ^{171}Yb, ^{172}Yb, ^{173}Yb, ^{175}Lu, ^{181}Ta and ^{182}W, were measured to correct for isobaric interference and calculation of the $^{176}Lu/^{177}Hf$ ratio. Internal normalization and mass bias corrections were performed after Lapen et al. (2004), and performed automatically after sample measurement.

The standards Plešovise and FC5z were measured before, between unknowns and after for each analytical session, to control for instrumental drift.

2.4. Data reduction

The intensity vs time data for the U-Pb analysis were processed in IGOR Pro 6.12a with the Iolite 2.11 add-in software (Hellstrom et al. 2008) at the University of Houston. The software integrates the time signals and outputs isotope fractions. Further processing was done in Microsoft Excel, where the ^{202}Hg and the natural ratio of ^{202}Hg/^{204}Hg (Zadnik et al. 1989) used to correct the ^{204}Pb abundance so that further unradiogenic Pb could be corrected for in the samples . Time integrated correction was also conducted, related to the standards Plešovise described by Sláma et al. (2008), and FC5z (an equivalent of FC1) as described by Woodhead and Hergt (2005) for the zircons, and corrected to the Madagascar, Yates and Bear standards for the apatite data.

The U-Pb data was analyzed with Isoplot v4.15 after Ludwig (2008), and all propagation of errors were performed after (Ludwig 1998). Concordance is set to be percentage deviations of the calculated ^{206}Pb/^{238}U age to ^{207}Pb/^{206}Pb age of the same grain, and is referred to as discordance in this thesis. In this thesis, all grains with discordance $-5\% < sample < 5\%$ are considered concordant.

The ^{176}Hf/^{177}Hf value for the standard reference material was controlled to stay within measurement error, and did not drift during the analytical time.

3. Results

3.1. Grain description

The analyzed zircons from sample RT11 contained almost exclusively pink to purple colored grains in the grain size range of 50 to 400 µm. Grain shapes are dominantly euhedral, slightly elongated or cubical. CL imaging reveals mostly heterogeneous crystals with a fine lamination of growth zones, some crystals also show inherited cores (Figure 3.1). Fracturing and metamictization is not a major feature in this suite of grains.

CH2 revealed transparent to white and yellow colored zircons in the grain size range 20 to 200 µm, with a predominantly elongated habit. The grains vary from being euhedral to subhedral and with some grains being subrounded. CL imaging reveals both heterogeneous and homogeneous structures, showing either finely laminated growth zones or a uniform gray scale throughout the grain (Figure 3.2). Inherited cores, fractures and metamictization is rare in this suite of zircons.

Zircons from RM1 also ranges in coloring from transparent to white and yellow. Grain sizes ranges from 30 to 250 µm, on cubic to elongated, subrounded to rounded grains. CL imaging shows growth zoning with a high amount of metamictization and internal fracturing. Inherited cores with either a homogeneous

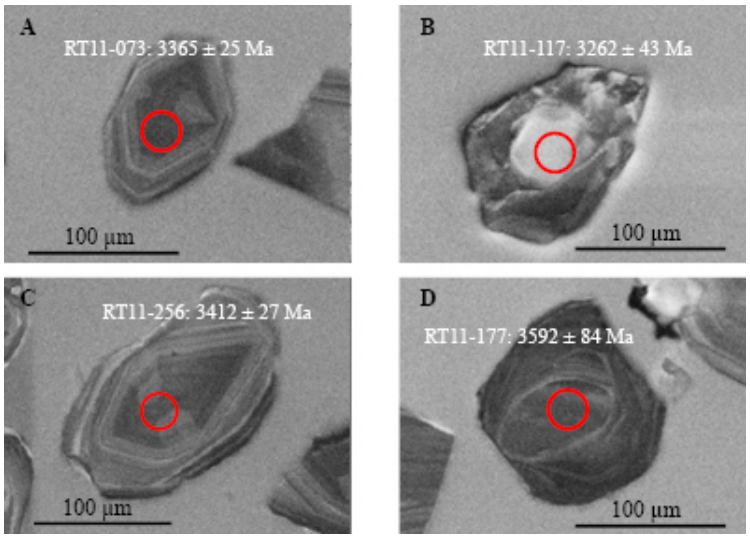

Figure 3.1.: CL images of four zircons from sample RT11. A and C showing euhedral zircons with growth zones. B, the youngest concordant zircon with some metamictization. D, zircon with inherited core, giving the oldest $^{207}Pb/^{206}Pb$ age of this sample. Red circles indicating placement of 25 μm analytical spot for U-Pb analysis.

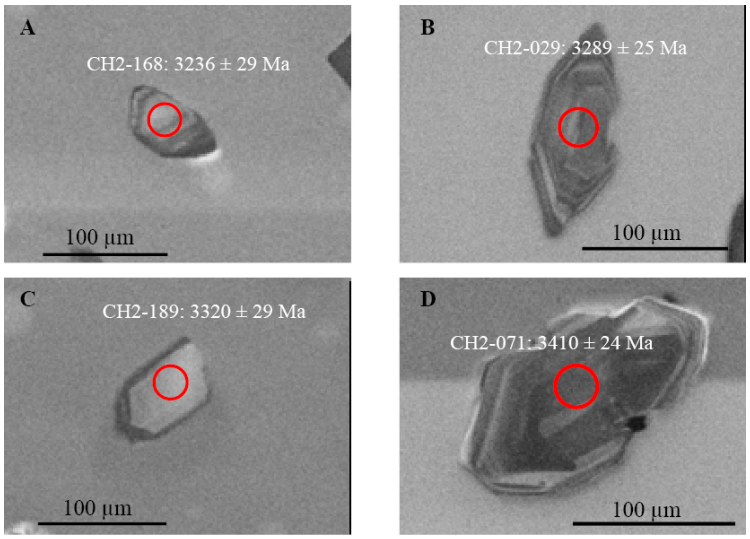

Figure 3.2.: CL images of four zircons from sample CH2. A, showing slightly subhedral zircon with growth zones. B, euhedral zircon with pronounced growth structure. C, broken zircon grain with homogeneous internal structure. D, example of large zircon grain with a chaotic core and laminated growth rim. Red circles indicating placement of 25 μm analytical spot for U-Pb analysis.

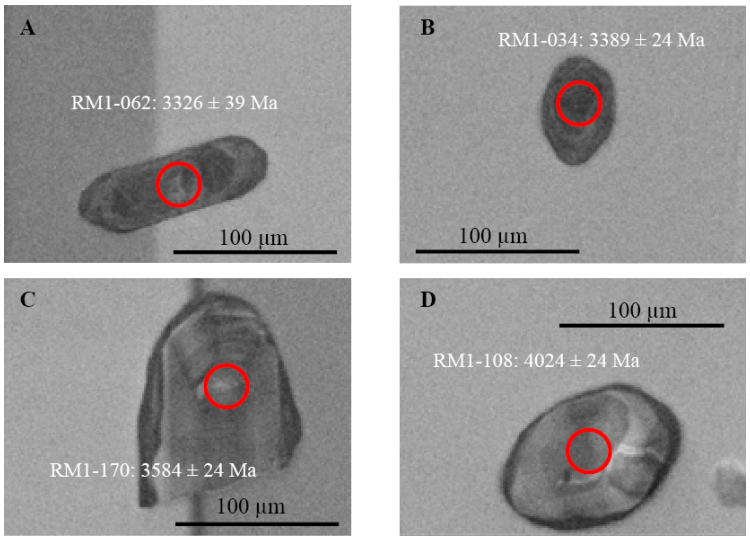

Figure 3.3.: CL images of four zircons from sample RM1. A, an elongated subhedral zircon with chaotic core and faint rim structure. B, subrounded zircon with faint growth zone structure. C, an elongated, but broken, zircon grain with faint growth zone structure and differentiated overgrowth. D, a rounded zircon grain, showing partly homogeneous and partly chaotic internal structure, producing the oldest concordant age measured in this thesis. Red circles indicating placement of 25 µm analytical spot for U-Pb analysis.

or chaotic interior is a common feature (Figure 3.3).

The suite of apatite grains measured for U-Pb geochronology in this thesis can be summarized in a joint description: Transparent to yellow grains with cubic to slightly elongated habit, with a roundness ranging from angular to rounded. Apatite grains size is quite uniform from all three samples, ranging from 75 to 200 µm. All CL images of the analyzed zircon grains and secondary electron maps of analyzed apatite grains is enclosed in Appendix A.

3.2. U-Pb ages

In total 880 zircon grains and 77 apatite grains and of three different samples from the Archean Singhbhum Craton were analyzed for U-Pb geochronology (307, 291 and 282 grains from RT11, CH2 and RM1 respectively), the full $^{207}Pb/^{206}Pb$ age and isotope ratio data set is presented in Appendix B. Initially 310 sample spots were measured for each sample, but some have been excluded on the basis of spot placement flaws (hitting inclusions etc.), measuring errors and/or low isotope count rates, producing extreme isotope ratio-errors.

The 307 analyzed grains from RT11 gives an upper intercept of 3384 ± 3.9 Ma, MSWD of 3.3, and a lower intercept at 909 ± 75 Ma in a concordia plot (Figure 3.4). 85 % of the grains from RT11 gives concordant $^{207}Pb/^{206}Pb$ ages with a continuous spread from 3262 ± 43 Ma to 3432 ± 29 Ma, with one older zircon, RT11-177, with an age of 3592 ± 84 Ma (uncertainties are given at the 2σ level), the distribution is presented in Figure 3.5. The mean $^{207}Pb/^{206}Pb$ age is 3379.7 ± 2.4 Ma, within uncertainty of the upper intercept of the concordia plot. The grain RT11-177 is a cubical, subangular, zircon crystal with the concordant analytical $^{207}Pb/^{206}Pb$ age of 3592 ± 84 Ma measured in an inherited core. The core has as an elongated and rounded structure, with a clear boundary, in the middle of the zircon grain (Figure 3.1D).

Out of 291 analyzed zircon grains in the sample CH2. Plotting 250 randomly selected data points in a concordia diagram, gives an calculated upper intercept of 3308.4 ± 7.6 Ma and lower intercept 573 ± 45 Ma (Figure 3.6), with MSWD = 15. The data forms a clear regression band from the upper to the lower intercept, but the high MSWD indicates that lead loss has happened in several smaller steps. 61 % data points are concordant, with $^{207}Pb/^{206}Pb$ ages ranging from 3232 ± 27 Ma to 3418 ± 25 Ma. The distribution is normally distributed around 3290 Ma, with an older, flat shoulder extending from 3360 to 3420 Ma (Figure 3.7).

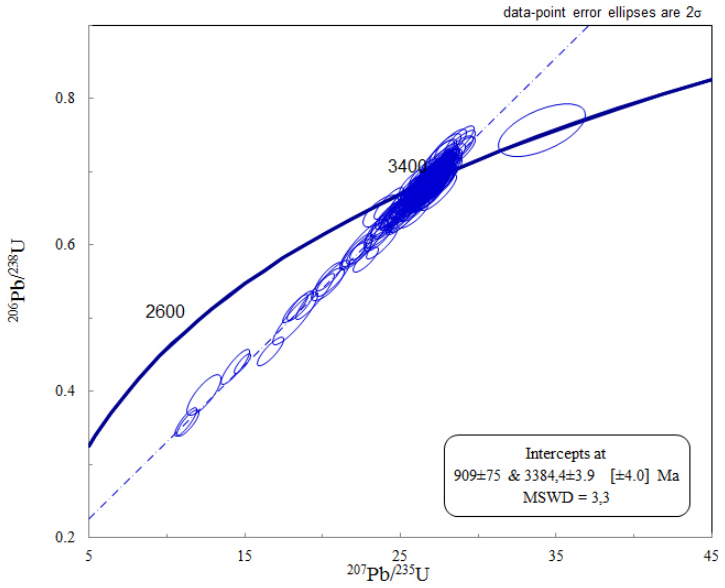

Figure 3.4.: Concordia plot showing the U-Pb data from sample RT11, blue ellipses representing data points with 2σ error, thick blue line is concordia curve. Upper intercept at 3384.4 ± 3.4 Ma with a lower intercept at 909 ± 75 Ma, MSWD $= 3.3$

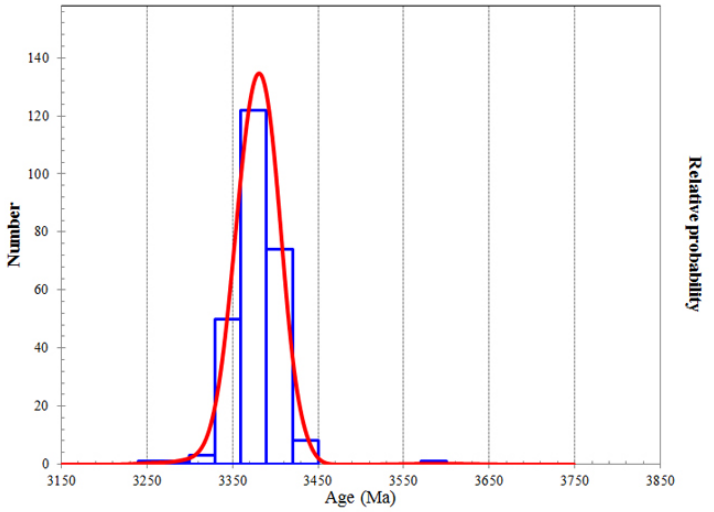

Figure 3.5.: Red line showing relative probability plot of the data points in sample RT11, showing a normal distribution around 3380 Ma, with one outlier at 3.6 Ga. Blue boxes plots number of zircons within the specified range.

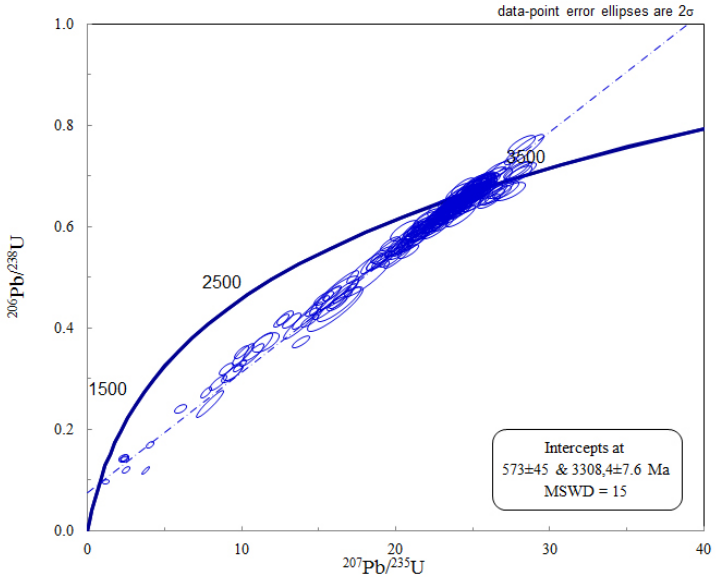

Figure 3.6.: Concordia plot showing the U-Pb data from sample CH2, blue ellipses representing data points with 2σ error, thick blue line is concordia curve. Upper intercept at 3308.4 ± 7.6 Ma with a lower intercept at 573 ± 45 Ma, MSWD $= 15$

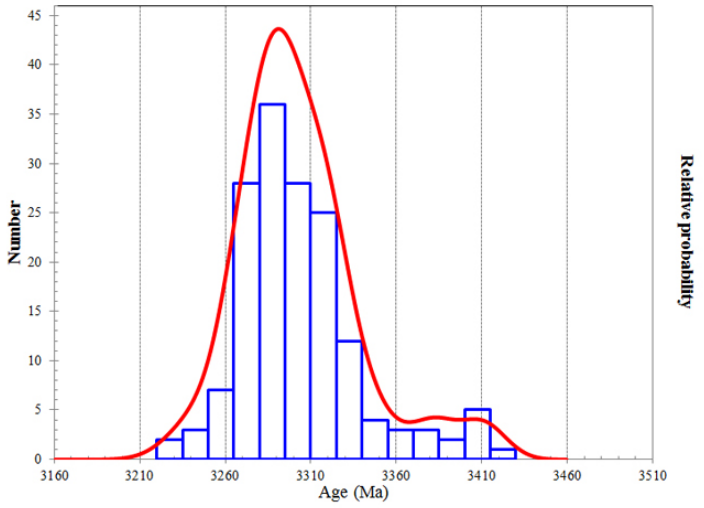

Figure 3.7.: Red line showing relative probability plot of the concordant $^{207}Pb/^{206}Pb$ ages in sample CH2, showing a normal distribution around 3290 Ma, with a right shoulder. Blue boxes plots number of zircons within the specified range.

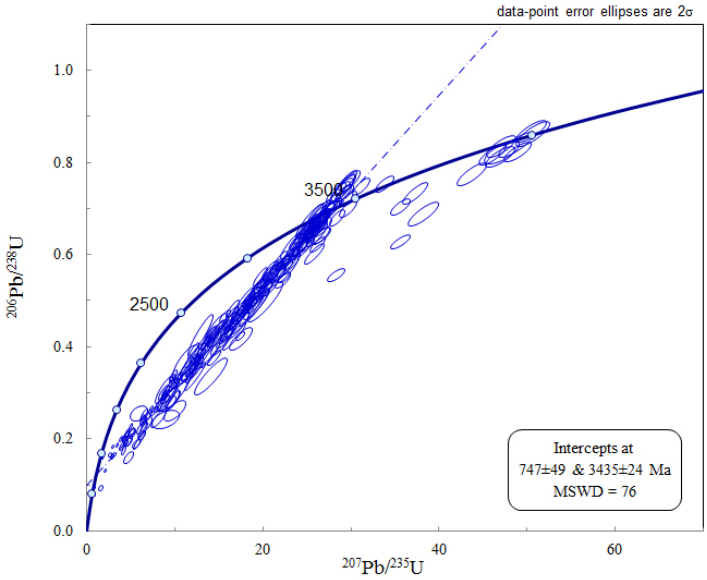

Figure 3.8.: Concordia plot showing the U-Pb data from sample RM1, blue ellipses representing data points with 2σ error, thick blue line is concordia curve.

The sample RM1 produced 282 data points, where 250 randomly selected points were plotted against the concordia line in Figure 3.8. At least two different populations can be observed in the data set, one major component plotting close the the mean calculated regression line, and one older component plotting further to the right. When observing the probability-density plot (Figure 3.9), two clear peaks is visible. One major component with a mean of 3380 ± 11 Ma, possibly mixed with a very small component at 3.6 Ga (represented by one concordant grain of 3584 ± 24 Ma), and a minor, but completely separate, component with a mean age of 3969 ± 30 Ma.

Extracting the data points that makes up the visible older population from the concordia and probability-density plots, and re plotting separately, two sets of upper and lower intercepts can be extracted from the data (Figure 3.10). The major zircon component now plots with an upper and lower intercept of 3396 ± 14 and 715 ± 28 Ma respectively, and the minor component regresses to 3974 ± 58 Ma upper and 1188 ± 570 Ma lower intercepts, separating the two

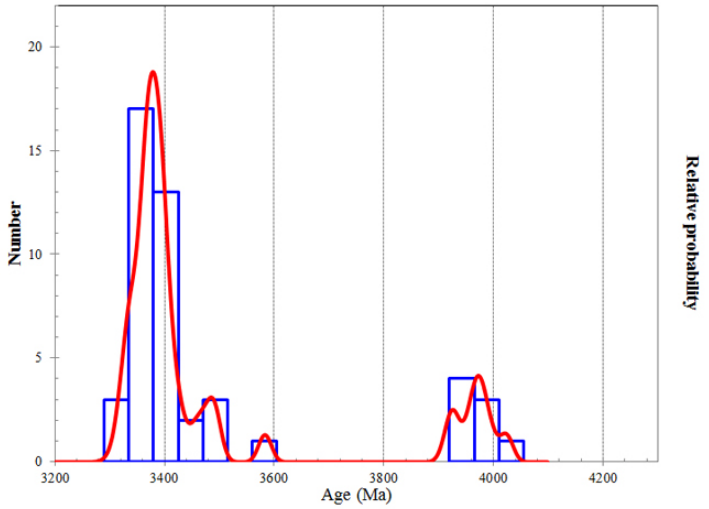

Figure 3.9.: Red line showing relative probability plot of the concordant $^{207}Pb/^{206}Pb$ ages in sample RM1. Blue boxes plots number of zircons within the specified range. Two separate populations are observed in the distribution, with one major peak at 3380 Ma, with a tail to the right, and one smaller peak at 3975 Ma.

populations with approximately 600 My. RM1 was the sample providing the least amount of concordant results, at only 17 %.

Similar to sample RT11, one grain, RM1-170, from sample RM1 gives a concordant $^{207}Pb/^{206}Pb$ age close to 3.6 Ga. Eight grains gives concordant $^{207}Pb/^{206}Pb$ ages close to 4.0 Ga, these are: RM1-038 at 3922±27 Ma, RM1-153 at 3927±25 Ma, RM1-129 at 3961±36 Ma, RM1-237 at 3961±28 Ma, RM1-169 at 3974±25 Ma, RM1-135 at 3977 ± 27 Ma, RM1-140 at 3994 ± 27 Ma and RM1-108 at 4024 ± 24 Ma, all within 4 % of the designated concordia criteria.

The apatites from sample RT11 and CH2 all produced radiogenic measurements, and only one grain was excluded on the basis of measurement error from sample CH2. Of the 32 measurements from RM1, only 14 spots gave analyzable data. $^{207}Pb/^{206}Pb$ ages from RT11 ranges from 3273±36 to 3498±66 Ma (concordance from 3.4 to -9.2 %) with a weighted mean of 3345 ± 10 Ma. Because near all

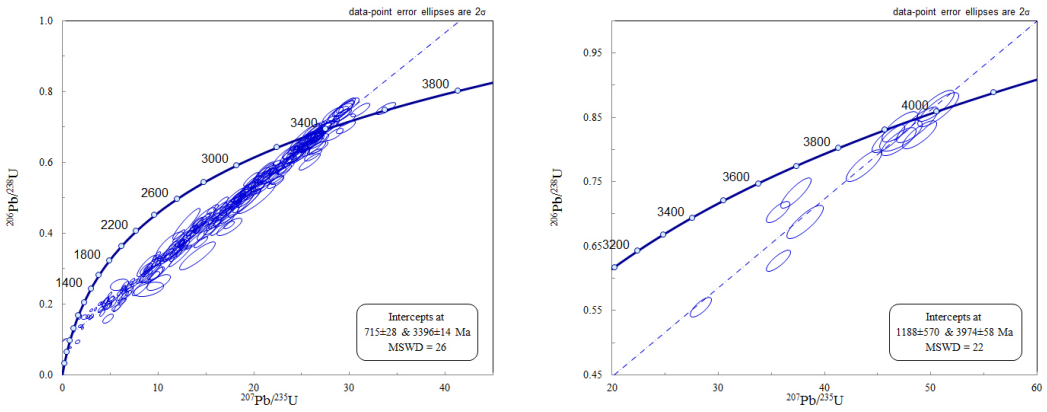

Figure 3.10.: Concordia plot showing the U-Pb data from sample RM1, split into the two components. Blue ellipses representing data points with 2σ error, thick blue line is concordia curve. The major age component constituting the youngest ages in the sample are plotted to the left, the minor, and older, component is plotted to the right.

data points exhibit negative concordance, most data points plots above the concordia curve (Figure 3.11), but it is possible to calculate an upper intercept of 3323 ± 22 Ma.

$^{207}Pb/^{206}Pb$ ages from the apatites of CH2 ranges from 3178 ± 72 to 3495 ± 66 Ma (with concordance from 25.8 to -9.2 %) with a weighted mean age of 3359 ± 16 Ma. Like RT11, most data points from CH2 apatites plots above the concordia curve (Figure 3.11). Regressing the data, produces an upper intercept age of 3349 ± 26 Ma.

The measured $^{207}Pb/^{206}Pb$ ages from the RM1 apatites ranges from 3322 ± 35 to 3647 ± 66 Ma (concordance ranges from -2.2 to -11.3 %) and a weighted mean age of 3395 ± 34 Ma. Plotting the 14 data points in a concordia diagram a regression line hitting a lower and upper intercept is not possible, because of the clustering of negative concordant data points above the concordia curve (Figure 3.12). A good approximation is to anchor the lower intercept to the one calculated for the zircon population of the same sample, and since two populations are identified in RM1, the lower intercept of the major fraction is

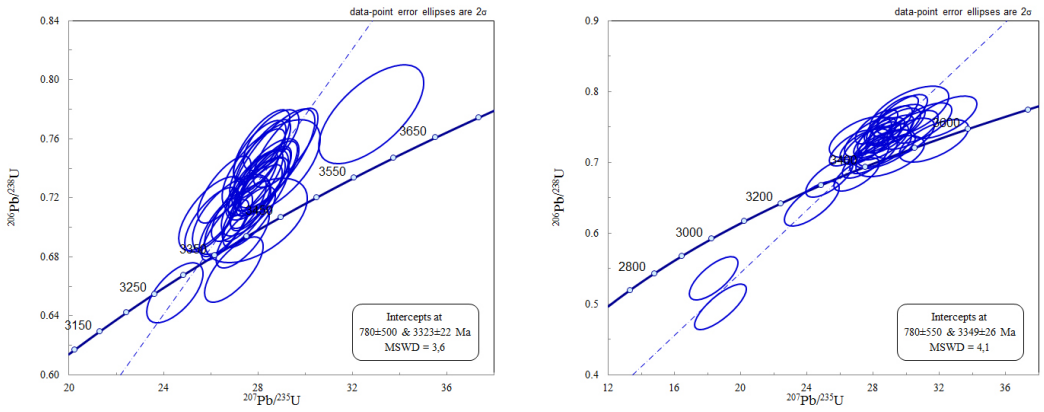

Figure 3.11.: Concordia plot of U-Pb data from the apatite grains from RT11 to the left and CH2 to the right. Blue circles represent data points with 2σ error, thick blue line is the concordia curve. The U-Pb data from the RT11 plots mostly above the concordia curve, but an upper intercept of 3323 ± 22 Ma is possible to calculate. The U-Pb apatite data from CH2 plots in a similar fashion above the concordia curve, with an upper intercept of 3349 ± 26 Ma.

chosen. Upper intercept for the apatites of RM1 is then calculated from the concordia regression to 3384 ± 44 Ma.

3.3. Hf-isotopes

The Hf composition of all analyzed concordant zircons from the three samples are presented in Appendix C. RT11 yielded zircons with initial $^{176}Hf/^{177}Hf$ values ranging from 0.28034 ± 0.00019 to 0.28067 ± 0.00015 translating into $\varepsilon_{Hf,t}$ values of -9.7 ± 4 to 1.2 ± 3.6 from 33 individual zircons. All values are either chondritic ($\varepsilon_{Hf,t} = 0$) or subchondritic ($\varepsilon_{Hf,t} < 0$), within analytical error, and is vertically distributed at the upper intercept age from the U-Pb concordia (Figure 3.4, under the curve representing depleted mantle evolution in a ε_{Hf} vs. $^{207}Hf/^{206}Pb$ age plot (Figure 3.13). 29 zircon grains has $\varepsilon_{Hf,t}$ values evenly distributed between 2 to -5 while three are less radiogenic with

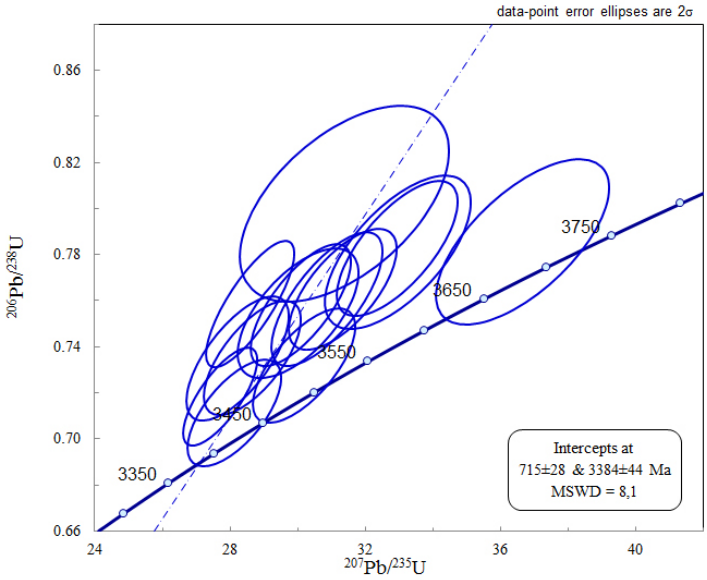

Figure 3.12.: Concordia plot of U-Pb data from the apatite grains from RM1. Blue circles represent data points with 2σ error, thick blue line is the concordia curve. The regression line is anchored to 715 Ma after the lower intercept calculated for the major zircon fraction of RM1, making it possible to deduce an upper intercept for this dataset.

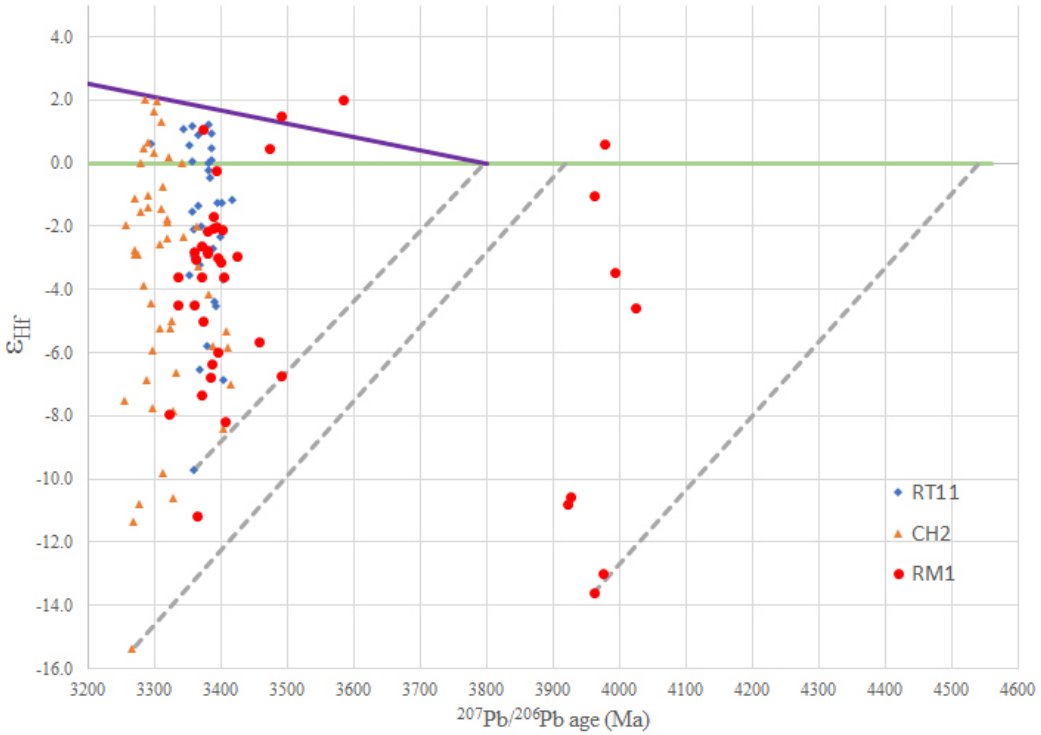

Figure 3.13.: ε_{Hf} vs. $^{207}Pb/^{206}Pb$ age plot the samples RT11 as blue diamonds, CH2 as orange triangles and RM1 as red circles. Purple line represents the Depleted Mantle evolution curve, the green line represents CHUR evolution. Stippled gray lines represents evolution trajectories for the grain with the lowest $\varepsilon_{Hf,t}$ value for each sample based on measured $^{176}Lu/^{177}Hf$ value. The intersection with the Depleted Mantle evolution curve (< 3800 Ma) represent separation from a depleted mantle reservoir, and similarly for intersection with the CHUR (> 3800 Ma) represents separation from a undifferentiated reservoir.

$\varepsilon_{Hf,t}$ from -5.8 to -9.7.

Initial $^{176}Hf/^{177}Hf$ for CH2 ranges from 0.28024 ± 0.00023 to 0.28072 ± 0.00013 translating to $\varepsilon_{Hf,t}$ values from -15.4 ± 6.3 to 2.0 ± 7.2 for 49 individual zircons. The $\varepsilon_{Hf,t}$ values ranges from suprachondritic to subchondritic within analytical error, but the errors produced are relatively high for this study. Arithmetic mean of σ for all $\varepsilon_{Hf,t}$ values are 4.6, ranging from 2.1 to 8.7. 24 grains has $\sigma < 4.0$ and these ranges from $\varepsilon_{Hf,t}$ 2.0 to -7.8. The no grouping of data points

are observed in this sample (Figure 3.13).

Sample RM1 has two clearly separated age groupings, as presented in the previous section, these will be presented separately. 41 concordant zircons were analyzed for Hf-isotopes, where 33 zircons are from the major age population around 3.4 Ga, and eight zircons with an age close to 4.0 Ga. The younger population yielded initial $^{176}Hf/^{177}Hf$ values from 0.28029 ± 0.00010 to 0.28063 ± 0.00012, with $\varepsilon_{Hf,t}$ from -11.2 ± 2.4 to 2.0 ± 3.4. This population yields similar, slightly, suprachondritic to subchondritic values as the previous two samples (Figure 3.13). The second group, of older zircons, yields four chondritic to subchondritic values; 0.28003 ± 0.00011, 0.28009 ± 0.00012, 0.28018 ± 0.00015 and 0.280021 ± 0.00011 and four, near unradiogenic, subchondritic values of 0.27982 ± 0.00014, 0.27983 ± 0.00014, 0.27993 ± 0.00011 and 0.27993 ± 0.00014. The first group gives the $\varepsilon_{Hf,t}$ values -4.6 ± 2.5, $-3,4 \pm 2.7$, -1.0 ± 3.4 and 0.6 ± 2.5 respectively. The second group produces the $\varepsilon_{Hf,t}$ values -13.6 ± 3.1, -13.0 ± 3.1, -10.8 ± 2.7 and -10.6 ± 2.9, in the order listed above.

4. Discussion

The time of crystallization of the three TTG samples studied has been evaluated by *in situ* U-Pb isotope dating on zircon crystals extracted from the samples. The sample RT11 is dated to 3384.4 ± 3.9 Ma, CH2 to 3308.4 ± 7.6 Ma and RM1 has been determined to 3396 ± 14 Ma. The interpreted ages comes from the upper intercept calculated for the suite of concordant and discordant zircons plotted in Figure 3.4, 3.6 and 3.8.

The interpreted ages are supported by the apatite U-Pb ages, rendering slightly younger to time equivalent ages within uncertainty. RT11 yields an apatite U-Pb age of 3323 ± 22 Ma, a slightly younger age than the zircon U-Pb age. This fits with the lower closure temperature for apatites, and indicates a slow cooling process.

CH2 yields an apatite U-Pb age of 3349 ± 26 Ma, which is slightly higher than its zircon U-Pb age, but this can be explained by equilibrating processes and the readily acceptability of Pb in the apatite crystal. Where a magma resides isolated for a long period before crystallization, the radiogenic Pb produced during this time will be discriminated from the zircon, but can be incorporated in the apatite crystal, and thus elevate the radiogenic Pb and produce seemingly older ages. It is then probable that the apatite U-Pb age reflects a prolonged isolation of the magma suite, and the U-Pb age will represent the true timing of crystallization.

The apatite U-Pb age of 3384 ± 44 Ma is identical, within uncertainty, of the zircon U-Pb age, which indicates a more rapid cooling process than for the time equivalent RT11.

The zircon and apatite U-Pb data coupled with Hf-isotopic measurements indicates two time equivalent crustal generation events in sample RT11 and RM1, but with different provenance. CH2 represents a ∼100 My younger crustal generation, with a similar provenance to RT11.

The Hf-isotope data indicates a juvenile component mixed with one or more older components for all three samples. This interpretation is based on the uniform vertical spread in $\varepsilon_{Hf,t}$ values for all samples. RT11 and RM1 both shows one inherited zircon grain (core in RT11) of 3.6 Ga which is time equivalent with the oldest granitoide rocks in the neighboring Bastar Craton (Rajesh et al. 2009), but does not have an equivalent found in the Singhbhum Craton. CH2 exhibits quite negative $\varepsilon_{Hf,t}$ values, but due to high uncertainty the data does not allow for interpretation of any major unradiogenic component.

Interestingly, RM1, contained a small suite of ∼4.0 Ga zircons, with two distinct groups of Hf-isotope values. One group of chondritic zircons indicate a juvenile separation event around 4.0 Ga from CHUR, and one subchondritic group with close to the Solar System origin $^{176}Hf/^{177}Hf$ value.

For RT11 and CH2, Hf-model ages can be calculated against the Depleted Mantle Model, and generates T_{DMM} of up to 3.8 Ga which is consistent with the model. The eight zircons of 4.0 Ga however, indicates separation prior to what is modeled by the DMM, and therefore must derive from a chondritic reservoir or an enriched reservoir must have existed prior to 3.8 Ga.

Evaluating T_{CHUR} ages for the four subchondritic zircons with a crystallization age of ∼4.0 Ga, using the measured $^{176}Lu/^{177}Hf$, indicates separation from CHUR at ∼4.5 Ga. However, this implies that the crystallization at ∼4.0

Ga took place from a highly enriched source with similar $^{176}Lu/^{177}Hf$ as the zircon. Calculating the model age, with an assumed source $^{176}Lu/^{177}Hf$ ratio of Chaudhuri et al. (2018) (calculated from samples of the same location), gives model ages older than the formation of the Solar System! Thus implying that there had to exist an enriched reservoir as a source to these zircon grains at the formation of the Earth.

5. Conclusion

This thesis has performed U-Pb analysis of zircons and apatites from three TTG samples from the Singhbhum Craton of east India, and produced crystallization ages for the Singhbhum Granites of 3384.4 ± 3.9 Ma for RT11 and 3308.4 ± 7.6 Ma for CH2 and the OMGT of 3396 ± 14 Ma form sample RM1. Hf-isotope analysis reveals a mostly juvenile magma component for the two samples RT11 and CH2, but reworking of at least one 3.6 Ga component for RT11. RM1 reveals a much more complex provenance, with a similar juvenile component and reworking of a lesser 3.6 Ga source. RM1 also exhibit inherited zircons of $\sim$4.0 Ga xenocrysts with four out of eight inhabiting a juvenile $>$ 4.0 Ga component of CHUR separation, and four zircons exhibiting unradiogenic $^{176}Hf/^{177}Hf$ values, which indicates the existence of an enriched reservoir already depleted in Lu at the formation of the planet.

These results affirms that the Singhbhum Craton was the home for early crustal processes, which pushes back the timing of crustal differentiation from what is known today. The Singhbhum Craton contains important clues to the early history of the Earth, and will be an important provider of information for the continued exploration of the earliest geological processes.

5.1. Continued research

To further validate the findings of this thesis, the author would suggest further isotopic analyzes on the rocks studied here. Additional zircon U-Pb data, coupled with Hf-isotopic analyzes could confirm and expand upon the results gathered here, with the objective to further resolve the complex provenance of the rocks. Several isotopic investigations, like Sm-Nd and δ^{18}O, could be performed to either support or expand the preliminary findings of this thesis.

Bibliography

Andersen, T., Saeed, A., Gabrielsen, R. H., and Olaussen, S. (2011). Provenance characteristics of the Brumunddal sandstone in the Oslo Rift derived from U-Pb, Lu-Hf and trace element analyses of detrital zircons by laser ablation ICMPS. *Norwegian Journal of Geology* 91, 1–18.

Arndt, N. T. and Goldstein, S. L. (1987). Use and abuse of crust-formation ages. *Geology* 15(10), 893–895.

Bahlburg, H., Vervoort, J. D., Du Frane, S. A., Bock, B., Augustsson, C., and Reimann, C. (2009). Timing of crust formation and recycling in accretionary orogens: Insights learned from the western margin of South America. *Earth-Science Reviews* 97(1), 215–241. DOI: 10.1016/j.earscirev.2009.10.006.

Bodet, F. and Schärer, U. (2000). Evolution of the SE-Asian continent from U-Pb and Hf isotopes in single grains of zircon and baddeleyite from large rivers. *Geochimica et Cosmochimica Acta* 64(12), 2067–2091. DOI: 10.1016/S0016-7037(00)00352-5.

Bouvier, A., Vervoort, J. D., and Patchett, P. J. (2008). The Lu–Hf and Sm–Nd isotopic composition of CHUR: Constraints from unequilibrated chondrites and implications for the bulk composition of terrestrial planets. *Earth and Planetary Science Letters* 273(1), 48–57. DOI: 10.1016/j.epsl.2008.06.010.

Brown, M. and Rushmer, T. (2006). Evolution and Differentiation of the Continental Crust. Ed. by M. Brown and T. Rushmer. Cambrigde: Cambridge University Press, 553.

Chamberlain, K. R. and Bowring, S. A. (2000). Apatite-feldspar U-Pb thermochronometer: A reliable, mid-range (450°C), diffusion-controlled system. *Chemical Geology* 172, 173–200. DOI: 10.1016/S0009-2541(00)00242-4.

Chaudhuri, T., Wan, Y., Mazumder, R., Ma, M., and Liu, D. (2018). Evidence of Enriched, Hadean Mantle Reservoir from 4.2-4.0 Ga zircon xenocrysts from Paleoarchean TTGs of the Singhbhum Craton, Eastern India. *Scientific Reports* 8, 1–12. DOI: 10.1038/s41598-018-25494-6.

Chew, D. M., Sylvester, P. J., and Tubrett, M. N. (2011). U-Pb and Th-Pb dating of apatite by LA-ICPMS. *Chemical Geology* 280, 200–216. DOI: 10.1016/j.chemgeo.2010.11.010.

Davis, D. W., Krogh, T. E., and Williams, I. S. (2003). Historical Development of Zircon Geochronology. *Reviews in Mineralogy and Geochemistry* 53(1), 145–181. DOI: 10.2113/0530145.

Dickin, A. P. (2005). Radiogenic isotope geology. Vol. 2nd Editio. Cambridge University Press, 509.

Egerton, R. F. (2016). Physical principles of electron microscopy: An introduction to TEM, SEM, and AEM, second edition. Springer, 196. DOI: 10.1007/978-3-319-39877-8.

Gehrels, G. and Pecha, M. (2014). Detrital zircon U-Pb geochronology and Hf isotope geochemistry of Paleozoic and Triassic passive margin strata of western North America. *Geosphere* 10(1), 49–65.

Griffin, W. L., Pearson, N. J., Belousova, E., Jackson, S. E., Achterbergh, E. van, O'Reilly, S. Y., and Shee, S. R. (2000). The Hf isotope composition of cratonic mantle: LAM-MC-ICPMS analysis of zircon megacrysts in kimberlites. *Geochimica et Cosmochimica Acta* 64(1), 133–147. DOI: 10.1016/S0016-7037(99)00343-9.

Hastie, A. R., Fitton, J. G., Bromiley, G. D., Butler, I. B., and Odling, N. W. (2016). The origin of Earth's first continents and the onset of plate tectonics. *Geology* 44(10), 855858. DOI: 10.1130/G38226.1.

Hawkesworth, C. J. and Kemp, A. I. S. (2006). Evolution of the continental crust. *Nature* 226, 144–162. DOI: 10.1038/nature05191.

Hawkesworth, C. J., Cawood, P. A., Dhuime, B., and Kemp, T. I. (2017). Earth's Continental Lithosphere Through Time. *Annual Review of Earth and Planetary Sciences* 45, 169–198. DOI: 10.1146/annurev-earth-063016-020525.

Hellstrom, J., Paton, C., Woodhead, J., and Hergt, J. (2008). Iolite: Software for spatially resolved LA-(QUAD and MC) ICPMS analysis. *Laser ablation ICP-MS in the Earth Sciences: current practices and outstanding issues*. Vancouver: Mineralogical Association of Canada, 343–348.

Horn, I., Rudnick, R. L., and McDonough, W. F. (2000). Precise elemental and isotope ratio determination by simultaneous solution nebulization and laser ablation-ICP-MS: Application to U-Pb geochronology. *Chemical Geology* 164, 281–301. DOI: 10.1016/S0009-2541(99)00168-0.

Jaffey, A. H., Flynn, K. F., Glendenin, L. E., Bentley, W. C. t., and Essling, A. M. (1971). Precision measurement of half-lives and specific activities of U 235 and U 238. *Physical Review C* 4(5), 1889–1906.

Johnson, T. E., Brown, M., Gardiner, N. J., Kirkland, C. L., and Smithies, R. H. (2017). Earth's first stable continents did not form by subduction. *Nature* 543(7644). DOI: 10.1038/nature21383.

Kinny, P. D. and Maas, R. (2003). Lu–Hf and Sm–Nd isotope systems in zircon. *Reviews in Mineralogy and Geochemistry* 53(1), 327–341.

Knudsen, T. L., Griffin, W., Hartz, E., Andresen, A., and Jackson, S. (2001). In-situ hafnium and lead isotope analyses of detrital zircons from the Devonian sedimentary basin of NE Greenland: a record of repeated crustal reworking. *Contributions to mineralogy and petrology* 141(1), 83–94. DOI: 10.1007/s004100000220.

Lapen, T. J., Mahlen, N. J., Johnson, C. M., and Beard, B. L. (2004). High precision Lu and Hf isotope analyses of both spiked and unspiked samples: a new approach. *Geochemistry, Geophysics, Geosystems* 5(1), 1–17.

Ludwig, K. R. (1998). On the Treatment of Concordant Uranium-Lead Ages. *Geochimica et Cosmochimica Acta* 62(4), 665–676. DOI: 10.1016/S0016-7037(98)00059-3.

Ludwig, K. R. (2008). User ' s Manual for Isoplot 3.70. A Geochronological Toolkit for Microsoft Excel. *Berkeley Geochronology Center Special Publication No. 4*.

Mange, M. A. and Maurer, H. F. W. (1992). Heavy Minerals in Colour. London: Chapman & Hall, 147.

Mattinson, J. M. (2010). Analysis of the relative decay constants of235U and238U by multi-step CA-TIMS measurements of closed-system natural zircon samples. *Chemical Geology* 275, 186–198. DOI: 10.1016/j.chemgeo.2010.05.007.

Mishra, S., Deomurari, M. P., Wiedenbeck, M., Goswami, J. N., Ray, S., and Saha, A. K. (1999). 207Pb/206Pb zircon ages and the evolution of the Singhbhum Craton, eastern India: An ion microprobe study. *Precambrian Research* 93(2-3), 139–151. DOI: 10.1016/S0301-9268(98)00085-0.

Mukhopadhyay, D. (2001). The Archaean Nucleus of Singhbhum: The Present State of Knowledge. *Gondwana Research* 4(3), 307–318. DOI: 10.1016/S1342-937X(05)70331-2.

Mukhopadhyay, J., Beukes, N. J., Armstrong, R. A., Zimmermann, U., Ghosh, G., and Medda, R. A. (2008). Dating the oldest greenstone in India: a 3.51-Ga precise U-Pb SHRIMP zircon age for dacitic lava of the southern Iron Ore Group, Singhbhum craton. *The Journal of Geology* 116(5), 449–461.

Rajesh, H., Mukhopadhyay, J., Beukes, N., Gutzmer, J., Belyanin, G., and Armstrong, R. (2009). Evidence for an early Archaean granite from Bastar craton, India. *Journal of the Geological Society*. DOI: 10.1144/0016-76492008-089.

Ramakrishnan, M. and Vaidyanadhan, R. (2008). Geology of India (Volume 1). Vol. 1. Bangalore: GSI Publications, 556.

Rollinson, H. (2007). Early Earth systems: a geochemical approach. 1st ed. Oxford, Malden, Carlton: Blackwell Publishing, 285.

Schaltegger, U., Schmitt, A. K., and Horstwood, M. S. (2015). U-Th-Pb zircon geochronology by ID-TIMS, SIMS, and laser ablation ICP-MS: Recipes, interpretations, and opportunities. *Chemical Geology* 402, 89–110. DOI: 10.1016/j.chemgeo.2015.02.028.

Scherer, E., Münker, C., and Mezger, K. (2001). Calibration of the lutetium-hafnium clock. *Science* 293(5530), 683–687.

Schoene, B. (2014). 4.10 - U–Th–Pb Geochronology. *Treatise on Geochemistry (Second Edition)*. Ed. by K. K. Turekian. Oxford: Elsevier, 341–378. DOI: 10.1016/B978-0-08-095975-7.00310-7.

Schoene, B., Crowley, J. L., Condon, D. J., Schmitz, M. D., and Bowring, S. A. (2006). Reassessing the uranium decay constants for geochronology using ID-TIMS U-Pb data. *Geochimica et Cosmochimica Acta* 70, 426–445. DOI: 10.1016/j.gca.2005.09.007.

Shaulis, B., Lapen, T. J., and Toms, A. (2010). Signal linearity of an extended range pulse counting detector: Applications to accurate and precise U-Pb dating of zircon by laser ablation quadrupole ICP-MS. *Geochemistry, Geophysics, Geosystems* 11(11).

Sláma, J., Košler, J., Condon, D. J., Crowley, J. L., Gerdes, A., Hanchar, J. M., Horstwood, M. S. A., Morris, G. A., Nasdala, L., and Norberg, N. (2008). Plešovice zircon—a new natural reference material for U–Pb and Hf isotopic microanalysis. *Chemical Geology* 249(1), 1–35.

Steiger, R. H. and Jäger, E. (1977). Subcommission on geochronology: Convention on the use of decay constants in geo- and cosmochronology. *Earth and Planetary Science Letters* 36(3), 359–362. DOI: 10.1016/0012-821X(77)90060-7.

Tait, J., Zimmermann, U., Miyazaki, T., Presnyakov, S., Chang, Q., Mukhopadhyay, J., and Sergeev, S. (2011). Possible juvenile Palaeoarchaean TTG magmatism in eastern India and its constraints for the evolution of the Singhbhum craton. *Geol. Mag.* 148(2), 340–347. DOI: 10.1017/S0016756810000920.

Thomson, S. N., Gehrels, G. E., Ruiz, J., and Buchwaldt, R. (2012). Routine low-damage apatite U-Pb dating using laser ablation-multicollector-ICPMS. *Geochemistry, Geophysics, Geosystems* 13(2), 1–23. DOI: 10.1029/2011GC003928.

Upadhyay, D., Chattopadhyay, S., Kooijman, E., Mezger, K., and Berndt, J. (2014). Magmatic and metamorphic history of Paleoarchean tonalite-trondhjemite-granodiorite (TTG) suite from the Singhbhum craton, eastern

India. *Precambrian Research* 252, 180–190. DOI: 10.1016/j.precamres.2014.07.011.

Vervoort, J. D. and Kemp, A. I. S. (2016). Clarifying the zircon Hf isotope record of crust-mantle evolution. *Chemical Geology* 425, 65–75.

Watson, E. B. and Harrison, T. M. (1983). Zircon saturation revisited: temperature and composition effects in a variety of crustal magma types. *Earth and Planetary Science Letters* 64(2), 295–304.

Wetherill, G. W. (1956). Discordant uranium-lead ages, I. *Eos, Transactions American Geophysical Union* 37(3), 320–326. DOI: 10.1029/TR037i003p00320.

Woodhead, J. D. and Hergt, J. M. (2005). A preliminary appraisal of seven natural zircon reference materials for in situ Hf isotope determination. *Geostandards and Geoanalytical Research* 29(2), 183–195. DOI: 10.1111/j.1751-908X.2005.tb00891.x.

Zadnik, M. G., Specht, S., and Begemann, F. (1989). Revised isotopic composition of terrestrial mercury. *International Journal of Mass Spectrometry and Ion Processes* 89, 103–110. DOI: 10.1016/0168-1176(89)85035-9.

Appendix A.

CL and SE2 images of analyzed grains

In this appendix, the reader will find cathodoluminescence (CL) images of all zircons analyzed in this thesis. All three samples RT11, CH2 and RM1 are covered, in that order. All spots are labeled with analysis number, red circles indicates the ∼25 µm spot placements for U-Pb analysis and light blue circles indicates ∼50 µm spot placement for Hf-isotope analysis. Following the CL images of zircons are the secondary electron (SE2) images utilized as grain maps for U-Pb analysis on apatites. All analytical spots are labeled with text and a red circle (∼50 µm size).

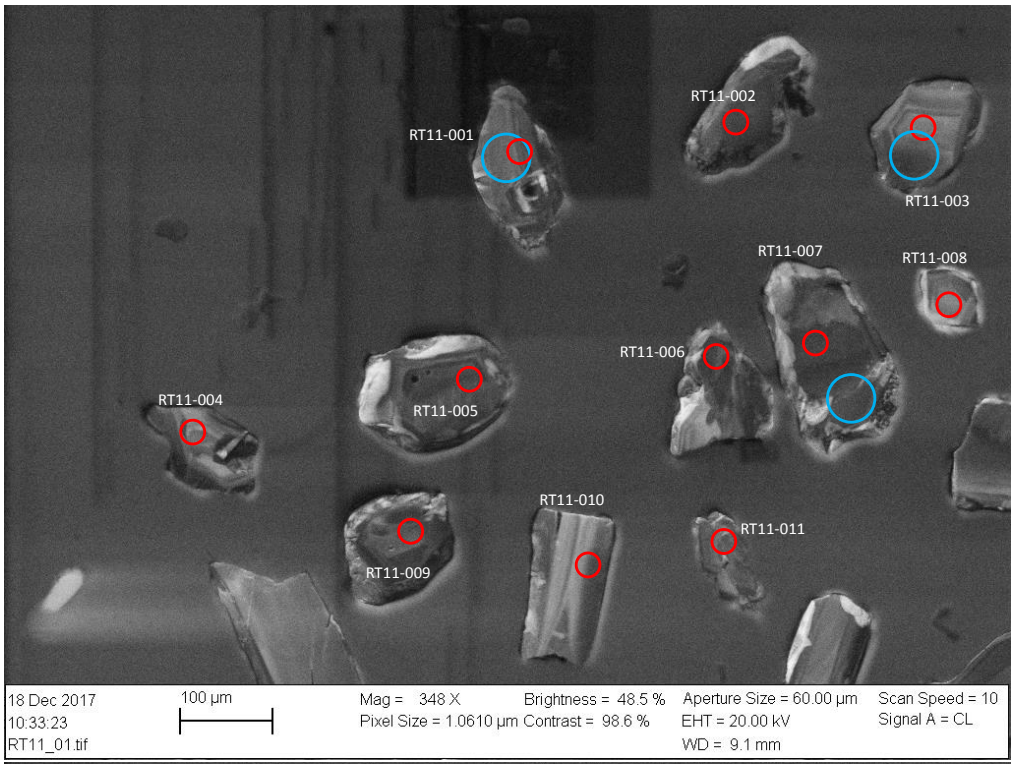
RT11-001
RT11-002
RT11-003
RT11-004
RT11-005
RT11-006
RT11-007
RT11-008
RT11-009
RT11-010
RT11-011
18 Dec 2017
10:33:23
RT11_01.tif
100 µm
Mag = 348 X
Pixel Size = 1.0610 µm
Brightness = 48.5 %
Contrast = 98.6 %
Aperture Size = 60.00 µm
EHT = 20.00 kV
WD = 9.1 mm
Scan Speed = 10
Signal A = CL

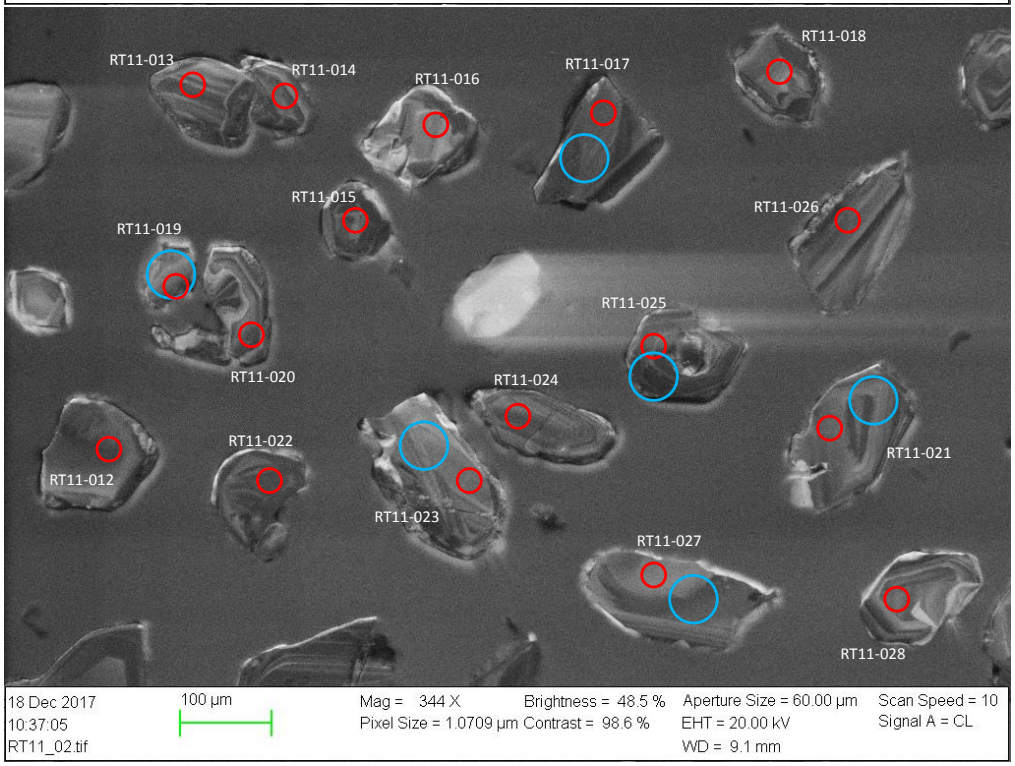
RT11-012
RT11-013
RT11-014
RT11-015
RT11-016
RT11-017
RT11-018
RT11-019
RT11-020
RT11-021
RT11-022
RT11-023
RT11-024
RT11-025
RT11-026
RT11-027
RT11-028
18 Dec 2017
10:37:05
RT11_02.tif
100 µm
Mag = 344 X
Pixel Size = 1.0709 µm
Brightness = 48.5 %
Contrast = 98.6 %
Aperture Size = 60.00 µm
EHT = 20.00 kV
WD = 9.1 mm
Scan Speed = 10
Signal A = CL

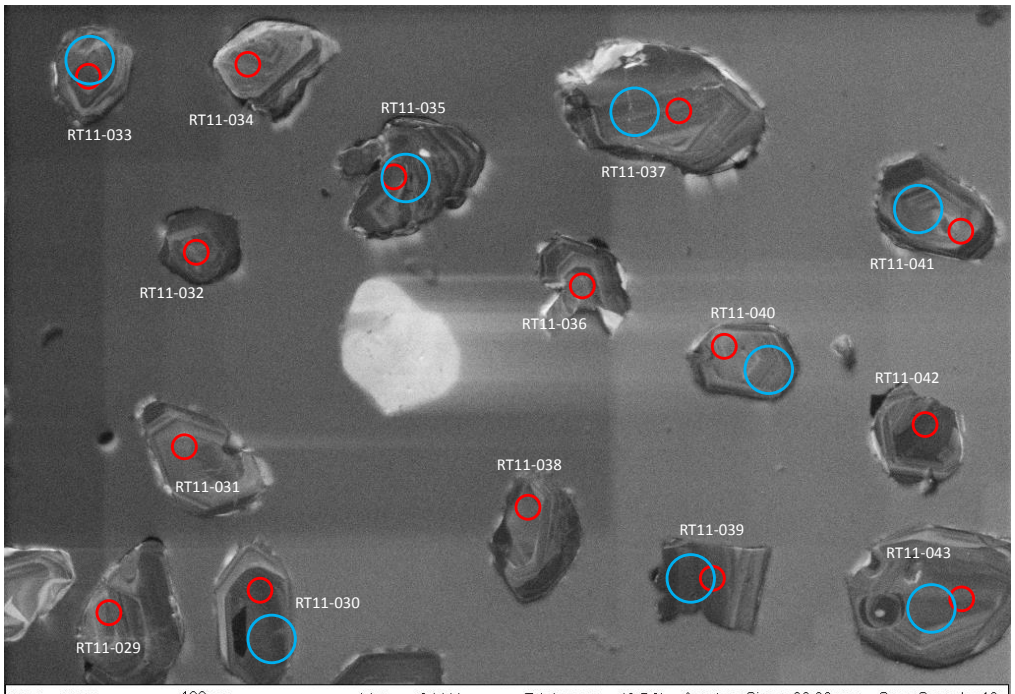
RT11-033
RT11-034
RT11-035
RT11-037
RT11-041
RT11-032
RT11-036
RT11-040
RT11-042
RT11-031
RT11-038
RT11-039
RT11-043
RT11-030
RT11-029
18 Dec 2017
10:52:14
RT11_03.tif
100 µm
Mag = 344 X
Pixel Size = 1.0709 µm
Brightness = 48.5 %
Contrast = 98.6 %
Aperture Size = 60.00 µm
EHT = 20.00 kV
WD = 9.1 mm
Scan Speed = 10
Signal A = CL

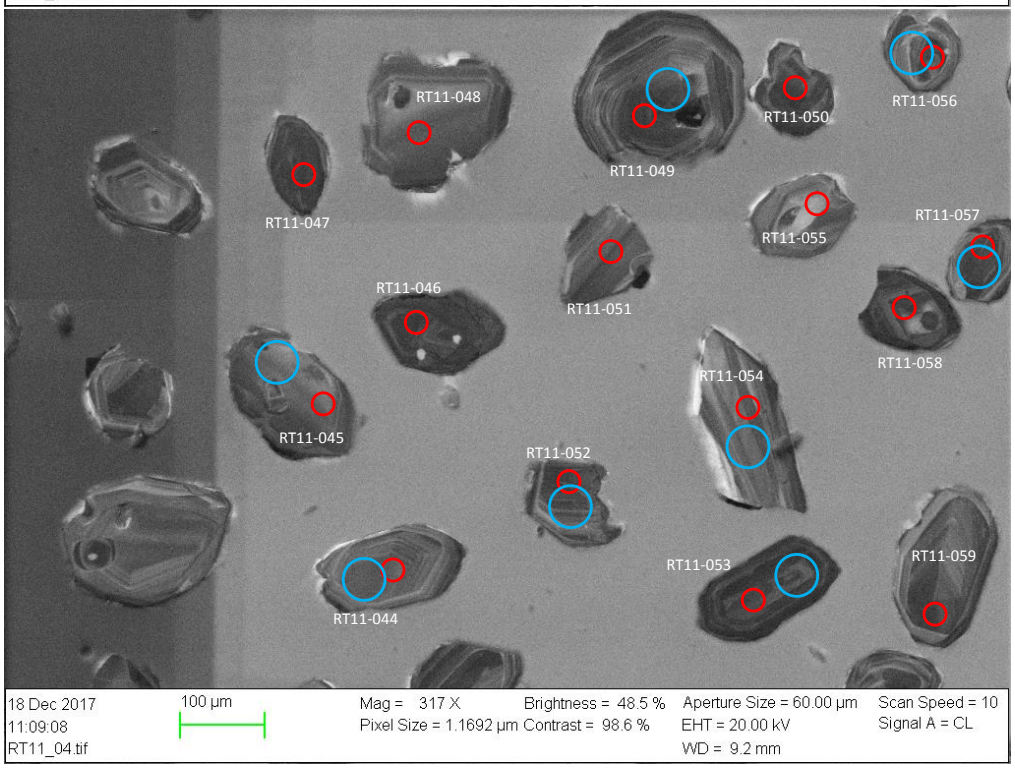
RT11-048
RT11-050
RT11-056
RT11-049
RT11-047
RT11-055
RT11-057
RT11-046
RT11-051
RT11-058
RT11-054
RT11-045
RT11-052
RT11-053
RT11-059
RT11-044
18 Dec 2017
11:09:08
RT11_04.tif
100 µm
Mag = 317 X
Pixel Size = 1.1692 µm
Brightness = 48.5 %
Contrast = 98.6 %
Aperture Size = 60.00 µm
EHT = 20.00 kV
WD = 9.2 mm
Scan Speed = 10
Signal A = CL

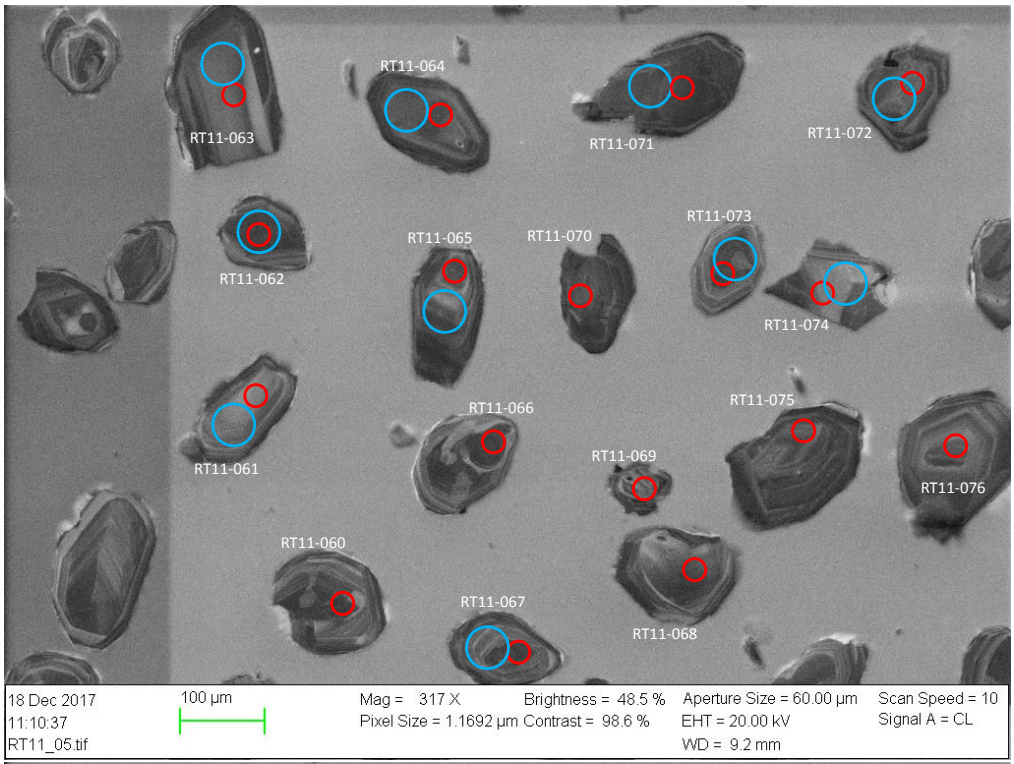
RT11-063
RT11-064
RT11-071
RT11-072
RT11-062
RT11-065
RT11-070
RT11-073
RT11-074
RT11-061
RT11-066
RT11-075
RT11-069
RT11-076
RT11-060
RT11-067
RT11-068
18 Dec 2017
11:10:37
RT11_05.tif
100 µm
Mag = 317 X
Pixel Size = 1.1692 µm
Brightness = 48.5 %
Contrast = 98.6 %
Aperture Size = 60.00 µm
EHT = 20.00 kV
WD = 9.2 mm
Scan Speed = 10
Signal A = CL

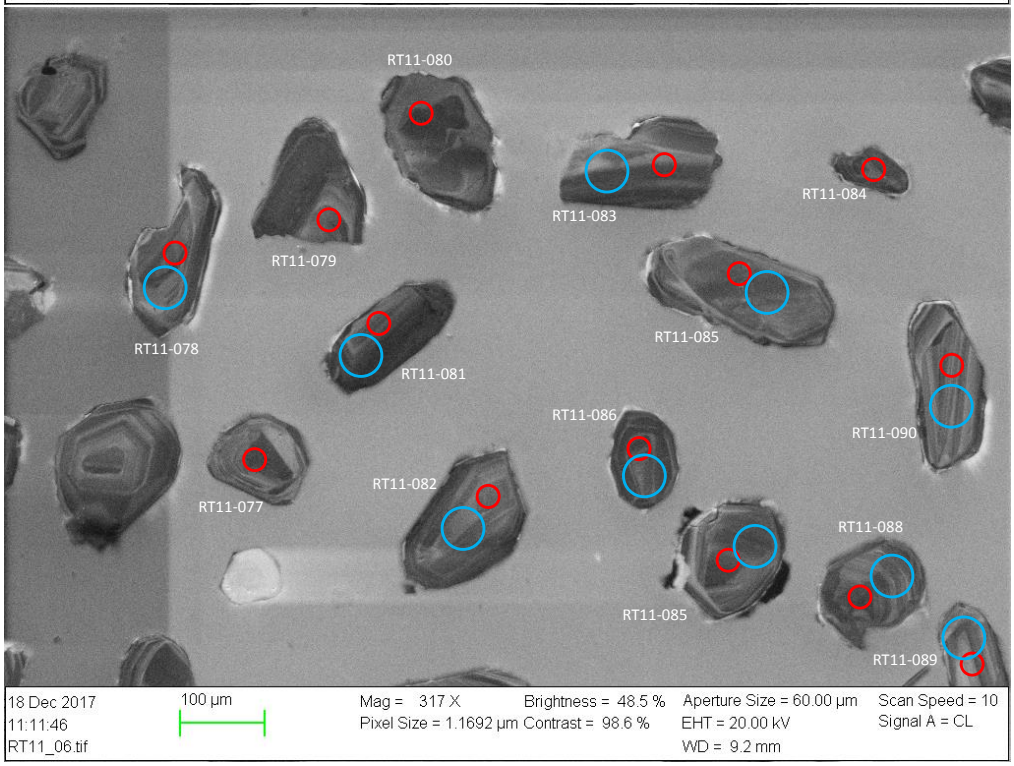
RT11-080
RT11-083
RT11-084
RT11-079
RT11-078
RT11-085
RT11-081
RT11-086
RT11-090
RT11-077
RT11-082
RT11-088
RT11-085
RT11-089
18 Dec 2017
11:11:46
RT11_06.tif
100 µm
Mag = 317 X
Pixel Size = 1.1692 µm
Brightness = 48.5 %
Contrast = 98.6 %
Aperture Size = 60.00 µm
EHT = 20.00 kV
WD = 9.2 mm
Scan Speed = 10
Signal A = CL

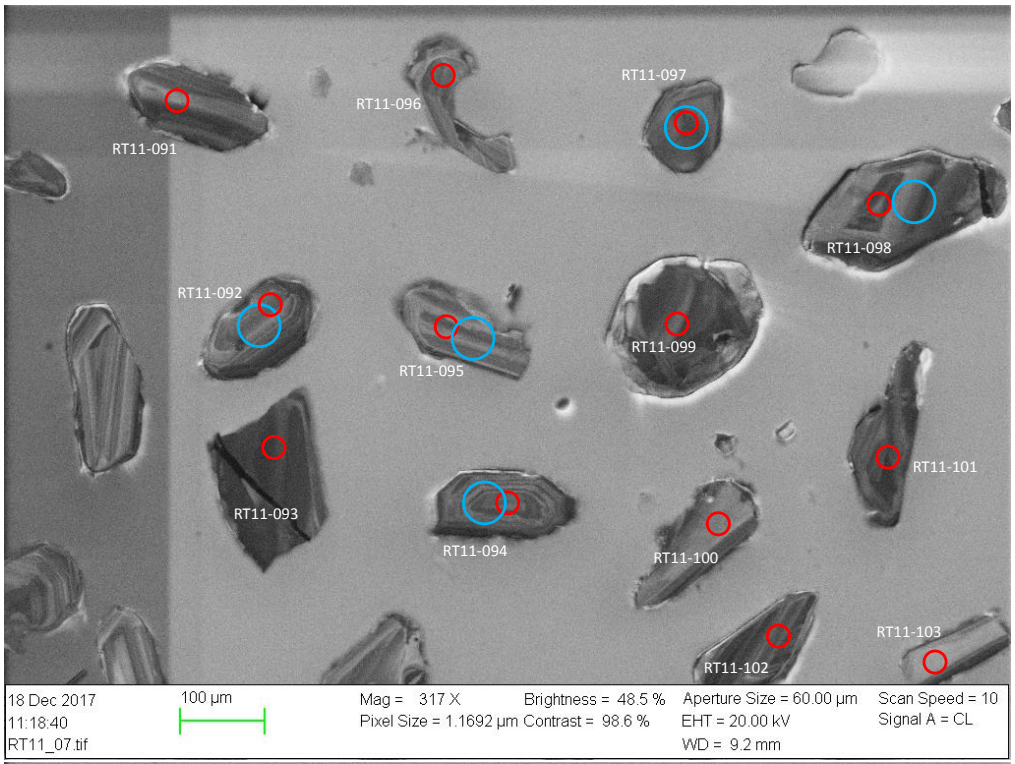
RT11-091
RT11-096
RT11-097
RT11-098
RT11-092
RT11-095
RT11-099
RT11-101
RT11-093
RT11-094
RT11-100
RT11-102
RT11-103
18 Dec 2017
11:18:40
RT11_07.tif
100 µm
Mag = 317 X
Pixel Size = 1.1692 µm
Brightness = 48.5 %
Contrast = 98.6 %
Aperture Size = 60.00 µm
EHT = 20.00 kV
WD = 9.2 mm
Scan Speed = 10
Signal A = CL

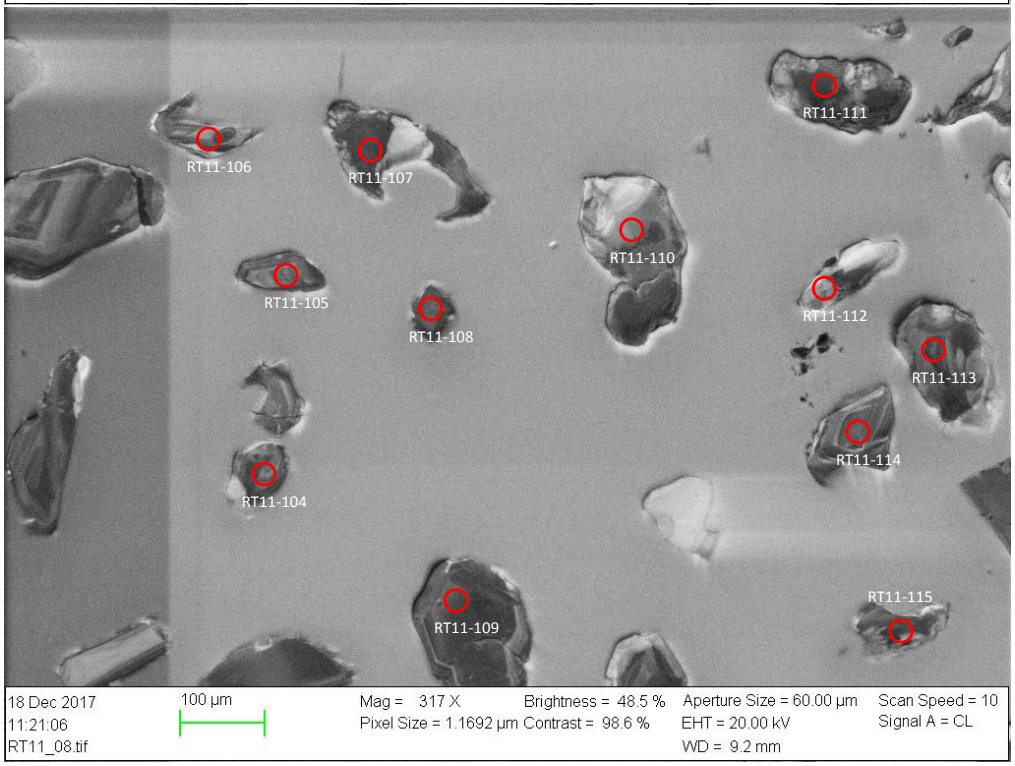
RT11-111
RT11-106
RT11-107
RT11-110
RT11-105
RT11-108
RT11-112
RT11-113
RT11-114
RT11-104
RT11-115
RT11-109
18 Dec 2017
11:21:06
RT11_08.tif
100 µm
Mag = 317 X
Pixel Size = 1.1692 µm
Brightness = 48.5 %
Contrast = 98.6 %
Aperture Size = 60.00 µm
EHT = 20.00 kV
WD = 9.2 mm
Scan Speed = 10
Signal A = CL

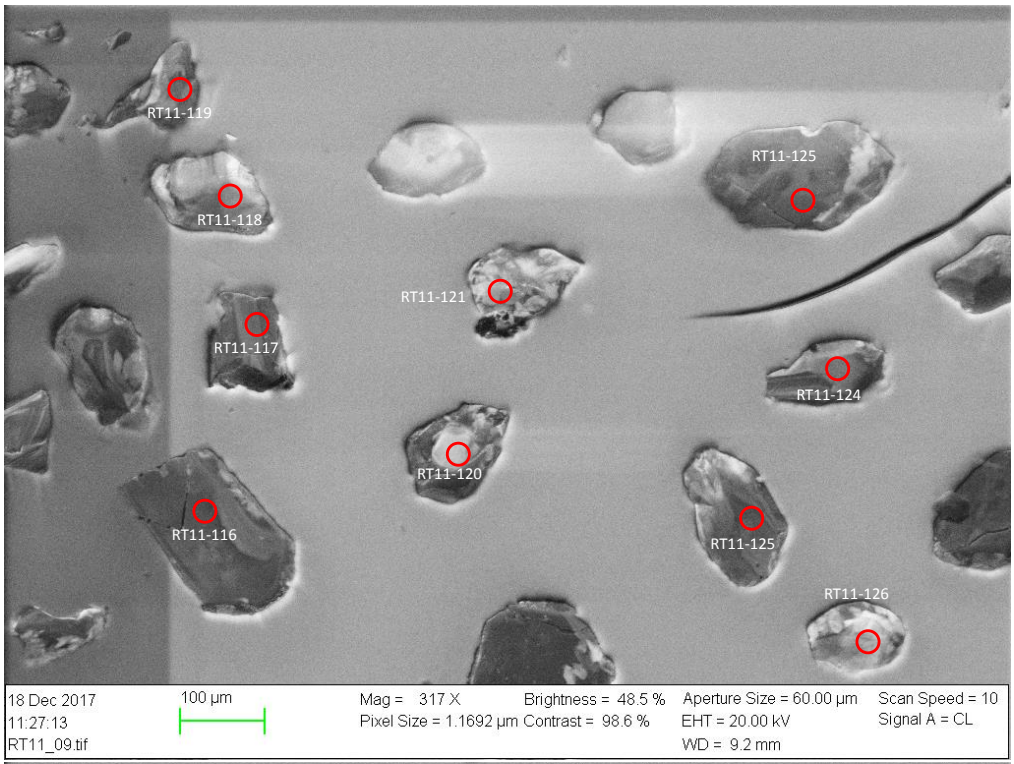
RT11-119
RT11-118
RT11-125
RT11-121
RT11-117
RT11-124
RT11-120
RT11-116
RT11-125
RT11-126
18 Dec 2017
11:27:13
RT11_09.tif
100 µm
Mag = 317 X
Pixel Size = 1.1692 µm
Brightness = 48.5 %
Contrast = 98.6 %
Aperture Size = 60.00 µm
EHT = 20.00 kV
WD = 9.2 mm
Scan Speed = 10
Signal A = CL

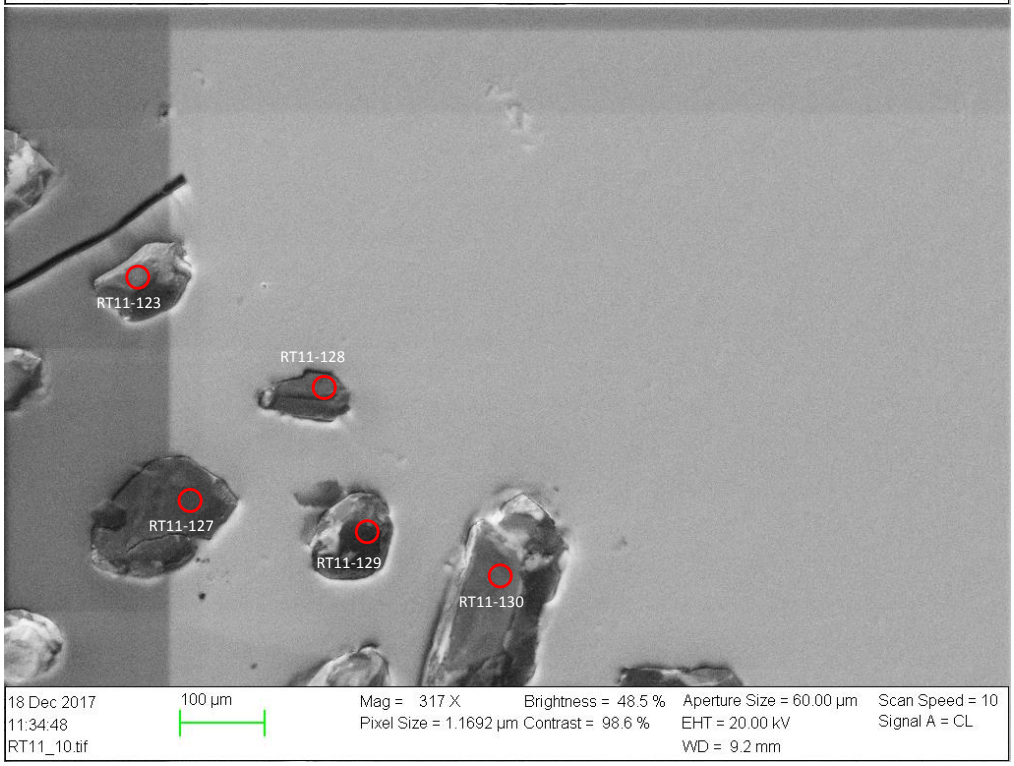
RT11-123
RT11-128
RT11-127
RT11-129
RT11-130
18 Dec 2017
11:34:48
RT11_10.tif
100 µm
Mag = 317 X
Pixel Size = 1.1692 µm
Brightness = 48.5 %
Contrast = 98.6 %
Aperture Size = 60.00 µm
EHT = 20.00 kV
WD = 9.2 mm
Scan Speed = 10
Signal A = CL

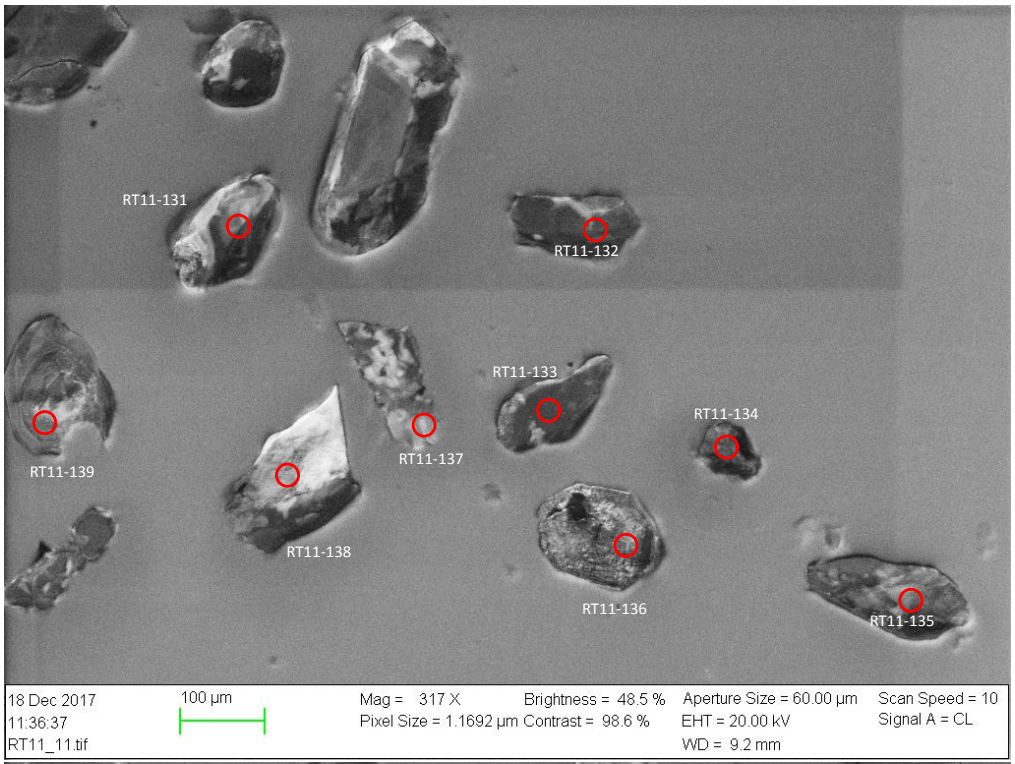
RT11-131
RT11-132
RT11-133
RT11-134
RT11-139
RT11-137
RT11-138
RT11-136
RT11-135
18 Dec 2017
11:36:37
RT11_11.tif
100 µm
Mag = 317 X
Pixel Size = 1.1692 µm
Brightness = 48.5 %
Contrast = 98.6 %
Aperture Size = 60.00 µm
EHT = 20.00 kV
WD = 9.2 mm
Scan Speed = 10
Signal A = CL

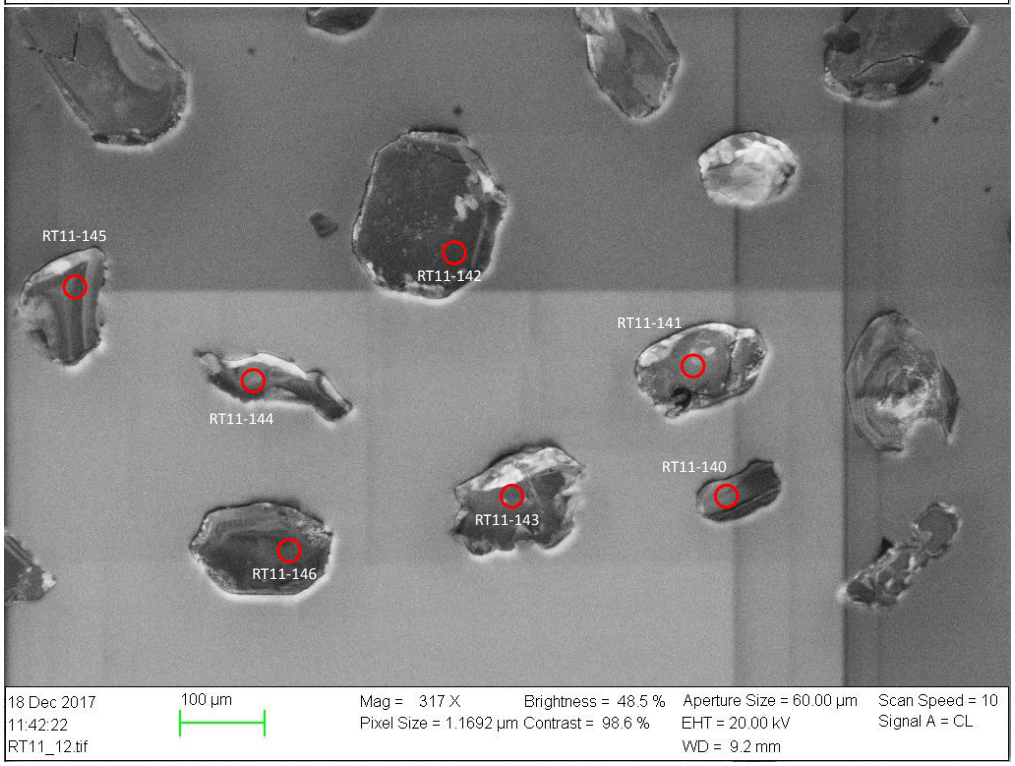
RT11-145
RT11-142
RT11-141
RT11-144
RT11-140
RT11-143
RT11-146
18 Dec 2017
11:42:22
RT11_12.tif
100 µm
Mag = 317 X
Pixel Size = 1.1692 µm
Brightness = 48.5 %
Contrast = 98.6 %
Aperture Size = 60.00 µm
EHT = 20.00 kV
WD = 9.2 mm
Scan Speed = 10
Signal A = CL

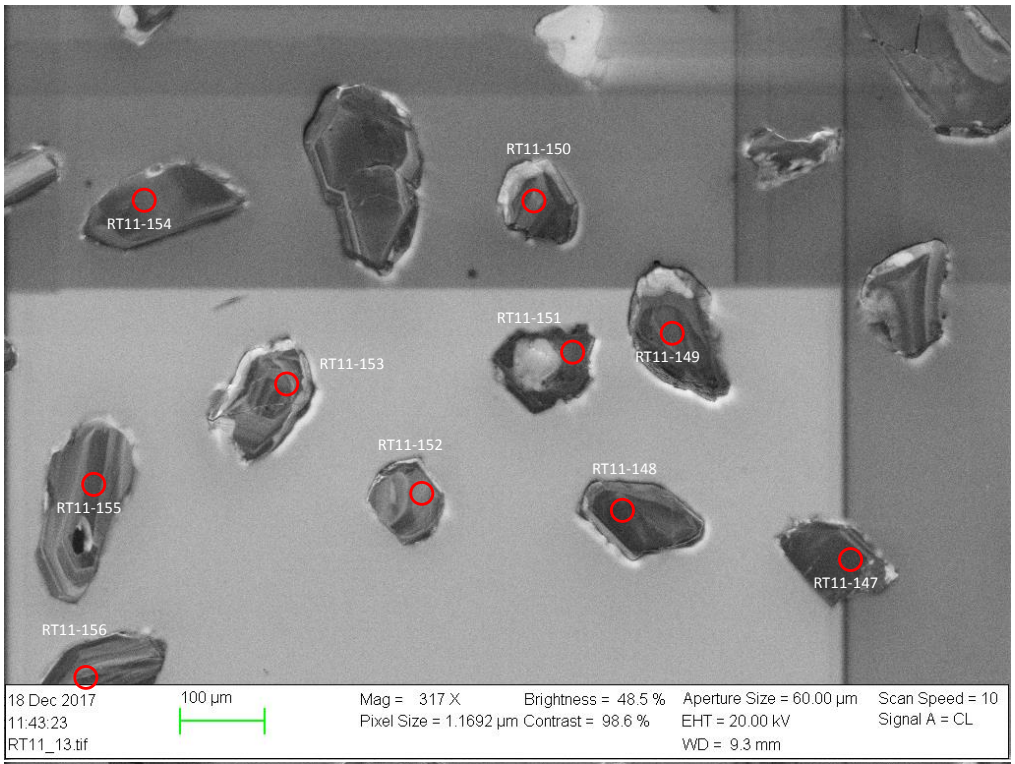
RT11-150
RT11-154
RT11-151
RT11-149
RT11-153
RT11-152
RT11-148
RT11-155
RT11-147
RT11-156
18 Dec 2017
11:43:23
RT11_13.tif
100 µm
Mag = 317 X
Pixel Size = 1.1692 µm
Brightness = 48.5 %
Contrast = 98.6 %
Aperture Size = 60.00 µm
EHT = 20.00 kV
WD = 9.3 mm
Scan Speed = 10
Signal A = CL

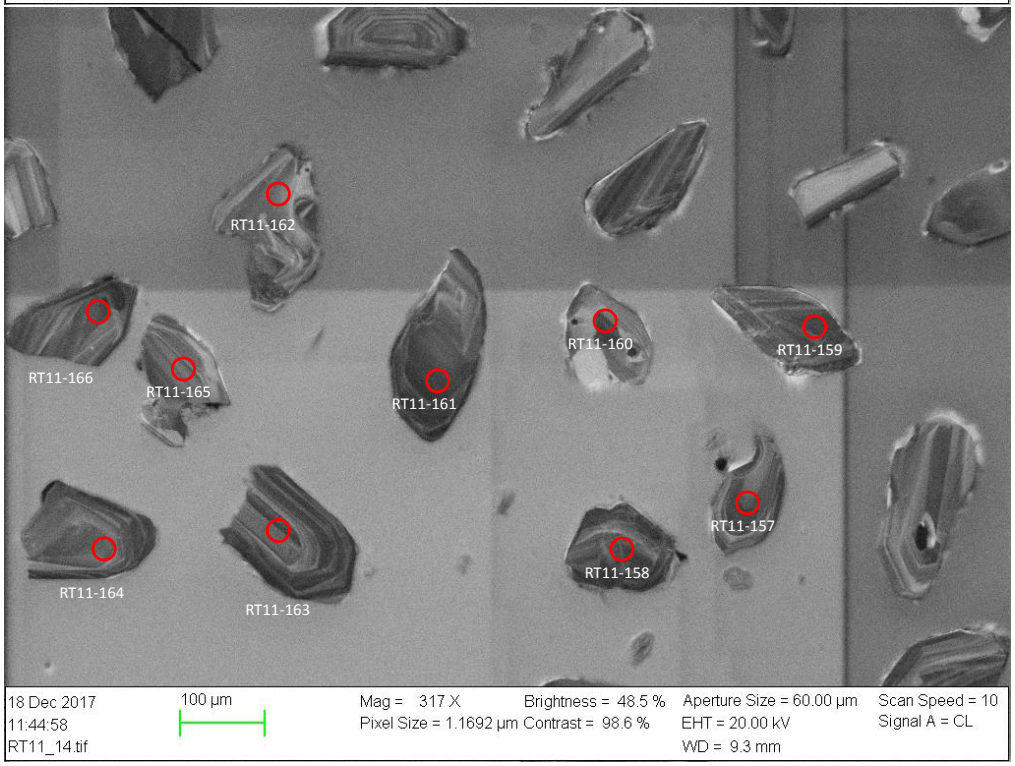
RT11-162
RT11-166
RT11-165
RT11-161
RT11-160
RT11-159
RT11-157
RT11-158
RT11-164
RT11-163
18 Dec 2017
11:44:58
RT11_14.tif
100 µm
Mag = 317 X
Pixel Size = 1.1692 µm
Brightness = 48.5 %
Contrast = 98.6 %
Aperture Size = 60.00 µm
EHT = 20.00 kV
WD = 9.3 mm
Scan Speed = 10
Signal A = CL

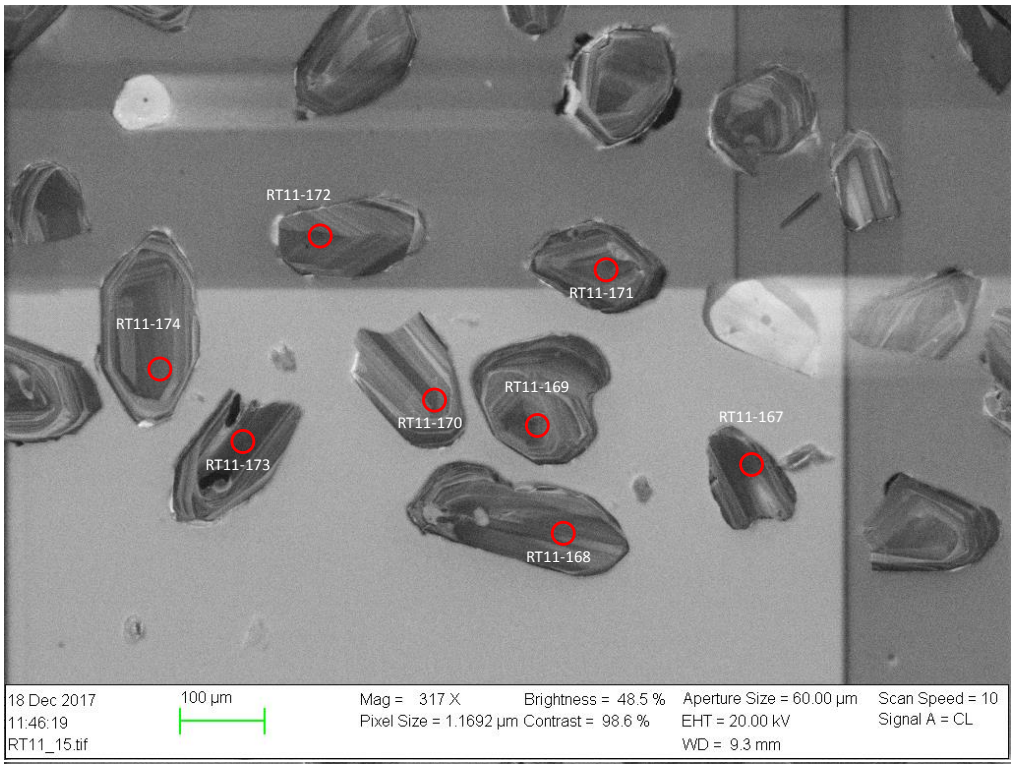
RT11-172
RT11-171
RT11-174
RT11-169
RT11-170
RT11-167
RT11-173
RT11-168
18 Dec 2017
11:46:19
RT11_15.tif
100 µm
Mag = 317 X
Pixel Size = 1.1692 µm
Brightness = 48.5 %
Contrast = 98.6 %
Aperture Size = 60.00 µm
EHT = 20.00 kV
WD = 9.3 mm
Scan Speed = 10
Signal A = CL

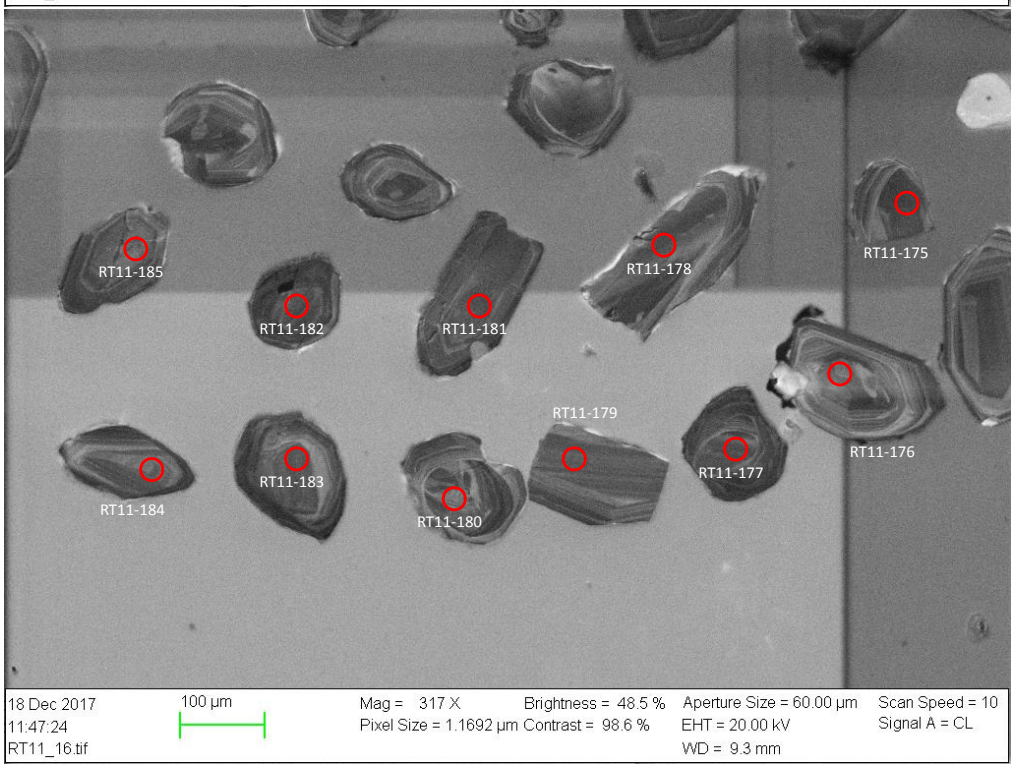
RT11-185
RT11-178
RT11-175
RT11-182
RT11-181
RT11-179
RT11-176
RT11-177
RT11-183
RT11-184
RT11-180
18 Dec 2017
11:47:24
RT11_16.tif
100 µm
Mag = 317 X
Pixel Size = 1.1692 µm
Brightness = 48.5 %
Contrast = 98.6 %
Aperture Size = 60.00 µm
EHT = 20.00 kV
WD = 9.3 mm
Scan Speed = 10
Signal A = CL

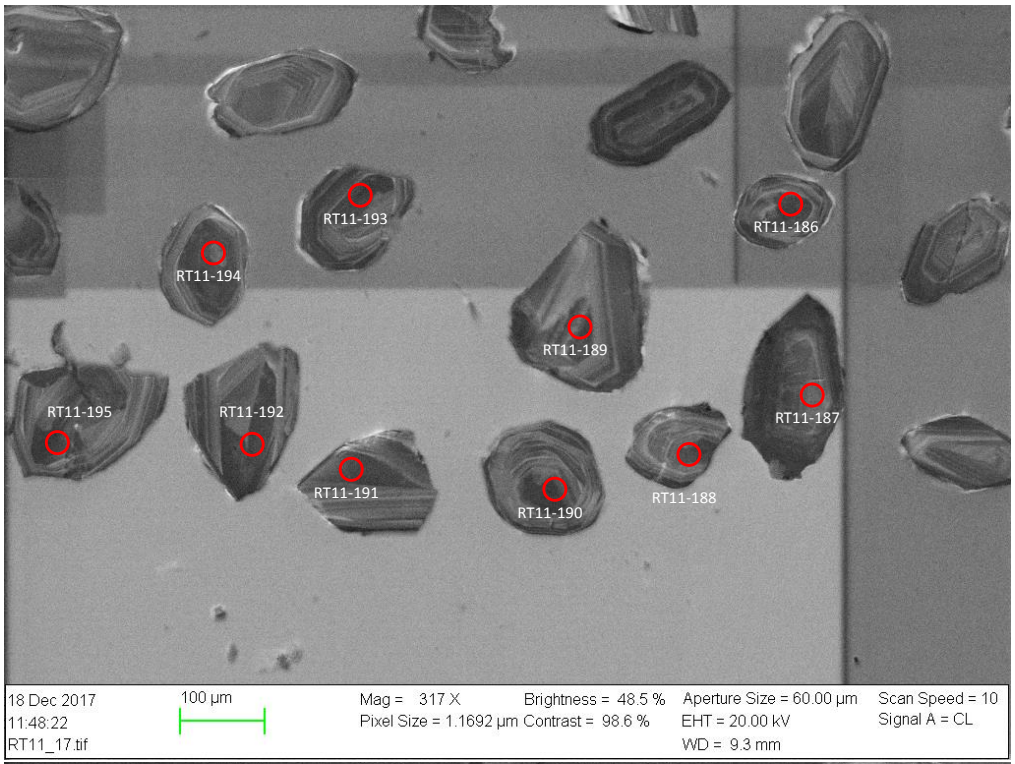
RT11-193
RT11-186
RT11-194
RT11-189
RT11-195
RT11-192
RT11-187
RT11-191
RT11-190
RT11-188
18 Dec 2017
11:48:22
RT11_17.tif
100 µm
Mag = 317 X
Pixel Size = 1.1692 µm
Brightness = 48.5 %
Contrast = 98.6 %
Aperture Size = 60.00 µm
EHT = 20.00 kV
WD = 9.3 mm
Scan Speed = 10
Signal A = CL

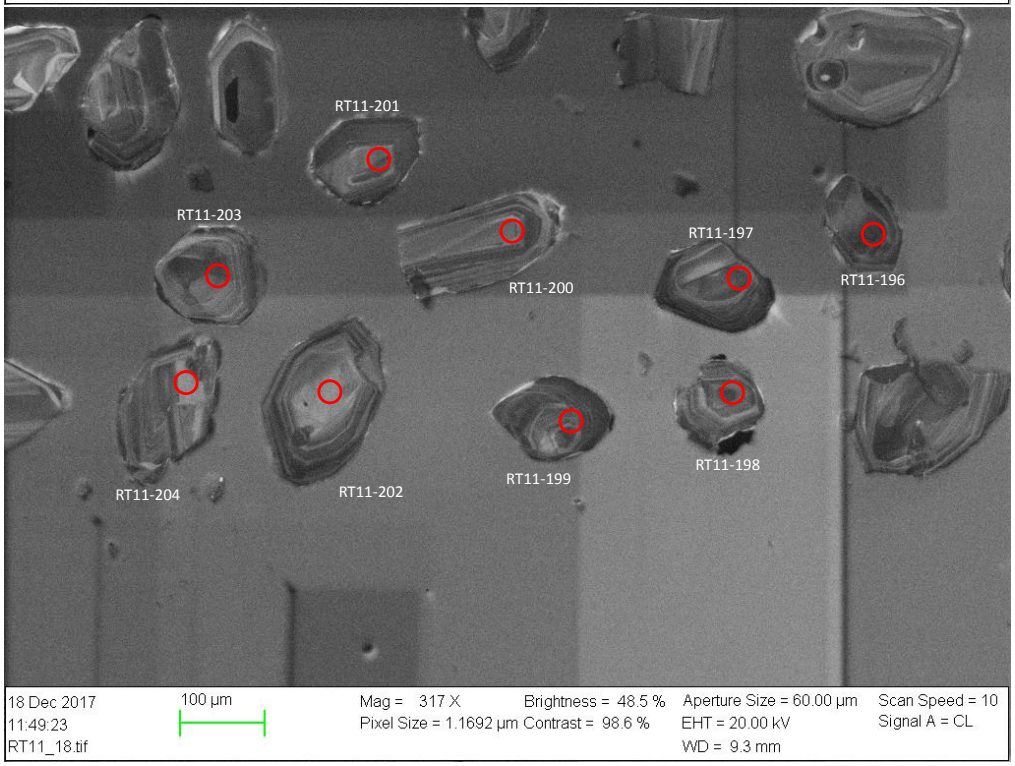
RT11-201
RT11-203
RT11-197
RT11-200
RT11-196
RT11-204
RT11-202
RT11-199
RT11-198
18 Dec 2017
11:49:23
RT11_18.tif
100 µm
Mag = 317 X
Pixel Size = 1.1692 µm
Brightness = 48.5 %
Contrast = 98.6 %
Aperture Size = 60.00 µm
EHT = 20.00 kV
WD = 9.3 mm
Scan Speed = 10
Signal A = CL

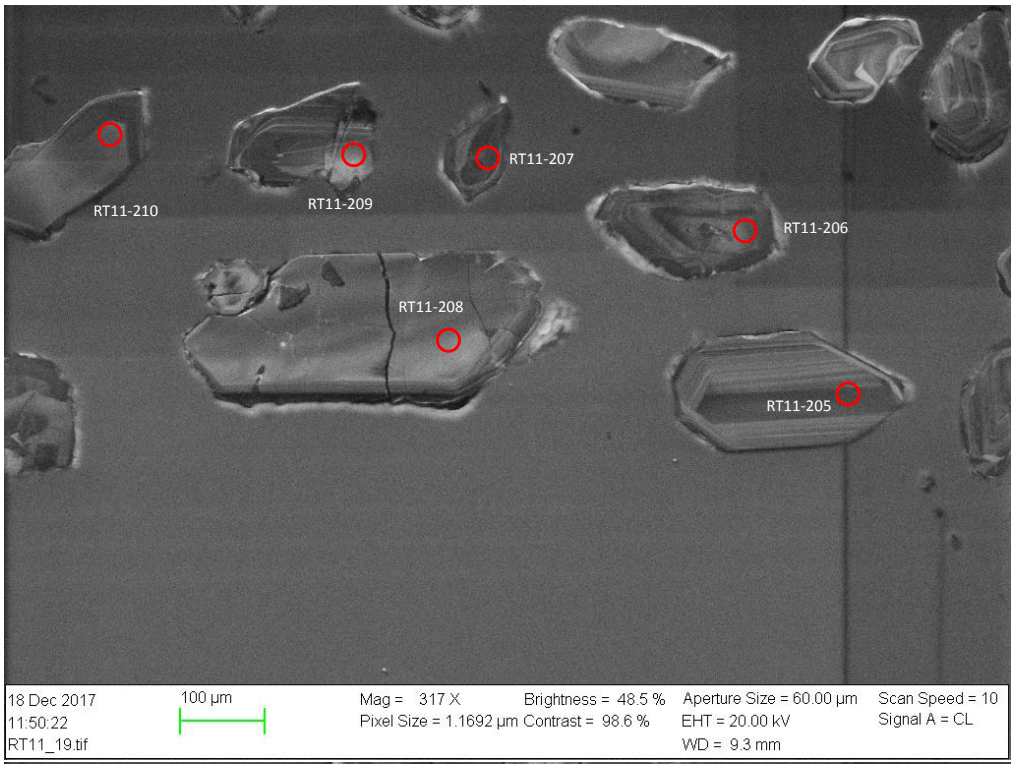
RT11-210
RT11-209
RT11-207
RT11-206
RT11-208
RT11-205
18 Dec 2017
11:50:22
RT11_19.tif
100 µm
Mag = 317 X
Pixel Size = 1.1692 µm
Brightness = 48.5 %
Contrast = 98.6 %
Aperture Size = 60.00 µm
EHT = 20.00 kV
WD = 9.3 mm
Scan Speed = 10
Signal A = CL

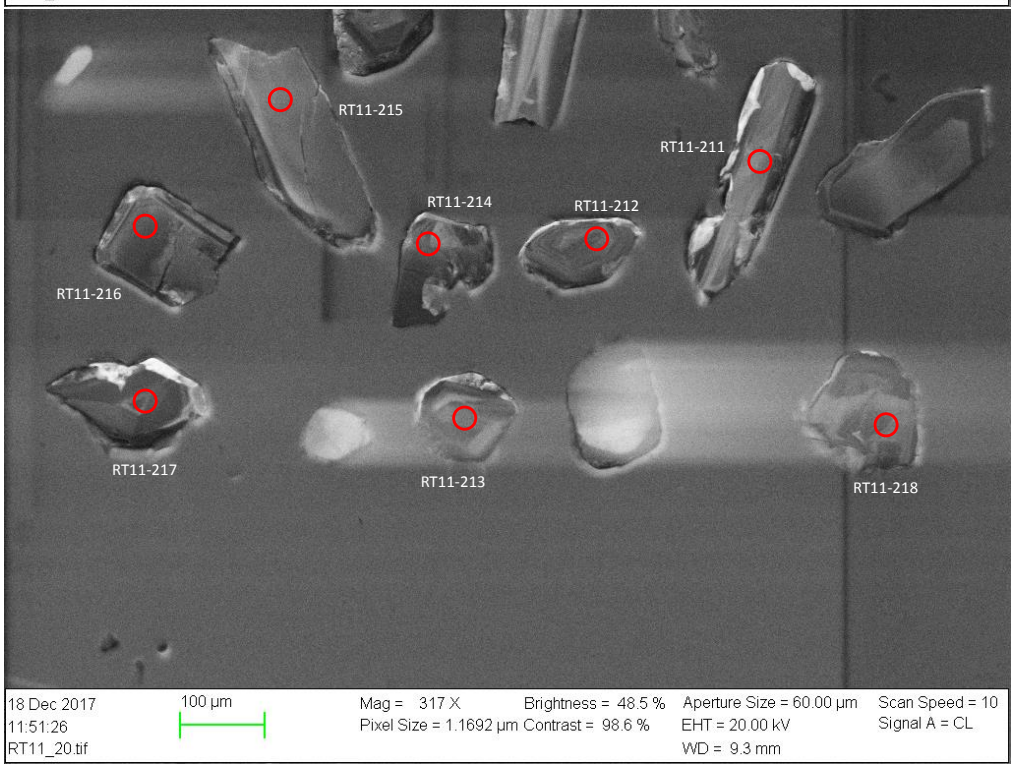
RT11-215
RT11-211
RT11-214
RT11-212
RT11-216
RT11-217
RT11-213
RT11-218
18 Dec 2017
11:51:26
RT11_20.tif
100 µm
Mag = 317 X
Pixel Size = 1.1692 µm
Brightness = 48.5 %
Contrast = 98.6 %
Aperture Size = 60.00 µm
EHT = 20.00 kV
WD = 9.3 mm
Scan Speed = 10
Signal A = CL

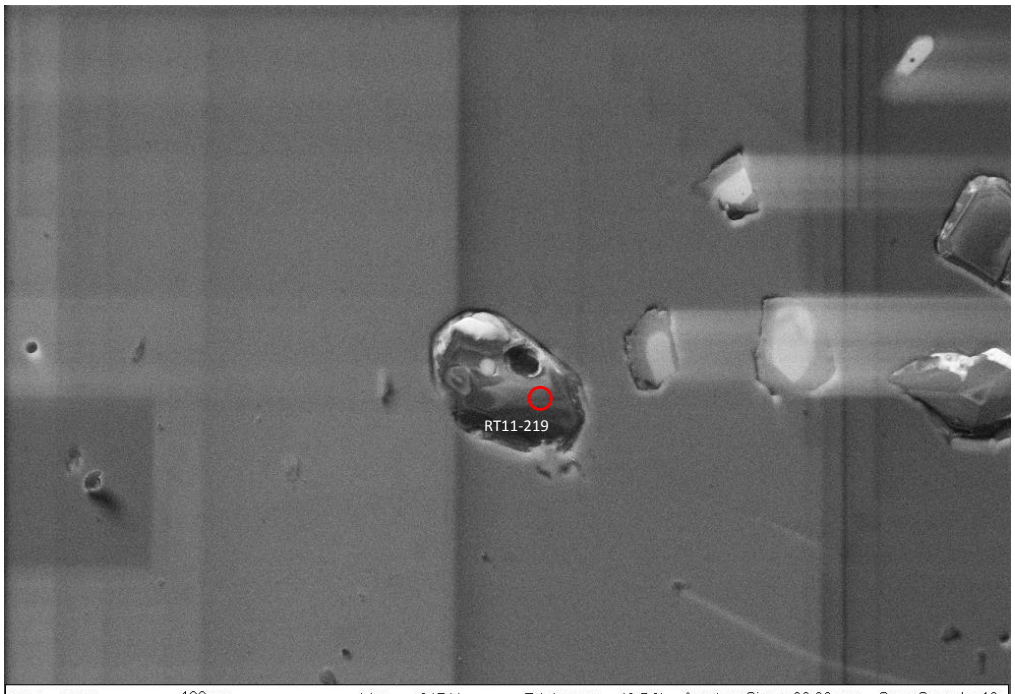
RT11-219
18 Dec 2017
11:58:07
RT11_21.tif
100 µm
Mag = 317 X
Pixel Size = 1.1692 µm
Brightness = 48.5 %
Contrast = 98.6 %
Aperture Size = 60.00 µm
EHT = 20.00 kV
WD = 9.3 mm
Scan Speed = 10
Signal A = CL

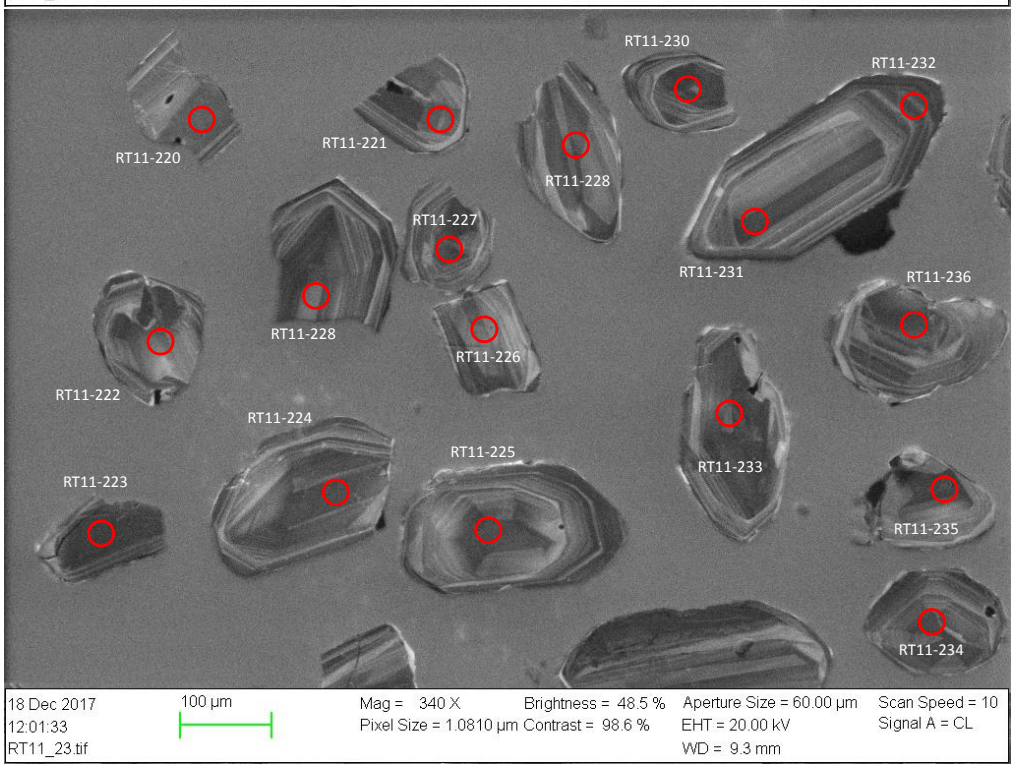
RT11-220
RT11-221
RT11-228
RT11-230
RT11-232
RT11-227
RT11-231
RT11-236
RT11-228
RT11-226
RT11-222
RT11-224
RT11-225
RT11-233
RT11-223
RT11-235
RT11-234
18 Dec 2017
12:01:33
RT11_23.tif
100 µm
Mag = 340 X
Pixel Size = 1.0810 µm
Brightness = 48.5 %
Contrast = 98.6 %
Aperture Size = 60.00 µm
EHT = 20.00 kV
WD = 9.3 mm
Scan Speed = 10
Signal A = CL

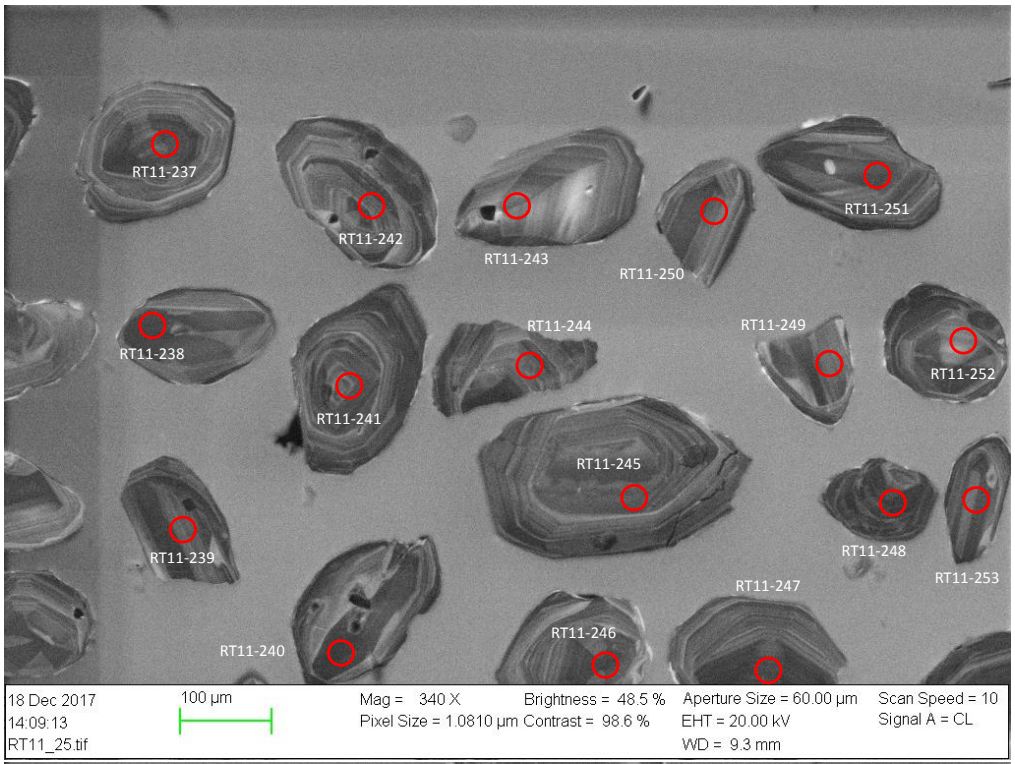
RT11-237
RT11-242
RT11-243
RT11-250
RT11-251
RT11-238
RT11-244
RT11-249
RT11-252
RT11-241
RT11-245
RT11-239
RT11-248
RT11-253
RT11-247
RT11-246
RT11-240
18 Dec 2017
14:09:13
RT11_25.tif
100 µm
Mag = 340 X
Pixel Size = 1.0810 µm
Brightness = 48.5 %
Contrast = 98.6 %
Aperture Size = 60.00 µm
EHT = 20.00 kV
WD = 9.3 mm
Scan Speed = 10
Signal A = CL

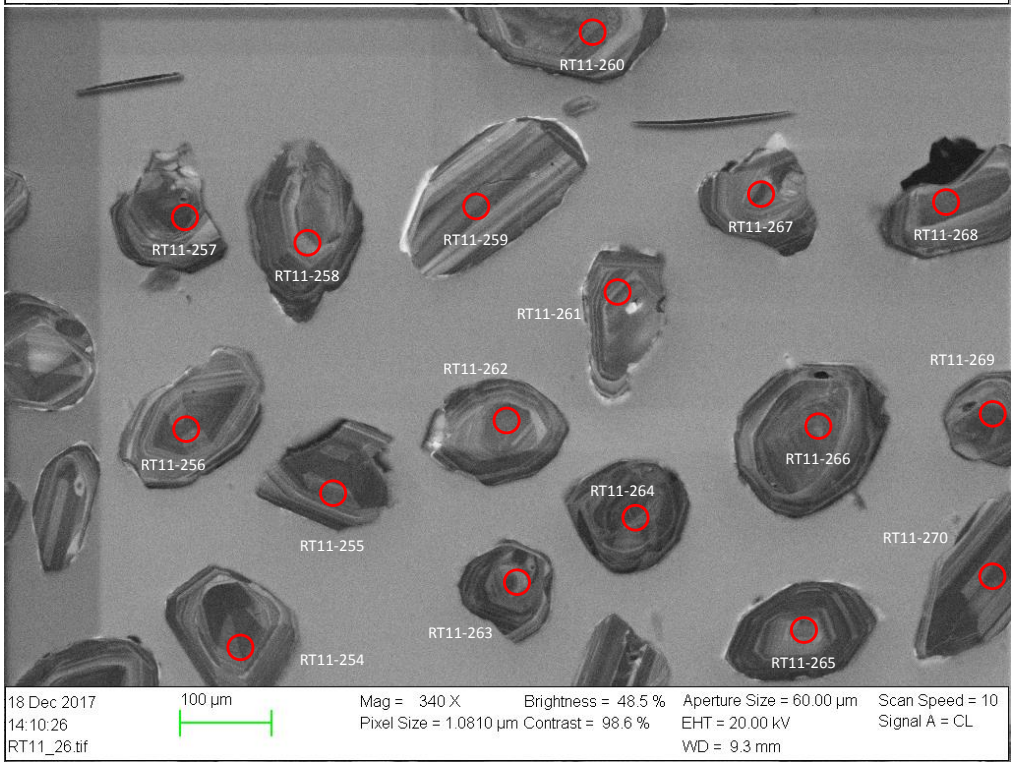
RT11-260
RT11-257
RT11-258
RT11-259
RT11-267
RT11-268
RT11-261
RT11-262
RT11-269
RT11-256
RT11-266
RT11-264
RT11-255
RT11-270
RT11-263
RT11-254
RT11-265
18 Dec 2017
14:10:26
RT11_26.tif
100 µm
Mag = 340 X
Pixel Size = 1.0810 µm
Brightness = 48.5 %
Contrast = 98.6 %
Aperture Size = 60.00 µm
EHT = 20.00 kV
WD = 9.3 mm
Scan Speed = 10
Signal A = CL

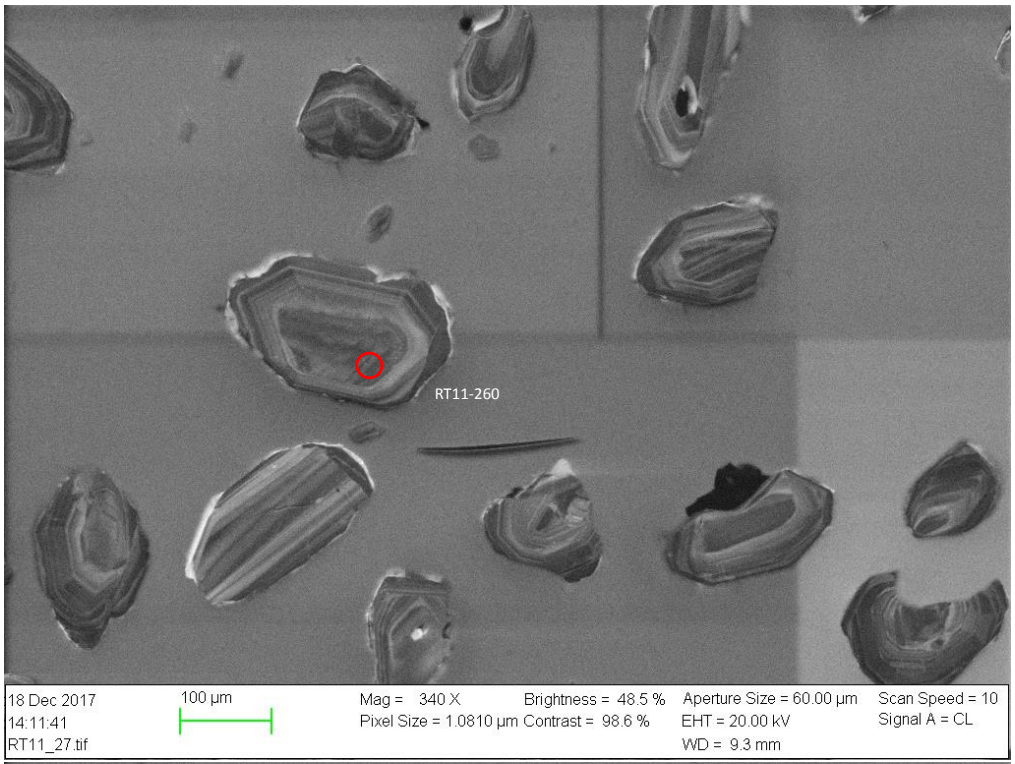
RT11-260
18 Dec 2017
14:11:41
RT11_27.tif
100 µm
Mag = 340 X
Pixel Size = 1.0810 µm
Brightness = 48.5 %
Contrast = 98.6 %
Aperture Size = 60.00 µm
EHT = 20.00 kV
WD = 9.3 mm
Scan Speed = 10
Signal A = CL

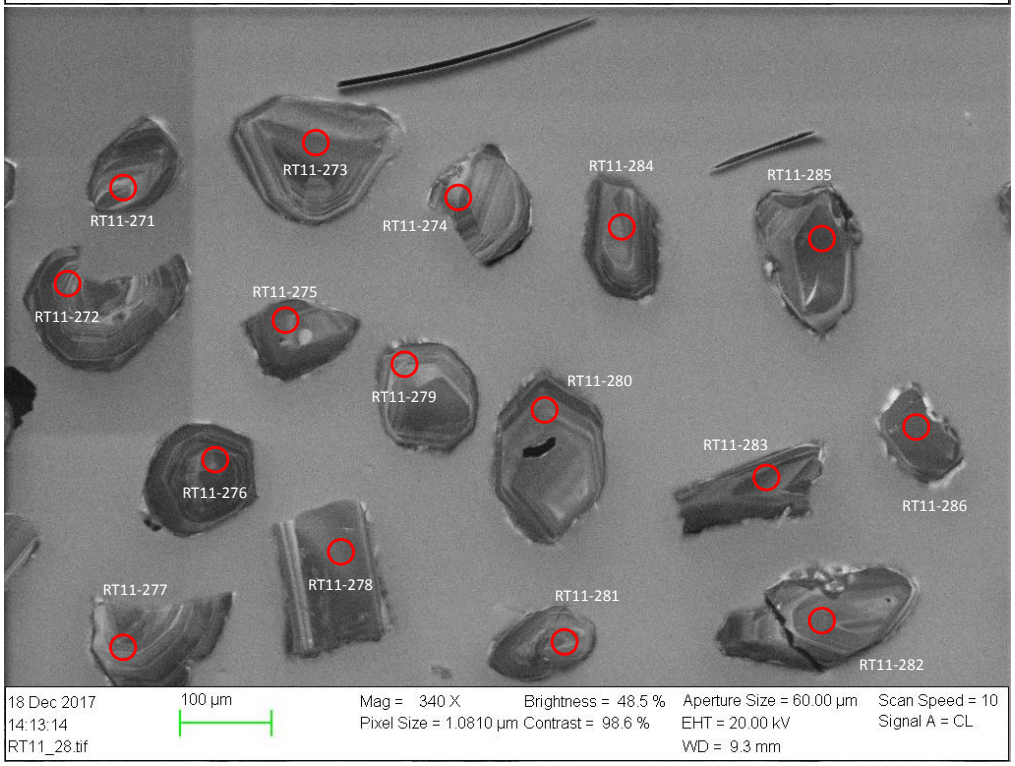
RT11-271
RT11-272
RT11-273
RT11-274
RT11-275
RT11-276
RT11-277
RT11-278
RT11-279
RT11-280
RT11-281
RT11-282
RT11-283
RT11-284
RT11-285
RT11-286
18 Dec 2017
14:13:14
RT11_28.tif
100 µm
Mag = 340 X
Pixel Size = 1.0810 µm
Brightness = 48.5 %
Contrast = 98.6 %
Aperture Size = 60.00 µm
EHT = 20.00 kV
WD = 9.3 mm
Scan Speed = 10
Signal A = CL

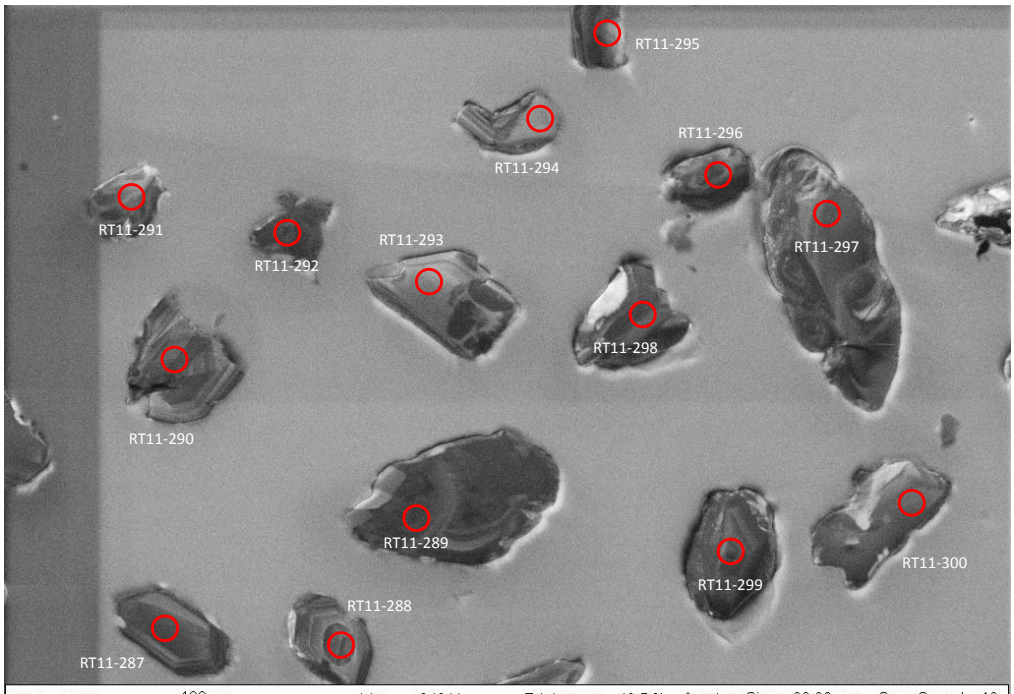
RT11-295
RT11-294
RT11-296
RT11-291
RT11-292
RT11-293
RT11-297
RT11-298
RT11-290
RT11-289
RT11-299
RT11-300
RT11-288
RT11-287
18 Dec 2017
14:20:36
RT11_29.tif
100 µm
Mag = 340 X
Pixel Size = 1.0810 µm
Brightness = 48.5 %
Contrast = 98.6 %
Aperture Size = 60.00 µm
EHT = 20.00 kV
WD = 9.3 mm
Scan Speed = 10
Signal A = CL

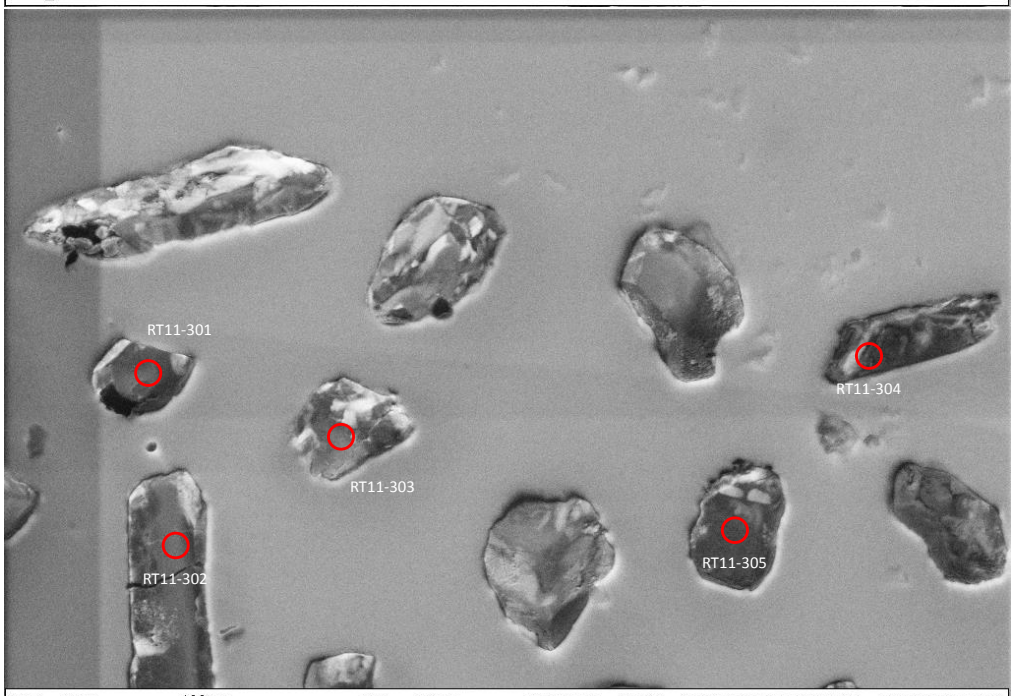
RT11-301
RT11-304
RT11-303
RT11-305
RT11-302
18 Dec 2017
14:21:46
RT11_30.tif
100 µm
Mag = 340 X
Pixel Size = 1.0810 µm
Brightness = 48.5 %
Contrast = 98.6 %
Aperture Size = 60.00 µm
EHT = 20.00 kV
WD = 9.3 mm
Scan Speed = 10
Signal A = CL

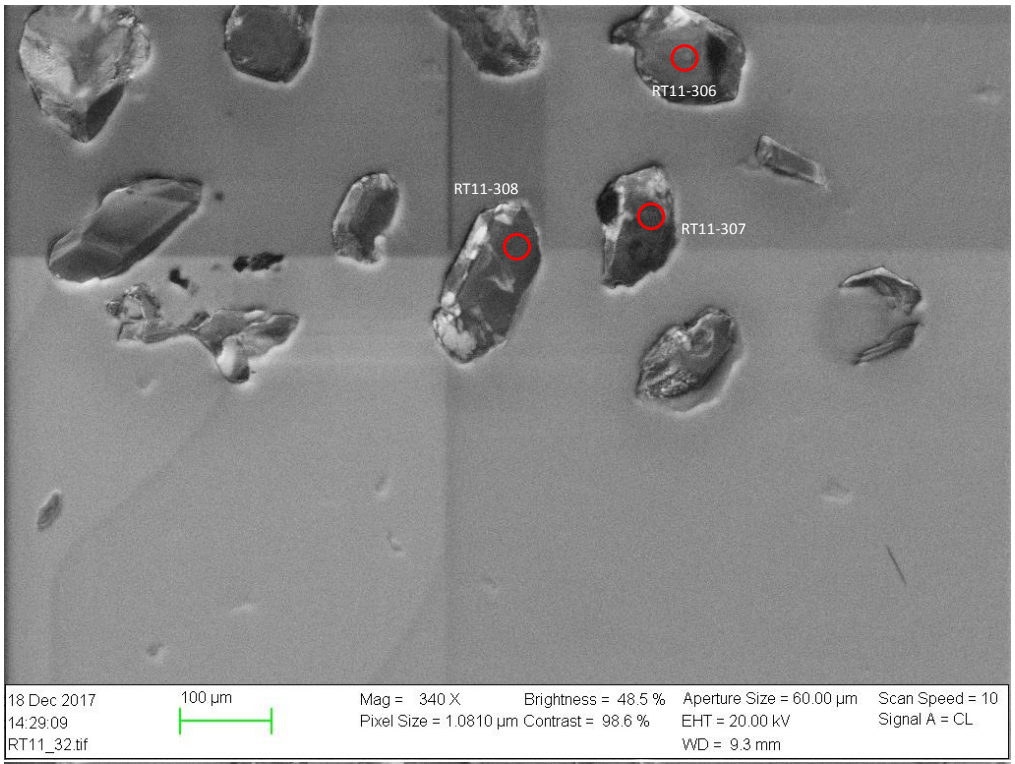
RT11-306
RT11-308
RT11-307
18 Dec 2017
14:29:09
RT11_32.tif
100 µm
Mag = 340 X
Pixel Size = 1.0810 µm
Brightness = 48.5 %
Contrast = 98.6 %
Aperture Size = 60.00 µm
EHT = 20.00 kV
WD = 9.3 mm
Scan Speed = 10
Signal A = CL

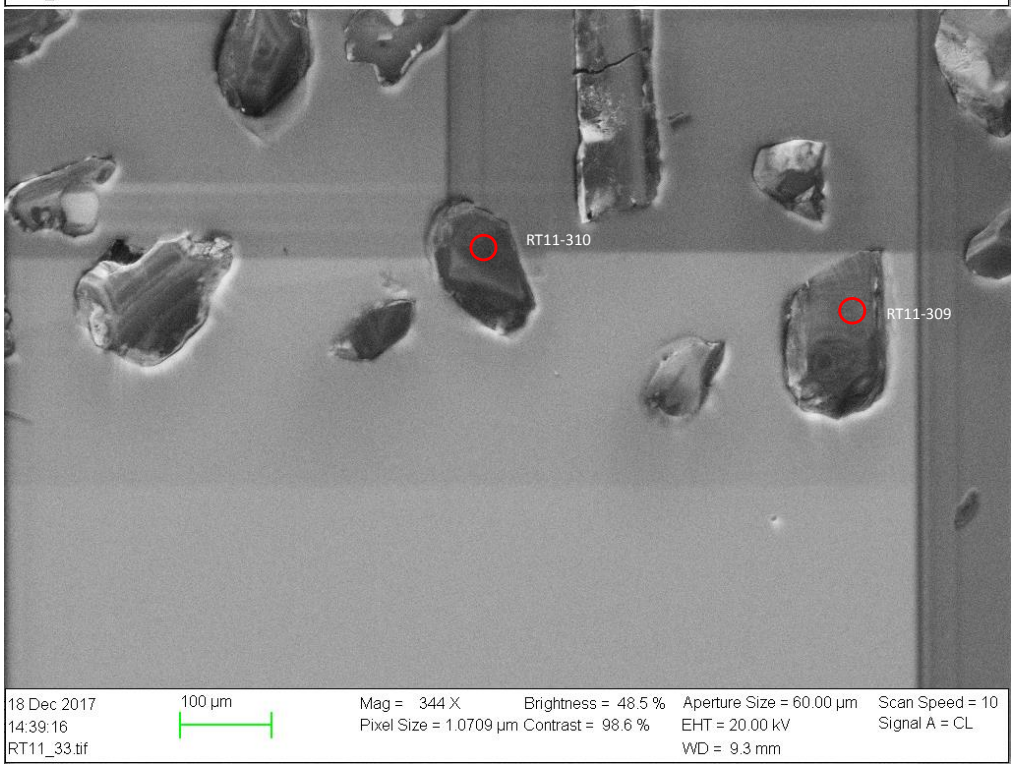
RT11-310
RT11-309
18 Dec 2017
14:39:16
RT11_33.tif
100 µm
Mag = 344 X
Pixel Size = 1.0709 µm
Brightness = 48.5 %
Contrast = 98.6 %
Aperture Size = 60.00 µm
EHT = 20.00 kV
WD = 9.3 mm
Scan Speed = 10
Signal A = CL

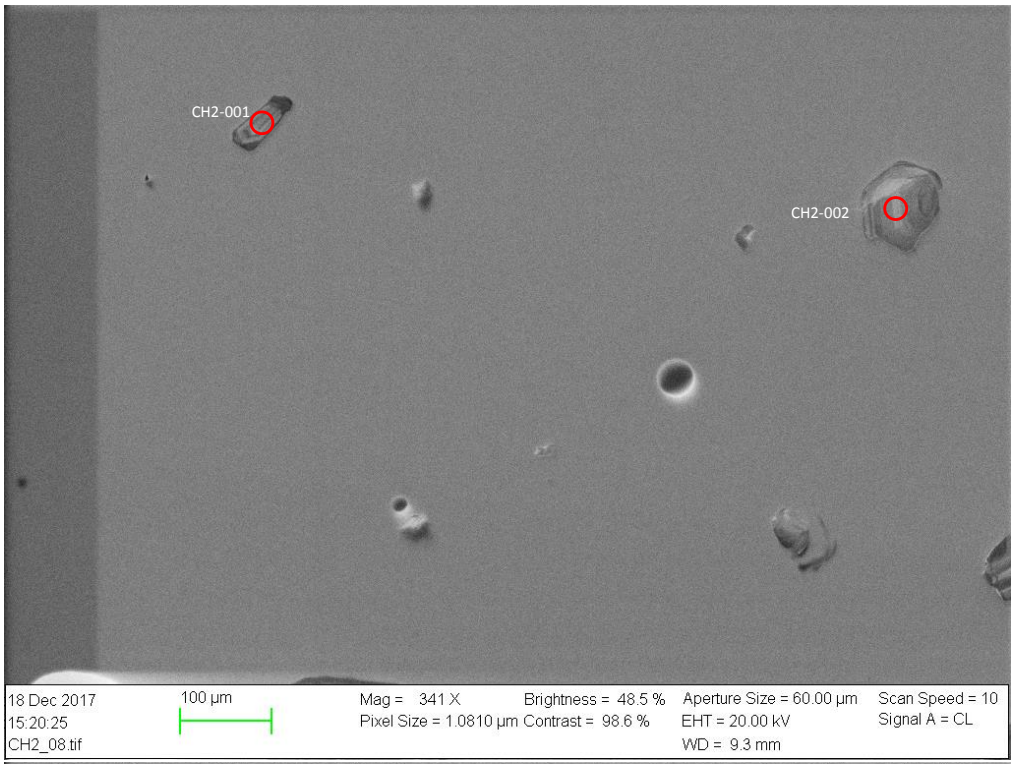
CH2-001
CH2-002
18 Dec 2017
15:20:25
CH2_08.tif
100 µm
Mag = 341 X
Pixel Size = 1.0810 µm
Brightness = 48.5 %
Contrast = 98.6 %
Aperture Size = 60.00 µm
EHT = 20.00 kV
WD = 9.3 mm
Scan Speed = 10
Signal A = CL

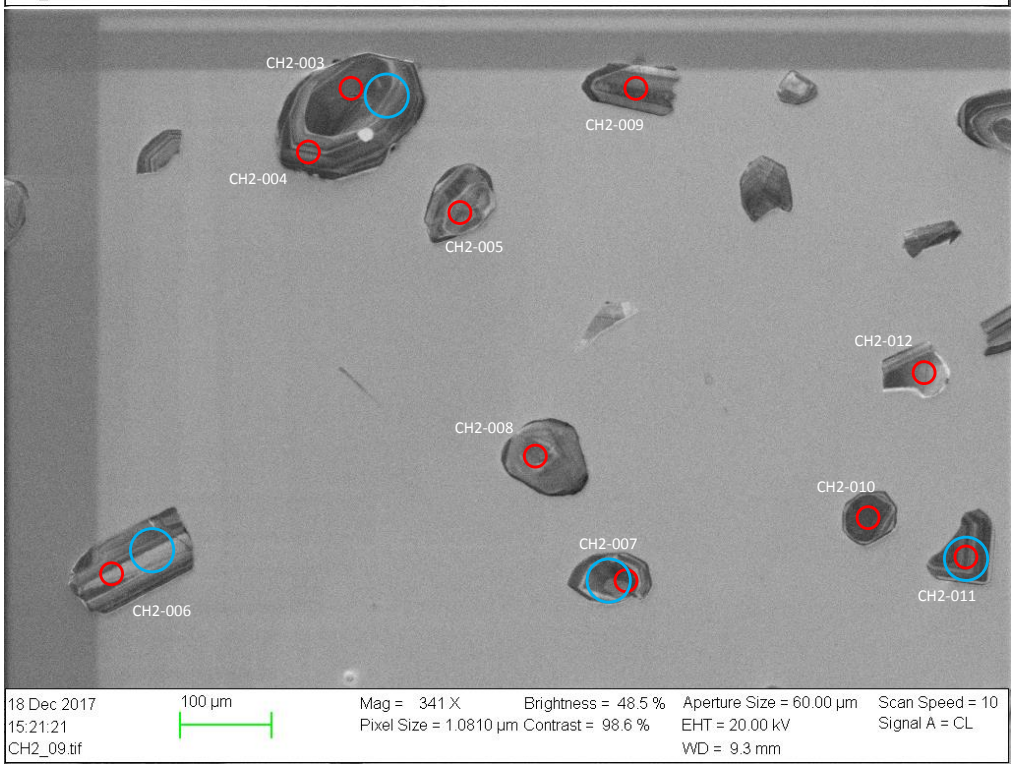
CH2-003
CH2-009
CH2-004
CH2-005
CH2-012
CH2-008
CH2-010
CH2-007
CH2-006
CH2-011
18 Dec 2017
15:21:21
CH2_09.tif
100 µm
Mag = 341 X
Pixel Size = 1.0810 µm
Brightness = 48.5 %
Contrast = 98.6 %
Aperture Size = 60.00 µm
EHT = 20.00 kV
WD = 9.3 mm
Scan Speed = 10
Signal A = CL

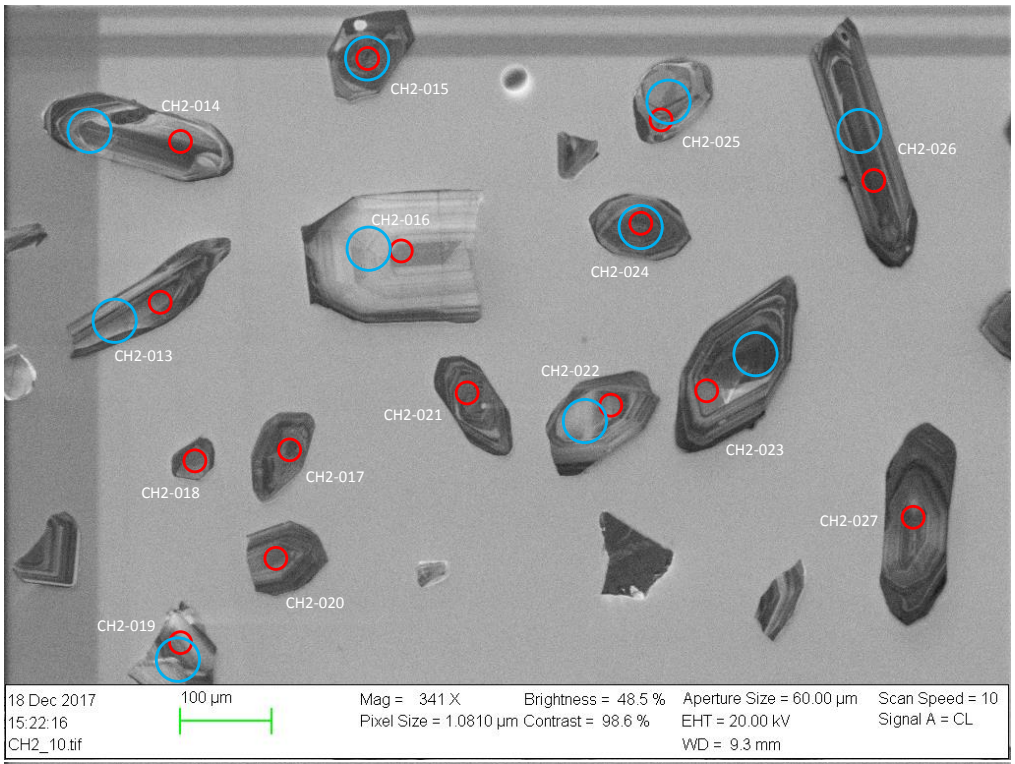
CH2-014
CH2-015
CH2-025
CH2-026
CH2-016
CH2-024
CH2-013
CH2-022
CH2-021
CH2-023
CH2-018
CH2-017
CH2-027
CH2-020
CH2-019
18 Dec 2017
15:22:16
CH2_10.tif
100 µm
Mag = 341 X
Pixel Size = 1.0810 µm
Brightness = 48.5 %
Contrast = 98.6 %
Aperture Size = 60.00 µm
EHT = 20.00 kV
WD = 9.3 mm
Scan Speed = 10
Signal A = CL

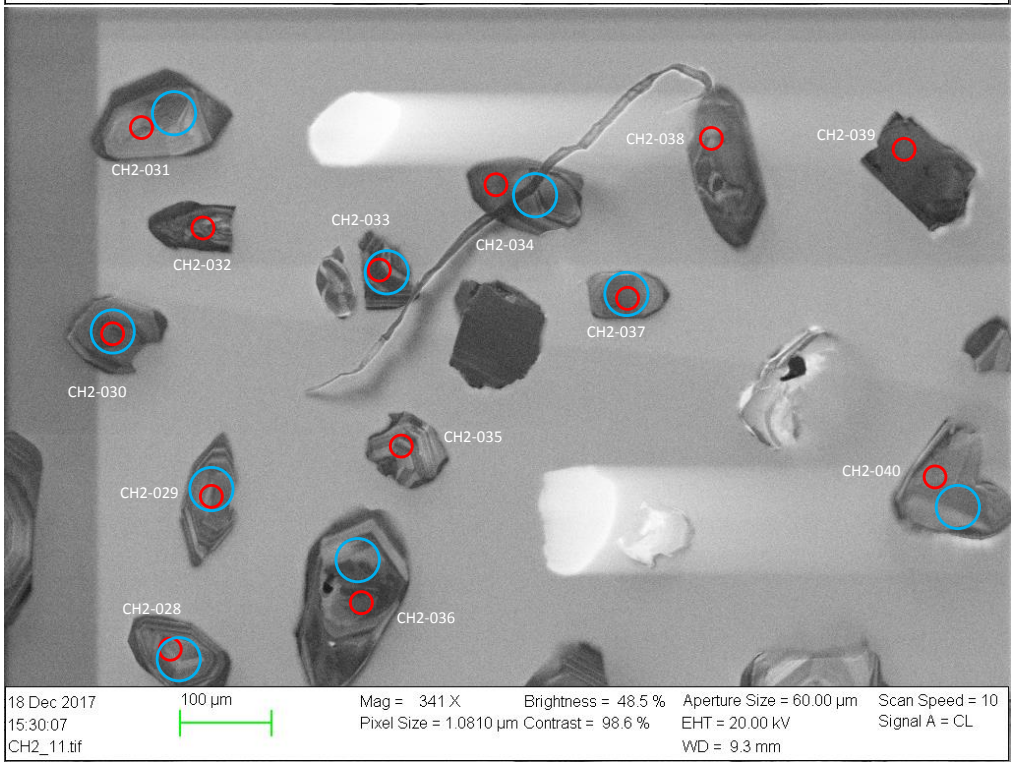
CH2-031
CH2-038
CH2-039
CH2-033
CH2-034
CH2-032
CH2-037
CH2-030
CH2-035
CH2-040
CH2-029
CH2-028
CH2-036
18 Dec 2017
15:30:07
CH2_11.tif
100 µm
Mag = 341 X
Pixel Size = 1.0810 µm
Brightness = 48.5 %
Contrast = 98.6 %
Aperture Size = 60.00 µm
EHT = 20.00 kV
WD = 9.3 mm
Scan Speed = 10
Signal A = CL

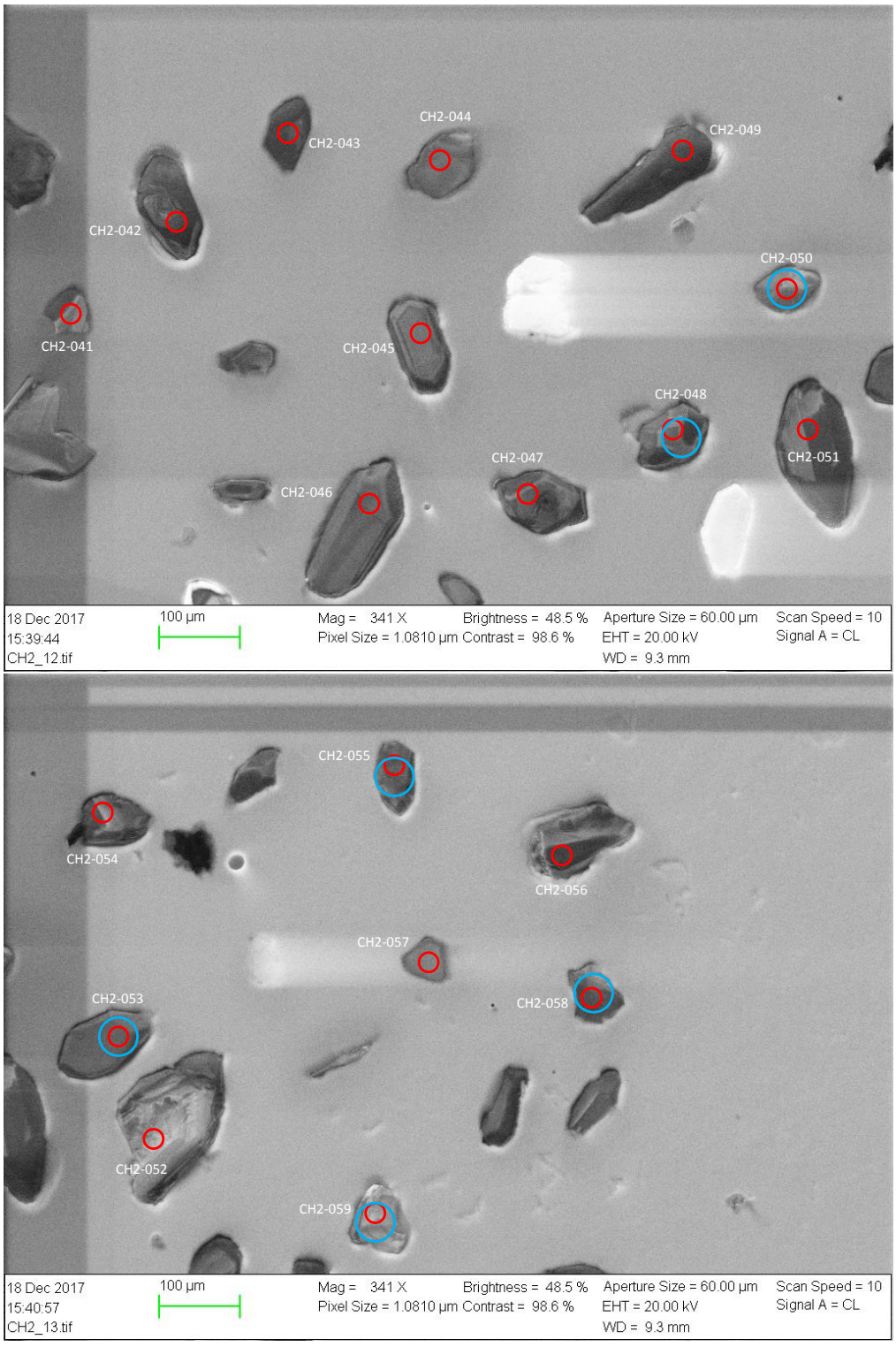
CH2-043
CH2-044
CH2-049
CH2-042
CH2-050
CH2-041
CH2-045
CH2-048
CH2-051
CH2-047
CH2-046
18 Dec 2017
15:39:44
CH2_12.tif
100 µm
Mag = 341 X
Pixel Size = 1.0810 µm
Brightness = 48.5 %
Contrast = 98.6 %
Aperture Size = 60.00 µm
EHT = 20.00 kV
WD = 9.3 mm
Scan Speed = 10
Signal A = CL
CH2-055
CH2-054
CH2-056
CH2-057
CH2-053
CH2-058
CH2-052
CH2-059
18 Dec 2017
15:40:57
CH2_13.tif
100 µm
Mag = 341 X
Pixel Size = 1.0810 µm
Brightness = 48.5 %
Contrast = 98.6 %
Aperture Size = 60.00 µm
EHT = 20.00 kV
WD = 9.3 mm
Scan Speed = 10
Signal A = CL

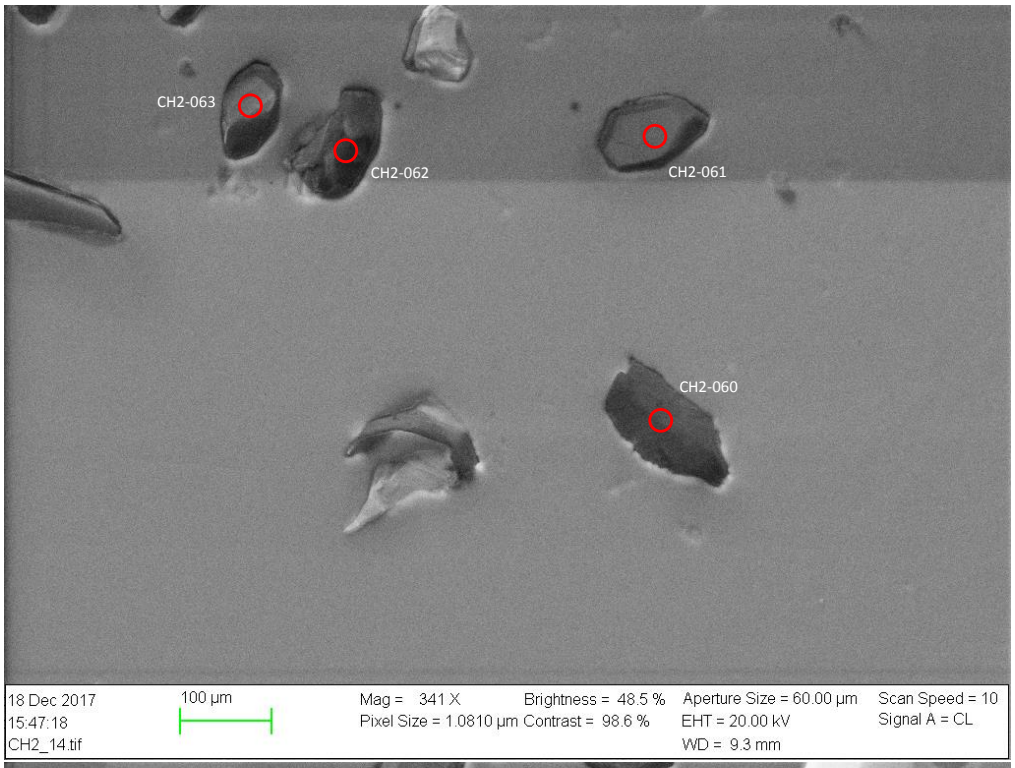
CH2-063
CH2-062
CH2-061
CH2-060
18 Dec 2017
15:47:18
CH2_14.tif
100 µm
Mag = 341 X
Pixel Size = 1.0810 µm
Brightness = 48.5 %
Contrast = 98.6 %
Aperture Size = 60.00 µm
EHT = 20.00 kV
WD = 9.3 mm
Scan Speed = 10
Signal A = CL

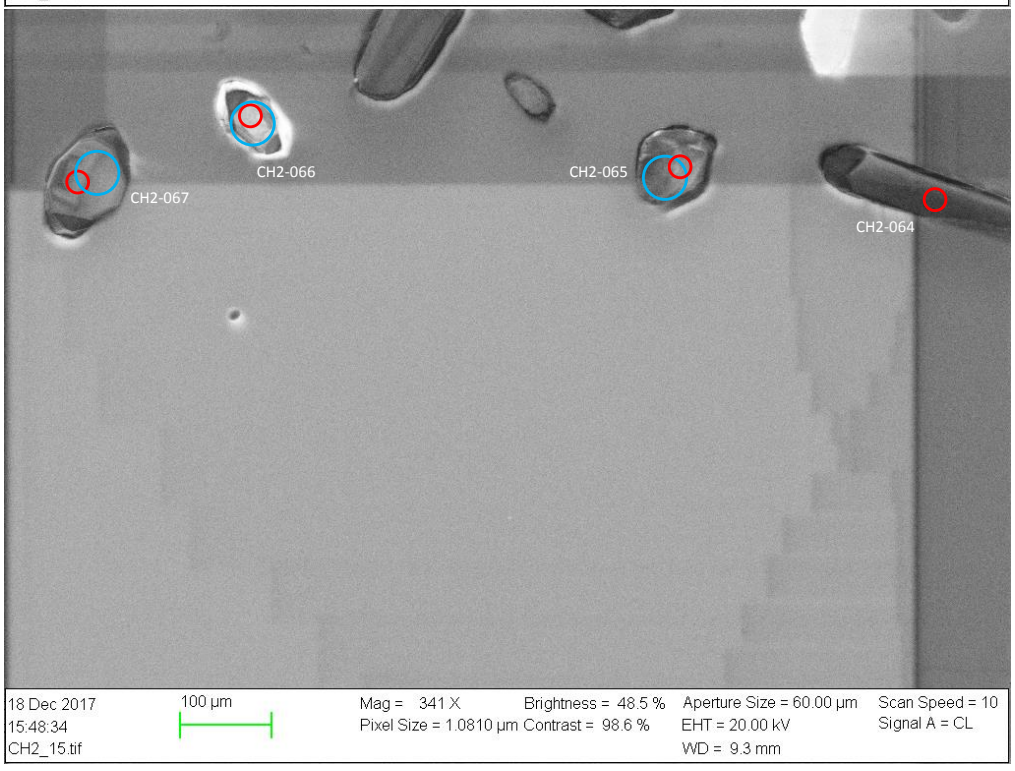
CH2-066
CH2-067
CH2-065
CH2-064
18 Dec 2017
15:48:34
CH2_15.tif
100 µm
Mag = 341 X
Pixel Size = 1.0810 µm
Brightness = 48.5 %
Contrast = 98.6 %
Aperture Size = 60.00 µm
EHT = 20.00 kV
WD = 9.3 mm
Scan Speed = 10
Signal A = CL

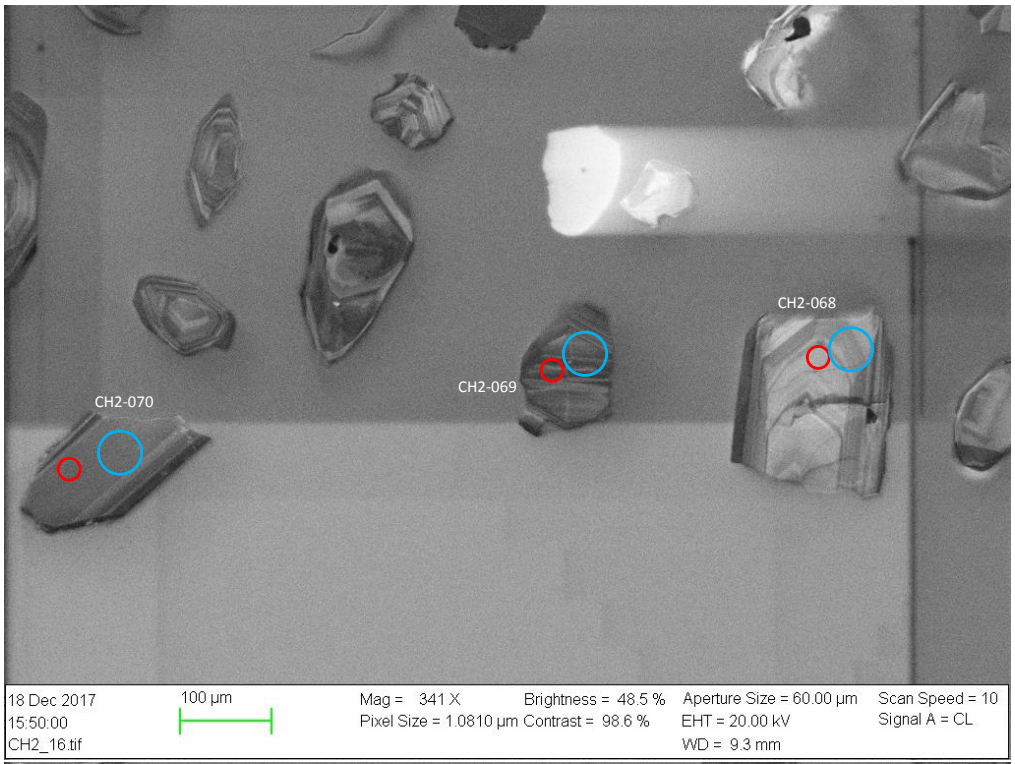
CH2-068
CH2-069
CH2-070
18 Dec 2017
15:50:00
CH2_16.tif
100 µm
Mag = 341 X
Pixel Size = 1.0810 µm
Brightness = 48.5 %
Contrast = 98.6 %
Aperture Size = 60.00 µm
EHT = 20.00 kV
WD = 9.3 mm
Scan Speed = 10
Signal A = CL

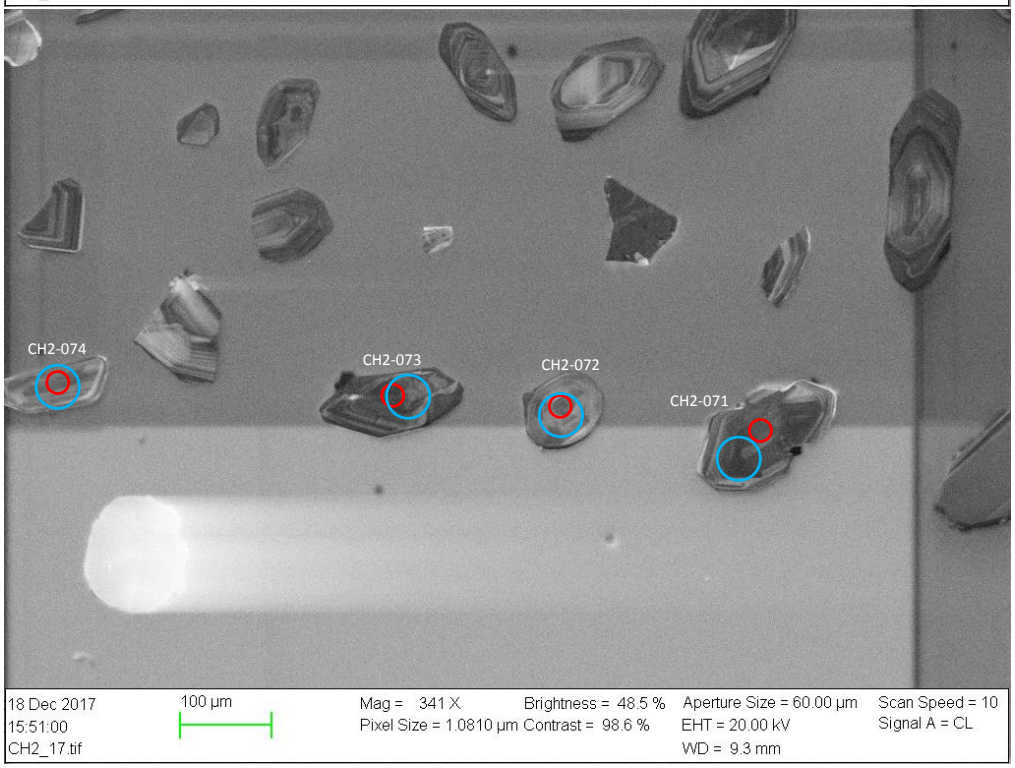
CH2-074
CH2-073
CH2-072
CH2-071
18 Dec 2017
15:51:00
CH2_17.tif
100 µm
Mag = 341 X
Pixel Size = 1.0810 µm
Brightness = 48.5 %
Contrast = 98.6 %
Aperture Size = 60.00 µm
EHT = 20.00 kV
WD = 9.3 mm
Scan Speed = 10
Signal A = CL

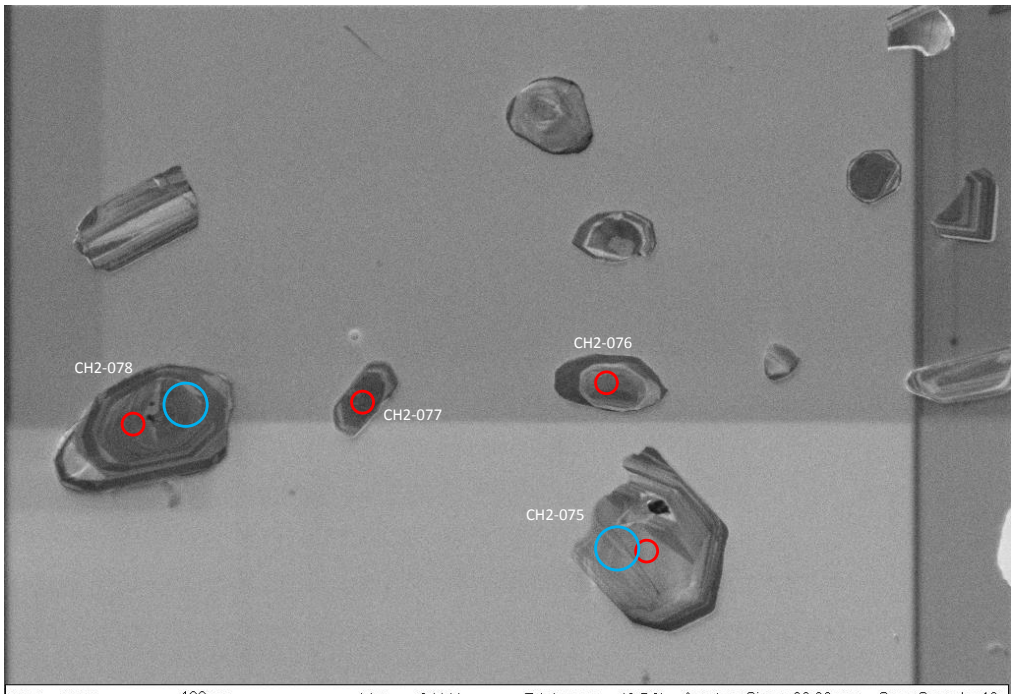
CH2-078
CH2-077
CH2-076
CH2-075
18 Dec 2017
15:51:57
CH2_18.tif
100 µm
Mag = 341 X
Pixel Size = 1.0810 µm
Brightness = 48.5 %
Contrast = 98.6 %
Aperture Size = 60.00 µm
EHT = 20.00 kV
WD = 9.3 mm
Scan Speed = 10
Signal A = CL

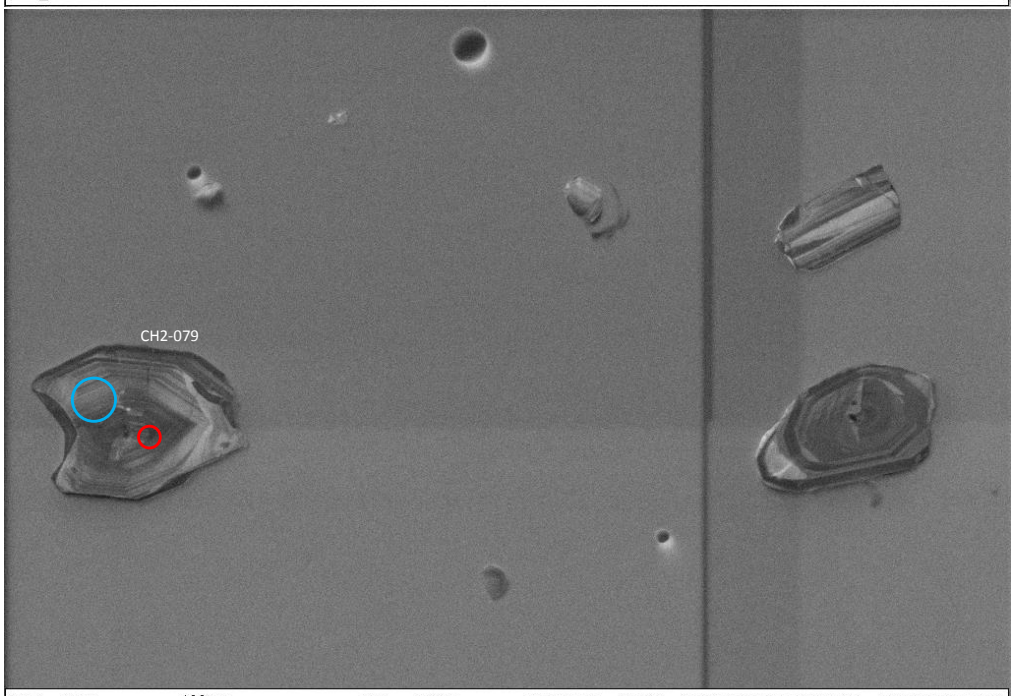
CH2-079
18 Dec 2017
15:54:09
CH2_20.tif
100 µm
Mag = 341 X
Pixel Size = 1.0810 µm
Brightness = 48.5 %
Contrast = 98.6 %
Aperture Size = 60.00 µm
EHT = 20.00 kV
WD = 9.3 mm
Scan Speed = 10
Signal A = CL


CH2-080
18 Dec 2017
15:12:29
CH2_06.tif
100 µm
Mag = 341 X
Pixel Size = 1.0810 µm
Brightness = 48.5 %
Contrast = 98.6 %
Aperture Size = 60.00 µm
EHT = 20.00 kV
WD = 9.3 mm
Scan Speed = 10
Signal A = CL

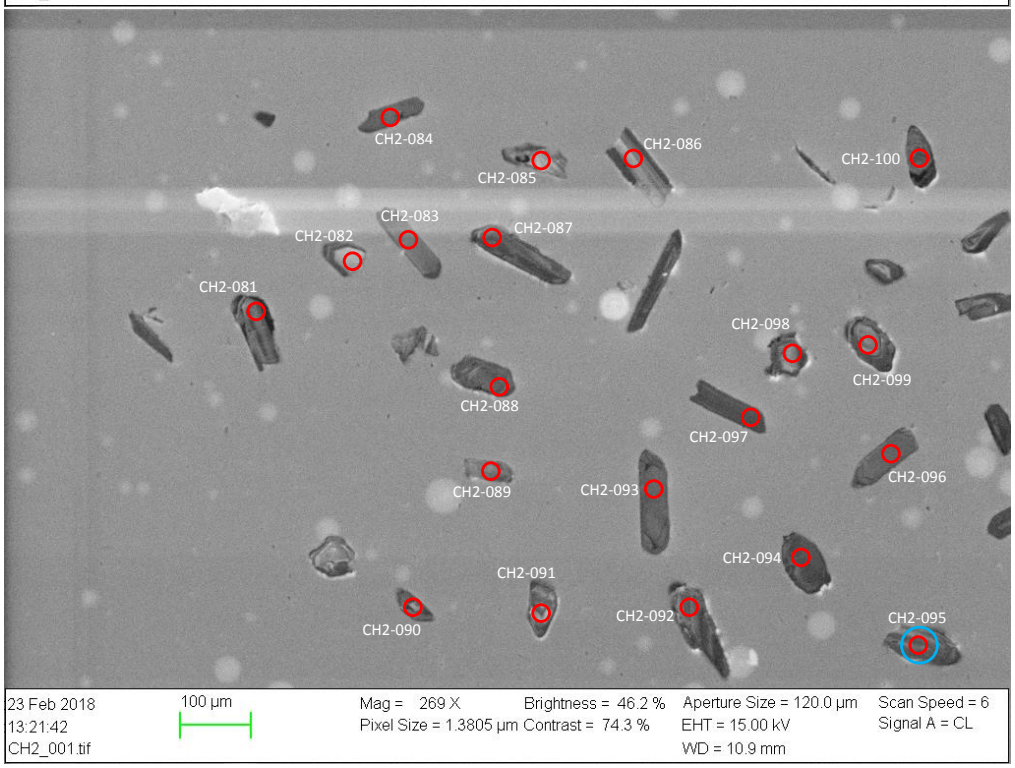
CH2-084
CH2-085
CH2-086
CH2-100
CH2-083
CH2-082
CH2-087
CH2-081
CH2-098
CH2-099
CH2-088
CH2-097
CH2-096
CH2-089
CH2-093
CH2-094
CH2-091
CH2-092
CH2-095
CH2-090
23 Feb 2018
13:21:42
CH2_001.tif
100 µm
Mag = 269 X
Pixel Size = 1.3805 µm
Brightness = 46.2 %
Contrast = 74.3 %
Aperture Size = 120.0 µm
EHT = 15.00 kV
WD = 10.9 mm
Scan Speed = 6
Signal A = CL

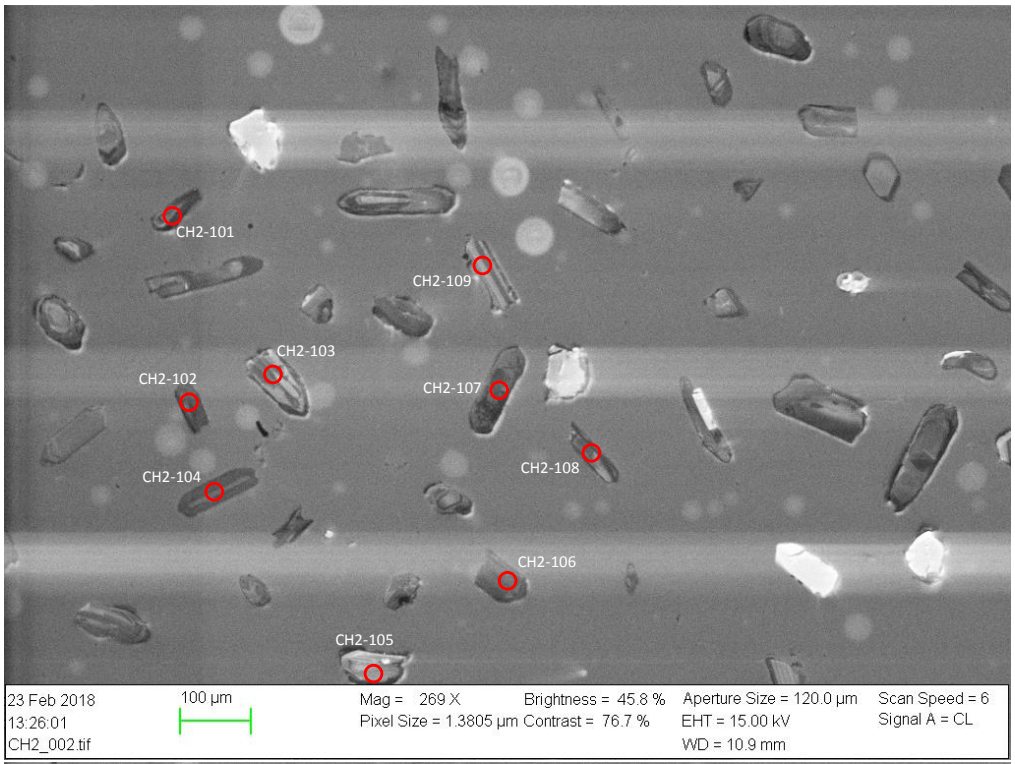
CH2-101
CH2-109
CH2-103
CH2-102
CH2-107
CH2-104
CH2-108
CH2-106
CH2-105
23 Feb 2018
13:26:01
CH2_002.tif
100 µm
Mag = 269 X
Pixel Size = 1.3805 µm
Brightness = 45.8 %
Contrast = 76.7 %
Aperture Size = 120.0 µm
EHT = 15.00 kV
WD = 10.9 mm
Scan Speed = 6
Signal A = CL

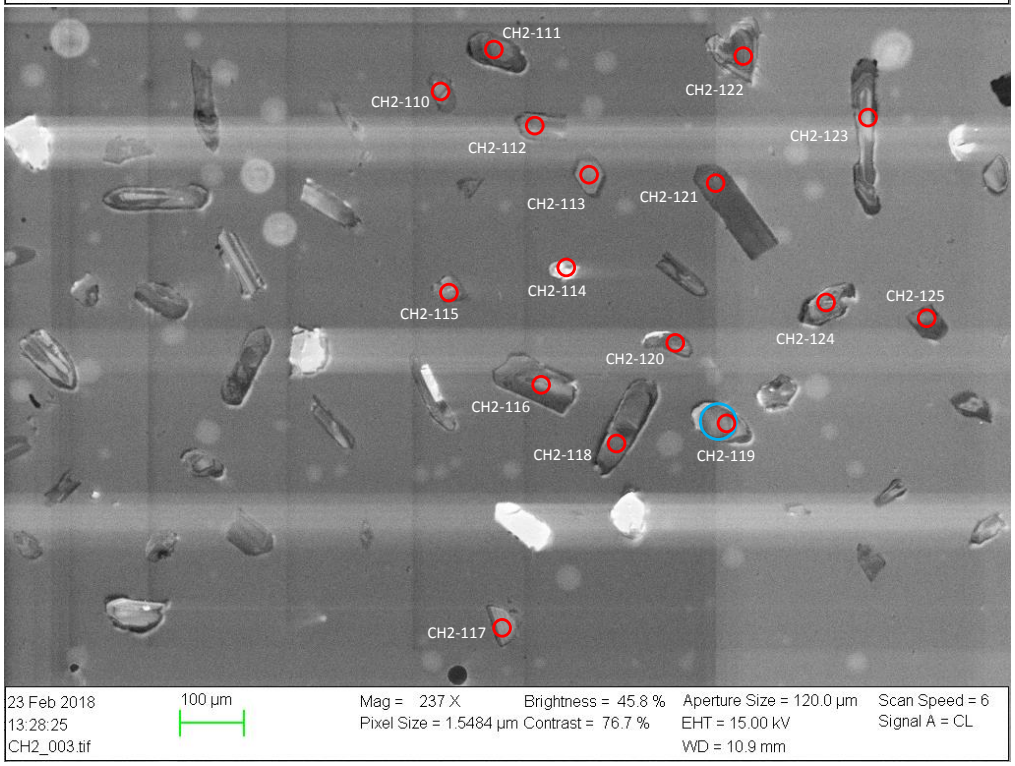
CH2-111
CH2-122
CH2-110
CH2-123
CH2-112
CH2-113
CH2-121
CH2-114
CH2-125
CH2-115
CH2-124
CH2-120
CH2-116
CH2-118
CH2-119
CH2-117
23 Feb 2018
13:28:25
CH2_003.tif
100 µm
Mag = 237 X
Pixel Size = 1.5484 µm
Brightness = 45.8 %
Contrast = 76.7 %
Aperture Size = 120.0 µm
EHT = 15.00 kV
WD = 10.9 mm
Scan Speed = 6
Signal A = CL

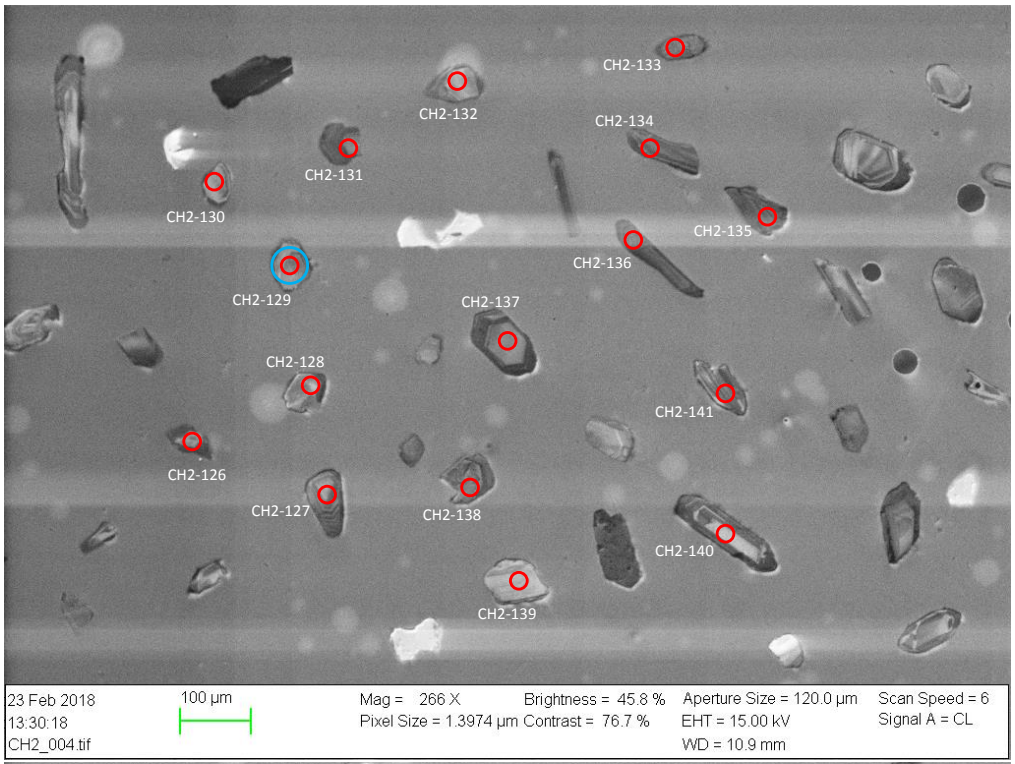
CH2-133
CH2-132
CH2-134
CH2-131
CH2-130
CH2-135
CH2-136
CH2-129
CH2-137
CH2-128
CH2-141
CH2-126
CH2-127
CH2-138
CH2-140
CH2-139
23 Feb 2018
13:30:18
CH2_004.tif
100 µm
Mag = 266 X
Pixel Size = 1.3974 µm
Brightness = 45.8 %
Contrast = 76.7 %
Aperture Size = 120.0 µm
EHT = 15.00 kV
WD = 10.9 mm
Scan Speed = 6
Signal A = CL

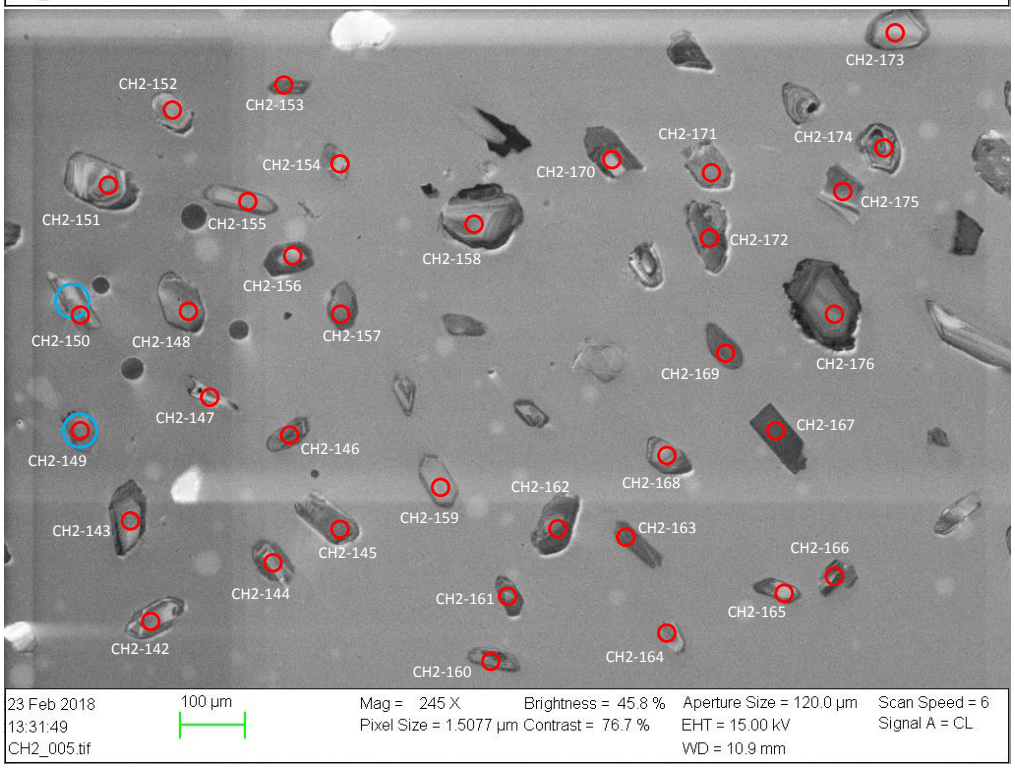
CH2-173
CH2-152
CH2-153
CH2-171
CH2-174
CH2-154
CH2-170
CH2-175
CH2-151
CH2-155
CH2-172
CH2-158
CH2-156
CH2-150
CH2-148
CH2-157
CH2-176
CH2-169
CH2-147
CH2-167
CH2-149
CH2-146
CH2-168
CH2-162
CH2-159
CH2-143
CH2-163
CH2-145
CH2-166
CH2-144
CH2-161
CH2-165
CH2-142
CH2-164
CH2-160
23 Feb 2018
13:31:49
CH2_005.tif
100 µm
Mag = 245 X
Pixel Size = 1.5077 µm
Brightness = 45.8 %
Contrast = 76.7 %
Aperture Size = 120.0 µm
EHT = 15.00 kV
WD = 10.9 mm
Scan Speed = 6
Signal A = CL

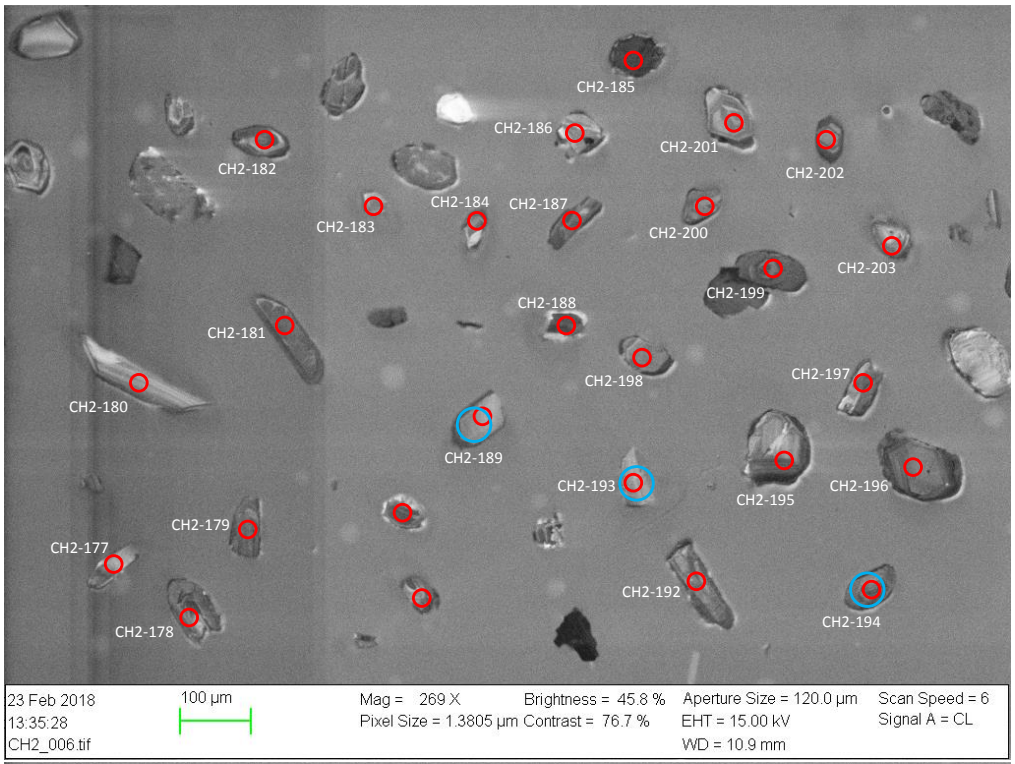
CH2-185
CH2-186
CH2-201
CH2-202
CH2-182
CH2-184
CH2-187
CH2-183
CH2-200
CH2-203
CH2-199
CH2-188
CH2-181
CH2-198
CH2-197
CH2-180
CH2-189
CH2-193
CH2-195
CH2-196
CH2-179
CH2-177
CH2-192
CH2-194
CH2-178
23 Feb 2018
13:35:28
CH2_006.tif
100 µm
Mag = 269 X
Pixel Size = 1.3805 µm
Brightness = 45.8 %
Contrast = 76.7 %
Aperture Size = 120.0 µm
EHT = 15.00 kV
WD = 10.9 mm
Scan Speed = 6
Signal A = CL

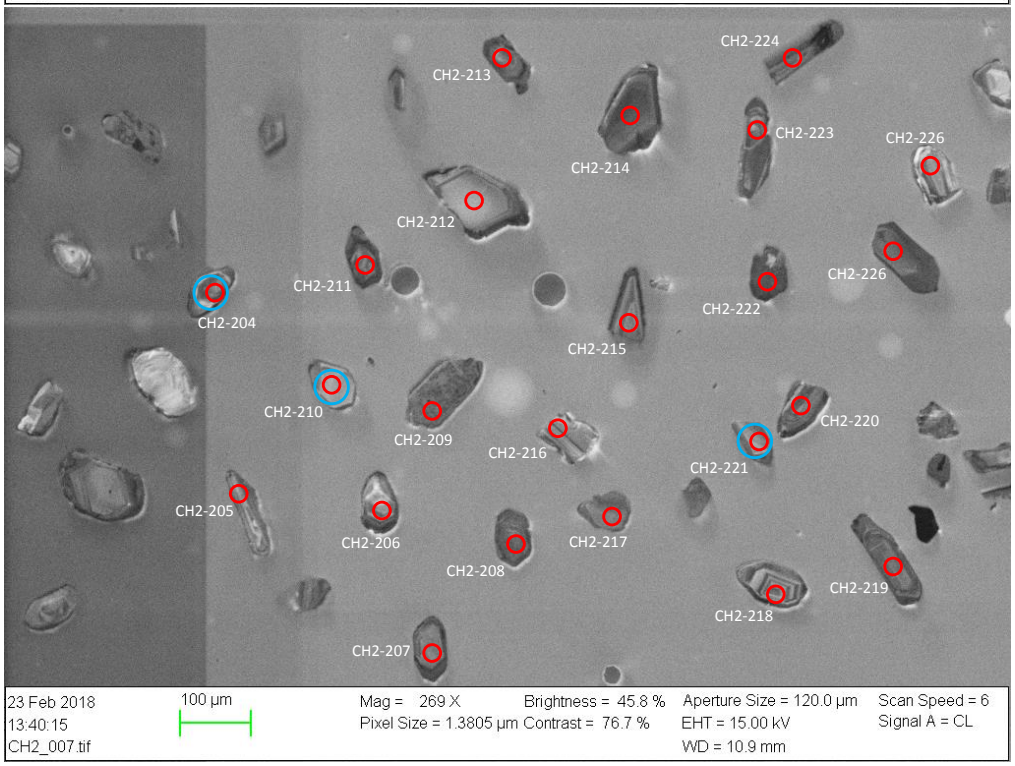
CH2-224
CH2-213
CH2-223
CH2-226
CH2-214
CH2-212
CH2-226
CH2-211
CH2-222
CH2-204
CH2-215
CH2-210
CH2-220
CH2-209
CH2-216
CH2-221
CH2-205
CH2-206
CH2-217
CH2-208
CH2-219
CH2-218
CH2-207
23 Feb 2018
13:40:15
CH2_007.tif
100 µm
Mag = 269 X
Pixel Size = 1.3805 µm
Brightness = 45.8 %
Contrast = 76.7 %
Aperture Size = 120.0 µm
EHT = 15.00 kV
WD = 10.9 mm
Scan Speed = 6
Signal A = CL

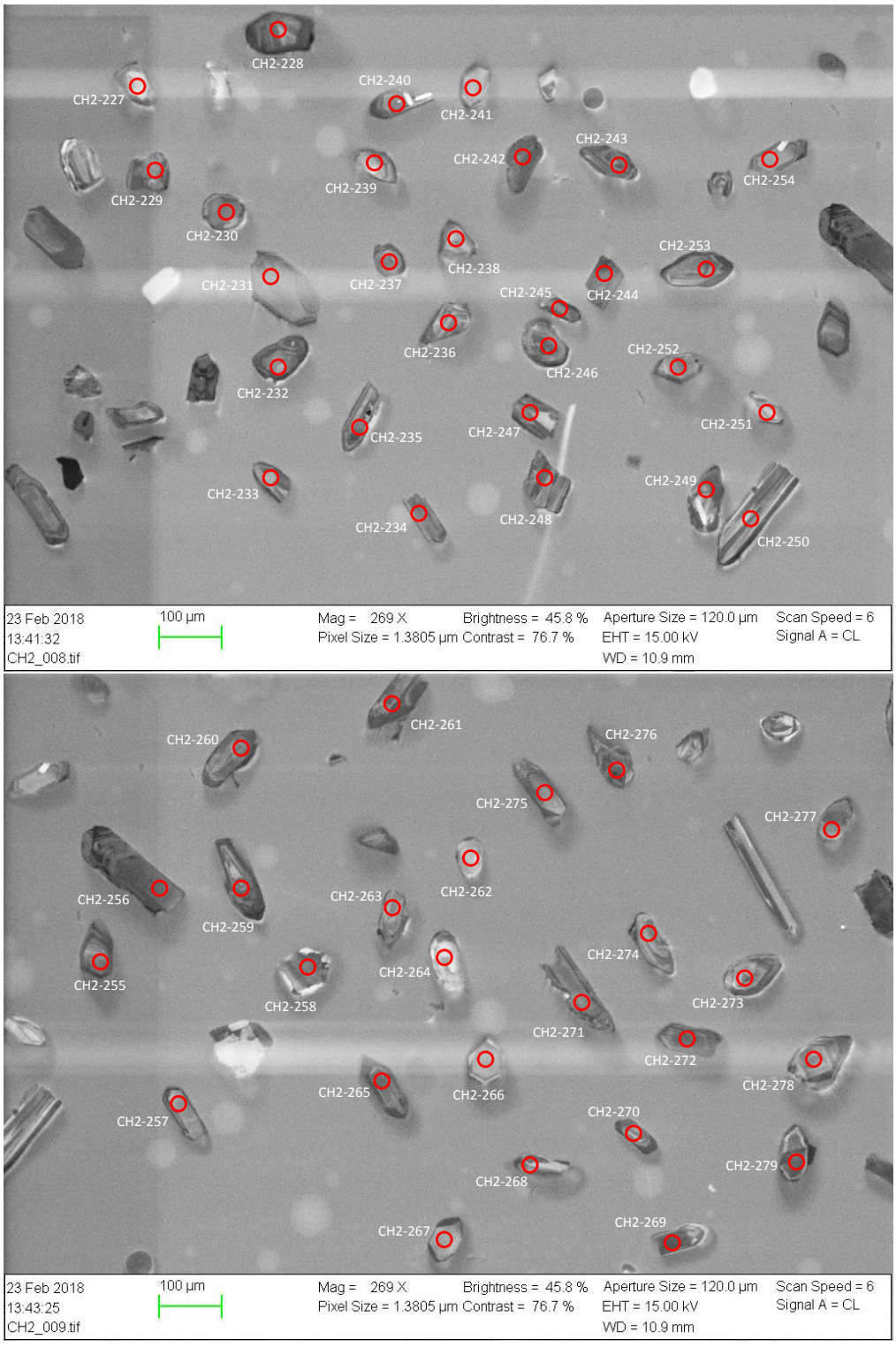
CH2-228
CH2-227
CH2-240
CH2-241
CH2-243
CH2-242
CH2-254
CH2-239
CH2-229
CH2-230
CH2-253
CH2-238
CH2-231
CH2-237
CH2-245
CH2-244
CH2-236
CH2-252
CH2-246
CH2-232
CH2-251
CH2-235
CH2-247
CH2-249
CH2-233
CH2-248
CH2-234
CH2-250
23 Feb 2018
13:41:32
CH2_008.tif
100 µm
Mag = 269 X
Pixel Size = 1.3805 µm
Brightness = 45.8 %
Contrast = 76.7 %
Aperture Size = 120.0 µm
EHT = 15.00 kV
WD = 10.9 mm
Scan Speed = 6
Signal A = CL
CH2-261
CH2-260
CH2-276
CH2-275
CH2-277
CH2-256
CH2-263
CH2-262
CH2-259
CH2-274
CH2-264
CH2-255
CH2-273
CH2-258
CH2-271
CH2-272
CH2-278
CH2-265
CH2-266
CH2-257
CH2-270
CH2-279
CH2-268
CH2-269
CH2-267
23 Feb 2018
13:43:25
CH2_009.tif
100 µm
Mag = 269 X
Pixel Size = 1.3805 µm
Brightness = 45.8 %
Contrast = 76.7 %
Aperture Size = 120.0 µm
EHT = 15.00 kV
WD = 10.9 mm
Scan Speed = 6
Signal A = CL

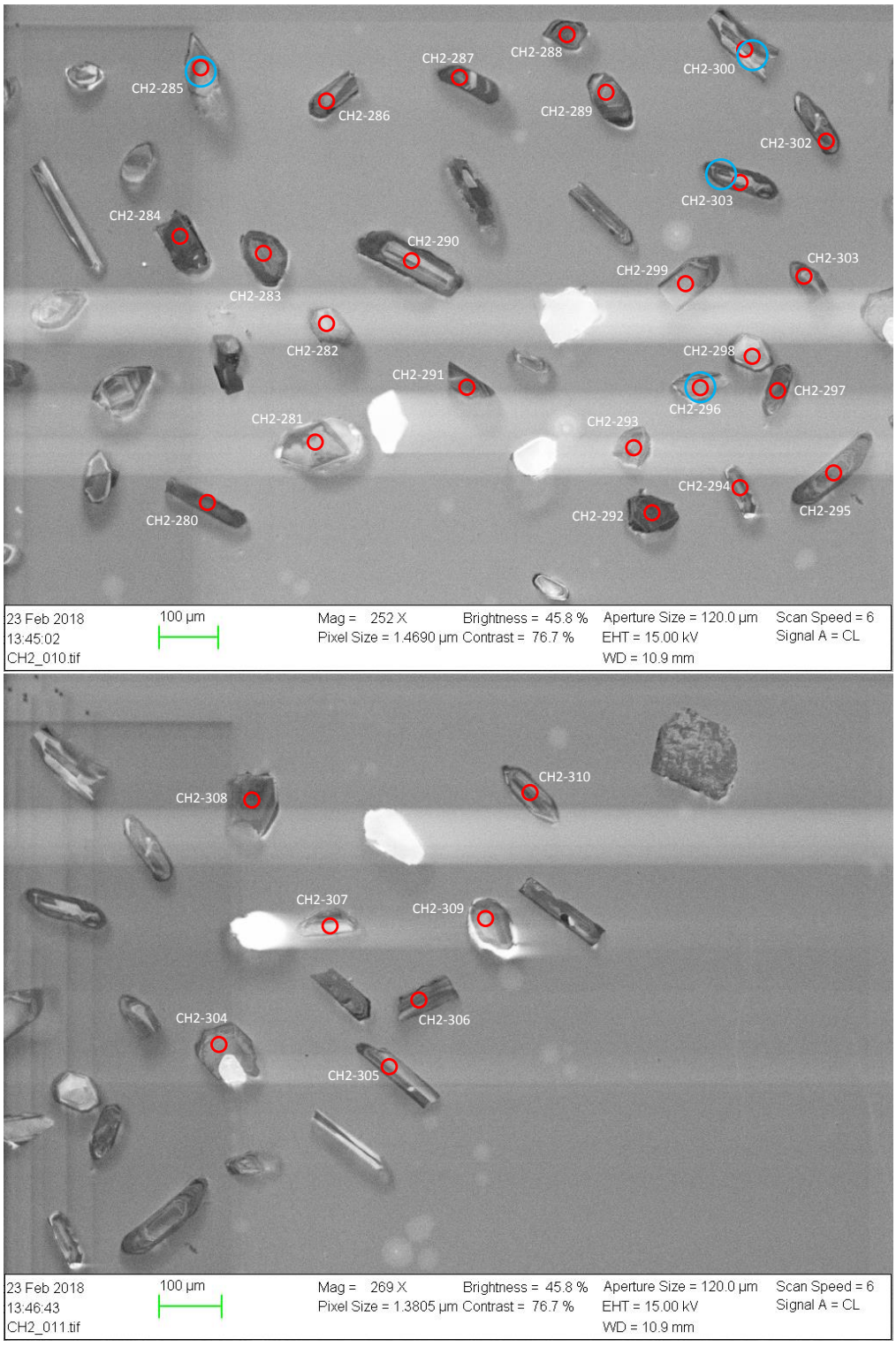
CH2-285
CH2-286
CH2-287
CH2-288
CH2-289
CH2-300
CH2-302
CH2-303
CH2-284
CH2-290
CH2-283
CH2-299
CH2-303
CH2-282
CH2-298
CH2-291
CH2-297
CH2-296
CH2-281
CH2-293
CH2-294
CH2-280
CH2-292
CH2-295
23 Feb 2018
13:45:02
CH2_010.tif
100 µm
Mag = 252 X
Pixel Size = 1.4690 µm
Brightness = 45.8 %
Contrast = 76.7 %
Aperture Size = 120.0 µm
EHT = 15.00 kV
WD = 10.9 mm
Scan Speed = 6
Signal A = CL
CH2-310
CH2-308
CH2-307
CH2-309
CH2-304
CH2-306
CH2-305
23 Feb 2018
13:46:43
CH2_011.tif
100 µm
Mag = 269 X
Pixel Size = 1.3805 µm
Brightness = 45.8 %
Contrast = 76.7 %
Aperture Size = 120.0 µm
EHT = 15.00 kV
WD = 10.9 mm
Scan Speed = 6
Signal A = CL

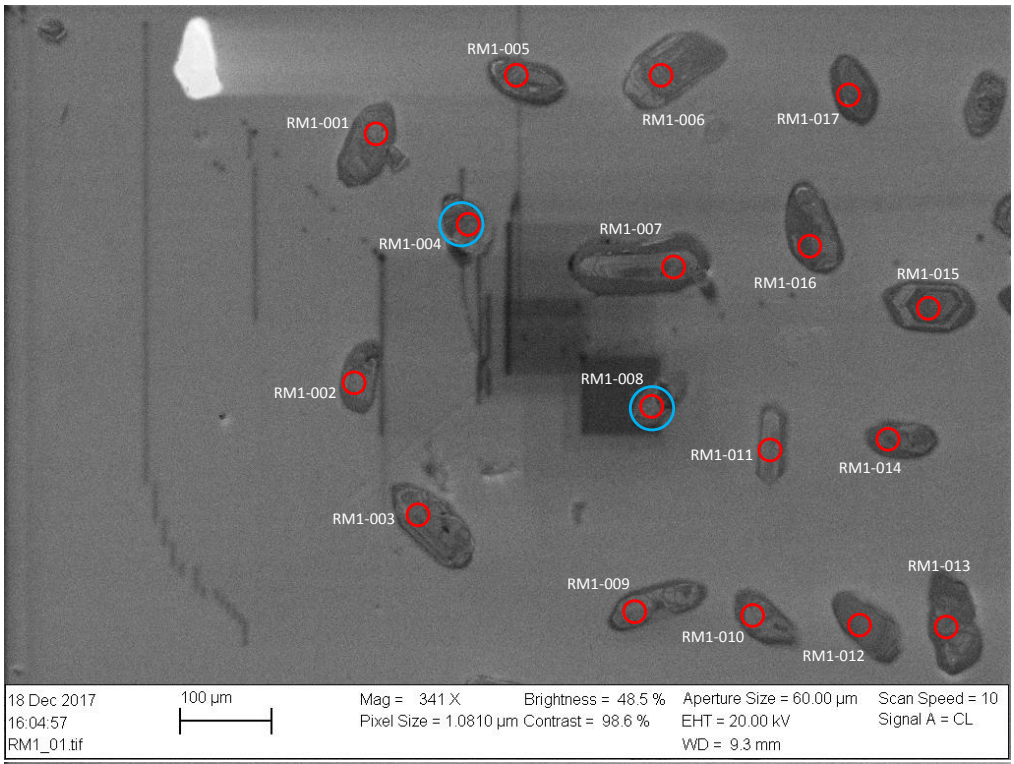
RM1-005
RM1-001
RM1-006
RM1-017
RM1-004
RM1-007
RM1-016
RM1-015
RM1-002
RM1-008
RM1-011
RM1-014
RM1-003
RM1-013
RM1-009
RM1-010
RM1-012
18 Dec 2017
16:04:57
RM1_01.tif
100 µm
Mag = 341 X
Pixel Size = 1.0810 µm
Brightness = 48.5 %
Contrast = 98.6 %
Aperture Size = 60.00 µm
EHT = 20.00 kV
WD = 9.3 mm
Scan Speed = 10
Signal A = CL

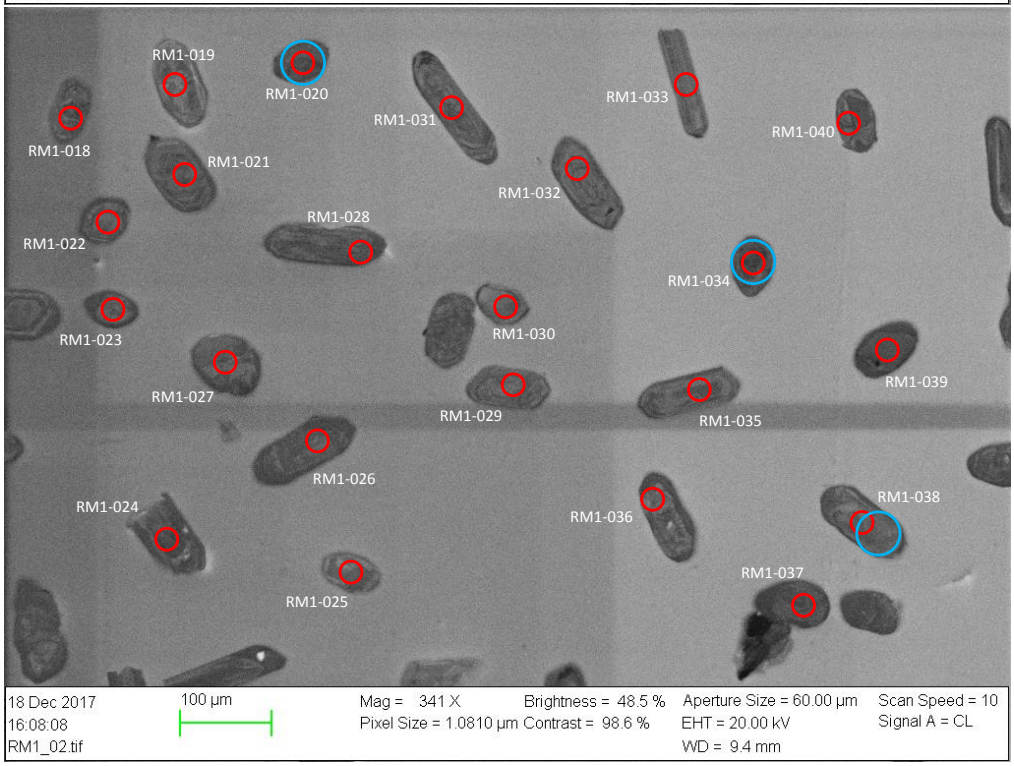
RM1-019
RM1-020
RM1-031
RM1-033
RM1-040
RM1-018
RM1-021
RM1-032
RM1-028
RM1-022
RM1-034
RM1-023
RM1-030
RM1-039
RM1-027
RM1-029
RM1-035
RM1-026
RM1-024
RM1-036
RM1-038
RM1-037
RM1-025
18 Dec 2017
16:08:08
RM1_02.tif
100 µm
Mag = 341 X
Pixel Size = 1.0810 µm
Brightness = 48.5 %
Contrast = 98.6 %
Aperture Size = 60.00 µm
EHT = 20.00 kV
WD = 9.4 mm
Scan Speed = 10
Signal A = CL

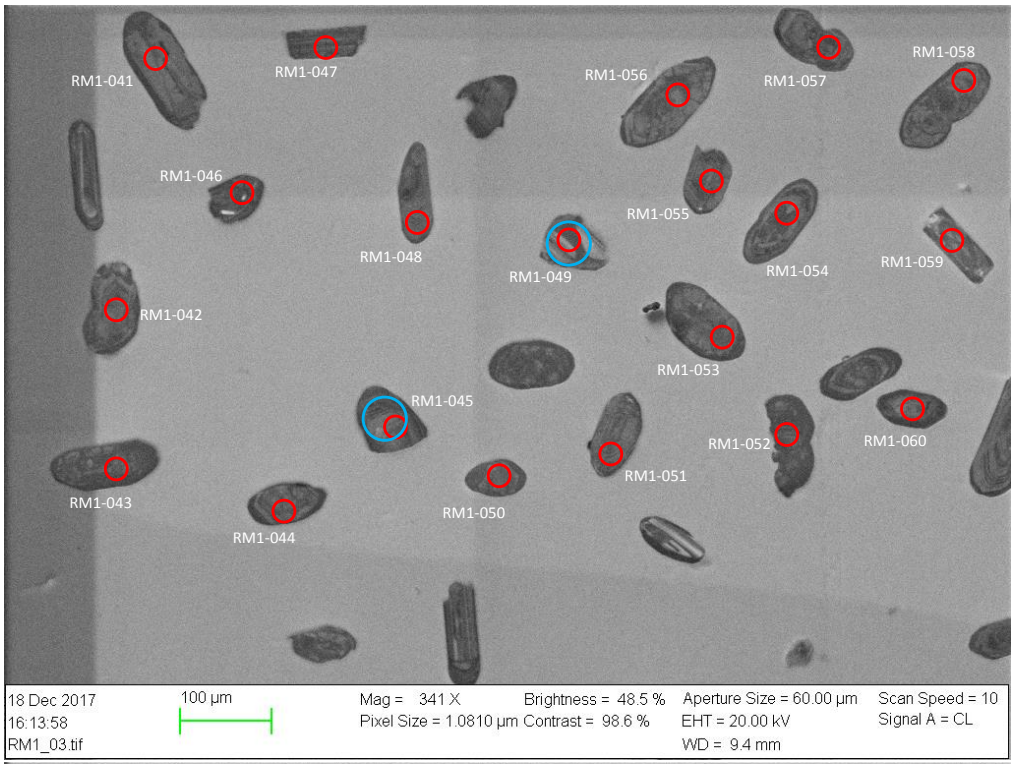
RM1-041
RM1-047
RM1-056
RM1-057
RM1-058
RM1-046
RM1-055
RM1-048
RM1-049
RM1-054
RM1-059
RM1-042
RM1-053
RM1-045
RM1-052
RM1-060
RM1-051
RM1-043
RM1-050
RM1-044
18 Dec 2017
16:13:58
RM1_03.tif
100 µm
Mag = 341 X
Pixel Size = 1.0810 µm
Brightness = 48.5 %
Contrast = 98.6 %
Aperture Size = 60.00 µm
EHT = 20.00 kV
WD = 9.4 mm
Scan Speed = 10
Signal A = CL

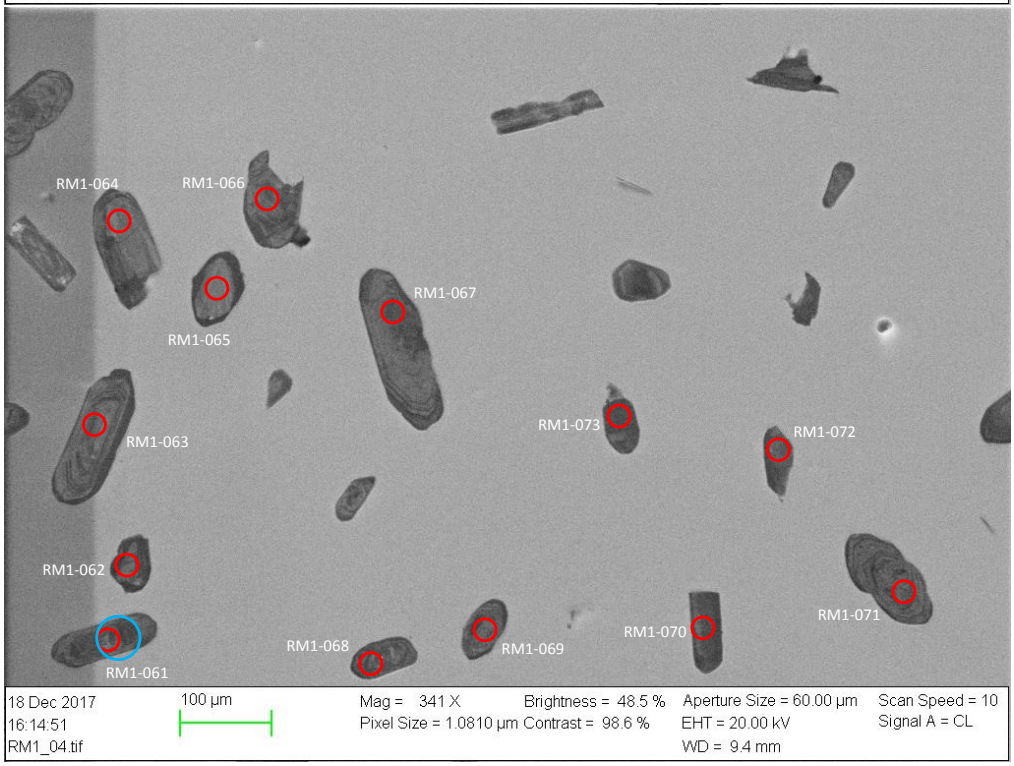
RM1-064
RM1-066
RM1-067
RM1-065
RM1-073
RM1-072
RM1-063
RM1-062
RM1-071
RM1-070
RM1-068
RM1-069
RM1-061
18 Dec 2017
16:14:51
RM1_04.tif
100 µm
Mag = 341 X
Pixel Size = 1.0810 µm
Brightness = 48.5 %
Contrast = 98.6 %
Aperture Size = 60.00 µm
EHT = 20.00 kV
WD = 9.4 mm
Scan Speed = 10
Signal A = CL

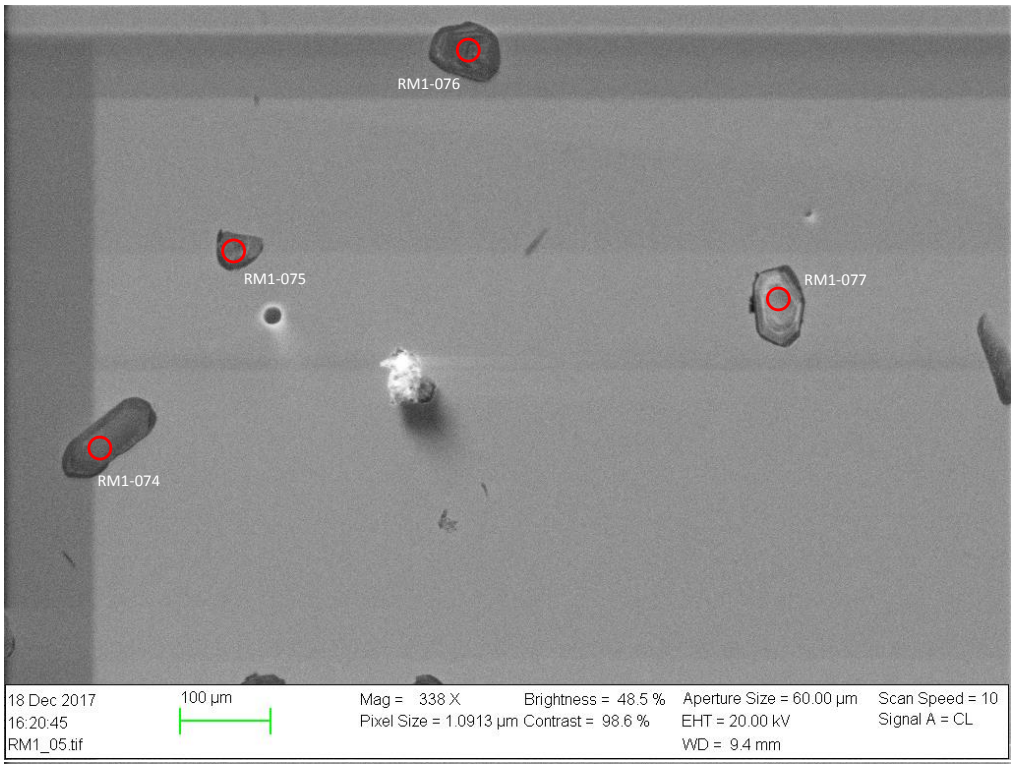
RM1-076
RM1-075
RM1-077
RM1-074
18 Dec 2017
16:20:45
RM1_05.tif
100 µm
Mag = 338 X
Pixel Size = 1.0913 µm
Brightness = 48.5 %
Contrast = 98.6 %
Aperture Size = 60.00 µm
EHT = 20.00 kV
WD = 9.4 mm
Scan Speed = 10
Signal A = CL

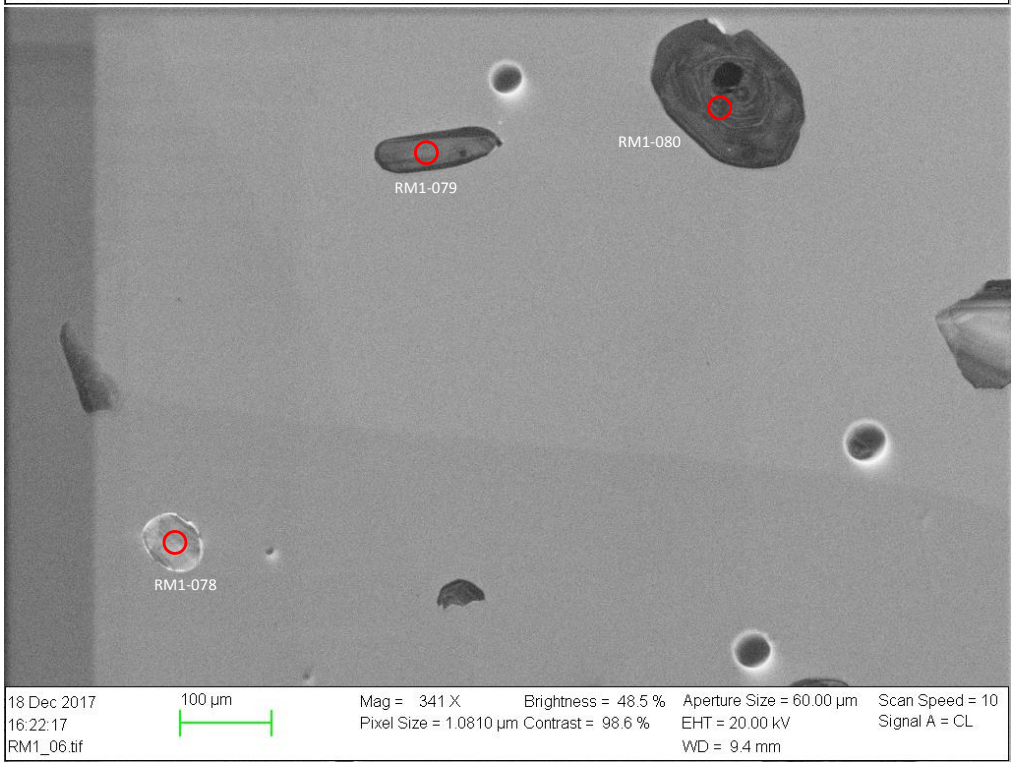
RM1-080
RM1-079
RM1-078
18 Dec 2017
16:22:17
RM1_06.tif
100 µm
Mag = 341 X
Pixel Size = 1.0810 µm
Brightness = 48.5 %
Contrast = 98.6 %
Aperture Size = 60.00 µm
EHT = 20.00 kV
WD = 9.4 mm
Scan Speed = 10
Signal A = CL

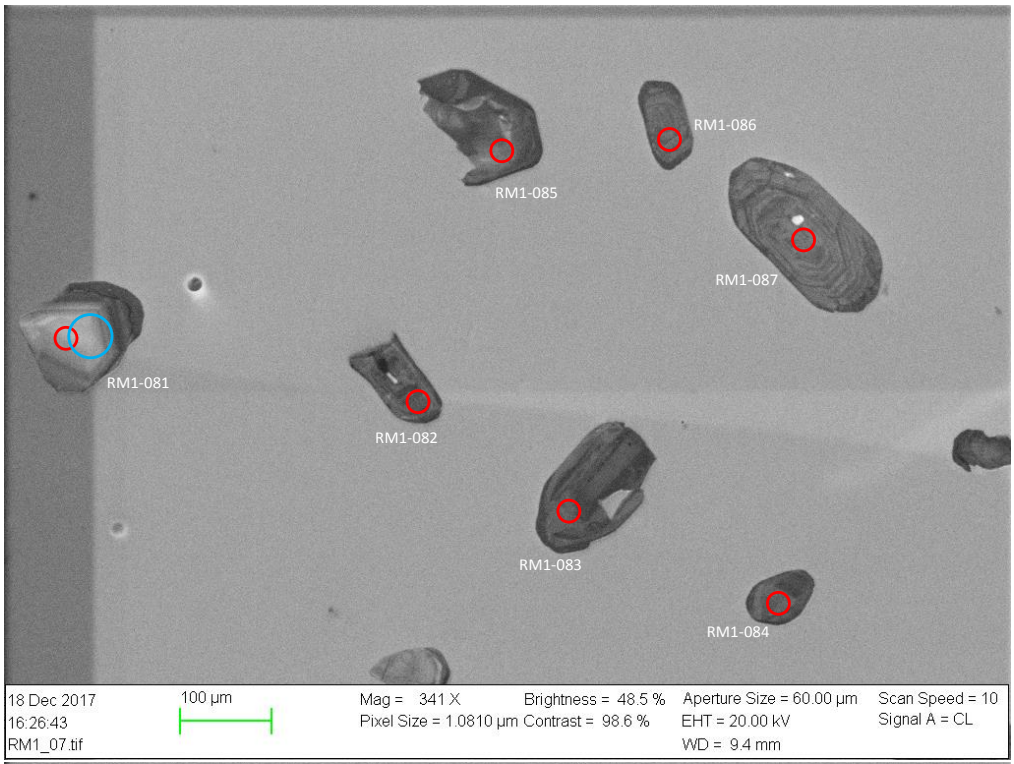
RM1-085
RM1-086
RM1-087
RM1-081
RM1-082
RM1-083
RM1-084
18 Dec 2017
16:26:43
RM1_07.tif
100 µm
Mag = 341 X
Pixel Size = 1.0810 µm
Brightness = 48.5 %
Contrast = 98.6 %
Aperture Size = 60.00 µm
EHT = 20.00 kV
WD = 9.4 mm
Scan Speed = 10
Signal A = CL

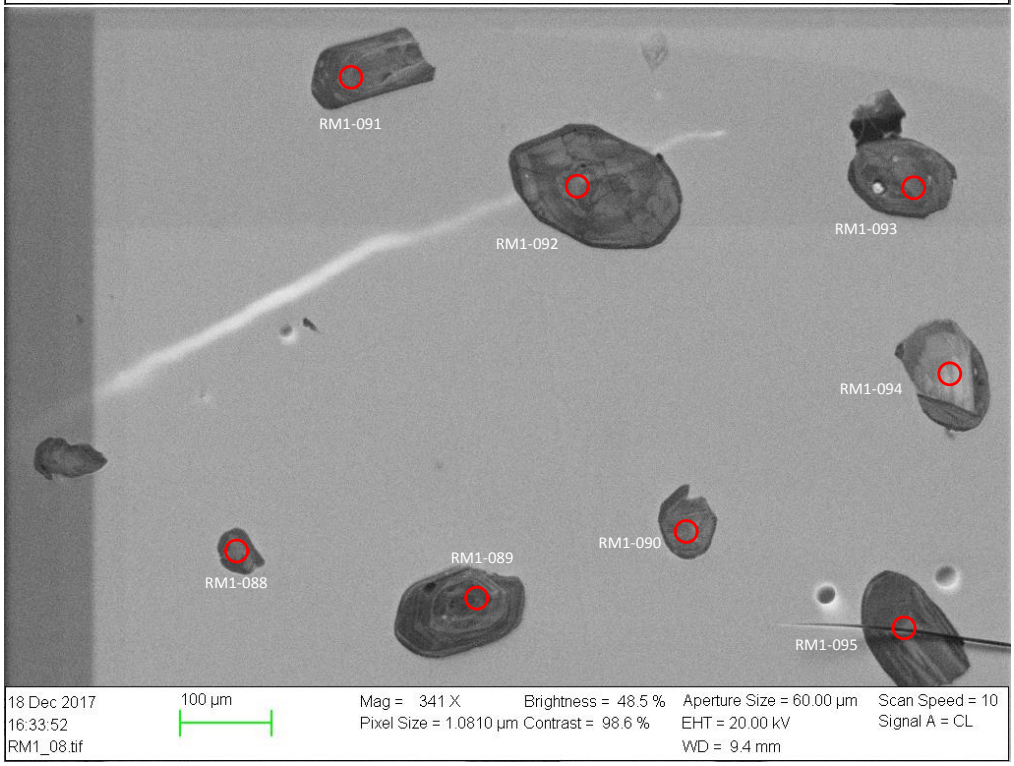
RM1-091
RM1-092
RM1-093
RM1-094
RM1-088
RM1-089
RM1-090
RM1-095
18 Dec 2017
16:33:52
RM1_08.tif
100 µm
Mag = 341 X
Pixel Size = 1.0810 µm
Brightness = 48.5 %
Contrast = 98.6 %
Aperture Size = 60.00 µm
EHT = 20.00 kV
WD = 9.4 mm
Scan Speed = 10
Signal A = CL

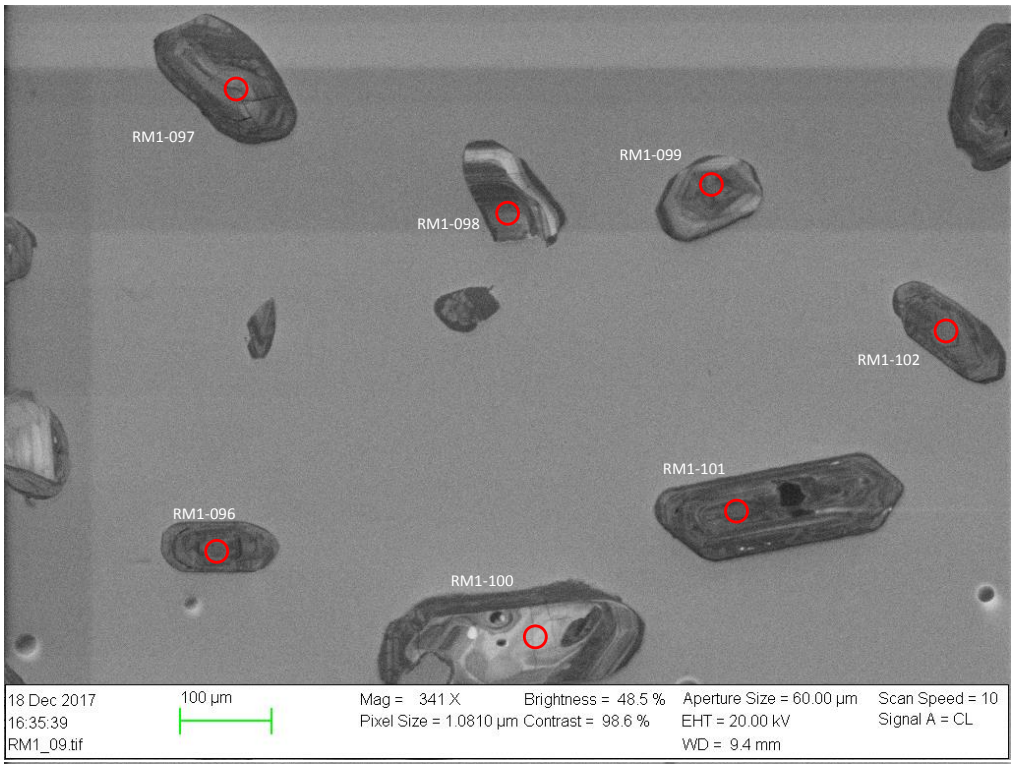
RM1-097
RM1-099
RM1-098
RM1-102
RM1-101
RM1-096
RM1-100
18 Dec 2017
16:35:39
RM1_09.tif
100 µm
Mag = 341 X
Pixel Size = 1.0810 µm
Brightness = 48.5 %
Contrast = 98.6 %
Aperture Size = 60.00 µm
EHT = 20.00 kV
WD = 9.4 mm
Scan Speed = 10
Signal A = CL

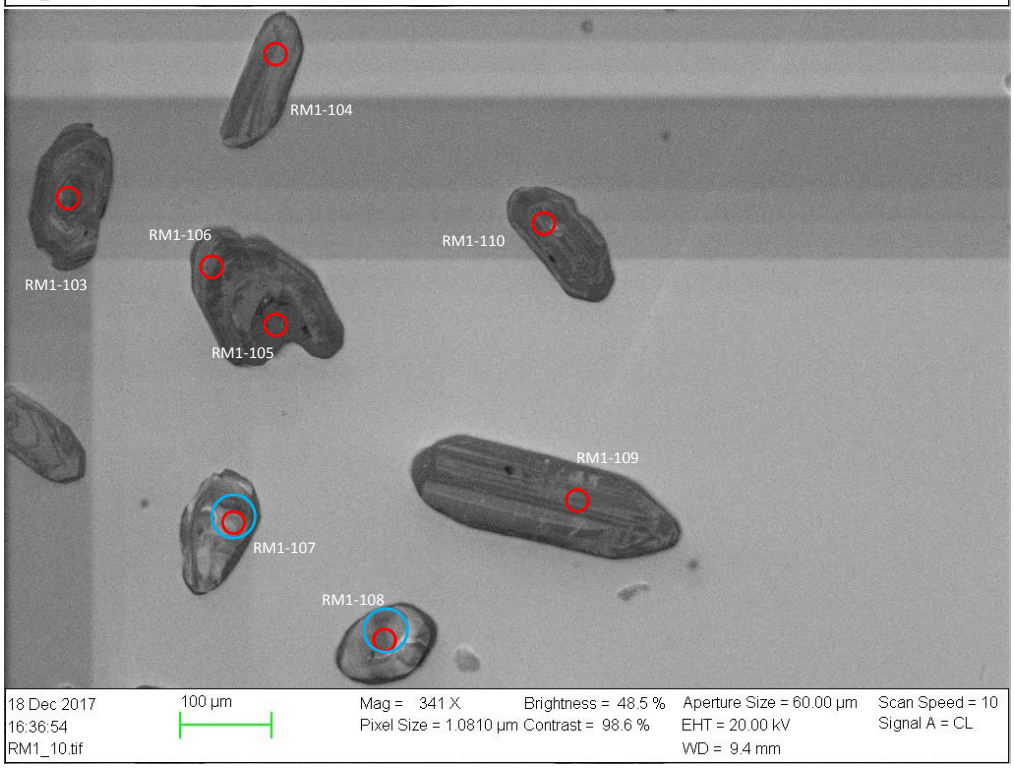
RM1-104
RM1-106
RM1-110
RM1-103
RM1-105
RM1-109
RM1-107
RM1-108
18 Dec 2017
16:36:54
RM1_10.tif
100 µm
Mag = 341 X
Pixel Size = 1.0810 µm
Brightness = 48.5 %
Contrast = 98.6 %
Aperture Size = 60.00 µm
EHT = 20.00 kV
WD = 9.4 mm
Scan Speed = 10
Signal A = CL

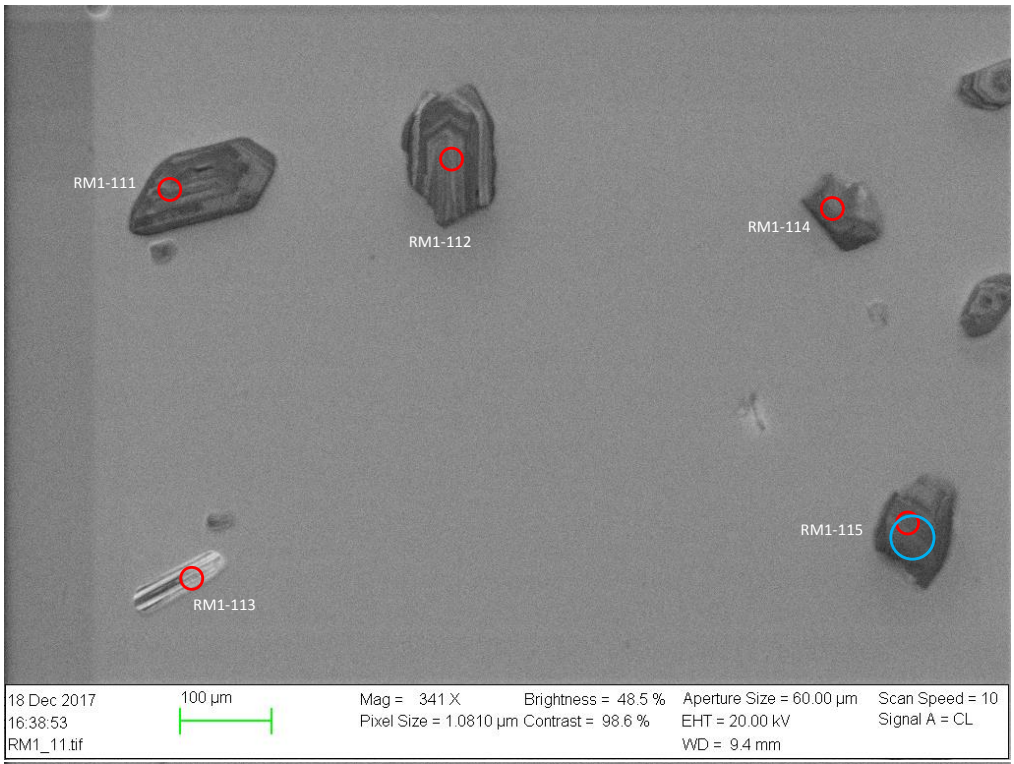
RM1-111
RM1-112
RM1-114
RM1-115
RM1-113
18 Dec 2017
16:38:53
RM1_11.tif
100 µm
Mag = 341 X
Pixel Size = 1.0810 µm
Brightness = 48.5 %
Contrast = 98.6 %
Aperture Size = 60.00 µm
EHT = 20.00 kV
WD = 9.4 mm
Scan Speed = 10
Signal A = CL

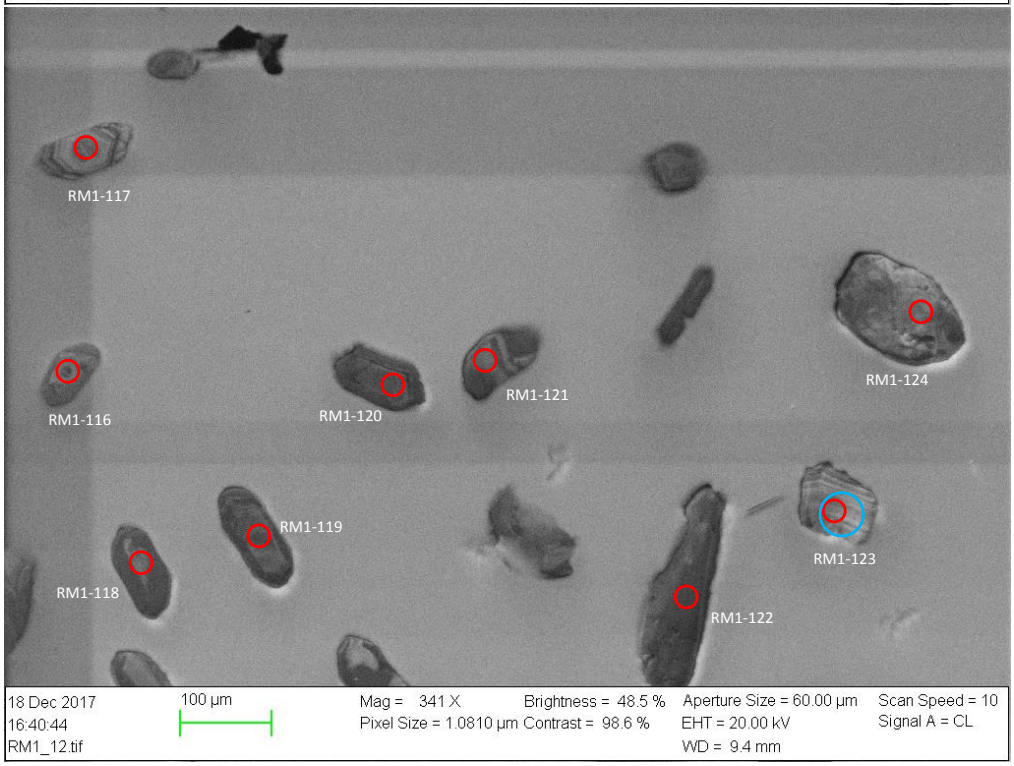
RM1-117
RM1-116
RM1-120
RM1-121
RM1-124
RM1-119
RM1-123
RM1-118
RM1-122
18 Dec 2017
16:40:44
RM1_12.tif
100 µm
Mag = 341 X
Pixel Size = 1.0810 µm
Brightness = 48.5 %
Contrast = 98.6 %
Aperture Size = 60.00 µm
EHT = 20.00 kV
WD = 9.4 mm
Scan Speed = 10
Signal A = CL

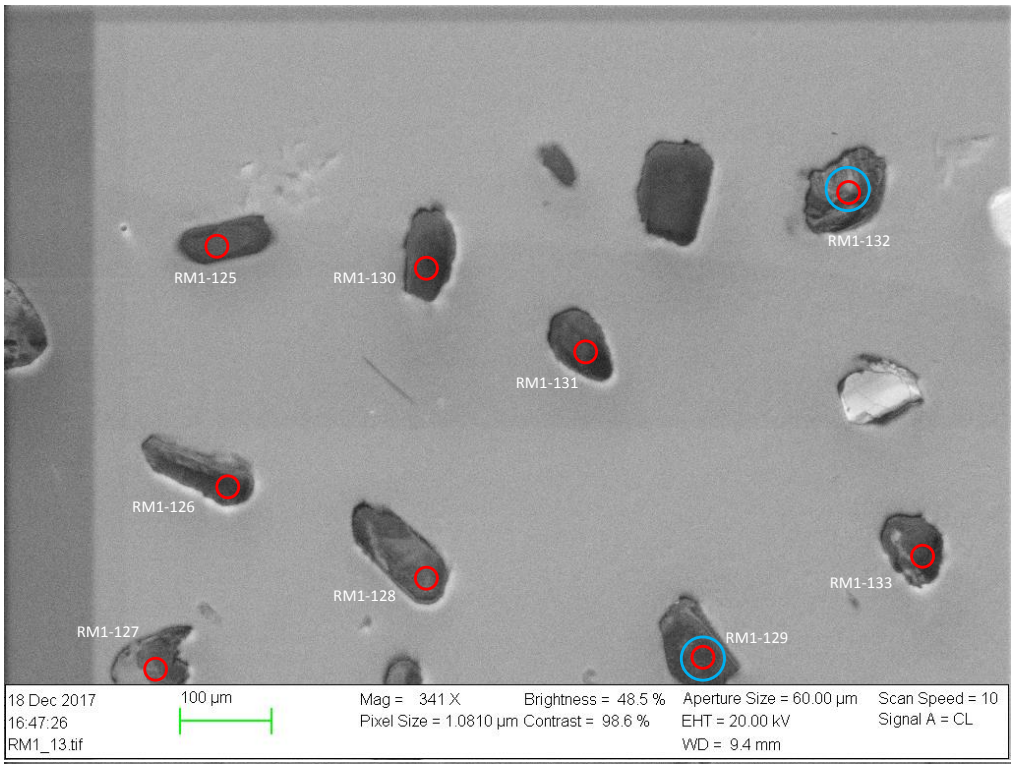
RM1-125
RM1-130
RM1-132
RM1-131
RM1-126
RM1-128
RM1-133
RM1-127
RM1-129
18 Dec 2017
16:47:26
RM1_13.tif
100 µm
Mag = 341 X
Pixel Size = 1.0810 µm
Brightness = 48.5 %
Contrast = 98.6 %
Aperture Size = 60.00 µm
EHT = 20.00 kV
WD = 9.4 mm
Scan Speed = 10
Signal A = CL

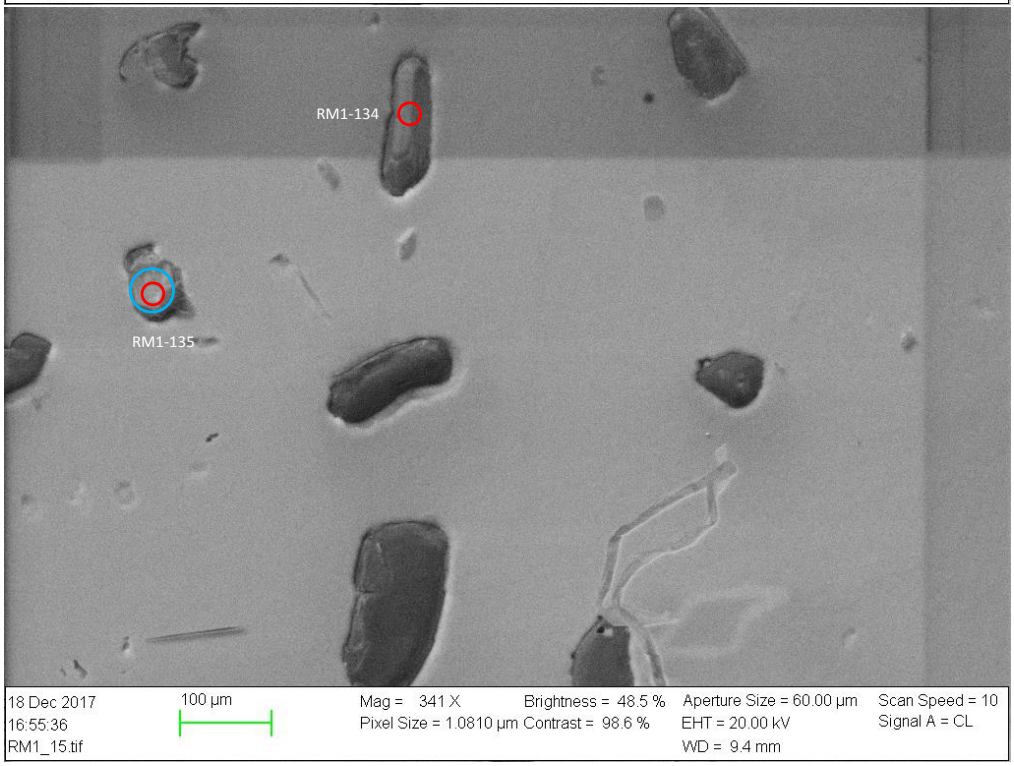
RM1-134
RM1-135
18 Dec 2017
16:55:36
RM1_15.tif
100 µm
Mag = 341 X
Pixel Size = 1.0810 µm
Brightness = 48.5 %
Contrast = 98.6 %
Aperture Size = 60.00 µm
EHT = 20.00 kV
WD = 9.4 mm
Scan Speed = 10
Signal A = CL

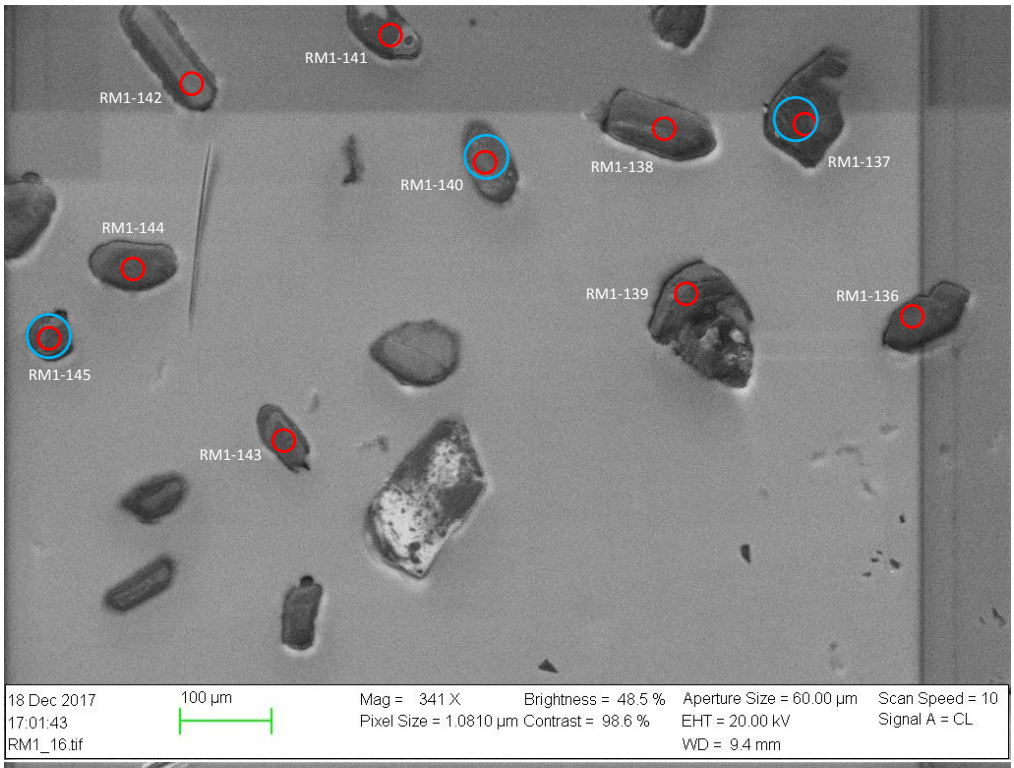
RM1-141
RM1-142
RM1-140
RM1-138
RM1-137
RM1-144
RM1-139
RM1-136
RM1-145
RM1-143
18 Dec 2017
17:01:43
RM1_16.tif
100 µm
Mag = 341 X
Pixel Size = 1.0810 µm
Brightness = 48.5 %
Contrast = 98.6 %
Aperture Size = 60.00 µm
EHT = 20.00 kV
WD = 9.4 mm
Scan Speed = 10
Signal A = CL

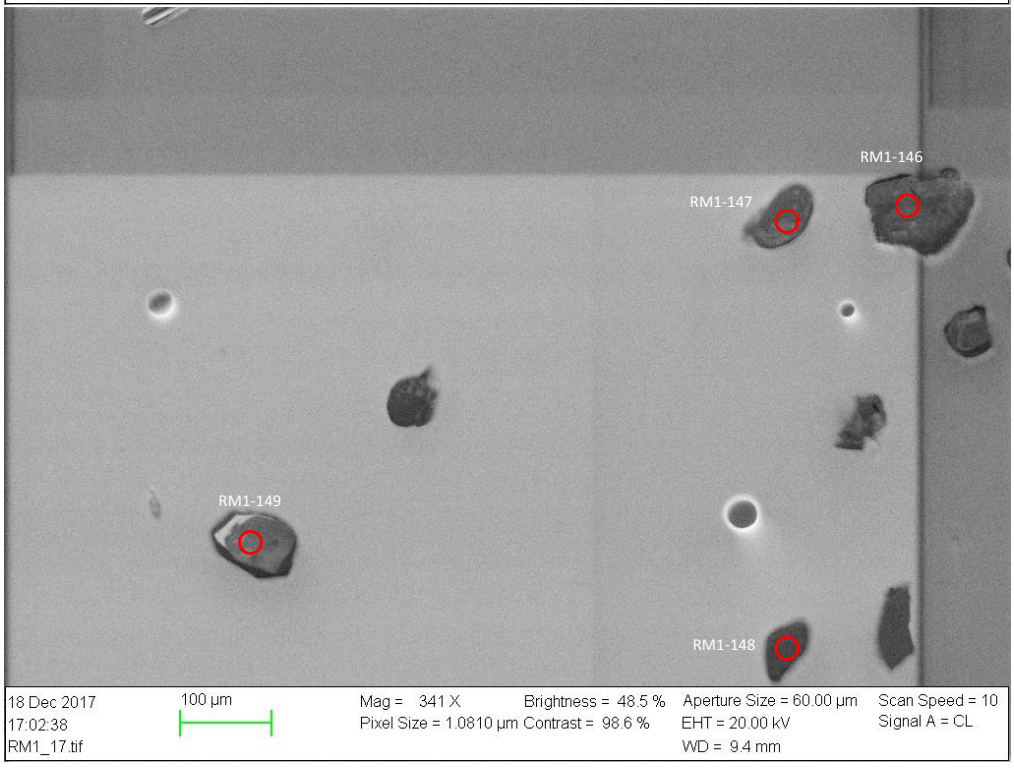
RM1-146
RM1-147
RM1-149
RM1-148
18 Dec 2017
17:02:38
RM1_17.tif
100 µm
Mag = 341 X
Pixel Size = 1.0810 µm
Brightness = 48.5 %
Contrast = 98.6 %
Aperture Size = 60.00 µm
EHT = 20.00 kV
WD = 9.4 mm
Scan Speed = 10
Signal A = CL

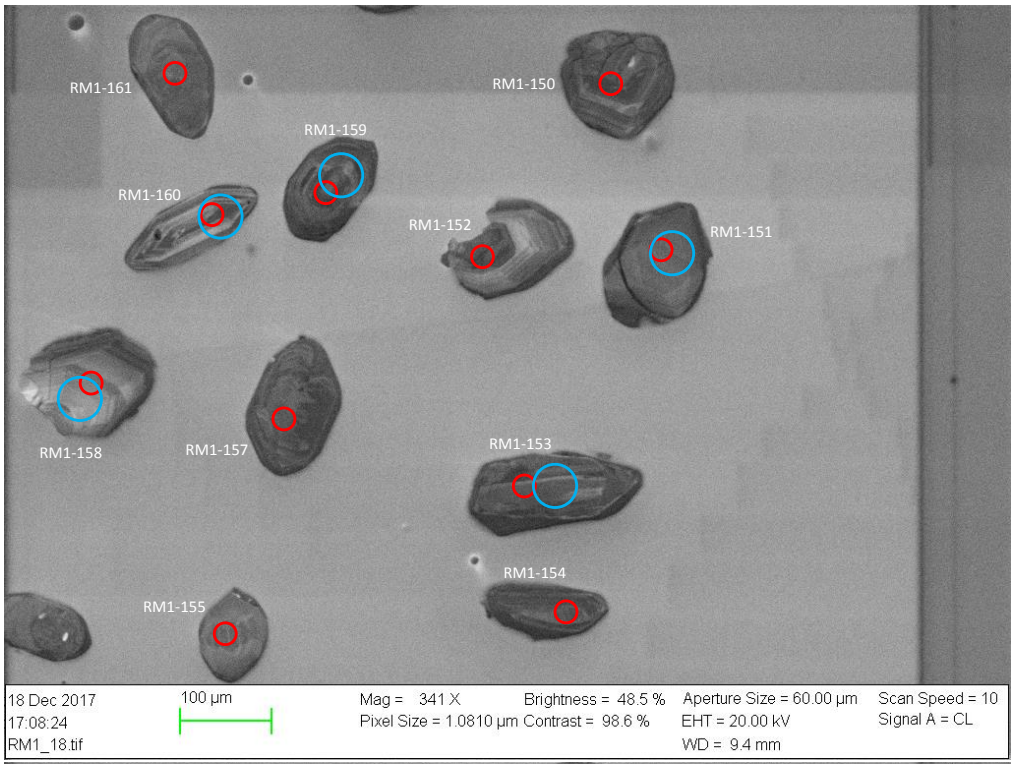
RM1-161
RM1-150
RM1-159
RM1-160
RM1-152
RM1-151
RM1-158
RM1-157
RM1-153
RM1-154
RM1-155
18 Dec 2017
17:08:24
RM1_18.tif
100 µm
Mag = 341 X
Pixel Size = 1.0810 µm
Brightness = 48.5 %
Contrast = 98.6 %
Aperture Size = 60.00 µm
EHT = 20.00 kV
WD = 9.4 mm
Scan Speed = 10
Signal A = CL

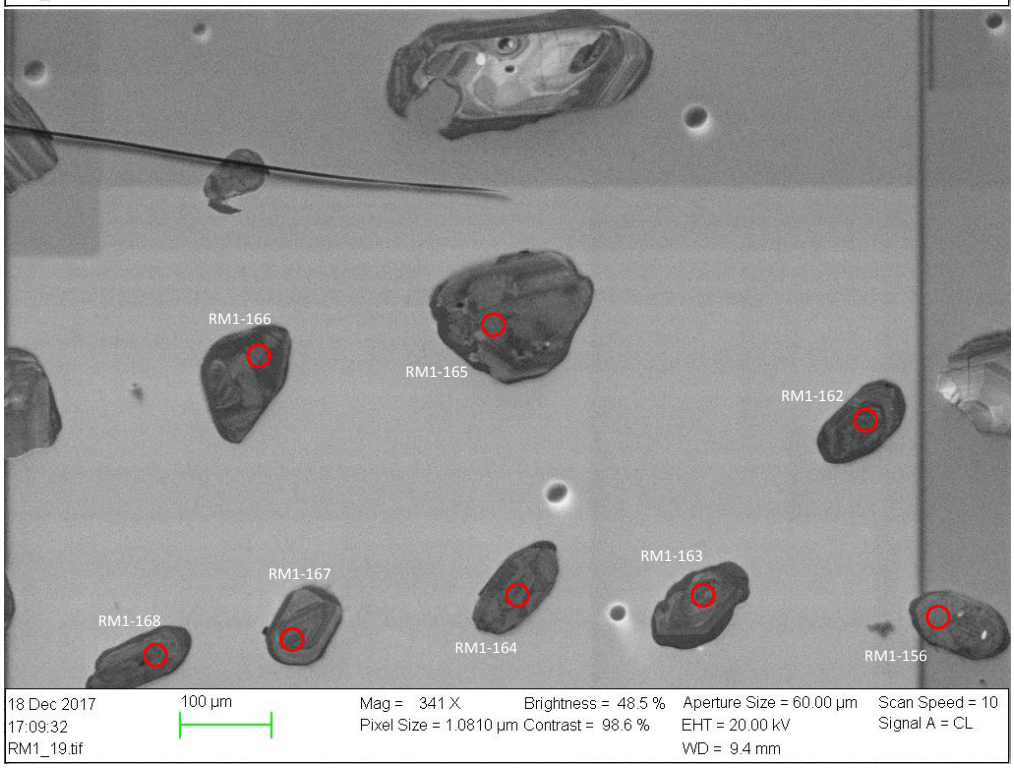
RM1-166
RM1-165
RM1-162
RM1-167
RM1-163
RM1-168
RM1-164
RM1-156
18 Dec 2017
17:09:32
RM1_19.tif
100 µm
Mag = 341 X
Pixel Size = 1.0810 µm
Brightness = 48.5 %
Contrast = 98.6 %
Aperture Size = 60.00 µm
EHT = 20.00 kV
WD = 9.4 mm
Scan Speed = 10
Signal A = CL

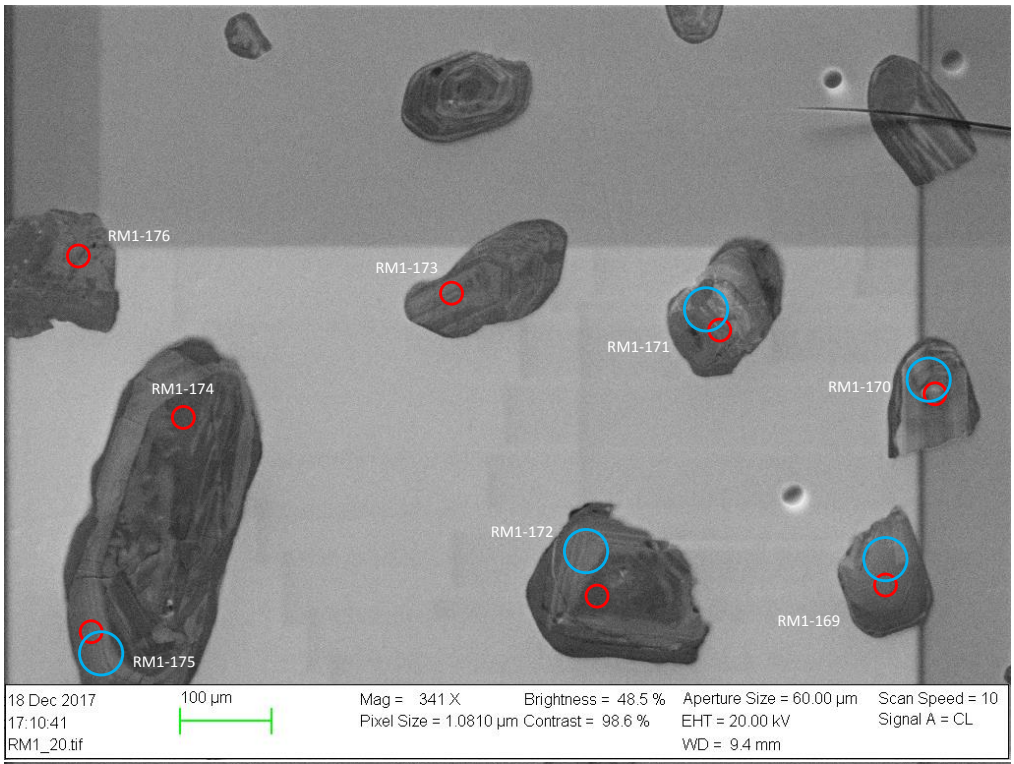
RM1-176
RM1-173
RM1-171
RM1-174
RM1-170
RM1-172
RM1-169
RM1-175
18 Dec 2017
17:10:41
RM1_20.tif
100 µm
Mag = 341 X
Pixel Size = 1.0810 µm
Brightness = 48.5 %
Contrast = 98.6 %
Aperture Size = 60.00 µm
EHT = 20.00 kV
WD = 9.4 mm
Scan Speed = 10
Signal A = CL

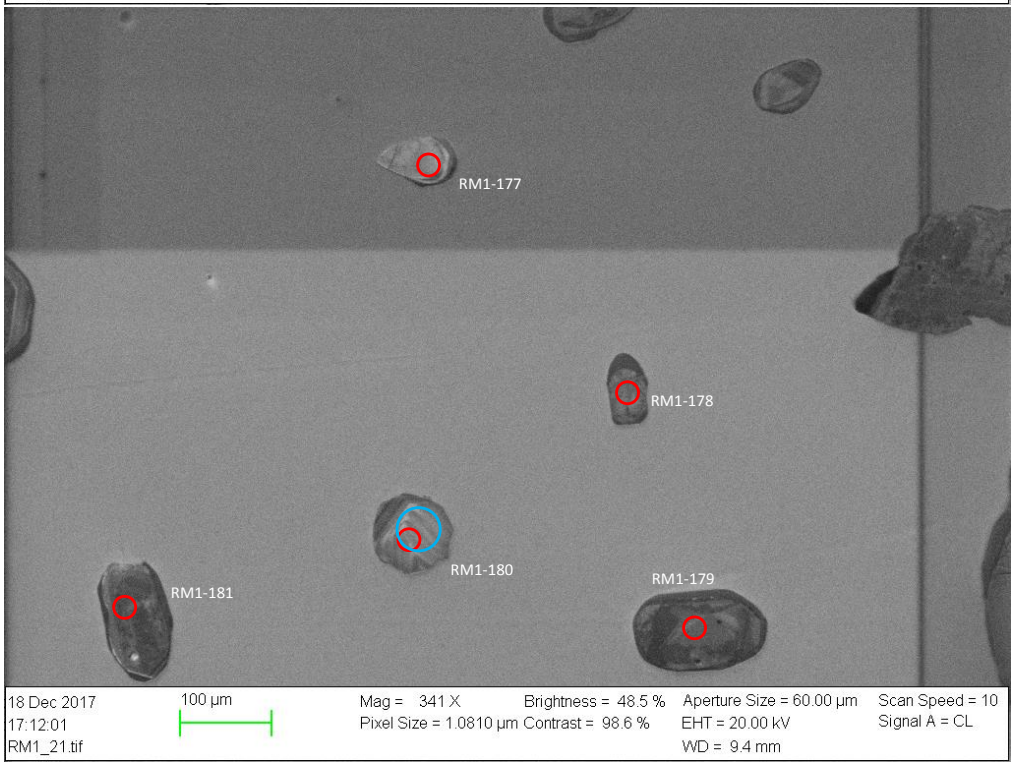
RM1-177
RM1-178
RM1-180
RM1-179
RM1-181
18 Dec 2017
17:12:01
RM1_21.tif
100 µm
Mag = 341 X
Pixel Size = 1.0810 µm
Brightness = 48.5 %
Contrast = 98.6 %
Aperture Size = 60.00 µm
EHT = 20.00 kV
WD = 9.4 mm
Scan Speed = 10
Signal A = CL

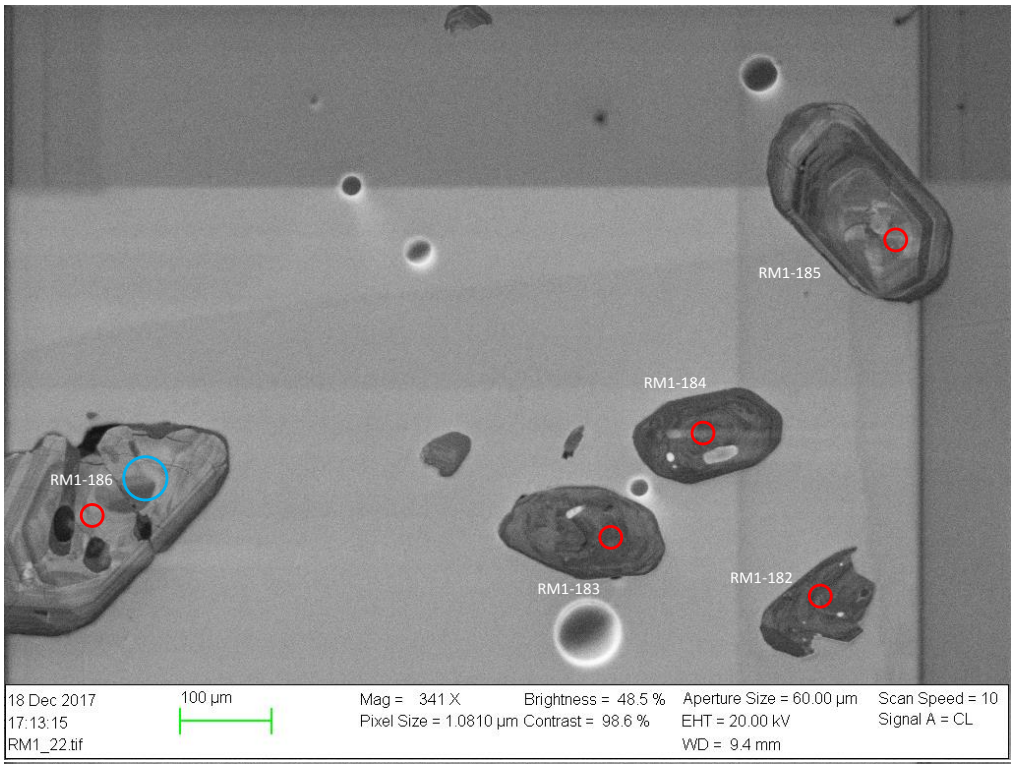
RM1-185
RM1-184
RM1-186
RM1-183
RM1-182
18 Dec 2017
17:13:15
RM1_22.tif
100 µm
Mag = 341 X
Pixel Size = 1.0810 µm
Brightness = 48.5 %
Contrast = 98.6 %
Aperture Size = 60.00 µm
EHT = 20.00 kV
WD = 9.4 mm
Scan Speed = 10
Signal A = CL

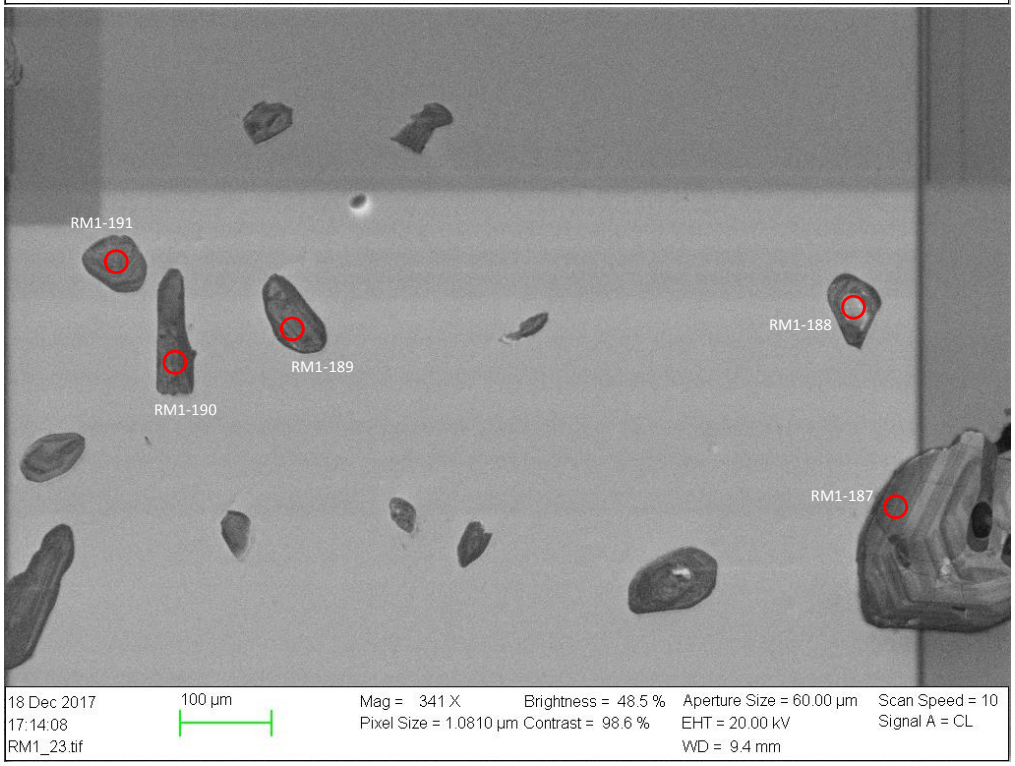
RM1-191
RM1-188
RM1-189
RM1-190
RM1-187
18 Dec 2017
17:14:08
RM1_23.tif
100 µm
Mag = 341 X
Pixel Size = 1.0810 µm
Brightness = 48.5 %
Contrast = 98.6 %
Aperture Size = 60.00 µm
EHT = 20.00 kV
WD = 9.4 mm
Scan Speed = 10
Signal A = CL

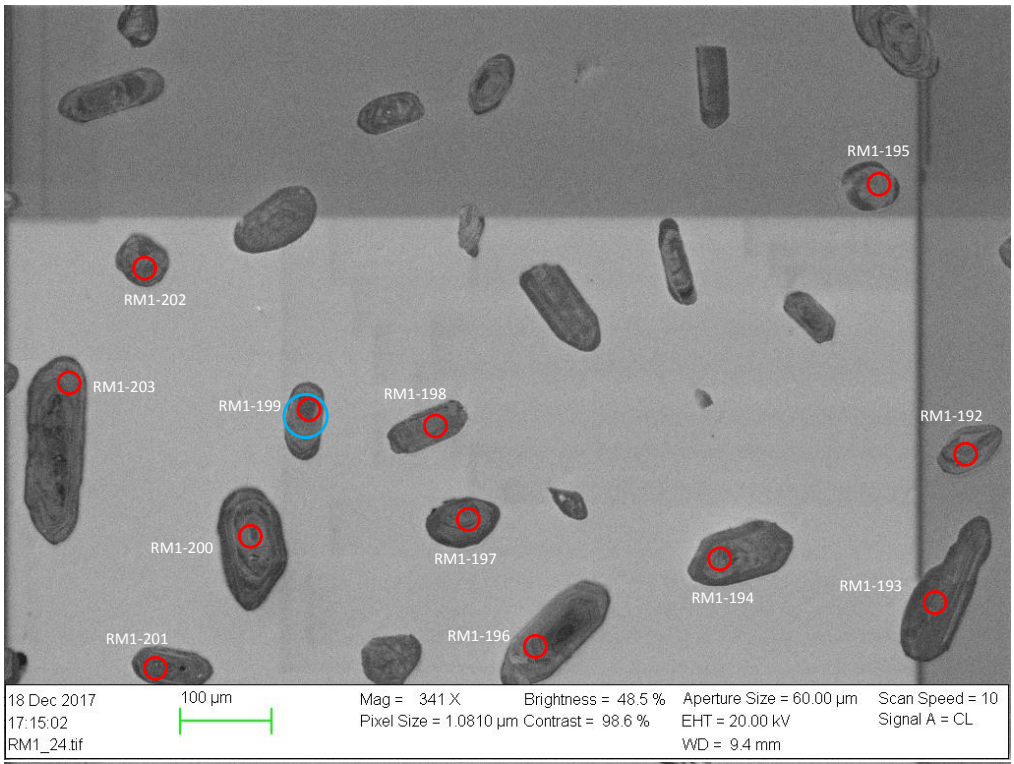
RM1-195
RM1-202
RM1-203
RM1-199
RM1-198
RM1-192
RM1-200
RM1-197
RM1-194
RM1-193
RM1-201
RM1-196
18 Dec 2017
17:15:02
RM1_24.tif
100 µm
Mag = 341 X
Pixel Size = 1.0810 µm
Brightness = 48.5 %
Contrast = 98.6 %
Aperture Size = 60.00 µm
EHT = 20.00 kV
WD = 9.4 mm
Scan Speed = 10
Signal A = CL

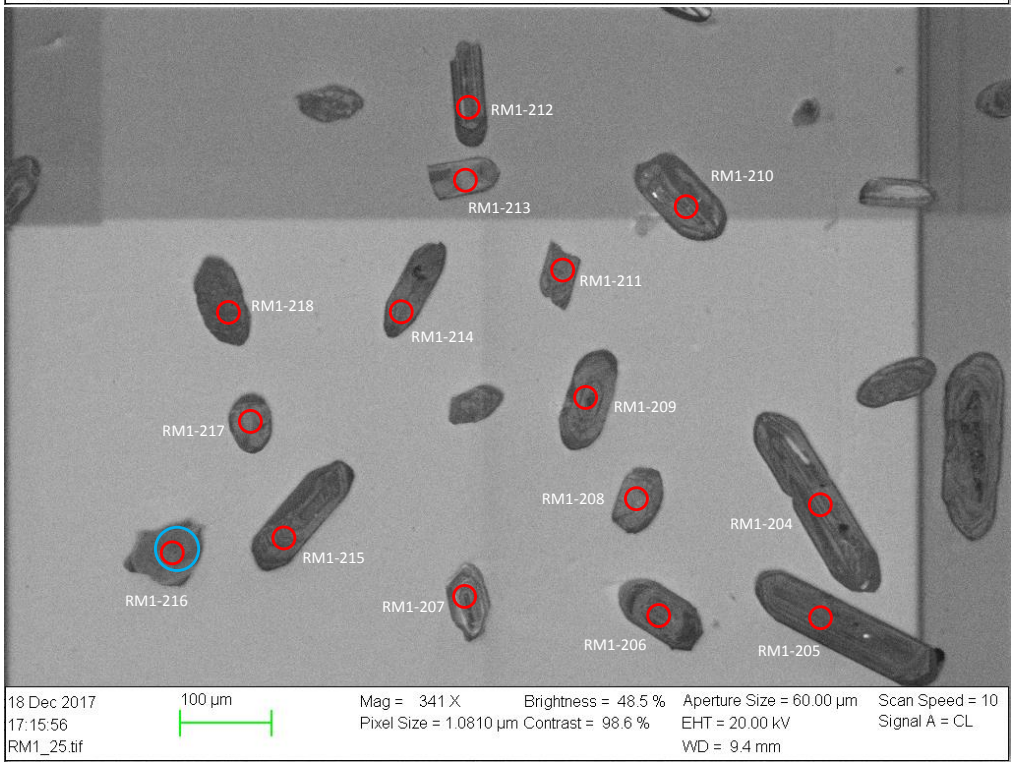
RM1-212
RM1-210
RM1-213
RM1-211
RM1-218
RM1-214
RM1-209
RM1-217
RM1-208
RM1-204
RM1-215
RM1-216
RM1-207
RM1-206
RM1-205
18 Dec 2017
17:15:56
RM1_25.tif
100 µm
Mag = 341 X
Pixel Size = 1.0810 µm
Brightness = 48.5 %
Contrast = 98.6 %
Aperture Size = 60.00 µm
EHT = 20.00 kV
WD = 9.4 mm
Scan Speed = 10
Signal A = CL

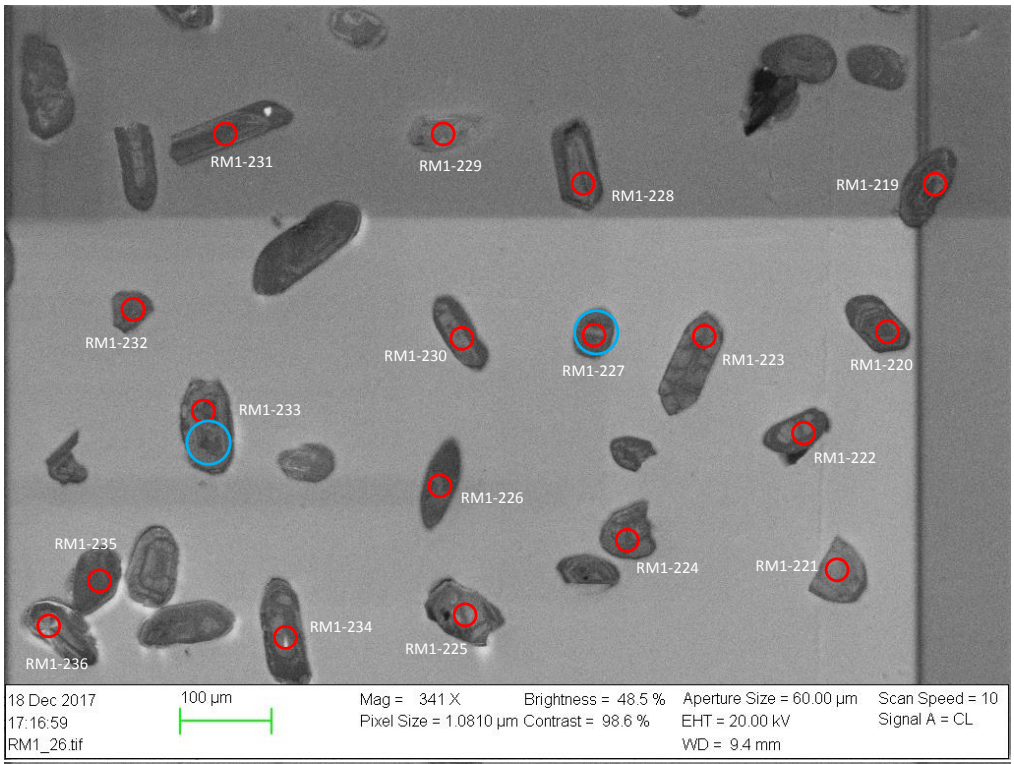
RM1-231
RM1-229
RM1-228
RM1-219
RM1-232
RM1-230
RM1-227
RM1-223
RM1-220
RM1-233
RM1-222
RM1-226
RM1-235
RM1-224
RM1-221
RM1-234
RM1-225
RM1-236
18 Dec 2017
17:16:59
RM1_26.tif
100 µm
Mag = 341 X
Pixel Size = 1.0810 µm
Brightness = 48.5 %
Contrast = 98.6 %
Aperture Size = 60.00 µm
EHT = 20.00 kV
WD = 9.4 mm
Scan Speed = 10
Signal A = CL

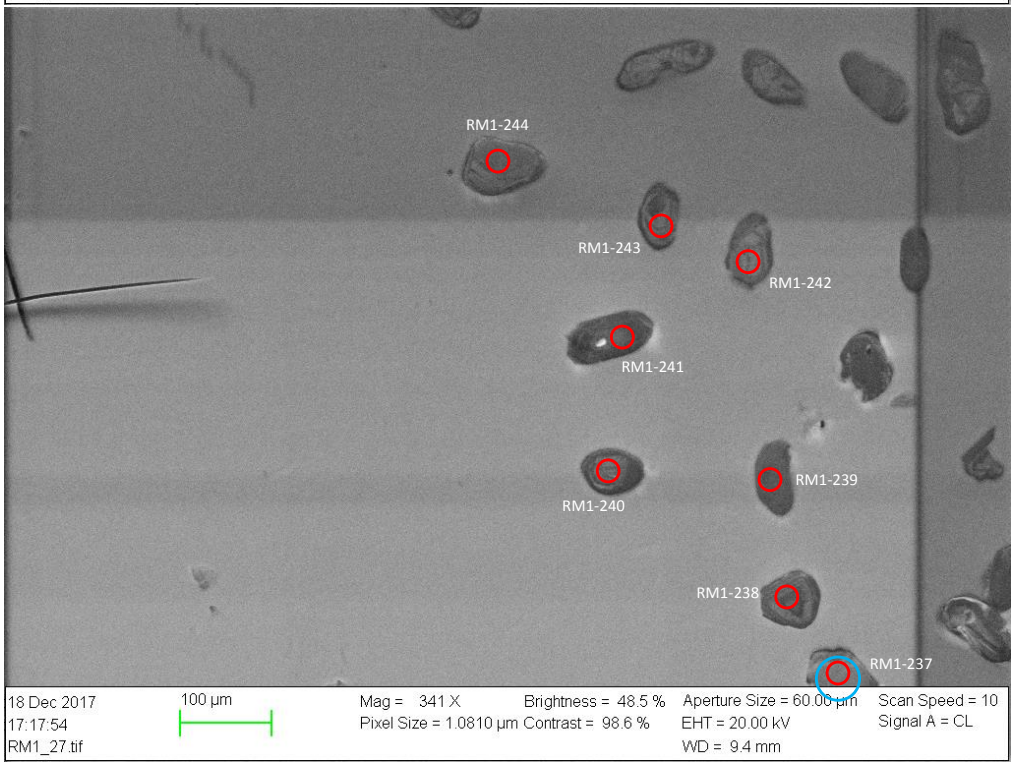
RM1-244
RM1-243
RM1-242
RM1-241
RM1-239
RM1-240
RM1-238
RM1-237
18 Dec 2017
17:17:54
RM1_27.tif
100 µm
Mag = 341 X
Pixel Size = 1.0810 µm
Brightness = 48.5 %
Contrast = 98.6 %
Aperture Size = 60.00 µm
EHT = 20.00 kV
WD = 9.4 mm
Scan Speed = 10
Signal A = CL

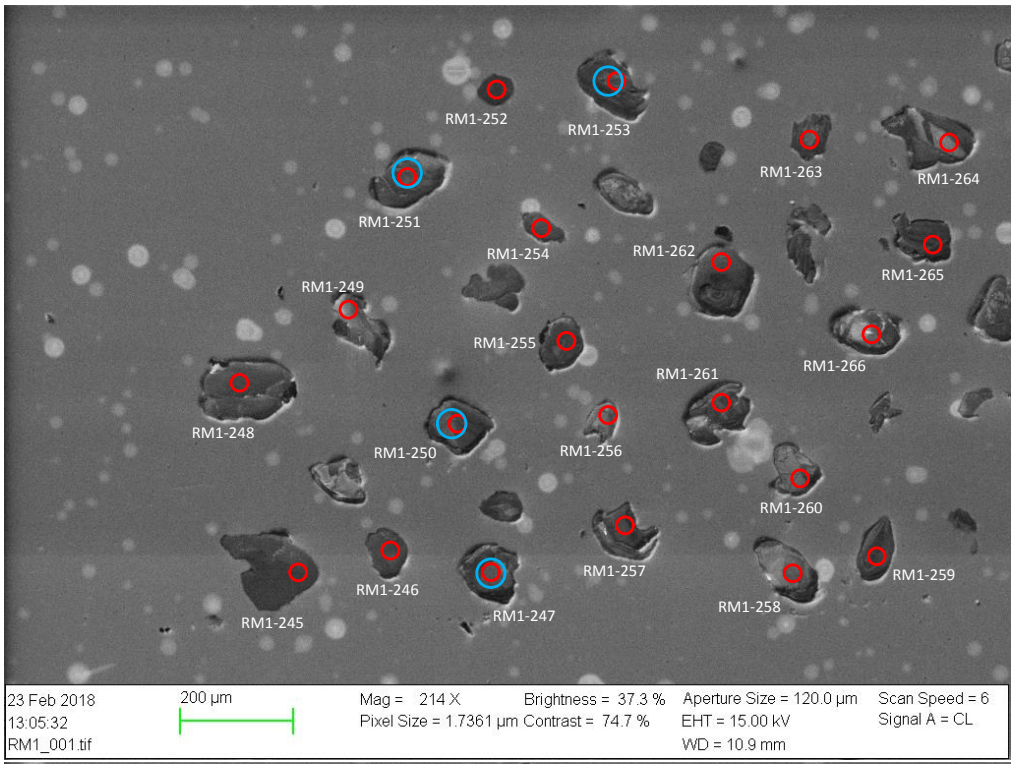
RM1-252
RM1-253
RM1-263
RM1-264
RM1-251
RM1-254
RM1-262
RM1-265
RM1-249
RM1-255
RM1-266
RM1-261
RM1-248
RM1-250
RM1-256
RM1-260
RM1-257
RM1-259
RM1-246
RM1-258
RM1-247
RM1-245
23 Feb 2018
13:05:32
RM1_001.tif
200 µm
Mag = 214 X
Pixel Size = 1.7361 µm
Brightness = 37.3 %
Contrast = 74.7 %
Aperture Size = 120.0 µm
EHT = 15.00 kV
WD = 10.9 mm
Scan Speed = 6
Signal A = CL

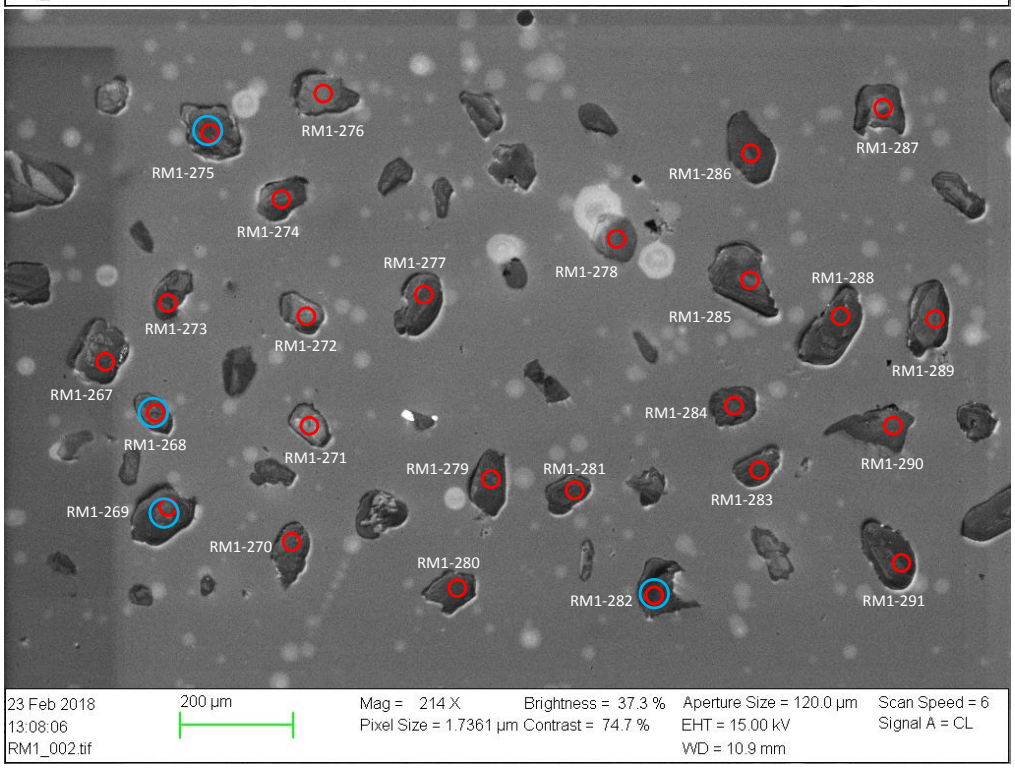
RM1-276
RM1-275
RM1-287
RM1-286
RM1-274
RM1-277
RM1-278
RM1-288
RM1-273
RM1-285
RM1-272
RM1-289
RM1-267
RM1-284
RM1-268
RM1-271
RM1-279
RM1-281
RM1-290
RM1-283
RM1-269
RM1-270
RM1-280
RM1-282
RM1-291
23 Feb 2018
13:08:06
RM1_002.tif
200 µm
Mag = 214 X
Pixel Size = 1.7361 µm
Brightness = 37.3 %
Contrast = 74.7 %
Aperture Size = 120.0 µm
EHT = 15.00 kV
WD = 10.9 mm
Scan Speed = 6
Signal A = CL

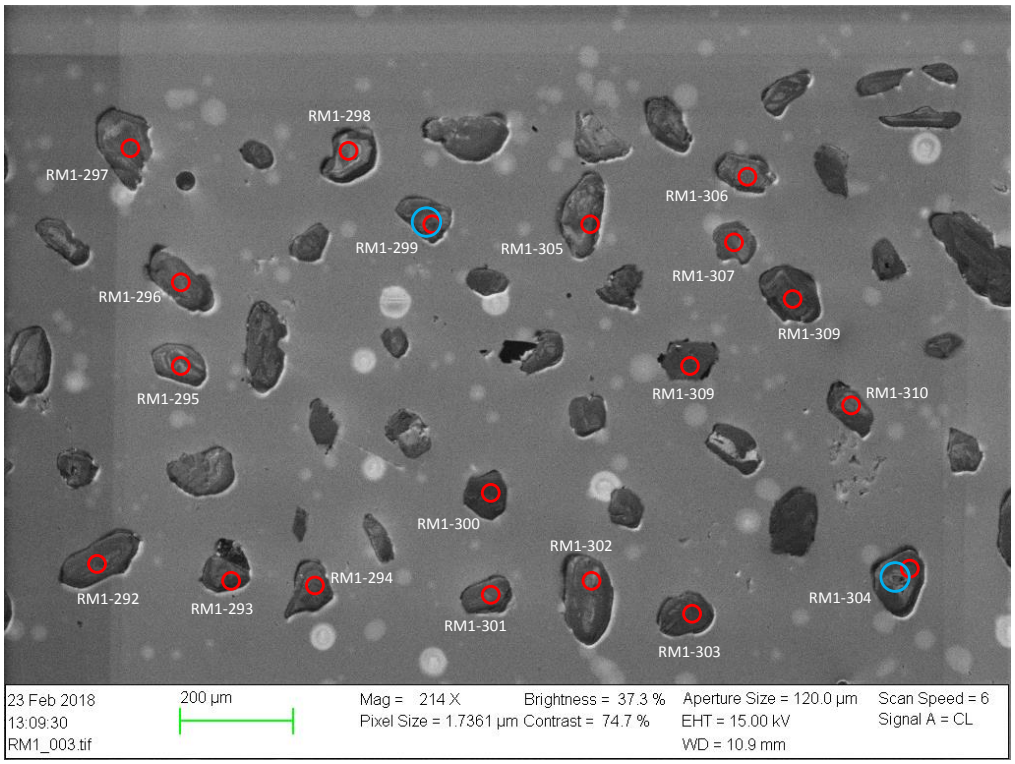
RM1-298
RM1-297
RM1-306
RM1-299
RM1-305
RM1-307
RM1-296
RM1-309
RM1-295
RM1-309
RM1-310
RM1-300
RM1-302
RM1-294
RM1-292
RM1-293
RM1-304
RM1-301
RM1-303
23 Feb 2018
13:09:30
RM1_003.tif
200 µm
Mag = 214 X
Pixel Size = 1.7361 µm
Brightness = 37.3 %
Contrast = 74.7 %
Aperture Size = 120.0 µm
EHT = 15.00 kV
WD = 10.9 mm
Scan Speed = 6
Signal A = CL

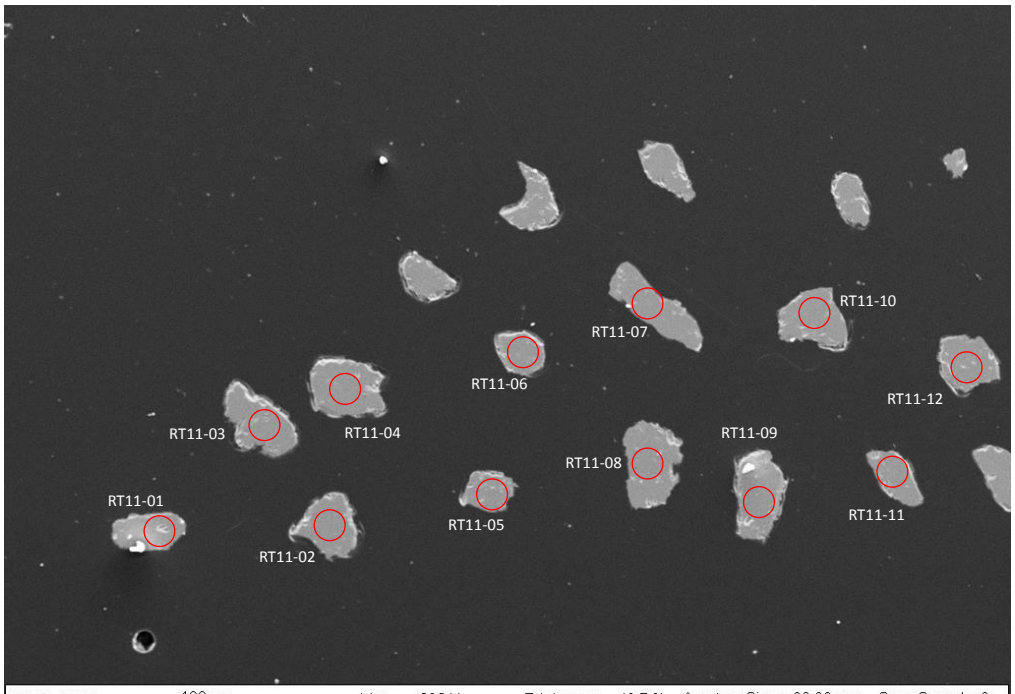
RT11-01
RT11-02
RT11-03
RT11-04
RT11-05
RT11-06
RT11-07
RT11-08
RT11-09
RT11-10
RT11-11
RT11-12
23 Feb 2018
10:10:36
RT11_001.tif
100 µm
Mag = 232 X
Pixel Size = 1.5914 µm
Brightness = 48.7 %
Contrast = 30.9 %
Aperture Size = 30.00 µm
EHT = 15.00 kV
WD = 20.2 mm
Scan Speed = 6
Signal A = SE2

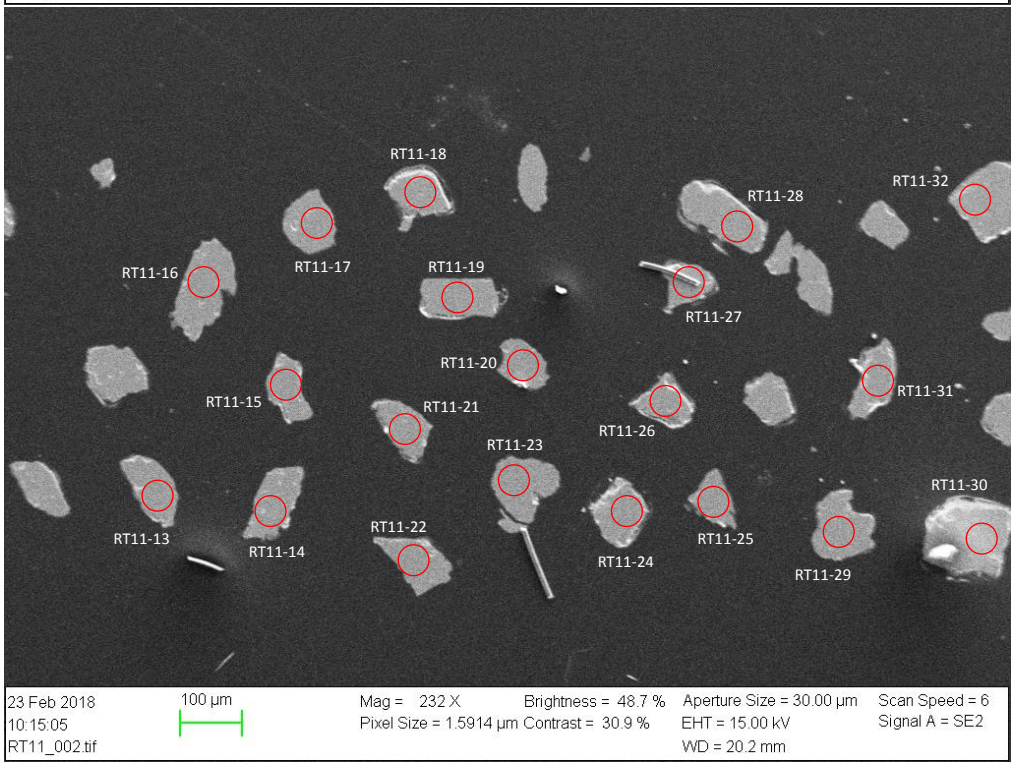
RT11-13
RT11-14
RT11-15
RT11-16
RT11-17
RT11-18
RT11-19
RT11-20
RT11-21
RT11-22
RT11-23
RT11-24
RT11-25
RT11-26
RT11-27
RT11-28
RT11-29
RT11-30
RT11-31
RT11-32
23 Feb 2018
10:15:05
RT11_002.tif
100 µm
Mag = 232 X
Pixel Size = 1.5914 µm
Brightness = 48.7 %
Contrast = 30.9 %
Aperture Size = 30.00 µm
EHT = 15.00 kV
WD = 20.2 mm
Scan Speed = 6
Signal A = SE2

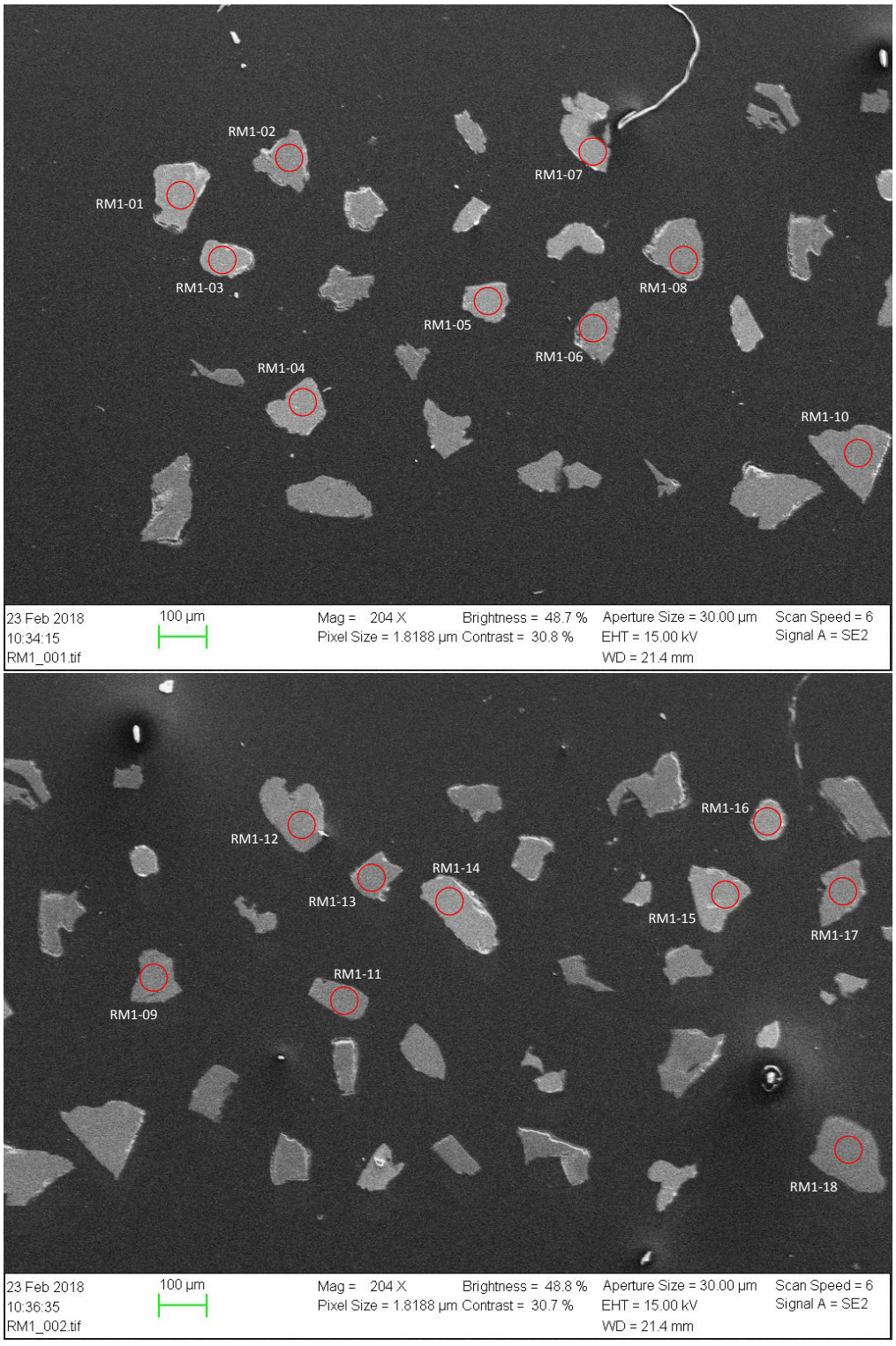
RM1-02
RM1-07
RM1-01
RM1-03
RM1-08
RM1-05
RM1-06
RM1-04
RM1-10
23 Feb 2018
10:34:15
RM1_001.tif
100 µm
Mag = 204 X
Pixel Size = 1.8188 µm
Brightness = 48.7 %
Contrast = 30.8 %
Aperture Size = 30.00 µm
EHT = 15.00 kV
WD = 21.4 mm
Scan Speed = 6
Signal A = SE2
RM1-16
RM1-12
RM1-14
RM1-13
RM1-15
RM1-17
RM1-11
RM1-09
RM1-18
23 Feb 2018
10:36:35
RM1_002.tif
100 µm
Mag = 204 X
Pixel Size = 1.8188 µm
Brightness = 48.8 %
Contrast = 30.7 %
Aperture Size = 30.00 µm
EHT = 15.00 kV
WD = 21.4 mm
Scan Speed = 6
Signal A = SE2

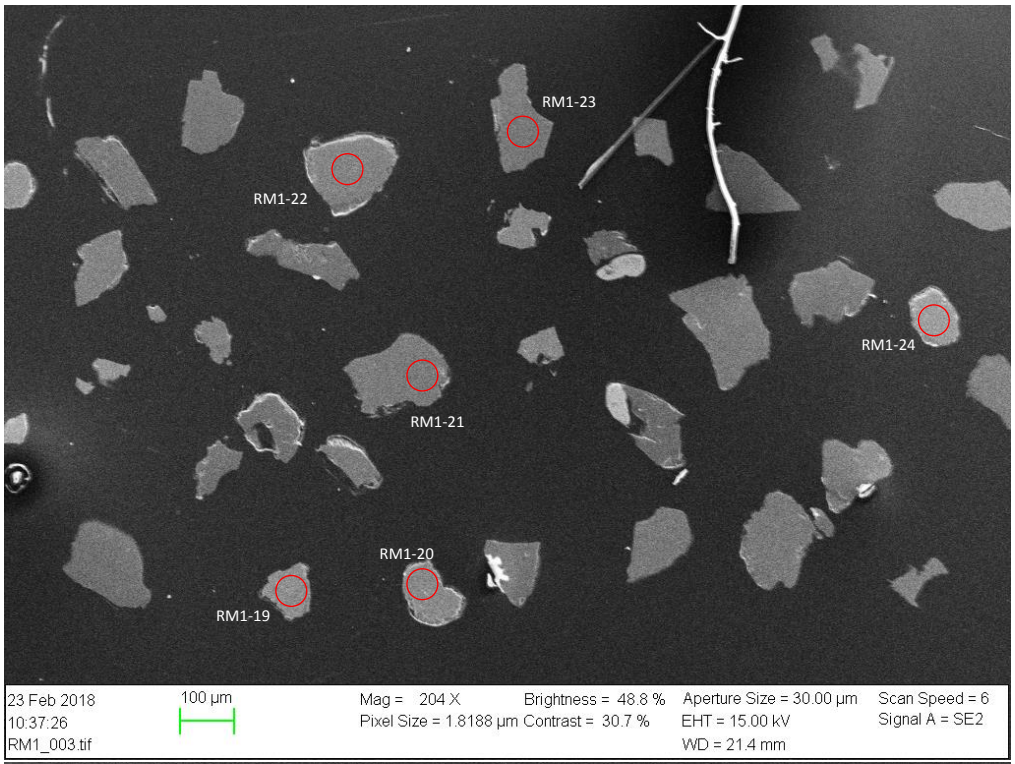
RM1-23
RM1-22
RM1-24
RM1-21
RM1-20
RM1-19
23 Feb 2018
10:37:26
RM1_003.tif
100 µm
Mag = 204 X
Pixel Size = 1.8188 µm
Brightness = 48.8 %
Contrast = 30.7 %
Aperture Size = 30.00 µm
EHT = 15.00 kV
WD = 21.4 mm
Scan Speed = 6
Signal A = SE2

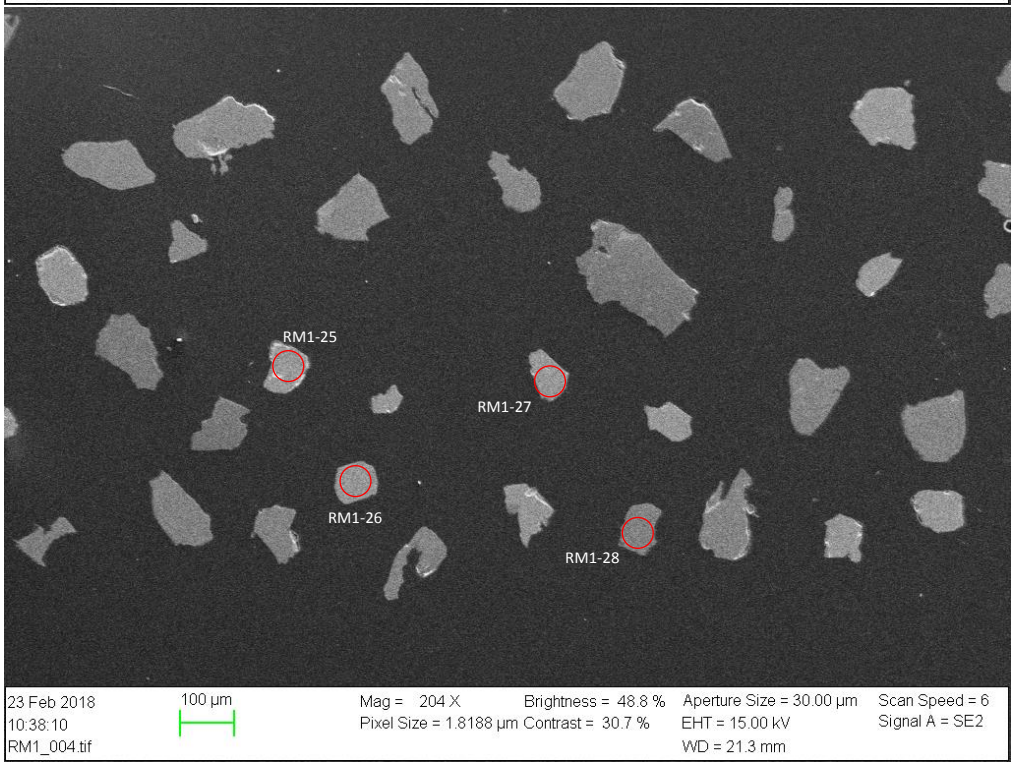
RM1-25
RM1-27
RM1-26
RM1-28
23 Feb 2018
10:38:10
RM1_004.tif
100 µm
Mag = 204 X
Pixel Size = 1.8188 µm
Brightness = 48.8 %
Contrast = 30.7 %
Aperture Size = 30.00 µm
EHT = 15.00 kV
WD = 21.3 mm
Scan Speed = 6
Signal A = SE2

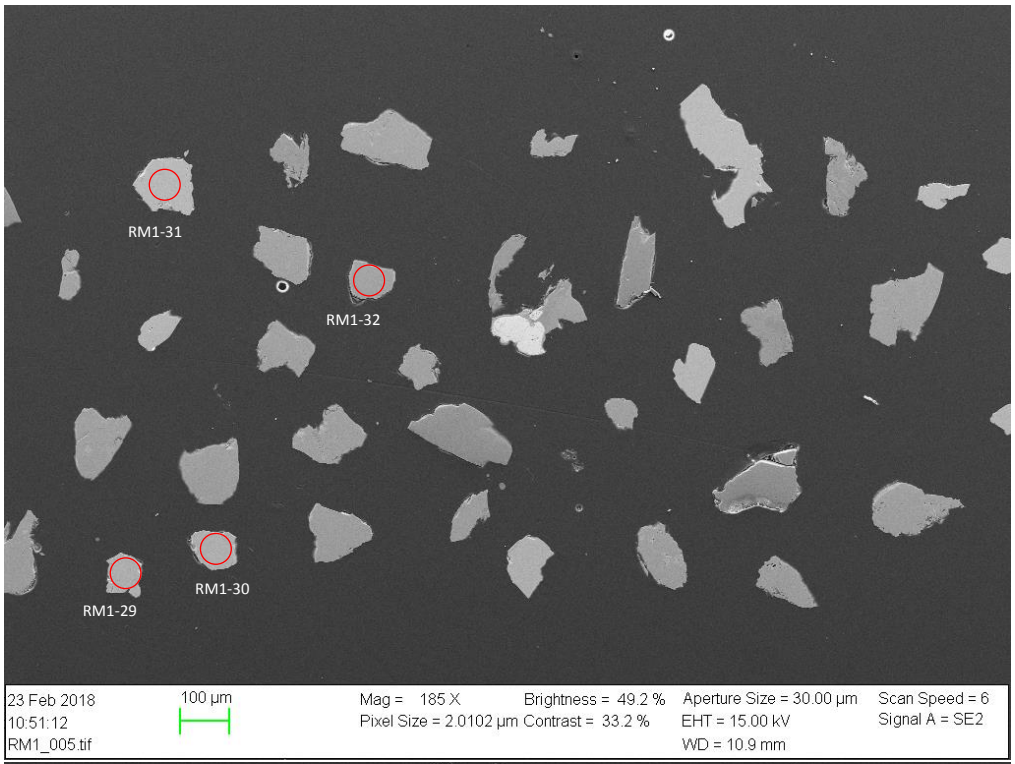
RM1-31
RM1-32
RM1-30
RM1-29
23 Feb 2018
10:51:12
RM1_005.tif
100 µm
Mag = 185 X
Pixel Size = 2.0102 µm
Brightness = 49.2 %
Contrast = 33.2 %
Aperture Size = 30.00 µm
EHT = 15.00 kV
WD = 10.9 mm
Scan Speed = 6
Signal A = SE2

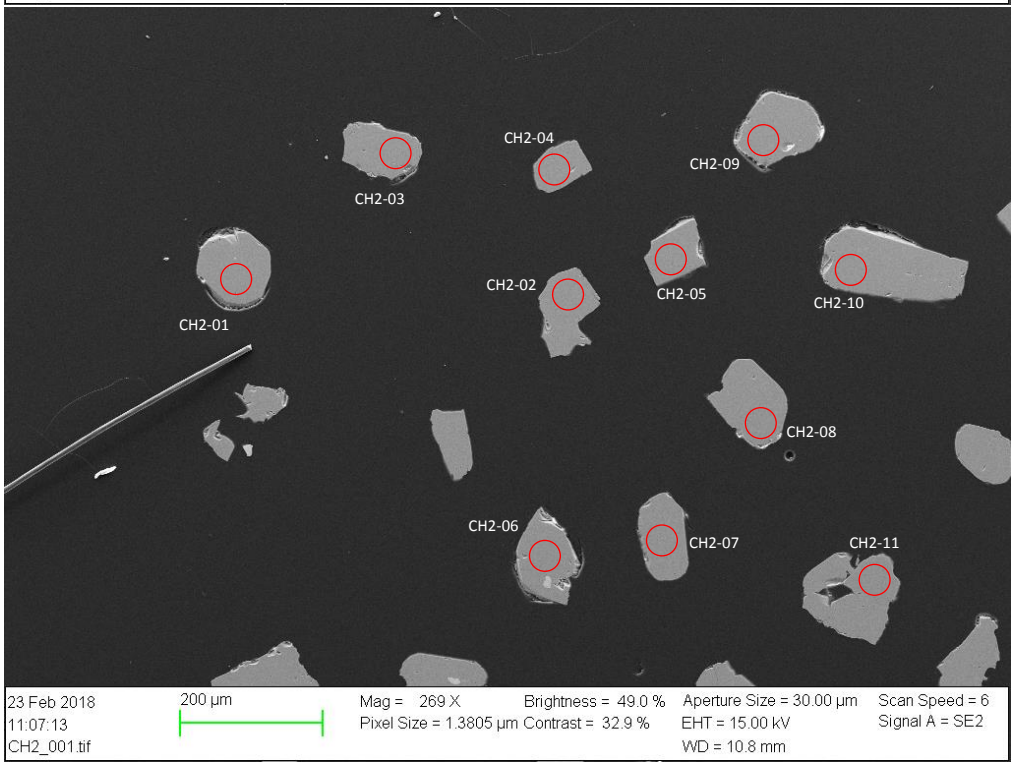
CH2-04
CH2-09
CH2-03
CH2-02
CH2-05
CH2-10
CH2-01
CH2-08
CH2-06
CH2-07
CH2-11
23 Feb 2018
11:07:13
CH2_001.tif
200 µm
Mag = 269 X
Pixel Size = 1.3805 µm
Brightness = 49.0 %
Contrast = 32.9 %
Aperture Size = 30.00 µm
EHT = 15.00 kV
WD = 10.8 mm
Scan Speed = 6
Signal A = SE2

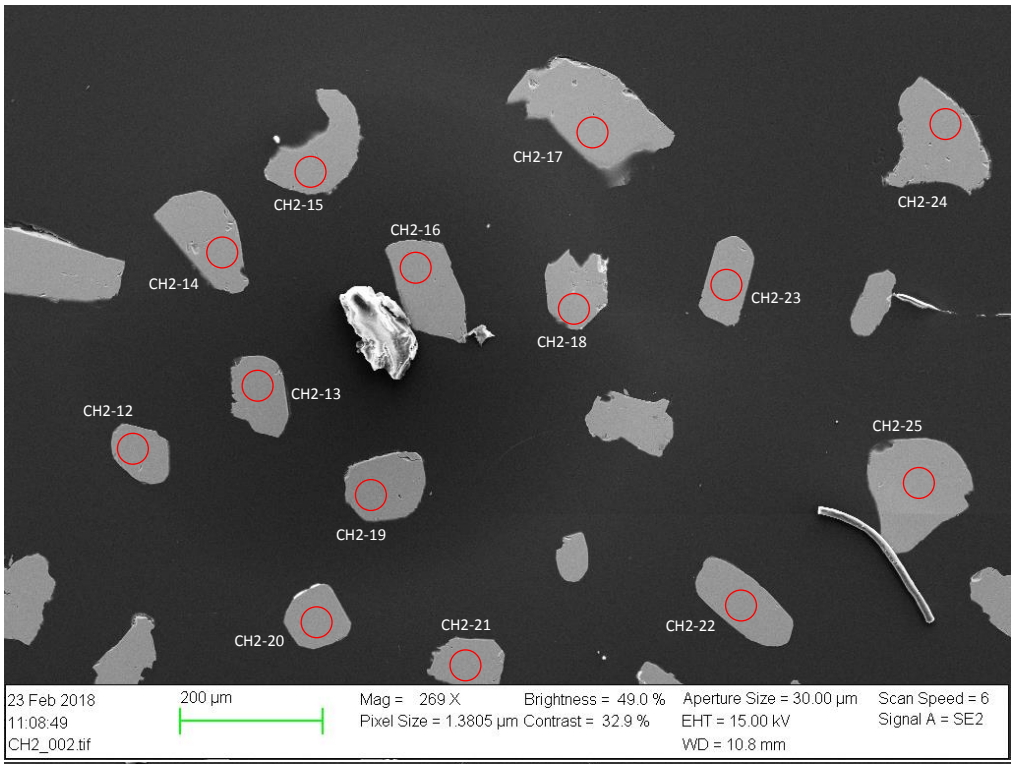
CH2-17
CH2-15
CH2-24
CH2-16
CH2-14
CH2-23
CH2-18
CH2-13
CH2-12
CH2-25
CH2-19
CH2-20
CH2-21
CH2-22
23 Feb 2018
11:08:49
CH2_002.tif
200 µm
Mag = 269 X
Pixel Size = 1.3805 µm
Brightness = 49.0 %
Contrast = 32.9 %
Aperture Size = 30.00 µm
EHT = 15.00 kV
WD = 10.8 mm
Scan Speed = 6
Signal A = SE2

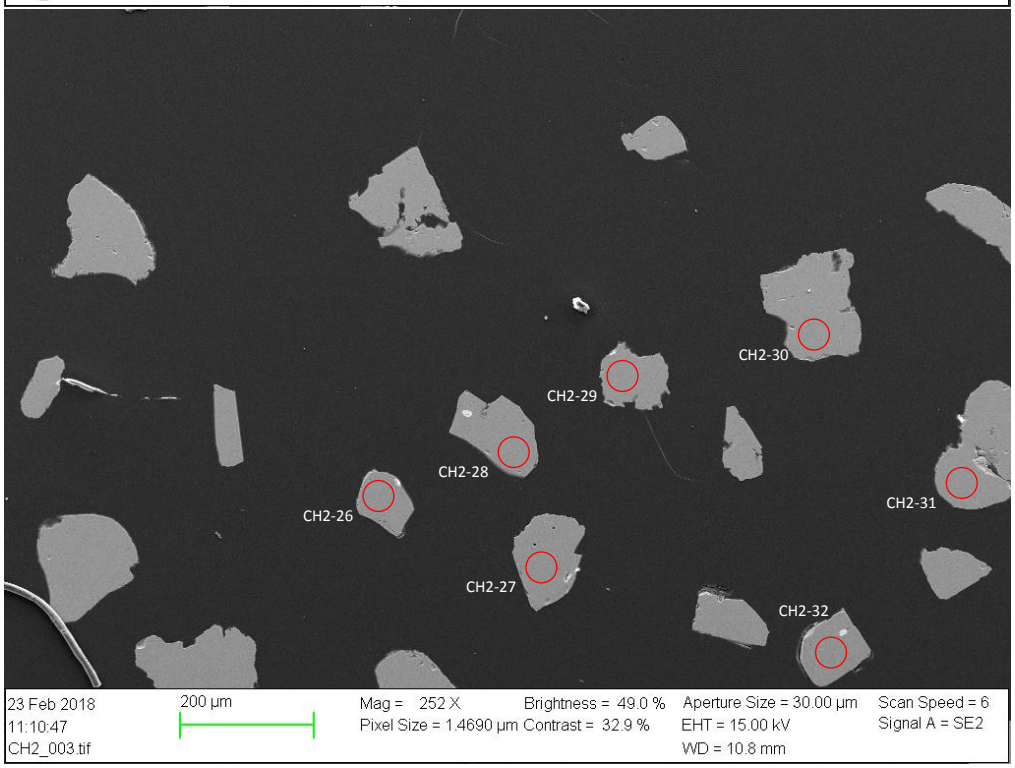
CH2-30
CH2-29
CH2-28
CH2-31
CH2-26
CH2-27
CH2-32
23 Feb 2018
11:10:47
CH2_003.tif
200 µm
Mag = 252 X
Pixel Size = 1.4690 µm
Brightness = 49.0 %
Contrast = 32.9 %
Aperture Size = 30.00 µm
EHT = 15.00 kV
WD = 10.8 mm
Scan Speed = 6
Signal A = SE2

Appendix B.

Tables of U-Pb data

In this appendix, the full tables of U-Pb data for both zircons and apatite are presented. Tables B.1, B.2 and B.3 presents zircon U-Pb data, and Table B.4 presents all U-Pb apatite data.

Table B.1.: U-Pb data from the sample RT11 showing all relevant isotope ratios and $^{207}Pb/^{206}Pb$ ages.

Analysis-#	$^{207}Pb/^{206}Pb$ Bias Corr.	% 2σ	$^{207}Pb/^{235}U$ Bias Corr.	% 2σ	$^{206}Pb/^{238}U$ Bias Corr.	% 2σ	corr. coef.	$^{207}Pb/^{206}Pb$ Age (Ma)	2σ	Discordance (%)
RT11-001	0.29091	1.61	27.48505	2.53	0.69081	1.95	0.771	3416	25	0.8
RT11-002	0.22900	2.68	11.21193	5.20	0.35795	4.45	0.857	3039	43	53.9
RT11-003	0.28869	1.77	26.89694	2.81	0.68112	2.17	0.775	3404	28	1.6
RT11-004	0.26944	2.05	19.52788	5.31	0.52980	4.90	0.922	3297	32	20.2
RT11-005	0.26015	1.63	18.24368	3.54	0.51262	3.14	0.888	3241	26	21.4
RT11-006	0.27378	1.75	22.15420	3.79	0.59145	3.36	0.886	3322	27	10.8
RT11-007	0.28429	1.69	26.38287	3.22	0.67827	2.75	0.852	3380	26	1.2
RT11-008	0.28573	1.67	27.82478	2.97	0.71167	2.45	0.826	3388	26	-2.3
RT11-009	0.28945	1.78	25.49094	3.75	0.64354	3.30	0.880	3408	28	6.3
RT11-010	0.28304	1.95	25.28071	3.02	0.65266	2.30	0.764	3373	30	4.1
RT11-011	0.27873	1.75	27.38825	3.31	0.71772	2.80	0.848	3350	27	-4.0
RT11-012	0.28250	1.90	27.35969	3.00	0.70736	2.32	0.773	3370	30	-2.3
RT11-013	0.27466	1.57	22.05624	2.84	0.58645	2.37	0.833	3327	25	11.7
RT11-014	0.28588	1.74	28.65072	3.26	0.73181	2.76	0.847	3389	27	-4.4
RT11-015	0.28193	1.65	27.68252	2.97	0.71693	2.47	0.831	3367	26	-3.4
RT11-016	0.28222	1.82	25.25525	2.95	0.65332	2.33	0.788	3369	28	3.9
RT11-017	0.28671	1.62	27.03120	2.89	0.68824	2.39	0.828	3394	25	0.4
RT11-018	0.28418	1.79	27.65285	2.93	0.71026	2.32	0.793	3380	28	-2.4
RT11-019	0.28851	1.61	26.94791	2.60	0.68166	2.05	0.787	3403	25	1.5
RT11-020	0.28043	1.83	27.33808	2.96	0.71138	2.32	0.784	3359	29	-3.1
RT11-021	0.28056	1.45	26.79237	2.48	0.69569	2.01	0.810	3360	23	-1.4
RT11-022	0.24749	1.59	14.86250	3.01	0.43785	2.56	0.849	3163	25	35.0
RT11-023	0.26918	1.69	24.24431	3.19	0.65661	2.71	0.849	3295	26	1.2
RT11-024	0.28684	1.75	28.65835	2.87	0.72827	2.27	0.792	3394	27	-3.8
RT11-025	0.28789	1.55	27.69604	2.82	0.70117	2.36	0.836	3400	24	-0.8
RT11-026	0.27844	1.76	27.88413	3.01	0.72979	2.44	0.811	3348	28	-5.3
RT11-027	0.28705	1.74	27.05309	3.13	0.68671	2.59	0.830	3395	27	0.7
RT11-028	0.29013	1.89	26.85839	3.10	0.67432	2.45	0.791	3412	29	2.6
RT11-029	0.29355	1.65	26.79255	2.67	0.66473	2.10	0.787	3430	26	4.3
RT11-030	0.28606	1.88	27.40063	3.02	0.69752	2.37	0.783	3390	29	-0.7
RT11-031	0.28931	1.62	26.89669	2.77	0.67666	2.25	0.812	3408	25	2.2
RT11-032	0.28067	1.53	24.03281	2.55	0.62313	2.03	0.799	3360	24	7.5
RT11-033	0.28518	1.62	27.63505	2.70	0.70513	2.16	0.799	3385	25	-1.7
RT11-034	0.28732	1.87	26.57175	3.23	0.67282	2.63	0.816	3397	29	2.3
RT11-035	0.28274	1.73	26.82462	2.94	0.69012	2.38	0.810	3372	27	-0.4
RT11-036	0.27701	1.65	25.06309	2.68	0.65804	2.12	0.788	3340	26	2.4
RT11-037	0.28293	1.57	26.76547	2.71	0.68793	2.21	0.815	3373	24	-0.1

Table B.1 continued from previous page

Analysis-#	$^{207}Pb/^{206}Pb$ Bias Corr.	% 2σ	$^{207}Pb/^{235}U$ Bias Corr.	% 2σ	$^{206}Pb/^{238}U$ Bias Corr.	% 2σ	corr. coef.	$^{207}Pb/^{206}Pb$ Age (Ma)	2σ	Discordance (%)
RT11-038	0.29013	1.53	26.92641	2.56	0.67479	2.06	0.803	3412	24	2.5
RT11-039	0.28217	1.76	26.36820	2.99	0.67934	2.42	0.808	3369	27	0.7
RT11-040	0.28053	1.82	26.48837	2.86	0.68633	2.21	0.771	3360	28	-0.4
RT11-041	0.28283	1.44	27.21821	2.59	0.69911	2.16	0.832	3372	22	-1.4
RT11-042	0.28724	1.59	23.79648	3.33	0.60176	2.92	0.878	3396	25	11.7
RT11-043	0.28000	1.49	26.50251	2.65	0.68741	2.19	0.828	3357	23	-0.6
RT11-044	0.28551	1.76	26.90461	2.82	0.68426	2.20	0.780	3387	27	0.7
RT11-045	0.27748	1.61	26.09553	2.73	0.68279	2.20	0.806	3343	25	-0.5
RT11-046	0.23111	2.94	11.34593	5.11	0.35638	4.19	0.819	3054	47	55.3
RT11-047	0.27604	1.76	24.03869	3.11	0.63208	2.57	0.825	3334	27	5.5
RT11-048	0.28182	1.70	25.85123	2.97	0.66571	2.44	0.819	3367	27	2.3
RT11-049	0.28013	1.73	26.40740	2.79	0.68402	2.19	0.784	3357	27	-0.2
RT11-050	0.28703	1.58	26.58918	2.58	0.67207	2.04	0.790	3395	25	2.4
RT11-051	0.28290	1.79	25.10699	2.77	0.64351	2.12	0.764	3373	28	5.2
RT11-052	0.28336	1.67	26.43853	2.91	0.67642	2.38	0.818	3375	26	1.3
RT11-053	0.27741	1.79	26.49018	2.80	0.69214	2.15	0.768	3342	28	-1.5
RT11-054	0.27932	1.88	25.89664	3.04	0.67189	2.39	0.785	3353	29	1.1
RT11-055	0.27940	1.87	25.54433	2.77	0.66247	2.05	0.740	3353	29	2.3
RT11-056	0.28576	1.59	26.64265	2.56	0.67547	2.01	0.784	3388	25	1.8
RT11-057	0.28396	1.79	26.77437	2.81	0.68302	2.16	0.771	3379	28	0.6
RT11-058	0.27767	1.69	24.65842	2.85	0.64321	2.29	0.805	3344	26	4.3
RT11-059	0.28802	1.70	26.71280	2.77	0.67165	2.19	0.791	3401	26	2.6
RT11-060	0.28452	1.58	25.06119	3.12	0.63778	2.69	0.862	3382	25	6.2
RT11-061	0.28519	1.80	26.85208	2.95	0.68141	2.33	0.791	3385	28	1.0
RT11-062	0.28050	1.69	26.32868	2.74	0.67921	2.15	0.786	3359	26	0.5
RT11-063	0.27981	1.83	25.96373	2.85	0.67133	2.18	0.765	3356	29	1.3
RT11-064	0.28442	1.89	27.23344	2.96	0.69263	2.28	0.770	3381	29	-0.4
RT11-065	0.28184	1.49	26.05531	2.64	0.66860	2.18	0.825	3367	23	1.9
RT11-066	0.27286	1.60	22.49712	2.75	0.59620	2.24	0.812	3316	25	9.9
RT11-067	0.28000	1.63	26.69464	2.95	0.68931	2.46	0.833	3357	25	-0.8
RT11-068	0.28518	1.59	26.50548	2.68	0.67190	2.16	0.805	3385	25	2.1
RT11-069	0.26940	2.24	20.64530	4.33	0.55392	3.70	0.856	3296	35	15.9
RT11-070	0.28007	1.81	25.53510	2.85	0.65892	2.19	0.771	3357	28	2.8
RT11-071	0.27942	1.68	27.01078	2.93	0.69830	2.41	0.820	3353	26	-1.9
RT11-072	0.28464	1.75	26.56593	2.90	0.67411	2.31	0.796	3382	27	1.7
RT11-073	0.28144	1.59	26.06193	2.53	0.66874	1.97	0.778	3365	25	1.8
RT11-074	0.28498	1.58	26.54792	2.95	0.67265	2.49	0.844	3384	25	2.0
RT11-075	0.28589	1.79	26.50658	2.93	0.66937	2.32	0.791	3389	28	2.5
RT11-076	0.28726	1.61	26.36233	2.69	0.66246	2.16	0.802	3397	25	3.6

Table B.1 continued from previous page

Analysis-#	$^{207}Pb/^{206}Pb$ Bias Corr.	% 2σ	$^{207}Pb/^{235}U$ Bias Corr.	% 2σ	$^{206}Pb/^{238}U$ Bias Corr.	% 2σ	corr. coef.	$^{207}Pb/^{206}Pb$ Age (Ma)	2σ	Discordance (%)
RT11-077	0.28628	1.43	26.66312	2.42	0.67222	1.95	0.805	3391	22	2.2
RT11-078	0.28180	1.64	26.62917	2.66	0.68197	2.09	0.787	3367	26	0.4
RT11-079	0.28718	1.64	26.67924	2.68	0.67034	2.12	0.792	3396	25	2.6
RT11-080	0.28014	1.68	27.37123	2.89	0.70491	2.35	0.814	3357	26	-2.5
RT11-081	0.28016	1.61	26.32897	2.92	0.67777	2.44	0.834	3358	25	0.6
RT11-082	0.28534	1.91	26.82755	2.96	0.67791	2.26	0.763	3386	30	1.4
RT11-083	0.28117	1.59	26.34143	2.76	0.67542	2.26	0.818	3363	25	1.0
RT11-084	0.28220	1.58	27.29839	2.70	0.69731	2.19	0.810	3369	25	-1.3
RT11-085	0.27949	1.92	26.36018	3.22	0.67982	2.59	0.803	3354	30	0.2
RT11-086	0.28449	1.74	27.26859	2.81	0.69080	2.20	0.785	3381	27	-0.2
RT11-087	0.28818	1.57	27.19632	2.73	0.68004	2.23	0.818	3402	24	1.6
RT11-088	0.28815	1.54	27.17367	2.71	0.67947	2.23	0.824	3401	24	1.7
RT11-089	0.28245	1.93	26.33576	3.24	0.67174	2.60	0.803	3370	30	1.7
RT11-090	0.28633	1.65	27.24077	2.76	0.68533	2.21	0.801	3391	26	0.7
RT11-091	0.28096	1.66	27.51509	2.97	0.70522	2.47	0.830	3362	26	-2.4
RT11-092	0.28199	1.71	27.44248	2.74	0.70069	2.15	0.783	3368	27	-1.7
RT11-093	0.28447	1.75	28.00291	2.75	0.70869	2.12	0.772	3381	27	-2.2
RT11-094	0.27835	1.96	26.77431	3.05	0.69243	2.34	0.766	3347	31	-1.4
RT11-095	0.28538	1.69	27.17586	2.90	0.68544	2.36	0.813	3386	26	0.5
RT11-096	0.28833	1.72	27.66025	2.77	0.69045	2.17	0.784	3402	27	0.4
RT11-097	0.28517	1.79	27.40037	2.94	0.69148	2.33	0.793	3385	28	-0.2
RT11-098	0.28791	1.70	27.08118	3.07	0.67685	2.55	0.831	3400	27	1.9
RT11-099	0.28942	1.71	27.72226	2.89	0.68919	2.33	0.807	3408	27	0.8
RT11-100	0.27884	1.76	25.70318	3.14	0.66318	2.60	0.827	3350	28	2.1
RT11-101	0.28060	1.75	27.53906	2.62	0.70591	1.94	0.743	3360	27	-2.5
RT11-102	0.28236	1.74	27.20954	2.89	0.69305	2.31	0.799	3370	27	-0.8
RT11-103	0.28820	1.73	27.28755	2.78	0.68088	2.18	0.783	3402	27	1.5
RT11-104	0.28485	1.78	25.99381	3.30	0.65618	2.78	0.842	3383	28	3.9
RT11-105	0.28530	1.61	27.04791	2.84	0.68165	2.34	0.824	3386	25	1.0
RT11-106	0.28158	1.74	26.45167	3.20	0.67538	2.69	0.840	3365	27	1.1
RT11-107	0.26289	2.88	18.25201	6.58	0.49911	5.91	0.899	3258	45	24.7
RT11-108	0.27389	1.83	25.28679	3.01	0.66367	2.39	0.794	3322	29	1.2
RT11-109	0.28447	1.73	27.50296	2.73	0.69495	2.12	0.775	3381	27	-0.7
RT11-110	0.27728	2.05	24.85462	3.76	0.64427	3.15	0.838	3341	32	4.1
RT11-111	0.22554	4.33	12.37737	7.17	0.39435	5.71	0.797	3015	69	40.6
RT11-112	0.29394	1.84	27.45512	3.54	0.67114	3.02	0.854	3432	29	3.6
RT11-113	0.28003	2.12	27.22729	3.72	0.69858	3.06	0.822	3357	33	-1.8
RT11-114	0.28642	1.82	27.09625	3.08	0.67968	2.48	0.807	3392	28	1.4
RT11-115	0.28379	2.08	26.30013	3.40	0.66578	2.69	0.792	3378	32	2.6

Table B.1 continued from previous page

Analysis-#	$^{207}Pb/^{206}Pb$ Bias Corr.	% 2σ	$^{207}Pb/^{235}U$ Bias Corr.	% 2σ	$^{206}Pb/^{238}U$ Bias Corr.	% 2σ	corr. coef.	$^{207}Pb/^{206}Pb$ Age (Ma)	2σ	Discordance (%)
RT11-116	0.28092	1.74	27.81137	2.81	0.71119	2.21	0.785	3362	27	-3.0
RT11-117	0.28260	1.81	27.95636	2.98	0.71061	2.36	0.794	3371	28	-2.7
RT11-118	0.28797	1.75	26.95942	2.92	0.67246	2.33	0.799	3400	27	2.5
RT11-119	0.29001	1.61	27.53165	2.67	0.68188	2.13	0.799	3411	25	1.7
RT11-120	0.26364	2.76	23.70855	3.90	0.64588	2.76	0.707	3262	43	1.5
RT11-121	0.27842	1.83	26.40362	3.02	0.68136	2.40	0.794	3348	29	-0.1
RT11-122	0.28076	2.13	26.96599	3.55	0.69012	2.85	0.801	3361	33	-0.7
RT11-123	0.28102	1.80	25.81734	3.32	0.66014	2.79	0.840	3362	28	2.8
RT11-124	0.27774	1.88	23.54552	3.13	0.60920	2.50	0.799	3344	29	8.9
RT11-125	0.28133	1.97	26.11386	3.14	0.66706	2.44	0.779	3364	31	2.0
RT11-126	0.27999	1.96	25.41602	4.00	0.65239	3.49	0.872	3357	31	3.6
RT11-127	0.28258	1.81	26.53124	3.15	0.67480	2.57	0.818	3371	28	1.3
RT11-128	0.27624	2.15	23.70860	3.54	0.61690	2.81	0.793	3336	34	7.6
RT11-129	0.26379	2.30	16.66742	4.25	0.45418	3.58	0.842	3263	36	35.1
RT11-130	0.28574	1.85	27.45631	3.25	0.69076	2.67	0.822	3388	29	0.0
RT11-131	0.28045	1.86	26.37703	3.17	0.67617	2.57	0.810	3359	29	0.8
RT11-132	0.26756	2.60	20.32268	4.26	0.54630	3.37	0.791	3286	41	16.8
RT11-133	0.28446	1.81	25.19473	3.56	0.63709	3.07	0.861	3381	28	6.3
RT11-134	0.27685	1.78	25.30975	3.32	0.65762	2.81	0.845	3339	28	2.4
RT11-135	0.25825	1.99	18.54047	3.73	0.51648	3.15	0.846	3230	31	20.2
RT11-136	0.28049	2.09	24.97858	3.42	0.64072	2.71	0.791	3359	33	5.2
RT11-137	0.27395	1.96	24.05600	4.41	0.63183	3.95	0.896	3323	31	5.2
RT11-138	0.23930	2.56	14.41045	5.15	0.43333	4.47	0.868	3109	41	33.9
RT11-139	0.28240	1.66	22.76787	2.94	0.58021	2.43	0.826	3370	26	14.2
RT11-140	0.28880	2.06	25.80252	3.26	0.64303	2.53	0.776	3405	32	6.3
RT11-141	0.28872	1.93	26.64273	3.25	0.66436	2.61	0.803	3404	30	3.6
RT11-142	0.28307	1.94	25.77842	3.28	0.65571	2.64	0.807	3374	30	3.7
RT11-143	0.27160	2.44	22.64069	5.40	0.60027	4.81	0.892	3309	38	9.1
RT11-144	0.28979	1.81	26.81601	3.17	0.66640	2.60	0.821	3410	28	3.5
RT11-145	0.27982	1.78	25.91546	3.15	0.66705	2.60	0.825	3356	28	1.8
RT11-146	0.28302	1.65	26.43324	2.79	0.67275	2.25	0.807	3373	26	1.6
RT11-147	0.28130	1.88	27.02814	2.89	0.69218	2.19	0.758	3364	29	-0.9
RT11-148	0.27818	1.63	26.45224	2.88	0.68508	2.37	0.824	3346	25	-0.6
RT11-149	0.28447	1.64	26.20277	2.55	0.66369	1.96	0.768	3381	25	3.0
RT11-150	0.28227	1.65	27.31625	2.98	0.69737	2.48	0.833	3369	26	-1.3
RT11-151	0.27806	1.76	24.71619	3.22	0.64108	2.69	0.837	3346	28	4.7
RT11-152	0.27691	1.81	26.17876	2.99	0.68193	2.38	0.796	3339	28	-0.5
RT11-153	0.28697	1.65	27.49351	3.00	0.69113	2.50	0.836	3395	26	0.2
RT11-154	0.28610	1.73	26.88880	2.82	0.67806	2.23	0.791	3390	27	1.5

Table B.1 continued from previous page

Analysis-#	$^{207}Pb/^{206}Pb$ Bias Corr.	% 2σ	$^{207}Pb/^{235}U$ Bias Corr.	% 2σ	$^{206}Pb/^{238}U$ Bias Corr.	% 2σ	corr. coef.	$^{207}Pb/^{206}Pb$ Age (Ma)	2σ	Discordance (%)
RT11-155	0.28496	1.70	27.19792	2.66	0.68866	2.04	0.768	3384	26	0.1
RT11-156	0.27564	2.11	24.57349	3.29	0.64335	2.52	0.767	3332	33	4.0
RT11-157	0.28279	1.83	27.25471	2.96	0.69557	2.33	0.786	3372	29	-1.0
RT11-158	0.27365	1.75	24.28818	3.08	0.64064	2.53	0.821	3321	27	4.0
RT11-159	0.27974	1.68	26.19294	2.80	0.67592	2.23	0.799	3355	26	0.7
RT11-160	0.29101	1.62	27.67533	2.86	0.68659	2.36	0.824	3417	25	1.3
RT11-161	0.28250	1.85	27.42330	3.07	0.70552	2.45	0.797	3371	29	-2.1
RT11-162	0.28277	1.64	26.54373	2.64	0.67841	2.07	0.783	3372	26	0.9
RT11-163	0.28249	1.83	25.96105	3.05	0.66424	2.44	0.799	3370	29	2.6
RT11-164	0.28934	1.72	26.96954	2.95	0.67379	2.40	0.814	3408	27	2.5
RT11-165	0.28396	1.93	27.05022	3.04	0.68868	2.34	0.771	3379	30	-0.1
RT11-166	0.28737	1.53	26.93739	2.70	0.67775	2.23	0.824	3397	24	1.8
RT11-167	0.29210	1.75	27.54519	2.82	0.68189	2.21	0.785	3422	27	2.0
RT11-168	0.28746	1.65	26.67795	2.92	0.67115	2.40	0.825	3398	26	2.6
RT11-169	0.28695	1.61	27.08134	2.61	0.68260	2.05	0.787	3395	25	1.1
RT11-170	0.28216	1.64	26.17881	2.91	0.67111	2.40	0.825	3369	26	1.7
RT11-171	0.28833	1.72	27.26902	3.18	0.68435	2.67	0.840	3402	27	1.1
RT11-172	0.28541	1.69	27.25761	2.76	0.69114	2.18	0.789	3386	26	-0.1
RT11-174	0.28477	1.64	27.34034	2.84	0.69495	2.32	0.817	3383	26	-0.6
RT11-175	0.28153	1.67	27.39200	2.71	0.70437	2.13	0.787	3365	26	-2.2
RT11-176	0.28765	1.83	25.80492	2.82	0.64961	2.15	0.760	3399	29	5.2
RT11-177	0.32593	5.48	34.06816	6.71	0.75699	3.87	0.577	3592	84	-1.2
RT11-178	0.28802	1.75	26.67098	2.84	0.67070	2.24	0.788	3401	27	2.7
RT11-179	0.28050	1.72	26.89019	2.76	0.69442	2.16	0.782	3359	27	-1.3
RT11-180	0.28575	2.68	27.55474	4.07	0.69860	3.06	0.752	3388	42	-0.9
RT11-181	0.28725	1.67	27.49286	2.73	0.69364	2.16	0.792	3396	26	-0.1
RT11-182	0.28577	1.57	26.54100	2.72	0.67315	2.22	0.816	3388	24	2.0
RT11-183	0.28248	1.61	26.65976	2.84	0.68411	2.34	0.823	3370	25	0.2
RT11-184	0.28406	1.73	27.16119	2.76	0.69317	2.15	0.780	3379	27	-0.5
RT11-185	0.27637	1.59	23.83315	2.59	0.62523	2.05	0.790	3336	25	6.5
RT11-186	0.28836	1.54	26.43766	2.85	0.66479	2.40	0.842	3402	24	3.5
RT11-187	0.28696	1.79	27.74578	3.02	0.70116	2.43	0.806	3395	28	-1.0
RT11-188	0.28156	1.56	26.87365	2.53	0.69221	2.00	0.789	3365	24	-0.8
RT11-189	0.28857	1.56	26.79726	2.83	0.67353	2.37	0.836	3404	24	2.4
RT11-190	0.28808	1.58	27.14523	2.57	0.68352	2.02	0.788	3401	25	1.2
RT11-191	0.28636	1.71	27.13275	2.76	0.68753	2.16	0.784	3392	27	0.5
RT11-192	0.28660	1.65	27.34867	2.47	0.69250	1.84	0.745	3393	26	-0.1
RT11-193	0.28454	1.62	27.38004	2.79	0.69837	2.28	0.815	3382	25	-1.0
RT11-194	0.28710	1.75	28.76890	2.91	0.72735	2.33	0.799	3396	27	-3.7

Table B.1 continued from previous page

Analysis-#	$^{207}Pb/^{206}Pb$ Bias Corr.	% 2σ	$^{207}Pb/^{235}U$ Bias Corr.	% 2σ	$^{206}Pb/^{238}U$ Bias Corr.	% 2σ	corr. coef.	$^{207}Pb/^{206}Pb$ Age (Ma)	2σ	Discordance (%)
RT11-195	0.28444	1.48	27.85347	2.68	0.71087	2.23	0.833	3381	23	-2.4
RT11-197	0.29173	1.67	26.63899	2.66	0.66299	2.07	0.779	3421	26	4.2
RT11-198	0.28338	1.69	27.34649	2.58	0.70073	1.96	0.757	3375	26	-1.5
RT11-199	0.28243	1.71	25.83641	3.20	0.66431	2.70	0.845	3370	27	2.5
RT11-200	0.28449	1.51	27.98177	2.56	0.71434	2.06	0.807	3381	24	-2.8
RT11-201	0.28823	1.49	26.54275	2.51	0.66939	2.02	0.806	3402	23	2.9
RT11-202	0.28313	1.71	26.33001	2.88	0.67603	2.32	0.805	3374	27	1.3
RT11-203	0.28435	1.58	26.93930	2.64	0.68877	2.11	0.801	3381	25	0.0
RT11-204	0.28019	1.73	24.82320	2.97	0.64412	2.42	0.814	3358	27	4.7
RT11-205	0.29102	1.77	28.00564	2.84	0.69971	2.23	0.783	3417	27	-0.2
RT11-206	0.28562	1.62	27.63159	2.74	0.70346	2.21	0.808	3388	25	-1.4
RT11-207	0.27811	1.84	27.52615	3.30	0.71976	2.73	0.829	3346	29	-4.3
RT11-208	0.28456	1.74	27.69045	2.80	0.70766	2.19	0.783	3382	27	-2.0
RT11-209	0.27885	1.81	28.21062	3.00	0.73577	2.39	0.797	3350	28	-5.8
RT11-210	0.28231	1.58	28.80086	2.73	0.74200	2.23	0.816	3369	25	-5.9
RT11-211	0.28485	1.79	26.38012	2.90	0.67373	2.29	0.788	3383	28	1.8
RT11-212	0.28496	1.84	28.10025	3.05	0.71742	2.43	0.797	3384	29	-3.0
RT11-213	0.27977	1.87	24.71872	3.56	0.64281	3.02	0.850	3355	29	4.8
RT11-214	0.28745	1.60	27.11765	2.75	0.68638	2.24	0.814	3398	25	0.8
RT11-215	0.28207	1.85	26.65130	2.90	0.68748	2.23	0.770	3368	29	-0.2
RT11-216	0.28408	1.82	26.64425	2.89	0.68246	2.24	0.777	3379	28	0.7
RT11-217	0.28426	1.73	26.93789	2.93	0.68957	2.36	0.806	3380	27	-0.1
RT11-218	0.28886	1.77	27.12114	2.85	0.68324	2.23	0.783	3405	28	1.4
RT11-219	0.28840	1.63	26.38747	2.81	0.66585	2.29	0.814	3403	25	3.3
RT11-220	0.29012	1.82	27.11563	2.77	0.68019	2.09	0.754	3412	28	1.9
RT11-221	0.28875	1.87	27.10283	2.79	0.68315	2.07	0.741	3405	29	1.3
RT11-222	0.28314	1.54	27.09139	2.90	0.69643	2.46	0.848	3374	24	-1.1
RT11-223	0.28681	1.54	27.46378	2.65	0.69698	2.16	0.815	3394	24	-0.5
RT11-224	0.29325	1.62	27.51474	2.73	0.68294	2.20	0.806	3429	25	2.1
RT11-225	0.28156	1.75	26.57016	2.68	0.68689	2.04	0.760	3365	27	-0.2
RT11-226	0.28878	1.72	27.30775	2.78	0.68833	2.18	0.784	3405	27	0.8
RT11-227	0.28155	1.50	26.69914	2.52	0.69025	2.02	0.804	3365	23	-0.6
RT11-228	0.28248	1.80	27.20720	2.89	0.70107	2.27	0.784	3370	28	-1.7
RT11-229	0.28425	1.58	26.43620	2.83	0.67698	2.35	0.829	3380	25	1.3
RT11-230	0.26711	1.87	20.43266	3.41	0.55681	2.85	0.836	3283	29	15.0
RT11-231	0.28985	1.59	27.32510	2.68	0.68621	2.16	0.804	3410	25	1.2
RT11-233	0.28337	1.77	26.50779	2.80	0.68089	2.16	0.773	3375	28	0.7
RT11-234	0.28546	1.41	26.04452	2.62	0.66407	2.21	0.844	3387	22	3.1
RT11-235	0.28739	1.65	25.93252	2.66	0.65675	2.08	0.784	3397	26	4.3

Table B.1 continued from previous page

Analysis-#	$^{207}Pb/^{206}Pb$ Bias Corr.	% 2σ	$^{207}Pb/^{235}U$ Bias Corr.	% 2σ	$^{206}Pb/^{238}U$ Bias Corr.	% 2σ	corr. coef.	$^{207}Pb/^{206}Pb$ Age (Ma)	2σ	Discordance (%)
RT11-236	0.27520	1.85	22.32749	2.96	0.59049	2.31	0.781	3330	29	11.2
RT11-237	0.28425	1.86	27.14252	3.02	0.69495	2.38	0.787	3380	29	-0.7
RT11-238	0.28347	1.45	26.20894	2.49	0.67288	2.02	0.812	3376	23	1.7
RT11-239	0.28637	1.83	25.82551	2.87	0.65629	2.21	0.771	3392	28	4.2
RT11-240	0.28472	1.44	26.26984	2.72	0.67141	2.31	0.848	3383	22	2.1
RT11-241	0.28412	1.71	26.84284	2.81	0.68738	2.23	0.794	3379	27	0.1
RT11-242	0.27413	1.90	25.84111	2.93	0.68579	2.24	0.763	3324	30	-1.4
RT11-243	0.27784	1.98	25.89962	2.80	0.67813	1.98	0.707	3345	31	0.1
RT11-244	0.28075	1.94	26.47765	2.95	0.68603	2.23	0.753	3361	30	-0.3
RT11-245	0.28643	1.98	26.16616	2.92	0.66448	2.15	0.734	3392	31	3.2
RT11-246	0.28236	1.68	26.10259	2.71	0.67235	2.12	0.783	3370	26	1.6
RT11-247	0.27661	1.88	26.55996	2.98	0.69830	2.30	0.774	3338	29	-2.3
RT11-248	0.28479	1.65	25.59298	2.72	0.65350	2.17	0.796	3383	26	4.3
RT11-249	0.27623	1.91	25.71237	2.84	0.67684	2.10	0.741	3335	30	0.0
RT11-250	0.27821	2.01	26.43296	3.17	0.69080	2.46	0.774	3347	31	-1.2
RT11-251	0.29027	1.80	26.75661	2.65	0.66999	1.95	0.735	3413	28	3.1
RT11-252	0.27955	1.85	26.31921	2.97	0.68422	2.32	0.781	3354	29	-0.3
RT11-253	0.28442	1.80	26.78993	2.82	0.68447	2.17	0.770	3381	28	0.5
RT11-254	0.27953	1.87	27.10681	3.01	0.70458	2.37	0.785	3354	29	-2.5
RT11-255	0.28572	1.91	27.04985	3.18	0.68779	2.55	0.801	3388	30	0.3
RT11-256	0.29018	1.73	26.95922	2.68	0.67487	2.05	0.765	3412	27	2.5
RT11-257	0.28437	1.55	25.88527	2.60	0.66113	2.09	0.803	3381	24	3.3
RT11-258	0.28069	1.82	25.19542	2.90	0.65186	2.25	0.778	3360	28	3.8
RT11-259	0.28461	1.69	25.72560	3.02	0.65632	2.51	0.830	3382	26	3.9
RT11-260	0.27907	1.74	25.93045	2.88	0.67456	2.30	0.798	3351	27	0.8
RT11-261	0.28490	1.83	26.51972	2.82	0.67540	2.14	0.760	3384	29	1.6
RT11-262	0.27950	1.60	24.62681	2.89	0.63920	2.40	0.831	3354	25	5.2
RT11-263	0.28395	1.68	25.21361	3.02	0.64405	2.51	0.832	3379	26	5.3
RT11-264	0.27018	1.81	20.48488	3.18	0.54984	2.61	0.822	3301	28	16.8
RT11-265	0.28813	1.68	26.59484	2.94	0.66925	2.41	0.821	3401	26	2.9
RT11-266	0.28658	1.74	26.68393	2.84	0.67498	2.25	0.790	3393	27	2.0
RT11-267	0.29189	1.69	27.35255	3.01	0.67919	2.49	0.827	3421	26	2.3
RT11-268	0.29365	1.62	27.05926	2.89	0.66775	2.40	0.828	3431	25	4.0
RT11-269	0.28546	1.74	27.43192	2.88	0.69622	2.29	0.796	3387	27	-0.7
RT11-270	0.29374	1.57	27.76860	2.70	0.68476	2.20	0.814	3431	24	2.0
RT11-271	0.28640	1.77	27.35269	2.69	0.69117	2.03	0.753	3392	28	0.1
RT11-272	0.28751	1.99	25.90612	3.03	0.65195	2.28	0.752	3398	31	4.9
RT11-273	0.28704	1.66	26.95752	2.85	0.67936	2.31	0.811	3395	26	1.5
RT11-274	0.27838	1.92	24.66563	3.43	0.64077	2.84	0.829	3348	30	4.8

Table B.1 continued from previous page

Analysis-#	$^{207}Pb/^{206}Pb$ Bias Corr.	% 2σ	$^{207}Pb/^{235}U$ Bias Corr.	% 2σ	$^{206}Pb/^{238}U$ Bias Corr.	% 2σ	corr. coef.	$^{207}Pb/^{206}Pb$ Age (Ma)	2σ	Discordance (%)
RT11-275	0.28348	1.61	26.18346	2.84	0.66779	2.34	0.824	3376	25	2.3
RT11-276	0.28918	1.67	27.40675	2.92	0.68503	2.40	0.821	3407	26	1.2
RT11-277	0.28894	1.61	26.73816	2.72	0.66871	2.19	0.807	3406	25	3.1
RT11-278	0.28299	1.62	26.57182	2.80	0.67833	2.28	0.815	3373	25	1.0
RT11-279	0.27914	1.82	26.57336	2.89	0.68753	2.25	0.777	3352	28	-0.7
RT11-280	0.28292	1.86	27.04982	3.00	0.69033	2.35	0.784	3373	29	-0.4
RT11-281	0.26699	1.76	22.76933	4.12	0.61515	3.73	0.904	3282	28	6.1
RT11-282	0.28127	1.72	27.42330	2.86	0.70284	2.29	0.799	3364	27	-2.1
RT11-283	0.28604	1.65	26.45763	2.81	0.66658	2.28	0.811	3390	26	2.9
RT11-284	0.28347	2.13	26.82421	3.08	0.68162	2.22	0.722	3376	33	0.7
RT11-285	0.28434	1.64	25.97770	2.82	0.65787	2.29	0.814	3381	26	3.6
RT11-286	0.28796	1.89	26.34891	3.07	0.65865	2.41	0.787	3400	29	4.2
RT11-287	0.28185	1.83	25.70677	3.24	0.65631	2.67	0.825	3367	29	3.4
RT11-288	0.28259	1.72	26.31123	2.82	0.66972	2.24	0.793	3371	27	1.9
RT11-289	0.28178	1.84	25.74146	3.33	0.65688	2.78	0.834	3367	29	3.3
RT11-290	0.28692	1.69	27.24013	2.86	0.68242	2.31	0.807	3395	26	1.1
RT11-291	0.27769	1.98	26.96596	3.27	0.69715	2.60	0.796	3344	31	-2.0
RT11-292	0.27799	1.80	23.60865	4.18	0.60946	3.77	0.902	3345	28	9.0
RT11-293	0.28420	1.96	26.44704	3.05	0.66755	2.34	0.767	3380	30	2.4
RT11-294	0.28719	1.71	27.06714	3.07	0.67580	2.54	0.829	3396	27	2.0
RT11-295	0.27544	1.93	22.12125	3.91	0.57563	3.40	0.870	3331	30	13.6
RT11-296	0.28229	1.66	26.34750	3.15	0.66869	2.68	0.850	3369	26	2.0
RT11-297	0.28385	1.65	27.33435	2.88	0.68965	2.36	0.820	3378	26	-0.2
RT11-298	0.27675	1.79	23.90072	3.97	0.61822	3.54	0.893	3338	28	7.5
RT11-299	0.27998	1.73	27.50073	2.97	0.70282	2.42	0.814	3357	27	-2.3
RT11-300	0.29325	1.81	26.62315	3.08	0.64932	2.49	0.809	3429	28	6.2
RT11-301	0.28743	2.00	27.27354	3.38	0.67763	2.73	0.807	3397	31	1.8
RT11-302	0.28165	1.77	26.40831	3.38	0.66927	2.88	0.852	3366	28	1.8
RT11-303	0.27465	1.83	24.35439	4.10	0.63253	3.67	0.895	3327	29	5.2
RT11-304	0.27505	1.73	22.93548	4.39	0.59441	4.03	0.919	3329	27	10.6
RT11-305	0.28529	1.64	27.38290	2.66	0.68386	2.10	0.788	3386	26	0.7
RT11-306	0.28552	1.75	27.83672	2.88	0.69409	2.29	0.796	3387	27	-0.4
RT11-307	0.22686	2.97	10.16103	6.00	0.31868	5.22	0.869	3024	48	69.4
RT11-308	0.28378	1.56	27.26574	2.52	0.68329	1.97	0.785	3378	24	0.5
RT11-309	0.28872	1.66	27.14669	2.99	0.66832	2.49	0.831	3404	26	3.1
RT11-310	0.28692	1.67	28.39721	2.72	0.70312	2.14	0.787	3395	26	-1.2

Table B.2.: U-Pb data from the sample CH2 showing all relevant isotope ratios and $^{207}Pb/^{206}Pb$ ages.

Analysis-#	$^{207}Pb/^{206}Pb$ Bias Corr.	% 2σ	$^{207}Pb/^{235}U$ Bias Corr.	% 2σ	$^{206}Pb/^{238}U$ Bias Corr.	% 2σ	corr. coef.	$^{207}Pb/^{206}Pb$ Age (Ma)	2σ	Discordance (%)
CH2-001	0.21678	3.46	11.03729	7.09	0.36375	6.18	0.873	2951	56	47.4
CH2-002	0.26806	1.97	24.83950	3.09	0.66054	2.38	0.770	3289	31	0.5
CH2-003	0.27315	1.62	25.01243	2.76	0.65148	2.23	0.808	3318	25	2.5
CH2-005	0.26577	1.72	24.72727	3.25	0.65980	2.76	0.848	3275	27	0.2
CH2-006	0.28557	1.66	27.12652	2.59	0.67266	1.99	0.767	3387	26	2.1
CH2-007	0.28945	2.14	27.39196	3.06	0.66919	2.18	0.713	3408	33	3.1
CH2-008	0.26075	4.06	16.10822	9.15	0.43635	8.20	0.896	3245	64	38.9
CH2-009	0.22475	3.02	7.96837	9.06	0.25011	8.55	0.943	3009	48	108.9
CH2-010	0.26598	1.65	20.82426	2.64	0.55185	2.06	0.780	3276	26	15.6
CH2-011	0.26927	1.80	25.42988	2.85	0.66446	2.21	0.775	3296	28	0.3
CH2-012	0.25681	3.21	16.34152	7.02	0.44756	6.24	0.889	3221	51	35.0
CH2-013	0.26942	1.58	25.73591	2.55	0.67170	2.01	0.786	3296	25	-0.6
CH2-014	0.27987	1.56	28.22412	2.59	0.70905	2.08	0.800	3356	24	-2.9
CH2-015	0.26510	1.71	24.85521	2.67	0.65917	2.05	0.767	3271	27	0.1
CH2-016	0.26231	2.01	23.52713	2.94	0.63059	2.15	0.729	3254	32	3.2
CH2-017	0.25316	1.75	16.45161	3.64	0.45693	3.19	0.876	3199	28	31.7
CH2-018	0.21271	3.55	9.46511	5.48	0.31294	4.17	0.761	2920	57	66.2
CH2-019	0.26502	1.83	25.74575	2.70	0.68340	1.98	0.735	3271	29	-2.7
CH2-020	0.26223	1.83	22.93083	3.18	0.61538	2.60	0.818	3254	29	5.2
CH2-021	0.24735	2.23	19.05560	5.68	0.54297	5.22	0.919	3162	35	13.0
CH2-022	0.26964	1.63	25.76389	2.59	0.67391	2.02	0.779	3298	25	-0.8
CH2-023	0.26246	1.75	25.62518	2.64	0.68907	1.97	0.747	3255	28	-3.7
CH2-024	0.26511	1.62	25.76370	2.85	0.68634	2.34	0.822	3271	26	-3.0
CH2-025	0.27052	1.65	25.55285	2.62	0.66758	2.04	0.778	3303	26	0.1
CH2-026	0.26470	1.69	23.63091	2.59	0.63142	1.96	0.757	3269	27	3.5
CH2-027	0.26334	1.62	21.28403	3.63	0.57215	3.25	0.896	3261	25	11.7
CH2-028	0.26847	1.57	25.01734	2.60	0.66019	2.07	0.797	3291	25	0.6
CH2-029	0.26820	1.58	25.16683	2.74	0.66536	2.24	0.817	3289	25	0.0
CH2-030	0.26625	1.50	24.51137	2.58	0.65335	2.10	0.813	3278	24	1.0
CH2-031	0.27439	1.91	24.71698	2.73	0.64167	1.95	0.714	3325	30	4.0
CH2-032	0.25210	1.78	18.79009	3.13	0.53142	2.57	0.822	3192	28	16.1
CH2-033	0.27116	1.55	24.56608	2.48	0.64656	1.93	0.780	3307	24	2.8
CH2-035	0.26551	1.92	13.85027	3.18	0.37305	2.54	0.797	3274	30	60.0
CH2-036	0.26434	1.77	22.98903	2.83	0.62252	2.21	0.781	3267	28	4.6
CH2-037	0.27127	1.64	24.49333	2.54	0.64695	1.94	0.764	3307	26	2.7
CH2-038	0.26888	2.19	23.58054	3.87	0.62916	3.19	0.824	3293	34	4.6
CH2-039	0.11781	10.15	2.35167	10.81	0.14335	3.71	0.344	1918	182	121.9

Table B.2 continued from previous page

Analysis-#	$^{207}Pb/^{206}Pb$ Bias Corr.	% 2σ	$^{207}Pb/^{235}U$ Bias Corr.	% 2σ	$^{206}Pb/^{238}U$ Bias Corr.	% 2σ	corr. coef.	$^{207}Pb/^{206}Pb$ Age (Ma)	2σ	Discordance (%)
CH2-040	0.27477	1.70	25.38912	2.53	0.66419	1.88	0.740	3327	27	1.2
CH2-041	0.26847	1.61	20.11729	3.64	0.54037	3.27	0.897	3291	25	18.1
CH2-042	0.24423	2.50	13.86392	6.57	0.40969	6.08	0.925	3142	40	41.8
CH2-043	0.25788	1.84	20.51915	3.97	0.57474	3.52	0.886	3228	29	10.2
CH2-044	0.26494	1.68	20.45525	3.01	0.55814	2.49	0.829	3270	26	14.3
CH2-045	0.25962	1.73	19.18150	3.13	0.53452	2.61	0.833	3238	27	17.2
CH2-046	0.27630	1.76	24.14542	2.82	0.63270	2.20	0.781	3336	28	5.5
CH2-047	0.27134	1.62	22.72855	2.99	0.60688	2.51	0.839	3308	25	8.1
CH2-048	0.26503	2.03	22.96210	3.02	0.62838	2.23	0.739	3271	32	4.0
CH2-049	0.08935	14.57	1.18992	15.01	0.09666	3.59	0.239	1407	279	136.3
CH2-050	0.27255	1.78	23.86470	2.83	0.63592	2.20	0.777	3314	28	4.4
CH2-051	0.25100	3.73	16.20788	7.00	0.46979	5.93	0.847	3185	59	28.2
CH2-052	0.26911	2.10	23.14901	3.09	0.62617	2.26	0.733	3295	33	5.0
CH2-053	0.27560	1.87	24.73531	2.85	0.65359	2.14	0.753	3332	29	2.7
CH2-054	0.22798	2.64	3.75769	5.79	0.12008	5.15	0.890	3032	42	314.4
CH2-055	0.28873	1.55	26.30266	2.94	0.66391	2.50	0.850	3404	24	3.6
CH2-056	0.21148	3.03	8.49164	5.30	0.29273	4.35	0.820	2911	49	75.7
CH2-057	0.26254	2.16	21.40142	3.22	0.59444	2.39	0.743	3256	34	8.2
CH2-058	0.27215	1.93	24.12317	3.06	0.64654	2.37	0.775	3312	30	2.9
CH2-059	0.27777	1.74	25.25153	2.74	0.66324	2.12	0.773	3344	27	1.9
CH2-061	0.27098	1.67	21.17050	2.78	0.57023	2.21	0.798	3305	26	13.5
CH2-062	0.15021	6.02	2.48415	7.62	0.12070	4.66	0.612	2343	103	218.7
CH2-063	0.26328	1.88	16.17985	3.13	0.44851	2.50	0.798	3260	30	36.4
CH2-064	0.26673	2.46	21.50484	3.39	0.58836	2.34	0.689	3281	39	9.9
CH2-065	0.29045	1.72	27.96467	2.63	0.70252	2.00	0.758	3414	27	-0.6
CH2-067	0.27741	1.77	25.12643	2.76	0.66064	2.12	0.768	3342	28	2.1
CH2-068	0.27318	2.06	24.77007	2.95	0.66119	2.12	0.717	3318	32	1.3
CH2-069	0.27507	1.66	25.92763	2.77	0.68713	2.22	0.800	3329	26	-1.4
CH2-070	0.28431	1.64	26.15884	2.51	0.67053	1.89	0.755	3380	26	2.1
CH2-071	0.28978	1.55	26.82063	2.58	0.67357	2.06	0.799	3410	24	2.6
CH2-072	0.27556	1.80	25.37158	2.88	0.66973	2.26	0.782	3332	28	0.7
CH2-073	0.27323	1.71	23.93458	2.76	0.63687	2.17	0.786	3318	27	4.4
CH2-074	0.28136	2.28	25.18675	3.53	0.65045	2.69	0.763	3364	36	4.1
CH2-075	0.27226	2.00	25.16246	3.00	0.67115	2.23	0.745	3313	31	0.0
CH2-076	0.25571	2.68	16.09164	7.57	0.45671	7.08	0.935	3214	42	32.4
CH2-077	0.27145	2.20	22.53296	3.79	0.60205	3.09	0.815	3308	34	8.8
CH2-078	0.27387	1.79	25.41512	2.70	0.67259	2.03	0.750	3322	28	0.1
CH2-079	0.27426	1.65	25.77108	2.59	0.68045	1.99	0.770	3324	26	-0.7
CH2-080	0.26977	1.86	24.65699	2.76	0.66120	2.04	0.739	3298	29	0.7

Table B.2 continued from previous page

Analysis-#	$^{207}Pb/^{206}Pb$ Bias Corr.	% 2σ	$^{207}Pb/^{235}U$ Bias Corr.	% 2σ	$^{206}Pb/^{238}U$ Bias Corr.	% 2σ	corr. coef.	$^{207}Pb/^{206}Pb$ Age (Ma)	2σ	Discordance (%)
CH2-081	0.25161	1.72	19.66439	2.70	0.56637	2.08	0.771	3189	27	10.1
CH2-082	0.26836	1.64	23.93559	2.46	0.64627	1.84	0.747	3290	26	2.3
CH2-083	0.27256	1.47	26.91661	2.93	0.71548	2.54	0.866	3315	23	-4.8
CH2-084	0.11943	5.92	2.38147	7.03	0.14445	3.79	0.539	1943	106	123.1
CH2-085	0.26302	1.58	23.84907	2.43	0.65675	1.85	0.759	3259	25	0.0
CH2-086	0.25862	1.71	21.90415	2.77	0.61337	2.18	0.786	3232	27	4.7
CH2-087	0.26487	1.48	23.38566	2.28	0.63934	1.73	0.760	3270	23	2.5
CH2-088	0.20427	2.91	9.01111	4.32	0.31941	3.19	0.738	2855	47	59.6
CH2-091	0.25976	1.52	24.38095	2.49	0.67921	1.97	0.792	3239	24	-3.1
CH2-092	0.24503	1.66	15.83307	2.85	0.46756	2.31	0.813	3147	26	27.1
CH2-093	0.18046	4.37	6.00790	5.26	0.24088	2.94	0.558	2651	72	90.4
CH2-094	0.26050	1.75	24.05902	2.67	0.66818	2.01	0.754	3244	28	-1.8
CH2-095	0.26718	1.43	24.30846	2.32	0.65818	1.82	0.785	3283	23	0.6
CH2-096	0.26792	1.45	24.05703	2.24	0.64949	1.71	0.764	3288	23	1.8
CH2-097	0.22339	2.79	10.70469	5.94	0.34660	5.24	0.883	2999	45	56.2
CH2-098	0.24122	2.11	15.32775	3.28	0.45958	2.52	0.767	3122	33	28.0
CH2-099	0.26048	1.68	21.32628	2.31	0.59212	1.59	0.688	3243	26	8.1
CH2-100	0.27393	1.40	24.89326	2.26	0.65718	1.77	0.786	3322	22	1.9
CH2-101	0.21872	3.54	9.36742	5.84	0.30967	4.65	0.796	2965	57	70.4
CH2-102	0.24282	2.20	14.27936	5.61	0.42519	5.16	0.920	3132	35	37.0
CH2-103	0.26459	1.43	23.30184	2.29	0.63673	1.80	0.783	3268	22	2.8
CH2-104	0.24300	2.05	14.92272	4.37	0.44396	3.86	0.883	3134	33	32.2
CH2-105	0.26703	1.58	22.75139	2.44	0.61594	1.86	0.763	3282	25	6.0
CH2-106	0.25891	2.30	22.07645	3.48	0.61642	2.61	0.750	3234	36	4.4
CH2-107	0.22101	2.28	12.84204	3.46	0.42006	2.61	0.753	2982	37	31.8
CH2-108	0.26047	1.56	21.72488	3.08	0.60294	2.65	0.861	3243	25	6.5
CH2-109	0.27548	1.49	23.07766	2.38	0.60557	1.85	0.779	3331	23	9.0
CH2-110	0.26294	1.54	22.55082	2.38	0.61997	1.81	0.763	3258	24	4.7
CH2-111	0.27071	1.59	23.44909	2.41	0.62616	1.82	0.752	3304	25	5.3
CH2-112	0.22469	4.77	11.55897	6.37	0.37188	4.22	0.663	3009	77	47.5
CH2-113	0.26947	1.60	24.44413	2.48	0.65573	1.88	0.761	3297	25	1.3
CH2-115	0.26536	1.52	23.59050	2.76	0.64266	2.31	0.835	3273	24	2.2
CH2-116	0.26726	1.45	21.86628	3.27	0.59144	2.93	0.897	3284	23	9.5
CH2-117	0.26797	1.86	24.10893	2.80	0.65038	2.09	0.748	3288	29	1.7
CH2-118	0.26417	1.62	21.95991	2.54	0.60096	1.95	0.770	3266	25	7.5
CH2-119	0.26770	1.50	24.64268	2.39	0.66549	1.86	0.778	3286	24	-0.1
CH2-120	0.28963	1.47	26.03007	2.35	0.64974	1.83	0.780	3409	23	5.6
CH2-121	0.23108	2.20	13.23179	3.70	0.41400	2.97	0.804	3054	35	36.6
CH2-122	0.26849	1.51	24.19282	2.34	0.65151	1.79	0.763	3291	24	1.7

Table B.2 continued from previous page

Analysis-#	$^{207}Pb/^{206}Pb$ Bias Corr.	% 2σ	$^{207}Pb/^{235}U$ Bias Corr.	% 2σ	$^{206}Pb/^{238}U$ Bias Corr.	% 2σ	corr. coef.	$^{207}Pb/^{206}Pb$ Age (Ma)	2σ	Discordance (%)
CH2-123	0.26536	1.70	23.62325	2.71	0.64368	2.12	0.780	3273	27	2.1
CH2-124	0.26724	1.68	28.14671	2.58	0.76156	1.96	0.759	3284	26	-10.1
CH2-125	0.27525	1.44	24.37735	2.41	0.64040	1.93	0.802	3330	22	4.3
CH2-126	0.25117	2.48	20.57638	3.68	0.59240	2.73	0.741	3186	39	6.1
CH2-127	0.26790	1.98	23.98366	2.69	0.64738	1.82	0.677	3288	31	2.1
CH2-128	0.26989	1.52	24.53874	2.41	0.65751	1.86	0.774	3299	24	1.2
CH2-129	0.27196	1.65	24.95562	2.64	0.66361	2.05	0.778	3311	26	0.8
CH2-130	0.27031	1.52	23.26293	2.83	0.62241	2.39	0.844	3302	24	5.7
CH2-131	0.25373	1.67	19.09900	3.00	0.54446	2.49	0.830	3202	26	14.2
CH2-132	0.26878	1.46	24.39906	2.54	0.65661	2.07	0.817	3293	23	1.1
CH2-133	0.26292	1.34	20.95319	2.33	0.57647	1.91	0.818	3258	21	10.9
CH2-134	0.26314	1.46	20.49061	2.56	0.56330	2.11	0.821	3259	23	13.1
CH2-135	0.26453	1.86	21.88351	3.42	0.59846	2.87	0.839	3268	29	8.0
CH2-136	0.21016	2.83	10.11237	5.91	0.34810	5.19	0.878	2901	46	50.5
CH2-137	0.26874	1.68	24.01628	2.69	0.64656	2.10	0.781	3292	26	2.3
CH2-138	0.26270	1.79	20.18724	2.83	0.55600	2.19	0.775	3257	28	14.2
CH2-140	0.26900	1.58	24.22427	2.43	0.65164	1.85	0.761	3294	25	1.7
CH2-141	0.26953	1.58	22.42902	2.55	0.60225	2.00	0.784	3297	25	8.4
CH2-142	0.26067	1.56	20.61008	2.83	0.57223	2.36	0.835	3245	24	11.1
CH2-143	0.26369	1.76	21.13787	2.92	0.58020	2.33	0.797	3263	28	10.5
CH2-144	0.25875	1.73	16.71258	3.79	0.46750	3.38	0.890	3233	27	30.6
CH2-145	0.20529	2.25	10.00391	3.66	0.35272	2.89	0.789	2863	37	46.9
CH2-146	0.27671	1.85	26.64715	2.93	0.69708	2.28	0.776	3338	29	-2.2
CH2-147	0.26543	1.35	20.50905	2.42	0.55933	2.01	0.829	3273	21	14.2
CH2-148	0.27794	1.43	25.78752	2.46	0.67168	2.00	0.813	3345	22	0.9
CH2-149	0.26739	1.34	24.68826	2.57	0.66845	2.19	0.852	3285	21	-0.5
CH2-150	0.26841	1.76	24.68546	2.68	0.66587	2.02	0.753	3291	28	-0.1
CH2-151	0.27028	2.01	25.25867	2.82	0.67672	1.98	0.702	3301	31	-1.0
CH2-152	0.26341	1.69	21.15708	2.60	0.58163	1.98	0.761	3261	27	10.2
CH2-153	0.26791	1.50	23.44727	2.90	0.63381	2.48	0.855	3288	24	3.8
CH2-154	0.26831	1.64	25.16150	2.56	0.67914	1.96	0.767	3290	26	-1.6
CH2-155	0.26689	1.23	22.52731	2.28	0.61132	1.92	0.842	3282	19	6.6
CH2-156	0.26394	1.60	23.45138	2.92	0.64351	2.44	0.836	3264	25	1.8
CH2-157	0.26461	1.62	23.50102	2.62	0.64328	2.06	0.785	3268	26	2.0
CH2-158	0.26918	1.53	25.67720	2.46	0.69093	1.92	0.781	3295	24	-2.8
CH2-159	0.26962	2.37	25.44469	3.30	0.68358	2.30	0.697	3298	37	-1.9
CH2-160	0.17353	4.61	4.06309	5.55	0.16962	3.09	0.556	2586	77	155.8
CH2-161	0.24565	1.65	15.90011	3.03	0.46893	2.54	0.838	3151	26	27.0
CH2-162	0.26543	1.58	23.41424	2.74	0.63911	2.24	0.817	3273	25	2.7

Table B.2 continued from previous page

Analysis-#	$^{207}Pb/^{206}Pb$ Bias Corr.	% 2σ	$^{207}Pb/^{235}U$ Bias Corr.	% 2σ	$^{206}Pb/^{238}U$ Bias Corr.	% 2σ	corr. coef.	$^{207}Pb/^{206}Pb$ Age (Ma)	2σ	Discordance (%)
CH2-163	0.25171	2.11	17.99107	5.24	0.51786	4.80	0.916	3189	33	18.5
CH2-164	0.20394	2.43	7.68752	3.83	0.27313	2.96	0.772	2852	40	83.1
CH2-165	0.26443	1.44	22.52199	2.29	0.61715	1.77	0.776	3267	23	5.3
CH2-166	0.27148	1.59	26.32903	2.44	0.70275	1.86	0.760	3308	25	-3.7
CH2-167	0.24687	2.94	15.99519	8.21	0.46951	7.66	0.934	3159	47	27.2
CH2-168	0.25919	1.82	22.84304	2.87	0.63867	2.22	0.774	3236	29	1.5
CH2-170	0.26706	1.72	25.41784	2.55	0.68975	1.88	0.738	3283	27	-3.0
CH2-171	0.27298	1.64	28.34412	3.66	0.75254	3.27	0.894	3317	26	-8.4
CH2-172	0.26852	1.57	25.73748	2.30	0.69471	1.69	0.733	3291	25	-3.3
CH2-173	0.27110	1.75	26.56873	2.64	0.71034	1.97	0.748	3306	27	-4.5
CH2-174	0.26965	1.64	25.38365	2.62	0.68231	2.05	0.782	3298	26	-1.7
CH2-175	0.27555	1.60	23.50259	2.47	0.61824	1.88	0.761	3332	25	7.3
CH2-176	0.27031	1.79	25.44297	2.47	0.68228	1.71	0.691	3302	28	-1.6
CH2-177	0.25712	1.61	19.14626	2.60	0.53977	2.04	0.785	3223	25	15.7
CH2-179	0.25738	1.44	21.13222	2.57	0.59520	2.13	0.829	3225	23	7.0
CH2-180	0.27097	1.74	25.67965	2.66	0.68700	2.01	0.756	3305	27	-2.0
CH2-181	0.26526	1.40	23.38393	2.56	0.63910	2.14	0.837	3272	22	2.6
CH2-182	0.27238	1.59	23.97668	2.53	0.63816	1.97	0.779	3314	25	4.1
CH2-183	0.27224	1.45	25.21804	2.64	0.67157	2.21	0.835	3313	23	-0.1
CH2-184	0.26718	1.52	25.22986	2.51	0.68461	1.99	0.795	3283	24	-2.4
CH2-185	0.26403	2.70	18.11672	6.47	0.49747	5.88	0.909	3265	42	25.3
CH2-186	0.28552	1.51	27.95883	2.57	0.70996	2.07	0.808	3387	24	-2.1
CH2-187	0.26646	1.73	24.33948	3.09	0.66227	2.56	0.828	3279	27	0.0
CH2-188	0.28259	1.75	24.21652	3.24	0.62131	2.72	0.841	3371	27	8.1
CH2-189	0.27350	1.88	25.19279	2.77	0.66784	2.03	0.733	3320	29	0.6
CH2-190	0.28353	1.43	27.80103	2.37	0.71092	1.89	0.799	3376	22	-2.6
CH2-192	0.22070	2.03	9.89250	3.59	0.32499	2.97	0.826	2980	33	64.1
CH2-193	0.26640	1.89	24.45903	2.88	0.66571	2.18	0.755	3279	30	-0.4
CH2-194	0.26980	1.52	24.94529	2.50	0.67039	1.98	0.792	3299	24	-0.3
CH2-195	0.27563	1.70	25.37066	2.74	0.66739	2.15	0.785	3332	27	1.0
CH2-196	0.26277	1.59	24.09300	2.42	0.66481	1.83	0.754	3257	25	-1.0
CH2-197	0.27334	1.52	25.48697	2.48	0.67608	1.95	0.788	3319	24	-0.4
CH2-198	0.26559	1.72	25.13528	2.70	0.68619	2.08	0.770	3274	27	-2.9
CH2-199	0.26135	1.43	20.08860	3.09	0.55733	2.74	0.887	3249	22	13.7
CH2-200	0.26551	1.72	24.76249	2.71	0.67622	2.10	0.772	3274	27	-1.8
CH2-201	0.26588	1.67	24.76524	2.67	0.67537	2.08	0.780	3276	26	-1.6
CH2-202	0.26737	1.64	23.73995	2.60	0.64379	2.01	0.774	3284	26	2.4
CH2-204	0.27473	1.46	25.65916	2.53	0.67719	2.06	0.817	3327	23	-0.3
CH2-206	0.26511	1.64	22.80669	3.05	0.62375	2.57	0.843	3271	26	4.6

Table B.2 continued from previous page

Analysis-#	$^{207}Pb/^{206}Pb$ Bias Corr.	% 2σ	$^{207}Pb/^{235}U$ Bias Corr.	% 2σ	$^{206}Pb/^{238}U$ Bias Corr.	% 2σ	corr. coef.	$^{207}Pb/^{206}Pb$ Age (Ma)	2σ	Discordance (%)
CH2-207	0.25907	1.58	21.46294	2.65	0.60066	2.13	0.803	3235	25	6.6
CH2-208	0.26807	1.48	24.12753	2.71	0.65256	2.28	0.839	3289	23	1.5
CH2-209	0.22026	1.74	12.57799	3.08	0.41403	2.54	0.825	2977	28	33.2
CH2-210	0.27156	1.52	25.09682	2.55	0.67006	2.05	0.805	3309	24	0.0
CH2-211	0.26864	1.52	24.64868	2.43	0.66520	1.89	0.780	3292	24	0.1
CH2-212	0.27027	1.66	24.50955	2.53	0.65746	1.91	0.756	3301	26	1.3
CH2-213	0.27070	1.73	22.77317	3.24	0.60989	2.73	0.845	3304	27	7.5
CH2-214	0.26841	1.59	24.13635	2.49	0.65191	1.92	0.769	3291	25	1.6
CH2-215	0.26890	1.92	24.04117	2.85	0.64816	2.10	0.739	3293	30	2.2
CH2-216	0.29118	1.59	26.65481	2.70	0.66363	2.18	0.809	3418	25	4.1
CH2-217	0.26592	1.65	19.64697	2.84	0.53561	2.31	0.814	3276	26	18.4
CH2-218	0.26554	2.04	23.01286	2.85	0.62825	1.99	0.698	3274	32	4.1
CH2-219	0.27500	1.56	23.77517	2.51	0.62672	1.97	0.784	3329	24	6.0
CH2-220	0.26722	1.62	23.33579	2.66	0.63306	2.10	0.791	3284	25	3.8
CH2-221	0.26263	1.82	23.51170	2.51	0.64894	1.73	0.690	3256	29	0.9
CH2-223	0.26474	1.96	21.96207	3.06	0.60132	2.35	0.768	3269	31	7.6
CH2-224	0.26973	1.67	23.01357	3.09	0.61843	2.60	0.841	3298	26	6.2
CH2-225	0.26825	1.76	23.05517	2.61	0.62296	1.93	0.739	3290	28	5.3
CH2-226	0.28990	1.48	26.31084	2.47	0.65783	1.98	0.801	3411	23	4.6
CH2-227	0.27221	1.59	23.76504	2.47	0.63277	1.89	0.767	3313	25	4.7
CH2-228	0.27694	1.67	24.20092	2.64	0.63337	2.04	0.774	3340	26	5.5
CH2-229	0.27009	1.53	21.42897	2.44	0.57503	1.90	0.778	3300	24	12.6
CH2-230	0.26665	1.50	23.65324	2.38	0.64290	1.85	0.777	3280	24	2.4
CH2-231	0.27249	1.97	23.85017	2.83	0.63433	2.03	0.717	3314	31	4.6
CH2-232	0.25727	1.82	18.76394	2.87	0.52857	2.22	0.775	3224	29	17.8
CH2-233	0.27269	1.66	23.41251	2.75	0.62221	2.20	0.798	3315	26	6.2
CH2-235	0.26831	1.33	24.35117	2.34	0.65770	1.92	0.822	3290	21	0.9
CH2-236	0.27147	1.62	23.64798	2.57	0.63127	2.00	0.777	3308	25	4.8
CH2-237	0.26870	1.57	21.75859	2.79	0.58681	2.30	0.826	3292	25	10.5
CH2-238	0.27104	1.89	22.57609	3.05	0.60359	2.40	0.786	3306	30	8.5
CH2-239	0.27462	1.63	24.13708	2.67	0.63691	2.11	0.792	3326	25	4.6
CH2-240	0.26759	1.58	23.72780	2.50	0.64255	1.94	0.776	3286	25	2.6
CH2-241	0.27541	1.85	24.56405	2.77	0.64628	2.06	0.743	3331	29	3.6
CH2-242	0.12044	11.01	2.33455	11.46	0.14045	3.18	0.277	1958	196	130.9
CH2-243	0.27284	1.57	23.85460	2.49	0.63349	1.94	0.778	3316	25	4.7
CH2-244	0.25189	1.90	14.40296	3.13	0.41430	2.49	0.794	3191	30	42.7
CH2-245	0.27490	1.72	22.54148	3.06	0.59413	2.52	0.826	3328	27	10.6
CH2-246	0.26801	1.78	21.71825	2.86	0.58715	2.24	0.783	3288	28	10.3
CH2-247	0.25999	1.66	21.15796	2.77	0.58964	2.22	0.800	3240	26	8.4

Table B.2 continued from previous page

Analysis-#	$^{207}Pb/^{206}Pb$ Bias Corr.	% 2σ	$^{207}Pb/^{235}U$ Bias Corr.	% 2σ	$^{206}Pb/^{238}U$ Bias Corr.	% 2σ	corr. coef.	$^{207}Pb/^{206}Pb$ Age (Ma)	2σ	Discordance (%)
CH2-248	0.27246	1.59	23.52139	2.51	0.62549	1.94	0.772	3314	25	5.7
CH2-249	0.26452	2.14	21.33322	4.64	0.58433	4.12	0.888	3268	34	10.1
CH2-250	0.26663	1.97	22.85963	2.88	0.62118	2.10	0.730	3280	31	5.2
CH2-251	0.26010	1.88	20.05662	3.10	0.55867	2.46	0.794	3241	30	13.2
CH2-252	0.26376	1.87	21.81636	2.84	0.59926	2.14	0.752	3263	29	7.7
CH2-253	0.26579	2.01	20.17483	3.05	0.54993	2.30	0.754	3275	32	15.8
CH2-254	0.27225	1.41	23.06214	2.50	0.61372	2.07	0.827	3313	22	7.3
CH2-255	0.27040	1.67	22.46061	2.57	0.60181	1.95	0.761	3302	26	8.6
CH2-256	0.26492	1.78	22.31248	2.73	0.61020	2.07	0.759	3270	28	6.4
CH2-257	0.27076	1.57	22.12049	2.77	0.59192	2.28	0.823	3304	25	10.1
CH2-258	0.27797	1.82	25.28596	2.95	0.65907	2.32	0.787	3345	28	2.4
CH2-259	0.26692	1.45	23.56565	2.55	0.63967	2.10	0.823	3282	23	2.9
CH2-260	0.26582	1.90	22.92015	3.19	0.62472	2.57	0.804	3275	30	4.6
CH2-261	0.24809	1.93	13.93365	3.78	0.40694	3.24	0.859	3167	31	43.8
CH2-262	0.27702	1.94	23.76679	2.78	0.62164	2.00	0.718	3340	30	7.1
CH2-263	0.27584	1.53	24.35122	2.47	0.63965	1.93	0.784	3333	24	4.5
CH2-265	0.27003	1.44	23.73314	2.52	0.63686	2.07	0.821	3300	23	3.8
CH2-266	0.26850	1.65	23.70061	2.53	0.63963	1.92	0.759	3291	26	3.2
CH2-267	0.27434	1.53	24.51204	2.54	0.64747	2.03	0.799	3325	24	3.2
CH2-268	0.27369	1.54	24.30567	2.45	0.64356	1.90	0.777	3321	24	3.6
CH2-269	0.27098	1.51	24.31071	2.41	0.65015	1.88	0.780	3305	24	2.3
CH2-270	0.26076	1.53	16.43248	2.60	0.45668	2.09	0.807	3245	24	33.7
CH2-271	0.27176	1.54	22.87454	2.40	0.61006	1.84	0.767	3310	24	7.7
CH2-272	0.26762	2.31	21.84842	3.51	0.59173	2.64	0.752	3286	36	9.6
CH2-273	0.26071	1.70	21.88118	2.83	0.60836	2.27	0.801	3245	27	5.8
CH2-274	0.27199	1.48	23.50570	2.43	0.62644	1.92	0.793	3311	23	5.5
CH2-275	0.27069	1.50	22.08547	2.52	0.59142	2.03	0.805	3304	23	10.2
CH2-276	0.26990	1.35	22.96784	2.26	0.61689	1.81	0.801	3299	21	6.4
CH2-277	0.27337	1.47	23.69579	2.41	0.62840	1.91	0.793	3319	23	5.5
CH2-278	0.27365	1.53	23.41143	2.57	0.62024	2.07	0.803	3321	24	6.7
CH2-280	0.25789	2.06	18.76742	3.55	0.52765	2.90	0.815	3228	32	18.1
CH2-281	0.28510	1.47	26.67143	2.38	0.67842	1.88	0.787	3385	23	1.3
CH2-282	0.27356	1.42	24.27711	2.43	0.64360	1.97	0.812	3320	22	3.6
CH2-283	0.26089	1.63	21.45046	3.14	0.59632	2.69	0.855	3246	26	7.6
CH2-284	0.26039	2.07	18.98341	4.17	0.52879	3.63	0.869	3243	33	18.4
CH2-285	0.27164	1.78	24.91101	2.51	0.66520	1.77	0.706	3309	28	0.6
CH2-286	0.27247	1.65	24.33034	2.56	0.64776	1.95	0.763	3314	26	2.9
CH2-287	0.27243	1.50	23.50548	2.62	0.62594	2.15	0.820	3314	24	5.7
CH2-288	0.27341	1.52	24.90954	2.54	0.66100	2.03	0.801	3319	24	1.4

Table B.2 continued from previous page

Analysis-#	$^{207}Pb/^{206}Pb$ Bias Corr.	% 2σ	$^{207}Pb/^{235}U$ Bias Corr.	% 2σ	$^{206}Pb/^{238}U$ Bias Corr.	% 2σ	corr. coef.	$^{207}Pb/^{206}Pb$ Age (Ma)	2σ	Discordance (%)
CH2-289	0.27081	1.52	25.21375	2.51	0.67556	1.99	0.793	3304	24	-0.8
CH2-290	0.26733	1.57	22.57462	2.81	0.61276	2.33	0.829	3284	25	6.5
CH2-291	0.26755	1.68	22.17853	2.67	0.60167	2.08	0.779	3285	26	8.1
CH2-292	0.26870	1.51	25.21319	2.57	0.68112	2.08	0.809	3292	24	-1.8
CH2-293	0.25772	1.76	20.70316	2.77	0.58316	2.14	0.773	3227	28	8.9
CH2-295	0.26597	1.48	24.13268	2.40	0.65879	1.90	0.789	3276	23	0.3
CH2-296	0.28153	1.72	26.44441	2.51	0.68206	1.83	0.729	3365	27	0.3
CH2-297	0.27063	1.60	24.26991	2.49	0.65126	1.91	0.768	3303	25	2.1
CH2-298	0.27306	1.75	25.06540	2.56	0.66668	1.87	0.730	3317	27	0.7
CH2-299	0.26762	1.68	25.34434	2.84	0.68787	2.29	0.807	3286	26	-2.7
CH2-300	0.26843	1.51	24.54918	3.13	0.66433	2.74	0.876	3291	24	0.1
CH2-301	0.26640	2.02	24.32115	3.21	0.66339	2.50	0.777	3279	32	-0.1
CH2-302	0.26660	1.56	23.53735	2.59	0.64160	2.06	0.797	3280	25	2.6
CH2-303	0.27197	1.60	27.48832	2.67	0.73456	2.14	0.800	3311	25	-6.8
CH2-304	0.21415	1.84	10.10015	3.21	0.34282	2.63	0.820	2931	30	54.1
CH2-305	0.26454	1.52	23.65328	2.54	0.64999	2.04	0.801	3268	24	1.1
CH2-306	0.26459	2.02	24.96593	2.97	0.68599	2.17	0.732	3268	32	-3.0
CH2-307	0.27276	1.72	26.45826	2.72	0.70531	2.11	0.775	3316	27	-3.7
CH2-308	0.27117	1.65	25.76050	2.62	0.69080	2.03	0.776	3307	26	-2.4
CH2-310	0.27071	1.76	24.37839	2.97	0.65500	2.39	0.805	3304	28	1.6

Table B.3.: U-Pb data from the sample RM1 showing all relevant isotope ratios and $^{207}Pb/^{206}Pb$ ages.

Analysis-#	$^{207}Pb/^{206}Pb$ Bias Corr.	% 2σ	$^{207}Pb/^{235}U$ Bias Corr.	% 2σ	$^{206}Pb/^{238}U$ Bias Corr.	% 2σ	corr. coef.	$^{207}Pb/^{206}Pb$ Age (Ma)	2σ	Discordance (%)
RM1-001	0.11818	3.09	3.00012	3.70	0.18326	2.04	0.550	1924	55	77.2
RM1-002	0.24331	1.93	14.57906	4.64	0.43232	4.22	0.910	3136	31	35.3
RM1-003	0.26780	1.68	17.17223	2.87	0.46241	2.33	0.812	3287	26	34.0
RM1-004	0.27379	1.64	24.87610	4.49	0.65486	4.18	0.931	3322	26	2.2
RM1-005	0.36517	1.66	35.63317	2.57	0.70296	1.96	0.763	3765	25	9.6
RM1-006	0.11625	6.35	2.66246	6.78	0.16489	2.38	0.351	1894	114	92.4
RM1-007	0.28363	1.57	24.12341	2.75	0.61211	2.26	0.820	3377	25	9.6
RM1-008	0.28682	1.43	26.02982	2.84	0.65290	2.45	0.864	3394	22	4.7
RM1-009	0.25622	1.56	12.46558	4.18	0.34987	3.88	0.928	3217	25	66.2
RM1-010	0.24263	1.74	12.52667	2.95	0.37115	2.38	0.808	3131	28	53.8
RM1-011	0.22268	1.95	12.15046	4.24	0.39187	3.76	0.888	2994	31	40.4
RM1-013	0.21657	3.30	5.95828	8.91	0.19749	8.27	0.929	2949	53	153.6
RM1-015	0.25136	2.37	14.56733	3.81	0.41584	2.97	0.781	3187	38	42.1
RM1-016	0.21175	2.43	8.94509	3.94	0.30306	3.10	0.787	2913	39	70.6
RM1-017	0.24338	2.59	11.96897	4.85	0.35277	4.10	0.845	3136	41	60.9
RM1-018	0.21674	3.40	6.27614	4.80	0.20769	3.39	0.706	2951	55	142.3
RM1-019	0.36540	1.64	37.31717	3.14	0.73244	2.68	0.854	3766	25	6.2
RM1-020	0.28527	1.69	27.92211	3.00	0.70191	2.47	0.825	3386	26	-1.3
RM1-022	0.23744	1.94	13.54337	3.63	0.40897	3.07	0.845	3097	31	40.0
RM1-023	0.22304	2.27	10.40705	3.65	0.33456	2.85	0.782	2997	36	60.9
RM1-024	0.28028	1.84	29.44150	2.97	0.75319	2.33	0.785	3358	29	-7.3
RM1-025	0.28790	1.49	24.64602	2.73	0.61383	2.29	0.837	3400	23	10.1
RM1-026	0.15486	4.15	3.98095	5.54	0.18434	3.67	0.662	2395	70	119.4
RM1-027	0.19704	2.21	6.49490	3.71	0.23639	2.98	0.804	2796	36	104.2
RM1-028	0.24183	3.66	11.41016	4.94	0.33839	3.32	0.672	3126	58	66.2
RM1-032	0.27956	1.49	29.62138	2.76	0.76051	2.33	0.843	3354	23	-8.1
RM1-034	0.28581	1.57	29.14585	2.62	0.73219	2.10	0.801	3389	24	-4.4
RM1-035	0.22807	2.33	11.20928	4.61	0.35294	3.97	0.863	3033	37	55.5
RM1-036	0.16984	3.09	5.09011	4.50	0.21525	3.26	0.725	2550	52	102.8
RM1-038	0.40520	1.83	47.09287	2.92	0.83511	2.28	0.779	3922	27	0.1
RM1-039	0.27886	1.99	19.08280	3.86	0.49180	3.30	0.856	3350	31	29.8
RM1-040	0.24875	3.66	9.83575	6.97	0.28424	5.94	0.852	3171	58	96.4
RM1-041	0.21019	4.59	6.76189	7.18	0.23143	5.53	0.769	2901	74	116.0
RM1-042	0.24701	1.92	12.34543	4.12	0.35964	3.64	0.884	3160	30	59.4
RM1-043	0.11526	3.33	2.10716	3.96	0.13158	2.15	0.542	1879	60	135.6
RM1-044	0.26282	1.91	18.39783	3.23	0.50395	2.60	0.806	3257	30	23.7
RM1-045	0.28106	1.76	27.89040	2.80	0.71457	2.18	0.777	3363	28	-3.3

Table B.3 continued from previous page

Analysis-#	$^{207}Pb/^{206}Pb$ Bias Corr.	% 2σ	$^{207}Pb/^{235}U$ Bias Corr.	% 2σ	$^{206}Pb/^{238}U$ Bias Corr.	% 2σ	corr. coef.	$^{207}Pb/^{206}Pb$ Age (Ma)	2σ	Discordance (%)
RM1-047	0.21329	4.67	5.58421	6.03	0.18863	3.81	0.633	2925	75	162.3
RM1-048	0.24722	1.78	16.55964	3.68	0.48274	3.23	0.876	3161	28	24.4
RM1-049	0.28395	1.64	27.56091	2.63	0.69970	2.06	0.781	3379	26	-1.3
RM1-050	0.28217	1.86	29.05484	3.85	0.74249	3.37	0.876	3369	29	-6.0
RM1-051	0.21697	1.94	8.85274	2.85	0.29462	2.08	0.731	2952	31	77.2
RM1-052	0.22641	2.96	8.70736	6.23	0.27780	5.48	0.880	3021	47	91.0
RM1-053	0.15673	3.29	4.47083	5.86	0.20612	4.85	0.828	2415	56	99.7
RM1-055	0.21077	3.48	6.37475	7.25	0.21867	6.36	0.877	2906	56	127.7
RM1-056	0.17372	5.50	5.07587	6.94	0.21133	4.23	0.610	2588	92	109.2
RM1-057	0.27127	1.85	23.23781	4.13	0.61976	3.69	0.894	3307	29	6.3
RM1-058	0.28559	1.67	24.76770	3.00	0.62763	2.49	0.831	3387	26	7.8
RM1-059	0.25969	2.24	17.78821	5.98	0.49587	5.55	0.927	3239	35	24.6
RM1-060	0.27793	7.30	10.03028	10.10	0.26133	6.98	0.691	3345	114	123.3
RM1-061	0.27454	2.49	25.45327	5.29	0.67196	4.66	0.882	3326	39	0.3
RM1-063	0.24375	2.42	13.13786	5.23	0.39088	4.63	0.886	3138	38	47.4
RM1-064	0.37035	1.85	28.34448	2.87	0.55518	2.19	0.763	3786	28	32.9
RM1-065	0.22279	4.86	9.39285	9.02	0.30591	7.61	0.843	2995	78	73.9
RM1-066	0.17293	3.64	4.17721	5.50	0.17532	4.13	0.750	2581	61	147.6
RM1-067	0.25863	2.13	16.30117	3.62	0.45759	2.92	0.807	3232	34	33.0
RM1-068	0.22324	6.68	11.23830	10.72	0.36559	8.39	0.783	2998	107	49.1
RM1-069	0.28571	2.58	19.03830	7.18	0.48405	6.70	0.933	3388	40	33.0
RM1-071	0.23216	2.48	11.61044	3.64	0.36648	2.66	0.731	3061	40	51.9
RM1-074	0.23990	4.60	11.81538	11.59	0.36091	10.63	0.918	3113	73	56.6
RM1-075	0.27365	3.29	15.26982	6.62	0.40888	5.74	0.867	3321	52	50.1
RM1-076	0.27200	2.57	16.42648	5.92	0.44252	5.33	0.901	3311	40	40.1
RM1-077	0.26050	4.48	14.23095	10.82	0.40028	9.85	0.910	3244	70	49.3
RM1-078	0.06695	7.09	0.87565	7.86	0.09582	3.38	0.430	832	148	40.9
RM1-079	0.24469	4.65	8.16376	8.33	0.24445	6.91	0.830	3145	74	122.9
RM1-080	0.26707	1.73	18.35947	3.13	0.50364	2.61	0.833	3283	27	24.7
RM1-081	0.28711	2.22	26.50862	3.32	0.67630	2.48	0.745	3396	34	1.9
RM1-082	0.25416	3.71	10.43201	10.03	0.30063	9.32	0.929	3205	59	89.0
RM1-083	0.28133	1.64	22.38548	3.12	0.58275	2.65	0.851	3364	26	13.6
RM1-084	0.28073	3.12	17.14127	6.36	0.44716	5.54	0.871	3361	49	40.9
RM1-085	0.30494	1.96	26.75332	2.96	0.64244	2.22	0.750	3489	30	9.0
RM1-086	0.20376	2.55	7.00382	4.66	0.25168	3.90	0.836	2851	42	96.8
RM1-087	0.18908	2.79	6.54143	4.46	0.25328	3.48	0.780	2728	46	87.3
RM1-088	0.23896	8.38	9.29712	10.81	0.28481	6.83	0.632	3107	133	92.2
RM1-089	0.27906	1.52	21.06600	2.80	0.55257	2.35	0.839	3351	24	18.1
RM1-090	0.20998	4.81	8.80002	9.31	0.30674	7.97	0.856	2899	78	68.0

Table B.3 continued from previous page

Analysis-#	$^{207}Pb/^{206}Pb$ Bias Corr.	% 2σ	$^{207}Pb/^{235}U$ Bias Corr.	% 2σ	$^{206}Pb/^{238}U$ Bias Corr.	% 2σ	corr. coef.	$^{207}Pb/^{206}Pb$ Age (Ma)	2σ	Discordance (%)
RM1-091	0.27178	1.76	19.97358	2.81	0.53770	2.19	0.780	3310	28	19.2
RM1-092	0.27639	1.84	18.93061	3.75	0.50106	3.27	0.872	3336	29	27.3
RM1-093	0.22205	3.60	8.38901	6.70	0.27635	5.65	0.843	2990	58	89.9
RM1-094	0.27351	2.71	20.92189	3.60	0.55947	2.36	0.656	3320	42	15.8
RM1-095	0.27206	2.44	16.11455	5.43	0.43316	4.85	0.893	3312	38	42.6
RM1-096	0.25109	2.00	12.12392	4.13	0.35306	3.62	0.875	3186	32	63.3
RM1-097	0.28642	1.75	25.32935	2.79	0.64654	2.18	0.780	3392	27	5.4
RM1-098	0.28896	1.65	24.47480	3.12	0.61915	2.65	0.849	3406	26	9.5
RM1-099	0.28310	1.49	20.64487	2.65	0.53300	2.20	0.828	3374	23	22.4
RM1-100	0.26857	2.12	18.76501	3.84	0.51061	3.20	0.834	3291	33	23.7
RM1-101	0.29113	1.58	25.65980	2.69	0.64378	2.17	0.810	3417	24	6.6
RM1-102	0.25000	2.14	13.71987	4.09	0.40080	3.48	0.851	3179	34	46.2
RM1-103	0.29192	1.73	23.36549	3.11	0.58446	2.59	0.832	3422	27	15.2
RM1-104	0.23508	3.56	9.25798	8.69	0.28752	7.92	0.912	3081	57	89.0
RM1-106	0.28718	1.80	23.70399	2.78	0.60242	2.12	0.761	3396	28	11.6
RM1-107	0.28421	1.75	26.57926	2.69	0.68242	2.04	0.758	3380	27	0.7
RM1-108	0.43392	1.64	48.94030	2.67	0.82290	2.11	0.790	4024	24	3.9
RM1-109	0.30780	1.66	26.21794	2.78	0.62137	2.23	0.802	3504	26	12.4
RM1-110	0.28344	1.83	20.26814	3.20	0.52154	2.63	0.822	3376	28	24.7
RM1-111	0.28340	1.82	21.75664	3.37	0.55852	2.84	0.841	3375	28	17.9
RM1-112	0.29284	1.74	22.78534	4.17	0.56597	3.79	0.909	3426	27	18.4
RM1-113	0.08123	5.02	1.82882	6.30	0.16374	3.80	0.603	1222	99	24.9
RM1-114	0.28618	1.81	29.94422	2.99	0.76078	2.38	0.796	3391	28	-7.1
RM1-115	0.28293	1.72	25.61415	3.24	0.65813	2.75	0.848	3373	27	3.4
RM1-117	0.24435	1.71	15.70335	2.96	0.46701	2.42	0.816	3142	27	27.1
RM1-118	0.27324	1.99	20.86935	4.87	0.55492	4.45	0.913	3318	31	16.5
RM1-119	0.27207	1.72	21.55602	2.91	0.57550	2.34	0.807	3312	27	12.9
RM1-120	0.28681	1.78	20.86634	3.28	0.52837	2.75	0.840	3394	28	24.0
RM1-121	0.26732	2.03	18.04603	3.77	0.48998	3.18	0.843	3284	32	27.6
RM1-122	0.29534	3.44	20.28143	7.89	0.49832	7.10	0.900	3440	53	31.8
RM1-123	0.28578	2.32	26.29600	3.31	0.66759	2.35	0.711	3388	36	2.7
RM1-124	0.40937	1.80	43.73581	3.15	0.77500	2.59	0.820	3937	27	6.3
RM1-125	0.27877	2.13	14.44524	4.12	0.37582	3.52	0.856	3350	33	62.7
RM1-126	0.30106	1.82	26.55945	3.03	0.63971	2.42	0.799	3469	28	8.7
RM1-127	0.28251	2.35	21.66565	3.36	0.55599	2.39	0.713	3371	37	18.2
RM1-128	0.26621	1.81	17.76612	3.29	0.48376	2.75	0.836	3278	28	28.7
RM1-129	0.41598	2.43	47.18573	3.43	0.82209	2.42	0.706	3961	36	2.3
RM1-130	0.24439	3.31	13.59302	8.40	0.40289	7.72	0.919	3143	53	43.9
RM1-131	0.27364	1.74	20.97189	4.30	0.55474	3.93	0.915	3321	27	16.6

Table B.3 continued from previous page

Analysis-#	$^{207}Pb/^{206}Pb$ Bias Corr.	% 2σ	$^{207}Pb/^{235}U$ Bias Corr.	% 2σ	$^{206}Pb/^{238}U$ Bias Corr.	% 2σ	corr. coef.	$^{207}Pb/^{206}Pb$ Age (Ma)	2σ	Discordance (%)
RM1-132	0.29338	2.03	26.73858	3.35	0.65954	2.66	0.795	3429	31	4.9
RM1-133	0.26927	12.40	8.99049	14.06	0.24158	6.63	0.472	3296	194	136.0
RM1-134	0.28504	2.04	24.30875	3.21	0.61692	2.48	0.771	3384	32	9.2
RM1-135	0.42042	1.77	48.72840	3.26	0.83827	2.73	0.839	3977	27	1.2
RM1-136	0.26557	1.66	20.81701	3.33	0.56683	2.88	0.867	3274	26	13.0
RM1-137	0.28875	1.93	26.30431	2.89	0.65865	2.14	0.743	3405	30	4.3
RM1-138	0.28294	2.67	19.25852	6.28	0.49205	5.68	0.905	3373	42	30.6
RM1-139	0.26850	2.13	17.34317	5.24	0.46689	4.79	0.914	3291	33	33.1
RM1-140	0.42516	1.79	50.71989	3.09	0.86216	2.51	0.814	3994	27	-0.4
RM1-141	0.24128	3.65	14.67328	7.18	0.43929	6.18	0.861	3122	58	32.9
RM1-142	0.26220	1.89	17.16544	3.51	0.47282	2.96	0.843	3254	30	30.3
RM1-143	0.26504	1.85	16.39477	3.83	0.44671	3.35	0.875	3271	29	37.3
RM1-144	0.27856	1.87	28.31198	3.10	0.73389	2.47	0.797	3349	29	-5.7
RM1-145	0.28289	1.58	27.06532	2.95	0.69076	2.49	0.843	3373	25	-0.5
RM1-146	0.28183	1.90	28.81323	3.01	0.73805	2.33	0.774	3367	30	-5.6
RM1-147	0.20955	3.66	8.73206	5.71	0.30078	4.37	0.767	2896	59	70.7
RM1-148	0.16860	12.38	5.95328	13.49	0.25486	5.36	0.398	2538	207	73.3
RM1-149	0.40088	2.05	38.17494	3.73	0.68726	3.11	0.834	3906	31	15.7
RM1-150	0.27621	1.65	23.94534	2.90	0.62560	2.39	0.823	3335	26	6.4
RM1-151	0.28636	1.84	27.73754	2.82	0.69881	2.13	0.757	3392	29	-0.8
RM1-152	0.28931	1.88	24.92459	2.91	0.62151	2.22	0.764	3408	29	9.3
RM1-153	0.40660	1.64	46.02852	2.75	0.81660	2.20	0.802	3927	25	2.0
RM1-155	0.28544	1.85	24.25986	3.04	0.61302	2.42	0.795	3387	29	9.8
RM1-156	0.25649	1.87	15.92215	2.70	0.44773	1.95	0.723	3219	29	34.8
RM1-157	0.27879	1.65	19.61679	2.66	0.50747	2.08	0.783	3350	26	26.5
RM1-158	0.28232	1.87	27.24076	2.83	0.69586	2.12	0.750	3370	29	-1.1
RM1-159	0.30528	1.76	29.63113	2.74	0.69996	2.11	0.768	3491	27	2.0
RM1-160	0.30179	1.70	28.43998	2.63	0.67957	2.01	0.763	3473	26	3.8
RM1-161	0.17442	4.62	4.76651	6.93	0.19706	5.17	0.746	2595	77	123.6
RM1-162	0.27723	1.66	22.36022	2.87	0.58159	2.34	0.816	3341	26	13.0
RM1-163	0.26904	2.01	15.97825	3.72	0.42823	3.12	0.841	3294	32	43.2
RM1-164	0.25325	2.09	11.83983	4.46	0.33711	3.94	0.883	3199	33	70.7
RM1-165	0.26800	1.52	18.56893	2.47	0.49960	1.94	0.787	3288	24	25.8
RM1-166	0.29388	1.60	22.44432	2.48	0.55069	1.90	0.764	3432	25	21.2
RM1-167	0.18500	1.89	6.32142	3.02	0.24639	2.36	0.779	2692	31	89.5
RM1-168	0.26435	2.45	12.33101	7.93	0.33637	7.55	0.951	3267	38	74.6
RM1-169	0.41967	1.70	50.47558	2.85	0.86731	2.28	0.801	3974	25	-1.4
RM1-170	0.32425	1.55	33.83375	2.48	0.75244	1.94	0.780	3584	24	-1.0
RM1-171	0.27594	1.65	26.02259	4.85	0.68012	4.56	0.940	3334	26	-0.4

Table B.3 continued from previous page

Analysis-#	$^{207}Pb/^{206}Pb$ Bias Corr.	% 2σ	$^{207}Pb/^{235}U$ Bias Corr.	% 2σ	$^{206}Pb/^{238}U$ Bias Corr.	% 2σ	corr. coef.	$^{207}Pb/^{206}Pb$ Age (Ma)	2σ	Discordance (%)
RM1-172	0.28912	1.68	26.47571	2.76	0.66046	2.20	0.794	3407	26	4.1
RM1-173	0.19851	2.11	7.26919	3.27	0.26412	2.49	0.763	2808	35	85.7
RM1-175	0.28078	1.92	25.95193	3.13	0.66672	2.48	0.790	3361	30	2.0
RM1-176	0.40951	1.53	35.62884	2.63	0.62765	2.14	0.813	3938	23	25.3
RM1-177	0.30231	4.99	14.08673	10.88	0.33618	9.67	0.889	3476	77	85.9
RM1-178	0.21507	7.39	4.76387	9.94	0.15982	6.65	0.669	2938	119	207.2
RM1-179	0.28545	1.80	23.02470	2.78	0.58202	2.11	0.761	3387	28	14.4
RM1-180	0.28488	1.79	26.45307	2.92	0.67007	2.30	0.789	3384	28	2.3
RM1-181	0.26479	2.40	14.00240	6.33	0.38170	5.86	0.925	3269	38	56.7
RM1-182	0.26062	1.87	15.72173	2.98	0.43547	2.32	0.779	3244	29	39.1
RM1-183	0.26459	1.83	19.36939	3.10	0.52850	2.51	0.807	3268	29	19.4
RM1-184	0.26573	1.82	19.56193	4.06	0.53152	3.63	0.894	3275	29	19.1
RM1-185	0.27789	1.96	20.65049	3.77	0.53661	3.22	0.855	3345	31	20.7
RM1-186	0.28400	1.76	26.79725	2.86	0.68144	2.25	0.787	3379	27	0.8
RM1-188	0.21918	2.55	8.98832	4.20	0.29623	3.34	0.796	2969	41	77.3
RM1-189	0.15597	3.25	4.46332	6.66	0.20674	5.81	0.873	2407	55	98.5
RM1-191	0.24114	2.66	14.33464	4.24	0.42976	3.30	0.778	3121	42	35.3
RM1-192	0.26484	4.00	17.15880	7.22	0.46844	6.01	0.832	3270	63	31.9
RM1-193	0.27420	2.19	21.33887	3.75	0.56275	3.05	0.811	3324	34	15.4
RM1-194	0.25852	1.58	19.73521	3.32	0.55210	2.93	0.880	3232	25	13.9
RM1-195	0.21976	3.41	12.94259	9.15	0.42599	8.49	0.928	2973	55	29.8
RM1-196	0.23646	2.13	12.23677	3.19	0.37436	2.37	0.744	3090	34	50.6
RM1-198	0.28629	2.21	16.74752	6.13	0.42329	5.71	0.932	3391	34	48.9
RM1-199	0.28130	2.70	25.78118	4.76	0.66325	3.92	0.824	3364	42	2.5
RM1-200	0.27215	1.93	18.15356	2.83	0.48277	2.07	0.733	3312	30	30.3
RM1-201	0.24552	4.04	9.51310	5.44	0.28054	3.65	0.670	3150	64	97.4
RM1-202	0.16894	3.48	4.46193	4.73	0.19125	3.21	0.678	2542	58	125.1
RM1-203	0.22508	2.20	9.75320	3.28	0.31381	2.44	0.743	3011	35	71.0
RM1-204	0.21162	3.00	7.59538	4.37	0.25996	3.18	0.727	2912	49	95.3
RM1-205	0.27237	2.18	15.40512	3.44	0.40970	2.67	0.774	3313	34	49.6
RM1-206	0.23767	1.90	14.13261	3.18	0.43077	2.54	0.801	3098	30	34.1
RM1-207	0.07775	10.53	0.83570	10.76	0.07787	2.25	0.209	1136	209	134.8
RM1-208	0.15811	3.19	4.57686	4.36	0.20978	2.97	0.681	2430	54	97.8
RM1-209	0.24079	1.79	13.53434	3.63	0.40738	3.16	0.870	3119	28	41.5
RM1-210	0.26939	1.71	18.44656	2.79	0.49631	2.20	0.790	3296	27	26.8
RM1-211	0.15833	1.87	4.96557	3.15	0.22736	2.53	0.804	2432	32	84.0
RM1-212	0.28088	2.63	18.20050	7.77	0.46976	7.31	0.941	3362	41	35.3
RM1-213	0.29566	1.79	26.20580	3.70	0.64261	3.24	0.876	3441	28	7.5
RM1-214	0.24076	2.74	11.78167	7.09	0.35479	6.54	0.922	3119	44	59.2

Table B.3 continued from previous page

Analysis-#	$^{207}Pb/^{206}Pb$ Bias Corr.	% 2σ	$^{207}Pb/^{235}U$ Bias Corr.	% 2σ	$^{206}Pb/^{238}U$ Bias Corr.	% 2σ	corr. coef.	$^{207}Pb/^{206}Pb$ Age (Ma)	2σ	Discordance (%)
RM1-215	0.14958	3.36	4.18803	4.06	0.20301	2.29	0.563	2336	57	95.9
RM1-216	0.27621	1.75	24.52965	3.01	0.64390	2.45	0.814	3335	27	4.0
RM1-217	0.27639	1.67	18.70418	2.77	0.49066	2.21	0.797	3336	26	29.5
RM1-218	0.13428	4.99	3.06674	5.73	0.16558	2.81	0.490	2149	87	117.4
RM1-219	0.28787	1.57	25.83736	2.75	0.65072	2.26	0.821	3400	24	5.1
RM1-220	0.26427	1.81	17.00457	3.10	0.46649	2.52	0.812	3266	28	32.2
RM1-221	0.24530	1.94	14.58434	5.73	0.43096	5.40	0.941	3149	31	36.2
RM1-222	0.26562	1.63	19.10191	2.93	0.52121	2.43	0.831	3274	26	21.0
RM1-223	0.21301	1.83	9.70674	2.99	0.33007	2.36	0.790	2923	30	58.8
RM1-224	0.14179	2.68	3.93091	3.63	0.20078	2.45	0.676	2244	46	90.1
RM1-225	0.27461	1.85	23.82892	2.97	0.62827	2.32	0.782	3326	29	5.8
RM1-227	0.29878	1.67	29.74467	2.52	0.72044	1.88	0.747	3458	26	-1.2
RM1-228	0.20083	4.58	6.25238	6.95	0.22523	5.23	0.752	2827	75	115.7
RM1-229	0.31078	1.76	25.84078	3.61	0.60136	3.16	0.874	3518	27	15.8
RM1-230	0.24895	1.60	15.07698	2.72	0.43787	2.20	0.809	3172	25	35.4
RM1-231	0.24440	1.99	12.76280	4.30	0.37703	3.82	0.887	3143	32	52.3
RM1-232	0.27736	1.71	26.39412	2.92	0.68676	2.37	0.812	3342	27	-0.9
RM1-233	0.28226	1.88	26.26802	3.53	0.67130	2.99	0.846	3369	29	1.7
RM1-234	0.19100	2.72	6.38210	4.22	0.24088	3.22	0.764	2745	45	97.1
RM1-235	0.21798	2.98	9.45215	5.18	0.31246	4.24	0.817	2960	48	68.7
RM1-237	0.41599	1.85	46.96202	2.89	0.81253	2.22	0.768	3961	28	3.2
RM1-238	0.27597	1.96	23.95729	4.13	0.62430	3.64	0.880	3334	31	6.5
RM1-239	0.28017	1.58	23.36521	3.25	0.59933	2.84	0.874	3358	25	10.8
RM1-240	0.24542	1.75	14.27898	3.61	0.41775	3.16	0.874	3149	28	39.8
RM1-242	0.13232	2.12	3.44849	3.06	0.18638	2.20	0.721	2124	37	92.6
RM1-243	0.22446	2.21	10.20984	4.33	0.32500	3.72	0.860	3007	36	65.6
RM1-244	0.27041	1.55	18.12172	2.64	0.47841	2.14	0.810	3302	24	30.9
RM1-245	0.24363	3.72	11.63034	7.89	0.34965	6.96	0.882	3138	59	62.2
RM1-246	0.18093	4.74	4.81906	6.34	0.19510	4.21	0.664	2656	78	131.0
RM1-247	0.30527	1.55	31.13349	2.60	0.74713	2.09	0.803	3491	24	-3.0
RM1-249	0.28691	1.93	29.27108	2.85	0.74750	2.09	0.735	3395	30	-5.7
RM1-250	0.29214	1.82	29.28150	2.71	0.73442	2.01	0.743	3423	28	-3.7
RM1-251	0.28052	1.72	25.09009	3.06	0.65542	2.53	0.826	3360	27	3.3
RM1-252	0.27474	2.91	19.02501	4.90	0.50747	3.94	0.804	3327	45	25.6
RM1-253	0.28818	2.09	26.68285	3.31	0.67854	2.56	0.774	3401	33	1.8
RM1-255	0.30030	1.99	22.27163	3.25	0.54353	2.57	0.790	3465	31	23.7
RM1-257	0.28178	1.61	22.38423	2.77	0.58218	2.26	0.815	3367	25	13.7
RM1-258	0.28829	1.82	25.43762	2.74	0.64665	2.04	0.745	3402	28	5.7
RM1-259	0.25730	1.94	16.46048	3.70	0.46884	3.15	0.852	3224	31	30.0

Table B.3 continued from previous page

Analysis-#	$^{207}Pb/^{206}Pb$ Bias Corr.	% 2σ	$^{207}Pb/^{235}U$ Bias Corr.	% 2σ	$^{206}Pb/^{238}U$ Bias Corr.	% 2σ	corr. coef.	$^{207}Pb/^{206}Pb$ Age (Ma)	2σ	Discordance (%)
RM1-260	0.21428	1.91	9.85369	3.42	0.33700	2.83	0.829	2932	31	56.5
RM1-261	0.27062	1.80	19.35877	3.65	0.52420	3.17	0.870	3303	28	21.5
RM1-262	0.12202	10.32	1.56004	11.51	0.09368	5.11	0.444	1981	183	242.8
RM1-263	0.28941	1.74	22.48804	3.15	0.56936	2.63	0.834	3408	27	17.2
RM1-264	0.27140	2.01	20.18498	3.28	0.54494	2.59	0.790	3308	31	17.9
RM1-265	0.28376	1.53	24.87003	2.46	0.64214	1.92	0.783	3377	24	5.5
RM1-266	0.30147	1.73	17.42662	2.58	0.42350	1.91	0.740	3471	27	52.4
RM1-267	0.25433	1.96	12.75948	3.27	0.36753	2.63	0.802	3206	31	58.7
RM1-268	0.27669	1.44	25.99506	2.83	0.68821	2.44	0.862	3338	22	-1.2
RM1-269	0.28124	1.87	25.61594	2.73	0.66716	1.99	0.729	3364	29	2.0
RM1-270	0.13148	5.03	2.90679	5.71	0.16192	2.69	0.472	2112	88	118.2
RM1-271	0.27344	1.69	21.94371	3.19	0.58757	2.71	0.849	3320	26	11.3
RM1-272	0.28526	1.33	22.62671	2.14	0.58070	1.67	0.783	3386	21	14.6
RM1-273	0.28452	2.24	23.24322	3.70	0.59798	2.95	0.797	3382	35	11.8
RM1-274	0.25437	1.90	14.39633	3.54	0.41423	2.99	0.844	3206	30	43.4
RM1-275	0.28245	1.63	25.57458	2.79	0.66261	2.27	0.813	3370	25	2.7
RM1-276	0.30544	3.71	17.44659	6.10	0.41795	4.84	0.793	3492	57	55.0
RM1-277	0.28294	1.44	24.14078	2.45	0.62420	1.98	0.809	3373	22	7.8
RM1-278	0.26802	2.17	18.17937	4.00	0.49615	3.37	0.841	3288	34	26.5
RM1-279	0.18846	2.62	5.99285	3.95	0.23256	2.96	0.749	2723	43	101.8
RM1-280	0.24542	2.82	13.01283	5.21	0.38771	4.38	0.841	3149	45	49.0
RM1-281	0.21860	2.73	6.89123	3.72	0.23037	2.52	0.678	2964	44	121.6
RM1-282	0.28030	1.60	25.60606	2.65	0.66743	2.11	0.796	3358	25	1.8
RM1-284	0.26708	1.94	19.87929	3.63	0.54356	3.06	0.845	3283	30	17.2
RM1-285	0.26877	1.64	21.29937	3.06	0.57859	2.58	0.843	3293	26	11.8
RM1-286	0.23563	3.16	10.91174	5.43	0.33801	4.42	0.813	3085	50	64.2
RM1-287	0.28082	1.35	24.57766	2.35	0.63865	1.92	0.817	3361	21	5.5
RM1-288	0.19138	3.56	5.30169	5.35	0.20209	4.00	0.747	2748	58	131.4
RM1-289	0.20923	3.84	7.04539	4.95	0.24556	3.12	0.630	2894	62	104.2
RM1-290	0.10270	11.31	2.29875	11.71	0.16319	3.04	0.260	1668	209	71.1
RM1-291	0.26625	1.61	21.20866	3.51	0.58012	3.12	0.888	3278	25	11.0
RM1-292	0.09847	9.76	1.86548	10.16	0.13792	2.82	0.277	1590	182	90.8
RM1-293	0.27745	1.63	21.74823	2.90	0.57045	2.40	0.827	3342	25	14.8
RM1-294	0.25437	1.54	16.66190	3.25	0.47651	2.87	0.881	3206	24	27.5
RM1-295	0.16986	2.49	6.22946	4.58	0.26667	3.84	0.839	2551	42	67.2
RM1-296	0.10821	6.27	2.27634	7.21	0.15290	3.56	0.494	1764	114	92.2
RM1-297	0.09774	9.92	1.80320	10.28	0.13403	2.69	0.262	1577	185	94.3
RM1-298	0.24315	2.71	10.37342	3.41	0.30981	2.07	0.607	3135	43	80.0
RM1-299	0.28771	1.53	27.53972	2.87	0.69479	2.43	0.847	3399	24	-0.1

Table B.3 continued from previous page

Analysis-#	$^{207}Pb/^{206}Pb$ Bias Corr.	% 2σ	$^{207}Pb/^{235}U$ Bias Corr.	% 2σ	$^{206}Pb/^{238}U$ Bias Corr.	% 2σ	corr. coef.	$^{207}Pb/^{206}Pb$ Age (Ma)	2σ	Discordance (%)
RM1-300	0.26269	2.91	15.66370	5.47	0.43258	4.64	0.847	3257	46	40.4
RM1-301	0.14665	2.62	4.52604	3.42	0.22355	2.19	0.641	2302	45	76.8
RM1-302	0.24286	2.03	12.48889	3.72	0.37227	3.11	0.837	3133	32	53.4
RM1-303	0.20392	3.79	6.97656	5.17	0.24752	3.51	0.679	2852	62	99.9
RM1-304	0.28635	1.83	27.66925	3.07	0.69866	2.46	0.803	3392	28	-0.8
RM1-305	0.20223	2.03	8.34882	3.61	0.29831	2.99	0.826	2838	33	68.5
RM1-306	0.21416	1.49	10.96676	2.45	0.36977	1.95	0.796	2931	24	44.4
RM1-307	0.10988	2.29	2.89931	3.39	0.19040	2.50	0.738	1792	42	59.4
RM1-308	0.27788	4.61	8.69423	6.58	0.22562	4.69	0.713	3345	72	154.8
RM1-309	0.27449	2.47	22.62834	4.70	0.59404	4.00	0.851	3326	39	10.5
RM1-310	0.21159	2.10	8.26303	3.73	0.28121	3.08	0.827	2912	34	82.1

Table B.4.: U-Pb data from apatites of the sample RT11, CH2 and RM1 showing all relevant isotope ratios and $^{207}Pb/^{206}Pb$ ages.

Analysis-#	$^{207}Pb/^{206}Pb$ Bias Corr.	% 2σ	$^{207}Pb/^{235}U$ Bias Corr.	% 2σ	$^{206}Pb/^{238}U$ Bias Corr.	% 2σ	corr. coef.	$^{207}Pb/^{206}Pb$ Age (Ma)	2σ	Discordance (%)
RT11-01	0.26541	2.31	26.57109	3.45	0.72551	2.55	0.741	3273	36	-7.0
RT11-29	0.26573	3.19	26.01560	4.31	0.70936	2.90	0.672	3275	50	-5.3
RT11-23	0.26871	2.54	26.06892	3.61	0.70514	2.56	0.709	3292	40	-4.4
RT11-30	0.26979	2.31	28.15155	3.45	0.75586	2.57	0.743	3299	36	-9.2
RT11-27	0.27057	3.09	24.48228	4.00	0.65593	2.54	0.634	3303	48	1.5
RT11-06	0.27149	2.30	28.08136	3.22	0.75168	2.26	0.701	3308	36	-8.5
RT11-32	0.27247	2.51	28.56366	3.36	0.75902	2.23	0.664	3314	39	-9.0
RT11-18	0.27423	2.09	28.17730	3.46	0.74767	2.76	0.797	3324	33	-7.7
RT11-15	0.27444	2.25	27.98195	3.45	0.74288	2.61	0.758	3325	35	-7.2
RT11-21	0.27582	2.32	26.64070	3.45	0.70237	2.55	0.740	3333	36	-2.9
RT11-14	0.27642	3.98	26.88277	5.05	0.70864	3.11	0.616	3337	62	-3.5
RT11-19	0.27715	1.85	27.78886	3.09	0.72945	2.47	0.800	3341	29	-5.5
RT11-11	0.27770	1.85	26.61385	3.03	0.69826	2.40	0.793	3344	29	-2.1
RT11-17	0.27772	2.39	27.18284	3.47	0.71237	2.52	0.727	3344	37	-3.6
RT11-04	0.27852	2.76	27.97007	3.85	0.72910	2.68	0.697	3348	43	-5.2
RT11-10	0.27906	1.94	28.02864	3.01	0.73176	2.30	0.765	3351	30	-5.4
RT11-03	0.27983	4.74	28.55711	5.94	0.74053	3.57	0.602	3356	74	-6.1
RT11-09	0.27995	3.22	28.65895	4.97	0.74576	3.79	0.762	3356	50	-6.6
RT11-24	0.28038	2.79	28.42166	3.83	0.73659	2.62	0.684	3359	44	-5.7
RT11-26	0.28040	1.99	28.27910	3.17	0.73130	2.47	0.778	3359	31	-5.2
RT11-25	0.28062	2.15	27.98515	3.44	0.72330	2.69	0.781	3360	34	-4.3
RT11-22	0.28066	2.16	28.23132	3.41	0.73129	2.64	0.774	3360	34	-5.1
RT11-02	0.28112	2.25	28.46137	3.51	0.73419	2.69	0.767	3363	35	-5.3
RT11-28	0.28114	2.01	27.93859	3.23	0.72021	2.52	0.781	3363	31	-3.9
RT11-08	0.28127	2.84	27.88400	4.17	0.72103	3.05	0.732	3364	44	-4.0
RT11-13	0.28172	1.88	27.49174	3.02	0.71105	2.36	0.783	3366	29	-2.9
RT11-12	0.28201	2.52	29.17813	3.84	0.75387	2.90	0.755	3368	39	-7.1
RT11-31	0.28284	2.24	27.61838	3.27	0.70714	2.39	0.729	3372	35	-2.3
RT11-20	0.28714	2.36	27.35829	3.37	0.69300	2.41	0.714	3396	37	0.0
RT11-07	0.28795	5.40	27.91421	6.34	0.70478	3.31	0.523	3400	84	-1.2
RT11-16	0.29281	2.67	26.98005	3.79	0.67128	2.69	0.710	3426	41	3.4
RT11-05	0.30676	4.30	32.79703	5.57	0.77664	3.53	0.634	3498	66	-5.7
CH2-06	0.24985	4.56	18.34559	6.53	0.53616	4.67	0.715	3178	72	14.7
CH2-32	0.26484	4.20	18.77157	6.78	0.49619	5.32	0.785	3270	66	25.8
CH2-01	0.27011	4.60	27.24266	5.64	0.73589	3.26	0.577	3300	72	-7.2

Table B.4 continued from previous page

Analysis-#	$^{207}Pb/^{206}Pb$ Bias Corr.	% 2σ	$^{207}Pb/^{235}U$ Bias Corr.	% 2σ	$^{206}Pb/^{238}U$ Bias Corr.	% 2σ	corr. coef.	$^{207}Pb/^{206}Pb$ Age (Ma)	2σ	Discordance (%)
CH2-18	0.27066	3.25	25.33474	4.57	0.67790	3.21	0.702	3304	51	-1.1
CH2-07	0.27081	2.97	26.69582	4.14	0.71993	2.88	0.697	3304	47	-5.6
CH2-23	0.27257	3.34	27.84124	4.57	0.73570	3.11	0.681	3315	52	-6.8
CH2-05	0.27423	2.66	28.18545	3.72	0.75043	2.61	0.700	3324	42	-8.0
CH2-27	0.27425	3.02	29.74726	4.26	0.76812	3.00	0.705	3324	47	-9.6
CH2-03	0.27620	3.93	24.28740	5.61	0.64183	4.00	0.714	3335	61	4.3
CH2-29	0.27629	2.93	27.53136	4.14	0.70259	2.93	0.707	3336	46	-2.8
CH2-08	0.27786	3.59	27.52349	4.51	0.72348	2.73	0.606	3345	56	-4.8
CH2-30	0.27816	3.06	27.01730	4.16	0.68330	2.82	0.679	3346	48	-0.4
CH2-13	0.27861	3.05	27.63978	4.32	0.72393	3.05	0.708	3349	48	-4.7
CH2-20	0.27875	2.95	28.47396	4.05	0.73830	2.78	0.686	3350	46	-6.1
CH2-02	0.27894	2.47	29.49155	3.44	0.77156	2.39	0.695	3351	39	-9.2
CH2-10	0.28032	2.91	28.90166	4.12	0.75283	2.92	0.709	3358	45	-7.3
CH2-25	0.28072	2.90	28.04735	4.21	0.71039	3.05	0.724	3361	45	-3.0
CH2-16	0.28157	2.99	28.25688	4.10	0.73159	2.81	0.686	3365	47	-5.0
CH2-21	0.28199	3.24	29.28160	4.36	0.74969	2.92	0.669	3368	50	-6.7
CH2-17	0.28413	2.83	29.01659	4.08	0.74027	2.94	0.721	3380	44	-5.5
CH2-11	0.28472	3.81	29.36442	4.92	0.75292	3.12	0.633	3383	59	-6.6
CH2-12	0.28554	5.18	30.16679	6.45	0.77112	3.85	0.596	3387	81	-8.2
CH2-24	0.28630	3.55	28.66561	4.66	0.72023	3.02	0.648	3391	55	-3.1
CH2-04	0.28643	3.24	28.62276	4.33	0.72951	2.87	0.664	3392	50	-4.0
CH2-19	0.28821	4.38	28.64694	5.37	0.71914	3.11	0.580	3402	68	-2.7
CH2-26	0.28888	3.84	29.89117	4.97	0.73424	3.16	0.636	3405	60	-4.1
CH2-22	0.29512	4.74	29.01225	5.81	0.70894	3.36	0.579	3438	73	-0.5
CH2-14	0.29546	3.42	30.22359	4.54	0.74623	2.98	0.657	3440	53	-4.3
CH2-31	0.29644	3.96	32.24692	5.09	0.76340	3.20	0.628	3445	61	-5.9
CH2-15	0.29896	3.59	30.96570	4.72	0.75538	3.07	0.651	3458	56	-4.7
CH2-28	0.30613	4.26	31.65466	5.41	0.73069	3.34	0.617	3495	66	-1.2
RM1-26	0.27390	2.23	28.59467	3.70	0.75868	2.96	0.798	3322	35	-8.8
RM1-03	0.27746	3.19	28.22120	4.39	0.73490	3.01	0.686	3342	50	-6.0
RM1-16	0.27873	2.13	27.71434	3.22	0.71831	2.41	0.749	3350	33	-4.1
RM1-15	0.28267	6.77	31.38473	8.03	0.80198	4.33	0.539	3371	105	-11.3
RM1-31	0.28379	3.04	28.66612	4.11	0.73520	2.77	0.674	3378	47	-5.0
RM1-01	0.28590	3.03	28.13844	4.02	0.71134	2.64	0.657	3389	47	-2.2
RM1-14	0.28669	2.79	30.09513	4.00	0.75811	2.86	0.715	3393	43	-6.8
RM1-27	0.28926	3.84	30.01552	4.90	0.75433	3.04	0.621	3407	60	-6.0
RM1-04	0.29294	3.08	30.86963	4.39	0.76082	3.13	0.712	3427	48	-6.1
RM1-07	0.29576	3.10	31.34318	4.17	0.76498	2.79	0.669	3442	48	-6.1
RM1-05	0.29785	2.98	30.19405	4.06	0.73185	2.76	0.679	3453	46	-2.6

Table B.4 continued from previous page

Analysis-#	$^{207}Pb/^{206}Pb$ Bias Corr.	% 2σ	$^{207}Pb/^{235}U$ Bias Corr.	% 2σ	$^{206}Pb/^{238}U$ Bias Corr.	% 2σ	corr. coef.	$^{207}Pb/^{206}Pb$ Age (Ma)	2σ	Discordance (%)
RM1-30	0.30621	3.19	32.94233	4.42	0.78277	3.07	0.693	3496	49	-6.3
RM1-25	0.30663	4.05	32.96319	5.33	0.78100	3.47	0.650	3498	63	-6.1
RM1-19	0.33786	4.32	36.66798	5.72	0.78541	3.74	0.654	3647	66	-2.5

Appendix C.

Hf-isotope data

Hf-isotope data for all measurements of the three samples RT11, CH2 and RM1 are compiled in Table C.1 in this appendix.

Table C.1.: Hf-isotope data from the samples RT11, CH2 and RM1. $^{176}Lu/^{177}Hf$ is measured value, $^{176}Hf/^{177}Hf_{initial}$ is back calculated to respective measured $^{207}Pb/^{206}Pb$ age in Ma, $\varepsilon_{i,CHUR}$ is difference per 10000 with respect to chondritic uniform reservoir (CHUR) at crystallization age, and T_{CHUR} and T_{DMM} one stage separation dates with respect to CHUR (Bouvier et al. 2008) or Depleted Mantle Model (DMM) of Griffin et al. (2000). λ_{Lu} after Scherer et al. (2001).

Analysis-#	$^{176}Lu/^{177}Hf$ mean	$^{176}Lu/^{177}Hf$ SE	$^{207}Pb/^{206}Pb$ Age	2σ	$^{176}Hf/^{177}Hf_{initial}$	2σ	$\varepsilon_{i,CHUR}$	$\varepsilon_{i,CHUR}\sigma$	T_{CHUR} Ma	T_{DMM} Ma
RT11-001	0.000914	0.000008	3416	25	0.28054	0.00010	-1.2	2.3	3466	3522
RT11-003	0.000876	0.000005	3404	28	0.28048	0.00013	-3.7	3.0	3564	3604
RT11-007	0.000928	0.000005	3380	26	0.28063	0.00017	1.2	3.6	3327	3406
RT11-019	0.001613	0.000030	3403	25	0.28039	0.00019	-6.9	3.7	3705	3723
RT11-021	0.000824	0.000002	3360	23	0.28055	0.00017	-2.1	3.5	3451	3510
RT11-023	0.000713	0.000006	3295	26	0.28067	0.00015	0.6	3.3	3268	3356
RT11-025	0.001104	0.000004	3400	24	0.28052	0.00011	-2.3	2.5	3501	3552
RT11-027	0.000723	0.000007	3395	27	0.28055	0.00015	-1.2	3.2	3449	3508
RT11-030	0.000974	0.000008	3390	29	0.28047	0.00018	-4.4	3.9	3579	3617
RT11-033	0.000940	0.000002	3385	25	0.28060	0.00012	0.1	2.6	3380	3450
RT11-039	0.001200	0.000013	3369	27	0.28051	0.00014	-3.2	3.0	3508	3558
RT11-040	0.000703	0.000005	3360	28	0.28053	0.00016	-2.9	3.4	3485	3538
RT11-045	0.000845	0.000007	3343	25	0.28065	0.00017	1.1	3.6	3296	3380
RT11-049	0.000958	0.000014	3357	27	0.28057	0.00018	-1.5	3.8	3424	3487
RT11-052	0.000960	0.000006	3375	26	0.28053	0.00019	-2.7	4.0	3490	3542
RT11-054	0.000805	0.000004	3353	29	0.28051	0.00016	-3.6	3.5	3506	3555
RT11-056	0.000923	0.000003	3388	25	0.28051	0.00015	-2.7	3.3	3506	3556
RT11-057	0.001615	0.000007	3379	28	0.28043	0.00018	-5.8	3.8	3634	3664
RT11-062	0.002006	0.000004	3359	26	0.28034	0.00019	-9.7	4.0	3791	3795
RT11-064	0.000978	0.000013	3381	29	0.28060	0.00020	0.0	4.1	3380	3450
RT11-067	0.000835	0.000005	3357	25	0.28065	0.00017	1.2	3.6	3305	3387
RT11-071	0.000960	0.000008	3353	26	0.28063	0.00019	0.6	3.9	3328	3407
RT11-072	0.000715	0.000005	3382	27	0.28059	0.00016	-0.2	3.4	3392	3460
RT11-073	0.001653	0.000006	3365	25	0.28057	0.00018	-1.4	3.7	3425	3489
RT11-074	0.000636	0.000004	3384	25	0.28058	0.00013	-0.5	2.9	3404	3470
RT11-078	0.001448	0.000021	3367	26	0.28063	0.00020	0.9	4.1	3328	3408
RT11-081	0.001268	0.000010	3358	25	0.28061	0.00020	0.0	4.2	3356	3431
RT11-087	0.001265	0.000012	3402	24	0.28055	0.00023	-1.2	4.6	3455	3514
RT11-089	0.001143	0.000016	3370	30	0.28055	0.00018	-2.0	3.9	3456	3515
RT11-090	0.000729	0.000002	3391	26	0.28046	0.00018	-4.5	3.8	3586	3623
RT11-092	0.000748	0.000003	3368	27	0.28042	0.00018	-6.5	3.8	3648	3675
RT11-095	0.000847	0.000005	3386	26	0.28061	0.00022	0.5	4.6	3366	3438
RT11-097	0.001101	0.000007	3385	28	0.28062	0.00020	0.9	4.2	3344	3421
CH2-002	0.000373	0.000005	3289	31	0.28046	0.00018	-6.9	3.8	3580	3618

Table C.1 continued from previous page

Analysis-#	$^{176}Lu/^{177}Hf$ mean	$^{176}Lu/^{177}Hf$ SE	$^{207}Pb/^{206}Pb$ Age	2σ	$^{176}Hf/^{177}Hf_{initial}$	2σ	$\varepsilon_{i,CHUR}$	$\varepsilon_{i,CHUR}\sigma$	T_{CHUR} Ma	T_{DMM} Ma
CH2-003	0.000977	0.000002	3318	25	0.28059	0.00041	-1.9	7.8	3399	3466
CH2-005	0.000631	0.000002	3275	27	0.28058	0.00015	-2.9	3.3	3400	3466
CH2-006	0.000717	0.000005	3387	26	0.28043	0.00026	-5.8	5.2	3635	3664
CH2-007	0.001812	0.000018	3408	33	0.28043	0.00012	-5.3	2.8	3645	3673
CH2-011	0.001113	0.000013	3296	28	0.28053	0.00013	-4.4	3.0	3489	3542
CH2-013	0.000586	0.000003	3296	25	0.28049	0.00025	-5.9	4.9	3550	3593
CH2-015	0.000404	0.000003	3271	27	0.28059	0.00027	-2.8	5.5	3389	3457
CH2-016	0.000208	0.000002	3254	32	0.28047	0.00037	-7.5	7.3	3572	3610
CH2-022	0.000437	0.000003	3298	25	0.28043	0.00039	-7.7	7.5	3626	3656
CH2-024	0.000860	0.000006	3271	26	0.28059	0.00018	-2.9	3.8	3395	3463
CH2-025	0.000443	0.000005	3303	26	0.28070	0.00037	2.0	7.2	3219	3315
CH2-026	0.000857	0.000005	3269	27	0.28035	0.00044	-11.4	8.4	3757	3767
CH2-028	0.000532	0.000004	3291	25	0.28067	0.00037	0.7	7.2	3262	3351
CH2-030	0.000390	0.000002	3278	24	0.28036	0.00033	-10.8	6.5	3735	3748
CH2-031	0.000278	0.000002	3325	30	0.28049	0.00032	-5.0	6.5	3536	3580
CH2-036	0.000487	0.000003	3267	28	0.28024	0.00032	-15.4	6.3	3919	3902
CH2-037	0.000865	0.000010	3307	26	0.28050	0.00017	-5.2	3.6	3533	3578
CH2-040	0.000371	0.000002	3327	27	0.28033	0.00033	-10.6	6.5	3777	3783
CH2-048	0.000332	0.000003	3271	32	0.28064	0.00021	-1.1	4.4	3319	3398
CH2-053	0.000557	0.000004	3332	29	0.28044	0.00045	-6.6	8.7	3614	3646
CH2-055	0.001196	0.000013	3404	24	0.28034	0.00029	-8.4	5.7	3768	3776
CH2-058	0.000737	0.000014	3312	30	0.28062	0.00021	-0.7	4.3	3343	3419
CH2-059	0.000157	0.000005	3344	27	0.28055	0.00020	-2.3	4.2	3443	3502
CH2-065	0.000843	0.000009	3414	27	0.28038	0.00032	-7.0	6.4	3714	3730
CH2-067	0.000490	0.000003	3342	28	0.28062	0.00026	0.0	5.3	3341	3417
CH2-070	0.001264	0.000015	3380	26	0.28048	0.00027	-4.1	5.3	3561	3602
CH2-071	0.001602	0.000007	3410	24	0.28041	0.00030	-5.8	5.8	3667	3691
CH2-073	0.001057	0.000009	3318	27	0.28057	0.00016	-2.4	3.4	3421	3485
CH2-074	0.001509	0.000013	3364	36	0.28055	0.00017	-2.0	3.7	3451	3511
CH2-075	0.000526	0.000002	3313	31	0.28037	0.00029	-9.8	5.9	3730	3743
CH2-078	0.000236	0.000002	3322	28	0.28064	0.00025	0.2	5.1	3313	3393
CH2-079	0.000658	0.000003	3324	26	0.28049	0.00031	-5.2	6.1	3547	3590
CH2-080	0.000492	0.000009	3298	29	0.28070	0.00018	1.6	3.8	3229	3323
CH2-095	0.000951	0.000011	3283	23	0.28055	0.00009	-3.9	2.1	3452	3511
CH2-119	0.000936	0.000008	3286	24	0.28072	0.00013	2.0	2.8	3198	3298
CH2-129	0.000618	0.000006	3311	26	0.28060	0.00013	-1.4	2.9	3372	3443
CH2-149	0.001202	0.000010	3285	21	0.28067	0.00010	0.5	2.2	3263	3353
CH2-150	0.000976	0.000014	3291	28	0.28062	0.00010	-1.4	2.3	3352	3427
CH2-189	0.000343	0.000006	3320	29	0.28059	0.00010	-1.8	2.4	3394	3461
CH2-193	0.000814	0.000015	3279	30	0.28062	0.00010	-1.5	2.4	3344	3420
CH2-194	0.002141	0.000018	3299	24	0.28066	0.00013	0.3	2.8	3283	3372
CH2-204	0.001041	0.000007	3327	23	0.28041	0.00015	-7.8	3.1	3666	3690

Table C.1 continued from previous page

Analysis-#	$^{176}Lu/^{177}Hf$ mean	$^{176}Lu/^{177}Hf$ SE	$^{207}Pb/^{206}Pb$ Age	2σ	$^{176}Hf/^{177}Hf_{initial}$	2σ	$\varepsilon_{i,CHUR}$	$\varepsilon_{i,CHUR}\sigma$	T_{CHUR} Ma	T_{DMM} Ma
CH2-210	0.000801	0.000004	3309	24	0.28057	0.00010	-2.6	2.4	3420	3483
CH2-221	0.001411	0.000030	3256	29	0.28062	0.00013	-1.9	2.8	3342	3419
CH2-285	0.000752	0.000002	3309	28	0.28068	0.00014	1.3	3.2	3253	3344
CH2-296	0.001307	0.000033	3365	27	0.28051	0.00010	-3.3	2.2	3508	3558
CH2-300	0.000740	0.000009	3291	24	0.28063	0.00014	-1.0	3.0	3335	3412
CH2-301	0.001697	0.000007	3279	32	0.28066	0.00008	0.0	2.1	3278	3366
RM1-004	0.000889	0.000004	3322	26	0.28041	0.00012	-7.9	2.7	3663	3688
RM1-008	0.003415	0.000025	3394	22	0.28042	0.00012	-6.0	2.5	3673	3697
RM1-020	0.000987	0.000011	3386	26	0.28041	0.00010	-6.3	2.3	3659	3684
RM1-034	0.001579	0.000010	3389	24	0.28054	0.00009	-1.7	2.1	3462	3520
RM1-038	0.000982	0.000003	3922	27	0.27993	0.00011	-10.8	2.7	4382	4290
RM1-045	0.000951	0.000010	3363	28	0.28029	0.00010	-11.2	2.4	3843	3838
RM1-049	0.000505	0.000004	3379	26	0.28052	0.00010	-2.8	2.4	3496	3547
RM1-081	0.000710	0.000004	3396	34	0.28050	0.00014	-3.0	3.2	3523	3570
RM1-107	0.000661	0.000007	3380	27	0.28054	0.00011	-2.2	2.6	3473	3528
RM1-108	0.001192	0.000008	4024	24	0.28003	0.00011	-4.6	2.5	4221	4155
RM1-115	0.000668	0.000003	3373	27	0.28046	0.00011	-5.0	2.6	3586	3623
RM1-123	0.000555	0.000001	3388	36	0.28053	0.00013	-2.0	3.2	3476	3530
RM1-129	0.000699	0.000006	3961	36	0.28018	0.00015	-1.0	3.4	4004	3974
RM1-135	0.000689	0.000002	3977	27	0.28021	0.00011	0.6	2.5	3951	3929
RM1-137	0.001079	0.000013	3405	30	0.28048	0.00014	-3.6	3.1	3560	3602
RM1-140	0.001205	0.000006	3994	27	0.28009	0.00012	-3.4	2.7	4141	4088
RM1-145	0.001159	0.000001	3373	25	0.28063	0.00012	1.1	2.7	3325	3405
RM1-151	0.000793	0.000001	3392	29	0.28053	0.00017	-2.0	3.8	3477	3532
RM1-153	0.000511	0.000013	3927	25	0.27993	0.00014	-10.6	2.9	4370	4281
RM1-158	0.000686	0.000001	3370	29	0.28050	0.00017	-3.6	3.8	3522	3569
RM1-159	0.000334	0.000002	3491	27	0.28033	0.00014	-6.7	3.1	3776	3782
RM1-160	0.001388	0.000009	3473	26	0.28055	0.00012	0.5	2.8	3453	3512
RM1-169	0.000541	0.000001	3974	25	0.27983	0.00014	-13.0	3.1	4519	4407
RM1-170	0.001265	0.000012	3584	24	0.28052	0.00016	2.0	3.4	3496	3548
RM1-171	0.001364	0.000005	3334	26	0.28050	0.00011	-4.5	2.6	3529	3576
RM1-172	0.001673	0.000003	3407	26	0.28035	0.00014	-8.2	3.0	3766	3774
RM1-175	0.000513	0.000001	3361	30	0.28052	0.00011	-3.0	2.7	3491	3543
RM1-180	0.000754	0.000011	3384	28	0.28040	0.00009	-6.8	2.3	3674	3697
RM1-186	0.000941	0.000009	3379	27	0.28052	0.00013	-2.9	2.9	3502	3553
RM1-216	0.001733	0.000013	3335	27	0.28053	0.00010	-3.6	2.3	3494	3547
RM1-227	0.001462	0.000009	3458	26	0.28039	0.00009	-5.7	2.1	3705	3723
RM1-233	0.001081	0.000002	3369	29	0.28053	0.00010	-2.6	2.4	3483	3537
RM1-237	0.001083	0.000001	3961	28	0.27982	0.00014	-13.6	3.1	4541	4424
RM1-247	0.000747	0.000004	3491	24	0.28056	0.00017	1.5	3.6	3427	3490
RM1-250	0.000596	0.000001	3423	28	0.28049	0.00015	-2.9	3.3	3548	3591
RM1-251	0.000873	0.000007	3360	27	0.28048	0.00012	-4.5	2.7	3553	3595

Table C.1 continued from previous page

Analysis-#	$^{176}Lu/^{177}Hf$ mean	$^{176}Lu/^{177}Hf$ SE	$^{207}Pb/^{206}Pb$ Age	2σ	$^{176}Hf/^{177}Hf_{initial}$	2σ	$\varepsilon_{i,CHUR}$	$\varepsilon_{i,CHUR}\sigma$	T_{CHUR} Ma	T_{DM} Ma
RM1-253	0.000862	0.000004	3401	33	0.28052	0.00010	-2.1	2.5	3492	3544
RM1-275	0.000840	0.000004	3370	25	0.28040	0.00013	-7.3	2.8	3685	3706
RM1-282	0.000872	0.000001	3358	25	0.28053	0.00020	-2.8	4.1	3478	3532
RM1-299	0.000957	0.000003	3399	24	0.28050	0.00017	-3.1	3.5	3534	3580
RM1-304	0.001191	0.000003	3392	28	0.28058	0.00013	-0.2	2.9	3402	3469